COMBUSTION AND EMISSION CHARACTERISTICS OF BIOFUELS IN DIESEL ENGINES

A thesis submitted for the degree of Doctor of Philosophy

By

ŁUKASZ ŁABĘCKI

School of Engineering and Design
Brunel University
United Kingdom

September 2010

ABSTRACT

This study was concerned with the performance of biofuels in diesel engines. Generally, the basic combustion and emission characteristics of Rapeseed Oil (RSO) and Soya Oil (SO) result in a lower in-cylinder pressure peak than diesel. This led to the reduction of Nitrogen Oxides (NO_x) emissions and to relatively high soot emissions. Further measurements of RSO were done in order to investigate the influence of injection pressure, injection timing and Exhaust Gas Recirculation (EGR) on combustion and emission characteristics. A high soot emission from RSO was reduced by increased injection pressure. Moreover, injection timing also had to be varied in order to reduce the soot emissions from RSO. The retarded injection timing (3 deg bTDC) and increased injection pressure (1200 bar) for the blend of 30% RSO resulted in a reduction of soot emission to the same level as from diesel fuel. Further investigation regarding the soot emissions was done for Rapeseed Methyl Ester (RME) under turbocharged engine operation. The application of the boost pressure resulted in stable engine operation at a late injection timing of 5 deg aTDC. A simultaneous reduction of soot and NO_x emissions has been achieved for RME at an injection timing of TDC and high EGR percentage (40 – 50 %).

The soot particles size distribution under different engine operating conditions for RME and diesel has also been investigated. Moreover, the characteristic of Electrostatic Mobility Spectrometer (EMS) and the design of primary dilution system have been provided in order to understand the influence of the dilution process and to obtain more real results. Generally, RME showed less particles concentration in the nucleation mode when compared to diesel. Moreover, high EGR caused a shift of the particles from the nucleation mode by agglomeration into the accumulation mode for both fuels. The effect of injection pressure could only be seen in the accumulation mode, where high injection pressure slightly reduced the concentration number. The soot emission was effectively reduced by the usage of the diesel particulate filter (DPF). For this purpose, the soot particles size distributions before and after the DPF have been measured at different engine speeds and loads. At low engine torque, the soot was effectively filtered while the operation under high engine loads resulted in low soot particle concentration especially in the nucleation mode, after the DPF.

ACKNOWLEDGEMENTS

I would like to honestly thank to my supervisors Dr Lionel Christopher Ganippa and Prof. Hua Zhao, as a second supervisor, for their enormous help and support during the study. In addition I am thankful to all whose have gave a possibility to utilize University's equipment and laboratories to finish this research.

Moreover, greatest acknowledge to technical stuff at Brunel University, especially to Kenneth Anstiss and Andy Selways for keeping the engine in very good condition, Clive Barrett for electronic support and John Langdon for always fast ordering.

I would like to thank to Shell, Johnson and Matthey and Regenatec companies for their contribution to my work such as new fuels and DPF filter. Regarding the Electrostatic Mobility Analyser I would like to thank to Wolfgang Winklmayr and Adreas Lindner from Tapcon for their help, support and common investigations on the system.

Additionally, I would like to thank to my wife for her sacrifice and support during a three years spent in the UK together.

Furthermore, big thanks to Polish Society at Brunel University for keeping me in good mood and well organized social time over past three years.

ABBREVATIONS

A/F	Air to fuel ratio
aTDC	After top dead centre
BDC	Bottom dead centre
BMEP	Brake mean effective pressure
BSFC	Brake specific fuel consumption
bTDC	Before top dead centre
BTX	Benzene, toluene, xylene
CAD	Crank angle degree
CCN	Cumulative concentration number
cHRR	Cumulative heat release rate
CI	Compression ignition
CME	Cottonseed methyl ester
CN	Cetane number
CO	Carbon monoxide
CO_2	Carbon dioxide
COV	Coefficient of variation
CRT	Continuously regenerating traps
CVS	Constant volume sampler
Df(pCN)	Particles diameter at the corresponding peak of the concentration number
DI	Direct injection
DMA	Differential mobility analyser
DOC	Duration of combustion
DPF	Diesel particulates filter
ECU	Engine control unit
EGR	Exhaust gas recirculation
EMS	Electrostatic mobility spectrometer
EOC	End of combustion
EUI	Electronic unit injectors
EVC	Exhaust valve closing
EVO	Exhaust valve opening
FAME	Fatty acid methyl ester
FCE	Faraday cup electrometer
FEFD	Full exhaust flow dilution
FID	Flame ionisation detection method
FILE	Forward illumination light extinction
HOME	Honge oil methyl ester
HRR	Heat release rate
HSDI	High speed direct injection diesel
ID	Ignition delay
IDI	Indirect injection
IVC	Inlet valve closing
IVO	Inlet valve opening
JOME	Jatropha oil methyl ester

LII	Laser induced incandescence
LTC	Low temperature combustion
MAF	Mass air flow
NDIR	Non dispersive infrared method
NO	Nitrogen monoxide
NO_2	Nitrogen dioxide
NO_x	Nitrogen oxides
PDR	Primary dilution ratio
PEFD	Partial exhaust flow dilution
PM	Particulate matter
PM_{10}	Particulate matters in diameter less than 10 µm
$PM_{2.5}$	Particulate matters in diameter less than 2.5 µm
ppm	Parts per million
PPO	Pure plant oil
PTD	Porous tube diluter
rDOP	Relative duration of premixed
RME	Rapeseed methyl ester
rpm	Revolutions per minute
RSO	Rapeseed oil
SCR	Selective catalytic reduction
SDR	Secondary dilution ratio
SfME	Sunflower methyl ester
SME	Soya methyl ester
SN	Smoke number
SO	Soya oil
SOC	Start of combustion
SOF	Soluble organic fraction
SOI	Start of injection
SOME	Sesame oil methyl ester
SVO	Straight vegetable oil
TDC	Top dead centre
TEM	Transmission electron microscopy
THC	Total hydrocarbons
UIS	Unit injector system
ULSD	Ultra low sulfur diesel
VOF	Volatile organic fraction

CONTENTS

TABLE OF FIGURES

TABLE OF TABLES

1 CHAPTER 1 - Introduction

1.1 Introduction

An increased interest in diesel engines, in recent years, is a result of their better thermal efficiency which can effectively yield better fuel economy. Moreover, combination of improved fuel economy and excellent performance characteristics have made diesel engines dominant in Europe. Recent improvement of the injection systems (common rail system) and application of supercharged or turbocharged engines satisfy the requirements regarding the output power. Moreover, the exhaust gaseous emissions are improved against older engine and injection systems. Unfortunately, the exhaust gaseous emissions of NO_x and soot from the compression ignition (CI) engine are still high and limited by the legislation norms. The researchers and recent published literature are focused on the reduction of these pollutants to required limits from the legislation norms. Generally, by the application of exhaust after treatment systems such as Diesel Particulate Filter (DPF) or Selective Catalytic Reduction (SCR), the Particulate Matter (PM) and NO_x can be reduced. The usage of DPF consists of the filtration of PM through the filter walls and the simultaneous periodic regeneration of the material. The Electrostatic Mobility Spectrometer (EMS) can be used for detailed analysis of soot particles size distribution in the exhaust tail pipe. Recent measurement of particle mass during legislation tests will be replaced by the measurement of soot concentration number as a small mass of PM could result in enormous concentration of small diameter particles, which has a negative effect on human health.

On the other hand, the effects of climate change forces the use of alternative, renewable fuels. In the case of diesel engines, the Straight Vegetable Oil (SVO), Pure Plant Oil (PPO) or Fatty Acid Methyl Ester (FAME) (biodiesel) can be used as a fuel. They offer a closed loop of the carbon cycle, which can reduce the greenhouse gases in the atmosphere. Moreover, they are biodegradable and environmental friendly. The usage of SVO/PPO in diesel engines requires the reduction of its viscosity to the comparable level of diesel fuel (2 - 4 cSt). A high viscosity of PPO (about 40 cSt) can be effectively reduced by heating the fuel to a temperature of around 80 degC. For this purpose, the heat exchanger or heater can be installed in the fuel lines. Another method is the transesterification process, where fatty acid methyl ester (biodiesel) is a product of the reaction of alcohol with PPO. It offers reduced viscosity and direct usage in diesel engines.

The emissions and combustion characteristics from the combustion of Rapeseed Oil (RSO) and Soya Oil (SO) are presented in this study. Moreover, the performance of RSO under different engine injection parameters and EGR rates is described. According to the usage of RSO, the high soot emissions from its combustion have been subjected to an attempt of its reduction to the diesel equivalent level of soot. Regarding the recent interest in particulate

matter measurement and reduction from diesel engines, a detailed characterisation via an EMS system has been done. Moreover, the designed primary dilution system allows more accurate measurements of soot particulate size under different engine operating conditions. The soot particles size distribution has also been measured before and after the DPF in order to study its filtration efficiency. The main objectives from this work are summarized in the following section.

1.2 Objectives

The objectives of this study are summarized below:

- Investigation of the performance of a diesel engine fueled by RSO and SO. Comparison of combustion and emission characteristics with diesel fuel.

- Investigation of the influence of varied injection pressure, timing and EGR on the combustion and emission characteristics of RSO and its blends with diesel.

- Reduction of the soot emissions from RSO to the equivalent level of diesel.

- Reduction of soot and NO_x emissions from rapeseed methyl ester (RME) and diesel fuel under turbocharged engine operation.

- Characterization via an electrostatic mobility analyser in order to obtain soot particles size distribution measurements.

- Investigation of the soot particle size distribution emitted from diesel and RME under different engine injection pressures, timings and EGR rates.

- Investigation of the Diesel Particulate Filter (DPF) efficiency by the measurement of the soot particulate size distribution before and after the filter.

2 CHAPTER 2 – Literature review

2.1 Classification of compression ignition engines

Internal combustion engines are widely used in the transportation sector around the world. The main principle is to convert the chemical energy from the fuel to effective mechanical energy. It can be done in two ways: as an internal or external combustion process. It distinguishes two types of combustion engines but this study is focused on internal combustion engines. Generally, internal combustion engines can be classified as follows, proposed by Heywood [1]:

- Application:
  - truck, locomotive, light aircraft, marine, portable power system, power generation
- Basic engine design (arrangement of cylinders):
  - in-line, V, radial, opposed, etc. (Figure 2.1.1)
- Working cycle:
  - four-stroke cycle (naturally aspirated, supercharged, turbocharged)
  - two-stroke (crankcase scavenged, supercharged, turbocharged)
- Valve or port design location:
  - overhead valves, underhead valves, rotary valves, cross-scavenged porting, loop-scavenged porting, through- or uniflow-scavenged
- Fuel:
  - gasoline, fuel oil, natural gas, liquid petroleum gas, alcohols, hydrogen, dual fuel
- Method of mixture preparation:
  - carburetion, fuel injection into the intake ports or intake manifold, fuel injection into the engine cylinder
- Method of ignition:
  - spark ignition, compression ignition
- Combustion chamber design:
  - open chamber (disc, wedge, hemisphere, bowl-in-piston)
  - divided chamber (swirl chambers, prechambers)
- Method of load control:
  - throttling of fuel and air together, control of fuel alone, combination of these
- Method of cooling:
  - water cooled, air cooled, uncooled (other than by natural convection and radiation)

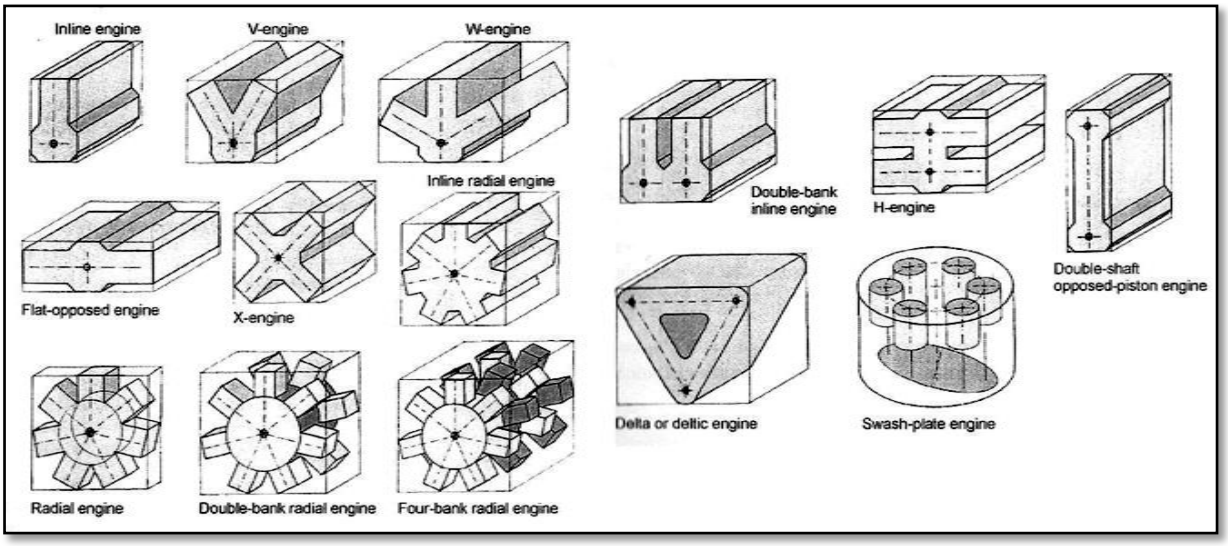

Fig. 2.1.1. Basic engine design (arrangement of cylinders) [2].

Compression ignition engines (mainly operating on diesel fuel) are preferably used in cars, trucks, locomotives, aircrafts, marines and power generators because of their higher thermal efficiency and durability compared to spark ignition (gasoline) engines. The first compression ignition engine was successfully introduced in 1892 by Rudolf Diesel (1858 – 1913) and was capable to run on coal dust and crude oil. It was a great opportunity to replace the old fashioned, poor thermal efficiency steam engines. Nowadays, more than 50% of passenger cars in Europe are driven by diesel engines. However, countries such as Luxembourg, Belgium, France and Spain noted even more than 75% [3]. Modern compression ignition engines are four-stroke, three (small passenger cars) to 12 cylinders (heavy-duty trucks), turbocharged, common rail direct injection fuel system with multiple hole piezo injectors.

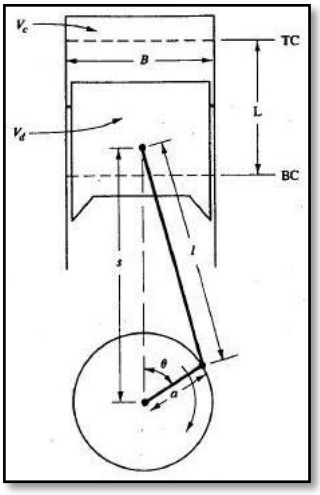

Fig. 2.1.2. Geometry of the crank-piston mechanism [1].

Internal combustion engines are based on a reciprocating-piston movement. A piston moves back and forth in a cylinder and transmits mechanical energy, from the combustion of the

fuel, by the connecting rod and crank mechanism to the drive shaft. In Figure 2.1.2, the geometry of the crank-piston mechanism is presented.

The four sequences (4 strokes) are referred to as a single engine cycle which is done during two revolutions of the crankshaft. The piston travels from top dead centre point (TDC) to bottom dead centre point (BDC) in half of revolution (1 stroke). The smallest possible volume occurs when the piston is in the TDC position and is called clearance volume V_c. The total volume V_t occurs when the piston is in the BDC position. The difference between the total volume V_t (piston in BDC position) and the clearance volume V_c is called a swept or displaced volume V_d and is used as a parameter to describe the engine capacity. The length from TDC to BDC is called an engine stroke. The compression ratio r_c is one of the most important engine parameters, which influences the overall thermal efficiency. Generally, the compression ratio can be calculated by the following Equation:

$$r_c = \frac{V_d + V_c}{V_c} \tag{2.1}$$

The compression ignition engines are usually manufactured with the compression ratio from 12 – 24 while spark ignition engines only from 8 – 12 [1,2]. In this case, a higher compression ratio results in a better thermal efficiency than spark ignition engines. Moreover, such a high compression ratio in diesel engines is used due to the cold start requirements where compressed air temperature has to be higher than self ignition temperature of injected fuel. Figure 2.1.3 shows the process of one full cycle for compression ignition engines.

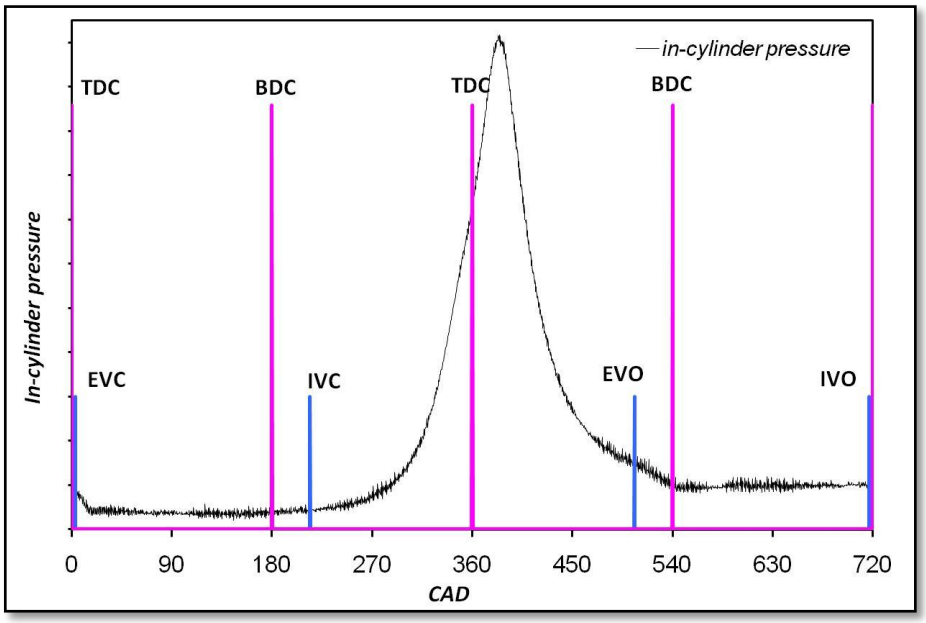

Fig. 2.1.3. Scheme of one engine cycle according to the in-cylinder pressure curve.

The full cycle of compression ignition engine consists of four sequences (strokes):

- Intake stroke (0 CAD – 180 CAD)

- the piston travels from TDC to BDC
- exhaust valve is already open
- shortly after TDC, the exhaust valve closes (EVC)
- the process of filling up with fresh air proceeds under the below atmospheric pressure

- Compression stroke (180 CAD – 360 CAD)
  - the piston travels from BDC to TDC
  - shortly after BDC, the inlet valve closes
  - exhaust valve is already closed
  - pressure inside cylinder rises
  - shortly before TDC (high pressure and temperature inside), the fuel is injected into combustion the chamber (start of injection (SOI))
  - depending on the local conditions and fuel properties the pre-mixing will ocure
  - after a few CAD, the fuel starts to burn (start of combustion (SOC))
  - after SOC, there is a rise in the in-cylinder pressure and temperature
  - depending on in-cylinder condition (local A/F ratio, mixing process, air entrainment, fuel vaporization, combustion temperature and pressure) the formation of combustion products begins
- Expansion stroke (360 CAD – 540 CAD)
  - the piston travels from TDC to BDC
  - inlet and exhaust valves are still closed
  - in-cylinder pressure raises up and reaches its peak, shortly after TDC (depends on SOI)
  - internal work done by combustion products is finally transmitted to the drive shaft after an internal and mechanical loss
  - shortly before BDC, the exhaust valve opens (EVO)
- Exhaust stroke (540 CAD – 720 CAD)
  - the piston travels from BDC to TDC
  - exhaust valve is already open
  - products of combustion are transmitted at higher pressure to the exhaust system
  - shortly before TDC, the inlet valve opens (IVO)

The overlap between IVO and EVC contributes to the better flushing of the combustion chamber by a new charge of fresh air. In some cases, negative valve overlap is used as an internal exhaust recirculation technique (EGR). The compression and expansion processes can be described as adiabatic processes by the following equations:

$$pV^{\gamma} = TV^{\gamma-1} = const \tag{2.2}$$

Where:

- p – in-cylinder pressure

- V – in-cylinder volume
- T – in cylinder temperature
- γ – adiabatic exponent

$$\gamma = \frac{C_p}{C_v} \tag{2.3}$$

Where:

- C_p – specific heat at constant pressure
- C_v – specific heat at constant volume

The difference between SOC and SOI is called an ignition delay (ID) and it is a time where the preflame reactions takes place, before the actual SOC (first appearance of flame). The main factors that influence the ID are as follows [2]:

- temperature of the charge
- density, viscosity, vaporization characteristics and ignitability of the fuel
- the pressure, time and characteristic of injection
- composition (fuel-oxygen ratio and amount of inert gases)
- turbulences inside combustion chamber

During the compression stroke, the in-cylinder temperature of compressed air has to be higher than the self ignition temperature of injected fuel to provide proper autoignition. According to ref. [2], the autoignition takes place in a range of local excess-air factor varying from 0.5 to 0.7. In addition to this, the high compression ratio allows the reach of higher in-cylinder temperatures of compressed air before injection. The overall combustion process can be shown as the heat release rate history according to CAD. Figure 2.1.4 shows a typical heat release rate diagram where the combustion phases for the compression ignition engine are illustrated [1].

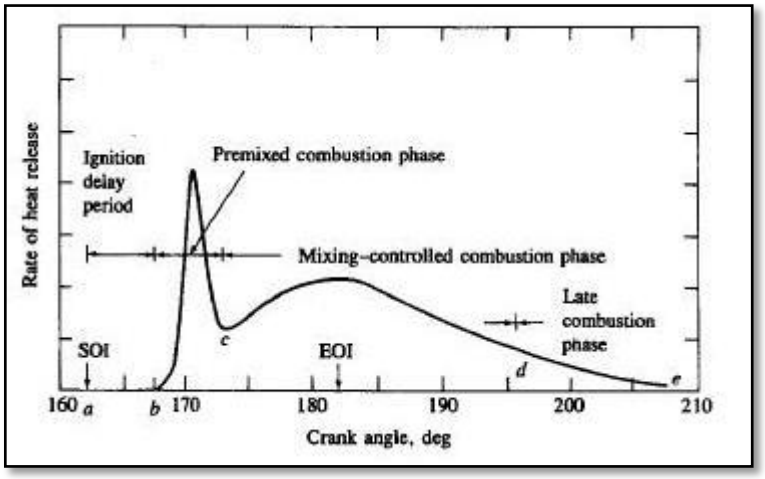

Fig. 2.1.4. Typical heat release rate history from diesel engine [1].

Typical diesel combustion consists of four combustion phases:

- Ignition delay: difference in time between SOC and SOI usually given in CAD
- Premixed combustion phase: in this phase, the hot air is mixed with fuel vapour (during the ID period) to their flammability limits, then burn rapidly resulting in a high heat release rate in a few CAD
- Mixing-controlled combustion phase: in this phase, the combustion is controlled by the ready to burn mixture formation rate. Usually, the heat rate decreases in a much longer period of time compared to the premixed phase
- Late combustion phase: in this phase, the heat may be released at a very low rate, usually because of small fractions of unburned fuel, energy release from soot or rich-fuel combustion products.

Moreover, each combustion cycle is different and strongly depends on engine operating conditions (load and speed), injection parameters (injection pressure, injection timing), engine temperature as well as ambient conditions. In this case, the combustion products are formed in different quantities as their formation strongly depends on the in-cylinder conditions such as pressure, heat rate, temperature, availability of oxygen, duration of ignition delay and injection or combustion.

2.1.1 Diesel exhaust emissions

In spite of the advantages of using compression ignition engines (high thermal efficiency and durability) there are drawbacks in the case of emissions. Compared to spark ignition engines, diesel engines produce more Nitrogen Oxides (NO_x) and Particulate Matter (PM). However, diesel engines emit relatively lower carbon monoxide (CO) and total un-burnt hydrocarbons (THC). Due to harmful effects on environment and human health of these pollutants, legislation norms have been proposed for all passenger cars in countries like Japan, the USA [4] and EU [5]. The European Union has suggested the EURO norms, which have been taken in to consideration since 1992 as a first norm EURO 1. The current EURO 5 standard started from 2009 and will be followed by EURO 6 in 2014. The previous and current EURO norms can be seen in Figure 2.1.1.1.

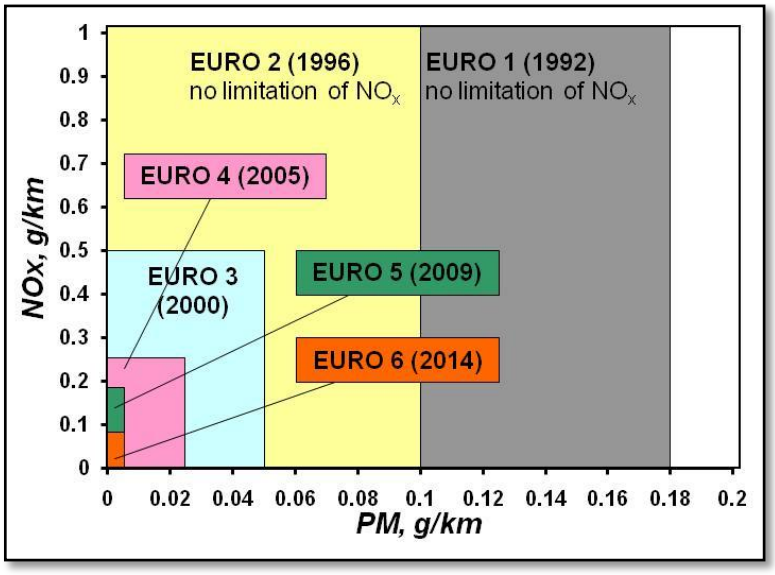

Fig. 2.1.1.1. Previous, current and future EURO norms for diesel passenger vehicles [5].

It can be seen that emission regulations become stricter from year to year. In 2014, EURO 6 predicts further reduction of NO_x emissions and the same level of PM emissions as the previous legislation. In order to meet future emission standards, new solutions for reduction of these pollutants have to be applied. One of the methods is installing different exhaust after treatment systems on the exhaust tail pipe, which significantly reduce NO_x and PM emissions.

As previously mentioned, NO_x emissions are one of the major pollutants emitted from diesel engines. Generally, NO_x consist mainly Nitrogen Monoxide (NO) and Nitrogen Dioxide (NO_2). It has been reported [6,7] that 10 to 30 percent of total NO_x is represented by NO_2 emission. The well known Zeldovich mechanism (1946) clearly describes the NO formation by the following reactions [1,2,8]:

$$O + N_2 = NO + N \tag{2.4}$$

$$N + O_2 = NO + O \tag{2.5}$$

$$N + OH = NO + H \tag{2.6}$$

The formation of the NO emission mainly occurs at high temperatures, in excess oxygen regions through reaction 2.4, leaving one free atom of nitrogen. It can be later combined with oxygen (reaction 2.5) or OH (reaction 2.6), already present in the combustion process, to form nitrogen monoxides. The already formed NO during combustion can be further converted to NO_2 by reaction 2.7. Afterwards, it can be also converted back to the form of NO by reaction 2.8 [1].

$$NO + HO_2 = NO_2 + OH \quad (2.7)$$

$$NO_2 + O = NO + O_2 \quad (2.8)$$

From the environmental and health point of view, NO_x are harmful. They can destroy the ozone in the atmosphere. Moreover, favourable conditions (presence of ammonia or moisture) lead to the formation of nitric acid vapour which is affecting human health mainly by respiratory and heart diseases [4].

Together with NO_x, particulate matter emissions are major pollutants from combustion in compression ignition engines. According to ref. [2], three definitions of particles emissions can be found regarding traffic regulations, the workplace and environment. Traffic regulations define particles as everything that can be filtered and weighted at temperature of 325 K. In the workspace, the overall mass of elementary carbon less than 5 μm is counted. In the environmental law, it is an overall mass detected with high volume samplers of less than 10 μm (PM_{10}) and less than 2.5 μm ($PM_{2.5}$) independent of their chemical composition. In the compression ignition engines, the soot is formed by cracking the complex hydrocarbons from the fuel composition and then producing solid carbon particles. The model of soot formation in diesel spray has been proposed by Dec [9] and it is illustrated in Figure 2.1.1.2.

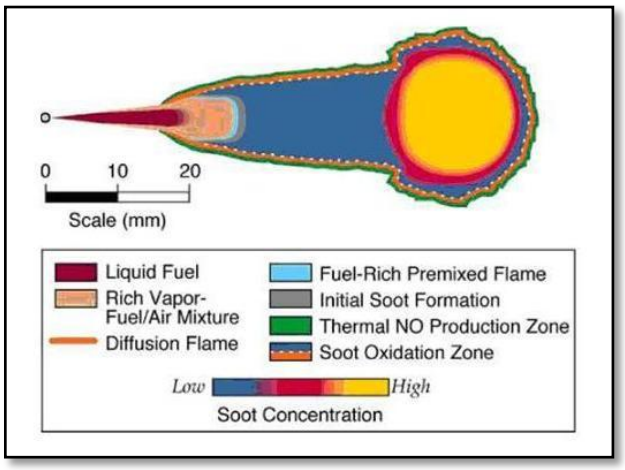

Fig. 2.1.1,2. Conceptual model of the soot formation process in diesel spray, proposed by Dec [9].

Generally, the single carbon particles are formed during the breakdown of the complex structure of fuel compounds. Additionally, it can be seen that the soot emission is formed in rich fuel/air mixture, preferably in the flame zone, during the diffusion combustion. On the periphery of the spray, soot particles start to oxidize. A higher rate of oxidation would produce less particles in the tail pipe. During the combustion and oxidizing processes, single solid carbon particles start to accumulate and agglomerate with each other to form aggregates. Generally, the particles from diesel combustion can be divided as carbonaceous

(soot particles), sulphate particles and soluble materials (mainly hydrocarbons) known as Soluble Organic Fraction or Volatile Organic Fraction (SOF/VOF). In the later stage of combustion, sulfur usually reacts with water vapour to form sulphuric acid and together with SOF/VOF may start to condense on the solid carbon particles at lower temperatures. In Figure 2.1.1.3 a detailed diagram of particulate matter composition is presented accordingly to the work done by Kittelson [10].

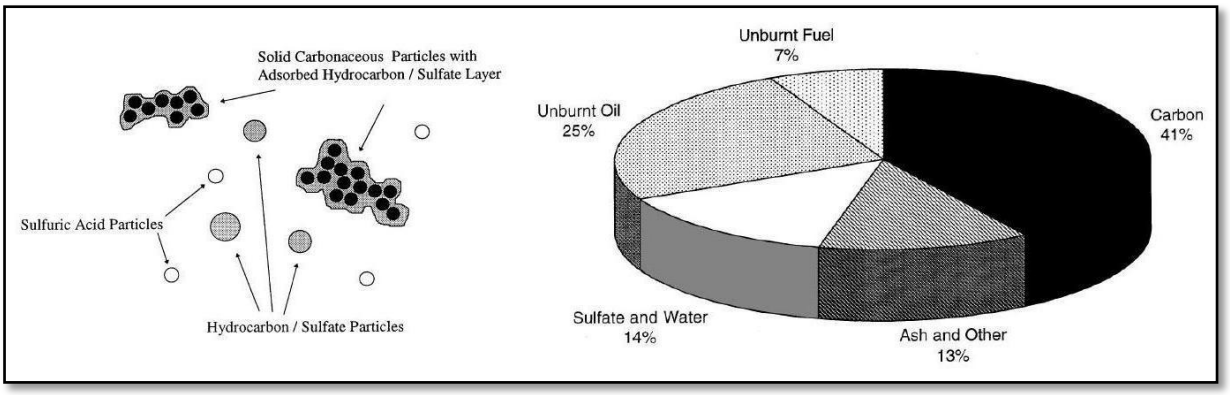

Fig. 2.1.1.3. Diagram soot particles composition from compression ignition engine [10].

The measurement of particulate matters can be done in the exhaust tail pipe or as early detection during the combustion usually in experimental optical engines. The measurement in the exhaust system is based on the filtration method (smoke number (SN)), soot mass measurements by the photo acoustic method, sampling for transmission electron microscopy (TEM) analysis and electrostatic classification (described in Section 2.3). Generally, the smoke number is measured as a light transmission rate through the filter paper on which sampled particles are collected. Usually, SN is determined via the Bosch scale, where the white filter corresponds to the value of 0 and totally black sample filter corresponds to the value of 10. The TEM technique has been used by many researchers to obtain detailed information about primary particle size, aggregates size and morphology of soot particles [11-14]. Usually, soot particles are collected on a small, around 3 mm in diameter, grid directly from the exhaust tail pipe or after dilution with air. The grids are further analyzed using transmission electron microscope. Usually, pictures of soot are determined in two resolutions. High magnification (above 40,000x) is used for diameter measurements and low (10,000x to 20,000x) for aggregate size, particle volume fraction and morphology measurements. Measurements in optical engines, with optical access to the combustion chamber allow the use of techniques such as Laser Induced Incandescence (LII) [15] or Forward Illumination Light Extinction (FILE) [16].

Particulate matters affect human health and the environment. The adverse effect of soot particles ($PM_{2.5}$ and PM_{10}) has been reported [17-19] while the influence of ultrafine particles (below 100nm) has not been fully understood but still generates interest. Generally, inhaling

particles affects the human body and may cause diseases such as asthma, lung cancer, cardiovascular issues, and in extreme cases premature death. From the environmental point of view, soot particles in the atmosphere may scatter and absorb solar and infrared radiation which can influence climate change. In the USA, the EPA sets limits for $PM_{2.5}$ and PM_{10} in the atmosphere. Similarly, in the EU, the European Commission has set limits for PM_{10} in the atmosphere which have become stricter from January 2010 (from 40 μg/m³ to 20 μg/m³ - yearly average) [5].

In the case of combustion products, NO_x and soot emissions become a major problem in conventional engines as they can be described by a well known NO_x – soot trade off. A reduction in NO_x emissions always results in higher soot emissions and vice versa. Generally less NO_x in the exhaust tile pipe can be achieved by decreasing the in-cylinder temperature either by using exhaust gas recirculation (EGR) or by retarding the injection timing. However, unfortunately, a reduced temperature environment is favourable for high soot emission. An exception from this conventional diesel trade off is Low Temperature Combustion (LTC) where simultaneous reduction of NO_x and soot can be achieved usually at very late injection parameters and high EGR rates [20-22].

The emissions of unburned hydrocarbons and carbon monoxide from compression ignition engines are usually much lower than those from spark ignition. They are both products of incomplete combustion, usually from engine operation at very rich A/F mixtures. Generally, the CO emission strongly depends on the stoichiometry of combustion. Usually, spark ignition engines operate at stoichiometry or a richer mixture, where the CO emission is very high. Under these conditions, a three-way catalyst has the highest possible efficiency (around 95%) of reduction of NO and oxidizing of CO and THC. However, in the case of conventional compression ignition engines, which are usually operated at lean mixtures, CO and THC are low enough to be considered minor pollutants [1]. Nevertheless, recent combustion techniques (LTC) provide a considerably high amount of these pollutants and they have to be taken in to consideration. Hydrocarbon emissions appear as total hydrocarbons which are usually measured as a concentration of carbon atoms in the exhaust gases. They are different in composition for various engines and operating conditions, especially for diesel combustion where the formation process is more complex. The major causes of THC emissions are summarized as follows [1]:

- Overmixing – local zones of mixtures leaner than combustion limit
- Undermixing – overfueling, rich mixtures from trapped fuel in the injector sac volume
- Wall quenching and misfires – low temperature of cylinder walls, very high cyclic variability in the combustion process

Carbon monoxide is colourless, odourless and tasteless gas which is lighter than air. It is highly toxic to humans and animals in higher quantities. As a result of incomplete combustion, humans can breathe CO without knowing of its presence in the ambient air causing breathing difficulties at a first stage, unconsciousness, deep poisoning or death in extreme situations. This is one of the most dangerous gases which humans can have contact with even in a household. Hydrocarbon vapour in high concentrations, especially benzene, toluene or xylene (BTX) is highly poisoneuous causing cancer, neurological diseases and death in extreme situations.

As a product of combustion, carbon dioxide emission is a dominant composition of exhaust gases from both spark ignition and compression ignition engines. As long as the fuel for these engines is a form of hydrocarbons, the main combustion process and production of CO_2 will be preceded by following the basic reaction 2.9:

$$C + O_2 = CO_2 + Energy \tag{2.9}$$

The carbon atoms are derived by the hydrocarbons from fuel composition. The combustion of fuel delivers a high amount of CO_2 into the atmosphere and eventually has a huge effect on the climate change. Recent research shows that the CO_2 concentration in the atmosphere is increasing from year to year [23]. The well known Keeling's curve [23-25] (Figure 2.1.1.4a) shows continuous results of measurement of CO_2 in the atmosphere. In addition to this, CO_2 concentration in the atmosphere is strongly linked to the fuel consumption (Figure 2.1.1.4b) and human activity.

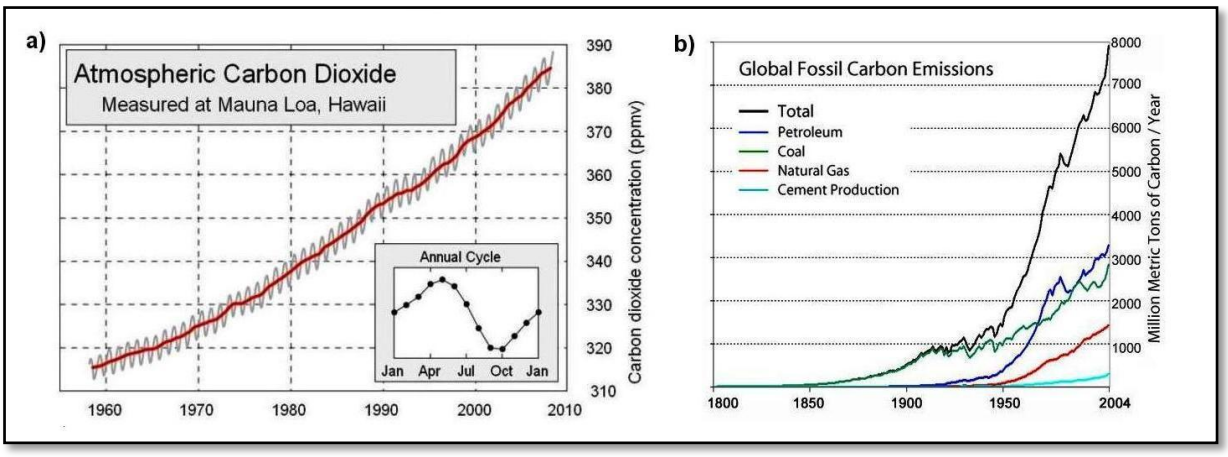

Fig. 2.1.1.4 Carbon dioxide effects: a) Keeling's curve [24], b) fossil fuels consumption [26].

Generally a high concentration of CO_2 in the atmosphere contributes to the effects of greenhouse gases which influence the global climate change. Based on this data, the fossil fuel consumption, caused by human activity, should be restricted or new renewable fuels should be proposed as they could reduce CO_2 in the air and avoid global climate change.

2.1.2 After treatment systems

In the case of compression ignition engines, after treatment systems reduce emissions such as: carbon monoxide, unburned hydrocarbons, nitrogen oxides and also soot particulates.

Oxidising catalysts are commonly used in both spark and compression ignition engines. Basically, they oxidise unburned hydrocarbons and carbon monoxide in the presence of catalytic materials which can be precious metals such as platinium (Pt), palladium (Pd) or Rhodium (Rh). The monolith substrate consists of small canals which in total give a cross-section area equal to the original tail pipe. The monolith can be made as an inorganic material (Al_2O_3, SiO_2, TiO_2), ceramic or metal with dispersed Pt, Pd or Rh on its surface. It allows a large reaction surface within a small space. The reactions of the oxidation of THC and CO are as follows [2]:

$$C_yH_n + \left(1 + \frac{n}{4}\right) O_2 \rightarrow yCO_2 + \frac{n}{2} H_2O \tag{2.10}$$

$$CO + \frac{1}{2} O_2 \rightarrow CO_2 \tag{2.11}$$

$$CO + H_2O \rightarrow CO_2 + H_2 \tag{2.12}$$

The efficiency of oxidizing catalysts is about 80 – 90 % for lean mixture combustion (mostly compression ignition combustion). When the engine is operated at gradually richer mixtures, the efficiency of catalyst decreases. However, such a high efficiency is possible only at high temperatures of catalytic converter, around 300 degC (activation temperature).

In the case of spark ignition engines, the NO_x emissions are easily reduced in three-way catalysts. It consists of the previously described oxidizing catalyst together with precious metal coating for NO_x reduction. When a very efficient oxidation of CO and THC proceeds at lean mixtures, with availability of oxygen in the exhaust composition, efficient reduction reactions of NO_x take place at rich mixture conditions. Thus, only a small window of engine fuel/air ratio regulation can be used in gasoline engines due to the highest possible three-way catalyst efficiency. Generally, NO/NO_2 reduction reactions are as follows [2]:

$$NO\ (or\ NO_2) + CO \rightarrow \frac{1}{2} N_2 + CO_2 \tag{2.13}$$

$$NO\ (or\ NO_2) + H_2 \rightarrow \frac{1}{2} N_2 + H_2O \tag{2.14}$$

$$\left(2 + \frac{n}{2}\right) NO\ (or\ NO_2) + C_yH_n \rightarrow \left(1 + \frac{n}{4}\right) N_2 + yCO_2 + \frac{n}{2} H_2O \tag{2.15}$$

As compression ignition engines mostly operate at lean mixtures new techniques are required to reduce NO_x emissions. In this case, the below methods can be used in diesel engines [2,8]:

- Active selective catalytic reduction (SCR) (active DENOx)

  The method is based on the addition of ammonia (NH_3) or urea ($CO(NH_2)_2$) into the exhaust tail pipe. Conversion efficiencies reach even 80% and proceed at the following reactions:

$$4NO + 4NH_3 + O_2 \rightarrow 4N_2 + 6H_2O \quad (2.16)$$

$$2NO_2 + 4NH_3 + O_2 \rightarrow 3N_2 + 6H_2O \quad (2.17)$$

$$NO + NO_2 + 2NH_3 \rightarrow 2N_2 + 3H_2O \quad (2.18)$$

$$4NO + 2(NH_2)_2CO + O_2 \rightarrow 4N_2 + 4H_2O + 2CO_2 \quad (2.19)$$

- Passive SCR (passive DENOx)

  This passive method (nothing added into the exhaust tail pipe) is based on utilizing hydrocarbons emissions to reduce NO_x emissions in the presence of catalysts. A major problem is a very narrow temperature window (160 – 220 degC) for platinum catalysts where these reactions occur [27,28]. However, with copper base zeolite it could be possible to reduce NO_x even up to 40% [29].

- NO_x traps

  This technique can be described by four fundamental reactions. At the presence of a catalytic converter, NO is transformed into NO_2 (reaction 2.20).

$$NO + \frac{1}{2}O_2 \rightarrow NO_2 \quad (2.20)$$

  Then, NO_2 reacts with metal oxides dispersed on the catalytic converter and forms storage material nitrate (reaction 2.21).

$$NO_2 + MeO \rightarrow Me - NO_3 \quad (2.21)$$

  As stored NO_2 increases the efficiency of nitrate formation is reduced, so in this case the storage materials have to be periodically regenerated. For this reason the engine must be briefly switched to rich mixture operation. Afterwards, at higher temperature, the storage material releases trapped NO_2 by using the following reaction 2.22:

$$Me - NO_3 \rightarrow NO + \frac{1}{2}O_2 \quad (2.22)$$

The NO then reacts with THC and CO presented in the exhaust gases during rich engine operation (reaction 2.23).

$$NO + HC(or\ CO) \rightarrow \frac{1}{2}N_2 + H_2O(or\ CO_2) \quad (2.23)$$

This method requires short periods of operation on a rich mixture which are easier to obtain by spark ignition engines rather than compression ignition engines where operation on rich mixtures provides maximum engine power.

To reduce soot particles emitted from compression ignition engines, diesel particulates filter (DPF) or soot traps have been proposed. Generally, soot particles are collected (filtered) on the monolith material. Different types of materials, such as ceramic monoliths, alumina-coated wire mesh, ceramic foam, ceramic fiber mat, woven silica-fiber rope wound on a porous tube are used to manufacture these filters [1]. Figure 2.1.2.1 presents DPF filters and the soot filtration process in ceramic monolith (commonly used).

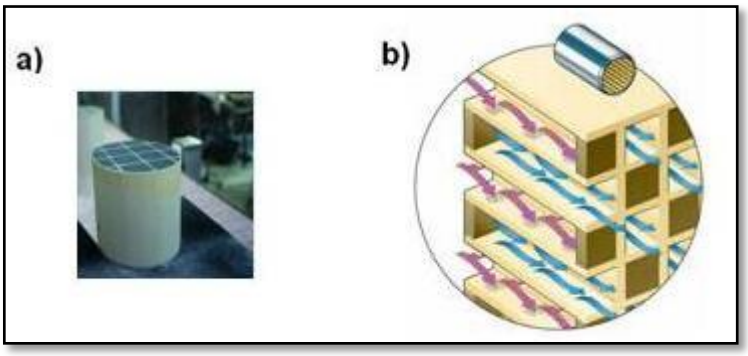

Fig. 2.1.2.1. DPF filter: a) size and design, b) ceramic monolith filtration method [30].

Raw exhaust gases, with soot particles, enter cells which are closed at the end and pass through walls. A major problem in this method is a back pressure build up when soot is gradually collected on the filtrating material. In this case, DPFs need to be periodically regenerated. The best way is to burn deposited soot by increasing exhaust gases temperature to that range where diesel soot particles start to ignite (about 500 to 600 degC). It can be done in two ways: positive regeneration (external heaters or fuel injection before DPF) or catalytic regeneration (addition of catalytic material which can decrease soot ignition temperature by up to 200 degC) [1,2]. The well known continuously regenerating trap (CRT) method effectively filtrates soot particles [31]. It consists of two sections, where the first is a platinum catalyst which generates more NO_2 from the exhaust's NO and the second is a soot trap. A high amount of NO_2 would oxidize soot continuously. Usually, this method is used in heavy duty diesel engines and is required to use a low sulfur fuel.

2.1.3 Diesel fuel injection

The occurrence of an autoignition in compression ignition engines depends on the time of injection of diesel fuel. The start of combustion usually occurs a few CADs after the SOI. Generally, the diesel fuel injection can be done in two different methods, indirect injection (IDI) and direct injection (DI). The in-direct injection method supplies the fuel injection into the pre-chamber which can be pre-combustion chamber or swirl chamber. Both of the applied techniques provide better mixing and faster combustion processes which allow increasing engine speed. Figure 2.1.3.1 shows different types of pre-combustion and swirl chambers used in compression ignition engines.

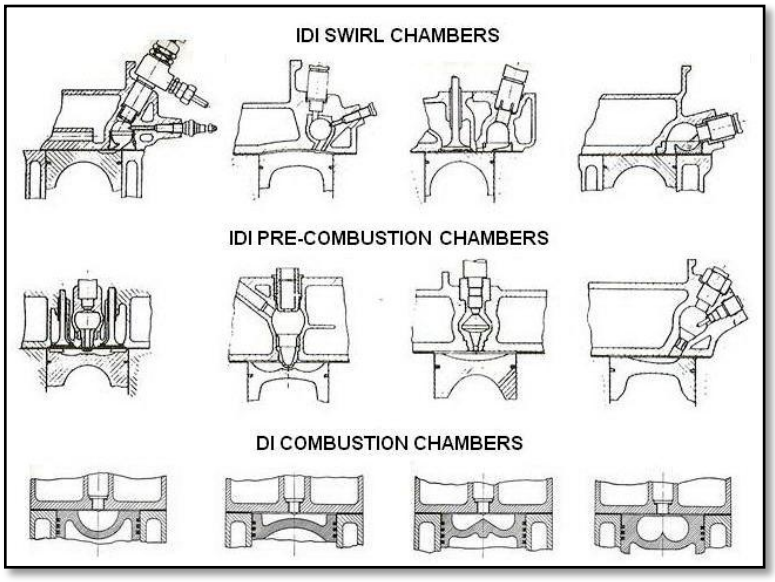

Fig. 2.1.3.1. Diagram of different types of combustion chambers in IDI and DI engines [8].

On the other hand, the direct injection system supplies the injection of the fuel directly into the engine cylinder. The combustion chamber is usually placed in the piston, which can have different shapes and designs. The most common combustion chamber shapes are presented in Figure 2.1.3.1.

Recent compression ignition engines are designed with a direct injection system. It allows using a more compact cylinder head design with four valves per cylinder. The swirl in the direct injection engines can be done by the shape of the inlet ports and also by the shape of the inlet valves. Beside DI or IDI systems, different injection pumps and injectors are applied. The old pump-line-nozzle system consists of a high pressure pump and lines which connect injectors. The Injector is designed to open its nozzle when high pressure pump provides the required pressure. The fuel quantity is regulated by the pump's plunger rotation as its position determines the volume of fuel to be pressurised and injected. This first system worked in indirect injection engines and could reach relatively low injection pressures. The application of DI engine requires much higher injection pressures as fuel needs to be mixed

and vaporized much quicker than in the case of IDI. For this purpose, the pump-nozzle system (PNU), also termed as unit injector system (UIS) or electronic unit injectors (EUI) was designed. Each of the cylinders has its own compact high pressure pump and injector in one casing. The fuel quantity is also regulated by the rotation of the pump's piston, but in this case it can be controlled electronically. The injection pressure of this system is much higher than in the pump-line-nozzle system. However, because of the complex design, poor reliability and expensive costs of production this system is in rare use. The common rail is the newest, fully electronically controlled system which can provide the highest injection pressure. It consists of one main high pressure injection pump which provides fuel into the common rail. All injectors (depends on cylinder quantity) are connected to the rail and filled by fuel at high pressure. Electronically controlled injectors lift their needles according to the signal from the Engine Control Unit (ECU), which is generally based on real time readings from sensors of engine phase, speed, vehicle speed, accelerator position, air flow etc. Figure 2.1.3.2a shows a basic diagram of modern common rail injection system.

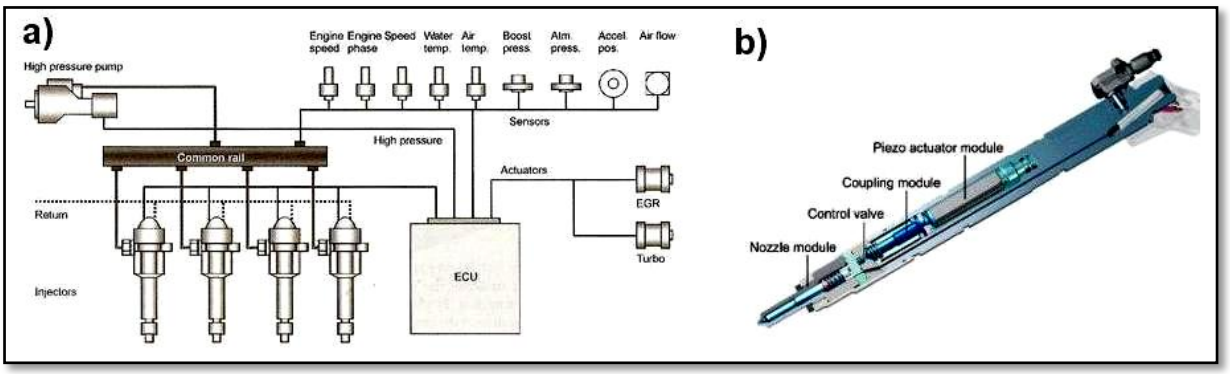

Fig. 2.1.3.2. Diagram of: a) modern common rail injection system, b) modern piezo injector [2].

In addition to this, injectors are electronically controlled by the electric coil and it is possible to approach different injection strategies such as dual injection or split injection. By applying an injector with a piezo actuator (piezo injector, Figure 2.1.3.2b) whose electrical response characteristics are much faster than those of the solenoid injectors, it is possible to distribute the same fuel quantity into five or six injections per cycle. This gives a much more uniform and controlled combustion with possible low NO_x and soot emissions. Additionally, the purpose of the ECU is to control all engine operating parameters such as injection timing, injection pressure, fuel quantity, injection strategy, etc., based on the current engine load, speed, temperatures or air flow. Generally, the engine control and output characteristic are determined by creating special maps programmed in the ECU memory. For instance, it can be the fuel or injection timing map where they depend on the engine operating conditions such as load and speed.

2.1.4 Advanced diesel combustion

Recent interest in new, more efficient combustion processes in diesel engines results in two main strategies: Low Temperature Combustion (LTC) and Homogeneous Charge Compression Ignition (HCCI). Figure 2.1.4.1 shows the equivalence ratio – temperature diagram with shaded areas of LTC and HCCI combustion modes.

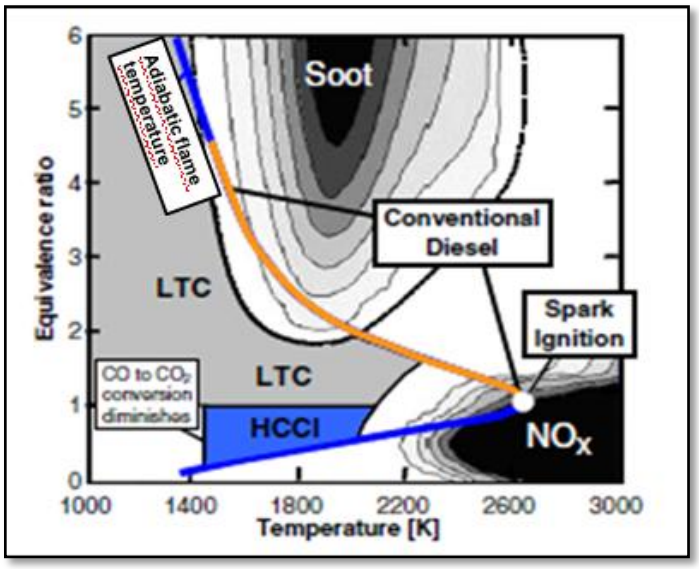

Fig. 2.1.4.1. The equivalence ratio – temperature diagram [32]

A reduction of NO_x and soot emissions for the requirements of further emission legislation norms can be done by the usage of these combustion modes in diesel engines. Generally, in HCCI mode, the air and fuel are premixed, then compressed and ignited. Usually the mixture is very diluted by the air or EGR, maintaining the equivalence ratio below 0.45. Such a high dilution causes low combustion temperature, where the NO_x formation is reduced. Moreover, a well mixed charge prevents the formation of the soot. This combustion strategy is still in the interest of researchers as a low load engine operation results in low combustion efficiency while the high load is limited by the excess of the in-cylinder pressure rise and eventually engine knock. The HCCI mode requires the modification of the diesel's fuel injection system to accommodate well mixing homogenous charge in the cylinder. The same principle of premixing the charge is utilised in LTC mode. This mode can be used in conventional direct injection diesel engines. Generally, it requires prolonged Ignition Delay (ID) for sufficient mixing of air and fuel. The longer ID delay can be achieved by very early injection in the compression stroke, providing the required time for well mixing. Moreover, longer ID occurs in very late injection, where mixing process takes place in the expansion stroke. Other techniques for achieving prolonged ID include the usage of cooled EGR, reduced compression ratio or late inlet valve closing [32]. The HCCI and LTC combustion modes significantly reduce NO_x and soot emissions but more research must be done in order to achieve a stable engine operation at high loads.

2.2 Vegetable oil and biodiesel as an alternative fuels in diesel engines

Increased world interest over the reduction of greenhouse gas emissions has forced energy providers to find alternative and renewable fuels as a replacement for fossil fuel. As renewable fuels, ethanol (from fermentation and distillation process) and biogas (mainly from communal and organic waste in process of fermentation) are proposed for spark ignition engines. In the case of compression ignition engines, vegetable oils and biodiesel have been proposed as a replacement for diesel fuel as their fuel properties are similar.

Generally, vegetable oils are termed as Straight Vegetable Oil (SVO) or Pure Plant Oil (PPO) in the combustion engine field. Biodiesel and PPO can be produced from different types of plants. Therefore, the usage of these fuels is often determined by the regions of cultivation and by the type of crop. Many publications confirmed that biodiesel and PPOs have been successfully used in diesel engines based on the production of rapeseeds, soybeans, jatrophas, olives, palms, coconuts, karanjas, sunflowers, corn, peanuts, waste cooking oils and even from oranges [33-35]. Vegetable oils are produced in different regions of the world. For instance, soya bean oil is mainly used in the USA, while rapeseed and sunflower oil in Europe, palm oil in South- East Asia, coconut oil in the Philippines, Jatropha and Karanja oil in India and also a production of biodiesel using recycled frying oil in Japan and other parts of the world [34,36].

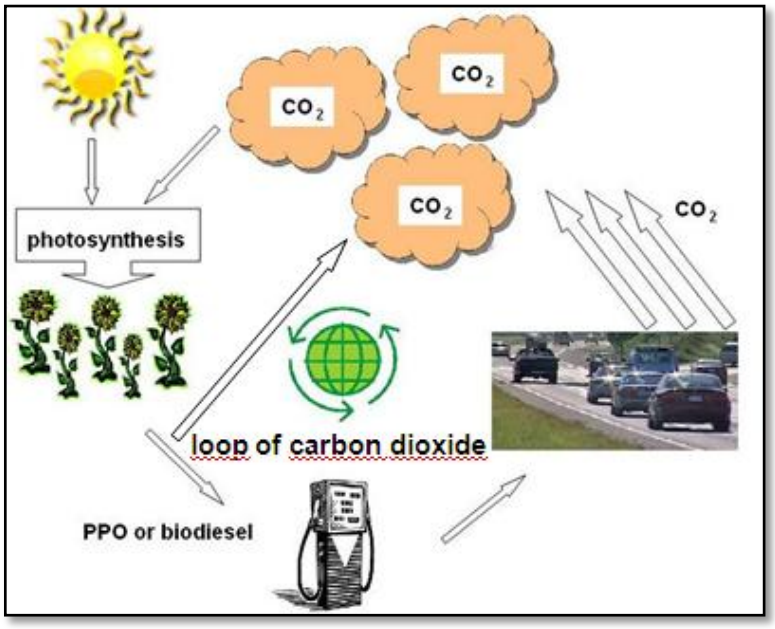

Fig. 2.2.1. Diagram of closed loop of carbon dioxide emission from the combustion of PPO or biodiesel.

In addition to this, 90% of CO_2 emission in the transportation sector is from the automobile [37]. Thus, the assumption from Kyoto protocol about the decrease in CO_2 emission could be done by partial or full replacement of diesel fuel by PPO or biodiesel. This is because their carbon dioxide emissions have a shorter carbon life cycle than those from the combustion of

petroleum diesel fuel [38-40]. Moreover, there are advantages over the CO_2 emissions because of the closed loop of carbon cycle through the use of SVO/PPO, as these emissions are absorbed by plants during the process of photosynthesis. An example of carbon closed cycle is shown in Figure 2.2.1. In the reality the closed carbon cycle is disturbed by the leakages of CO_2 to the atmosphere mainly during production and transportation of biodiesel or PPO.

2.2.1 Characterisation of pure plant oil/straight vegetable oil

The PPOs are different in chemical composition from diesel fuel and they mainly contain triglycerides in 90-98% and a minor percentage (1-5%) of free fatty acids, which provide different fuel properties. Triglycerides in SVOs have a very complex structure of three molecules of long chain fatty acids connected to a molecule of glycerol.

The fatty acid composition of the triglyceride molecules varies according to the types and the origins of the vegetable oil. Generally, they are saturated, monounsaturated and polyunsaturated (usually di or triunsaturated). The degree of unsaturation corresponds to the amount of carbon double bonds in the fatty acid structure. Figure 2.2.1.1 presents an example structure of saturated (palmitic acid), monounsaturated (oleic acid), diunsaturated (linoleic acid) and triunsaturated (linolenic acid) free fatty acids.

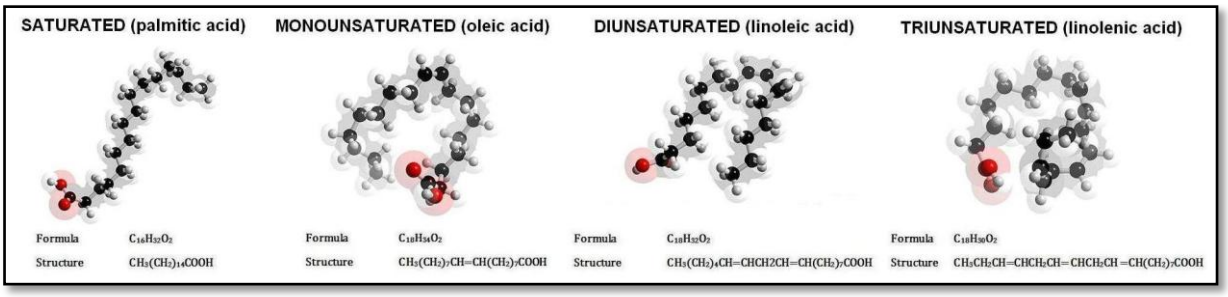

Fig. 2.2.1.1. Structure of different unsaturated fatty acids.

Different types of vegetable oil have a varied composition of fatty acids. Potentially, it can have an influence on the combustion process as it varies in carbon chain length and carbon double bonds (degree of unsaturation). Figure 2.2.1.2 shows the fatty acid composition of vegetable oils and fats from two different sources [33,41]. It can be seen that PPO from various origins have different composition which can influence the fuel chemical properties such as viscosity, density, cetane number and heating value. Table 2.2.1.1 presents a basic fuel properties comparison between the mainly used vegetable oils (different sources), PPO (described by DIN V 51605 standard) and diesel fuel (EN590 norm) [34,42-50]. The current DIN V 51605 is the newest standard describing the properties of PPO as a fuel in diesel engines. It could be seen that even for the same kind of oil, properties are varied from

source to source. On the other hand, it is obvious that there are differences between soya, rapeseed and jatropha oils because of various fatty acids compositions.

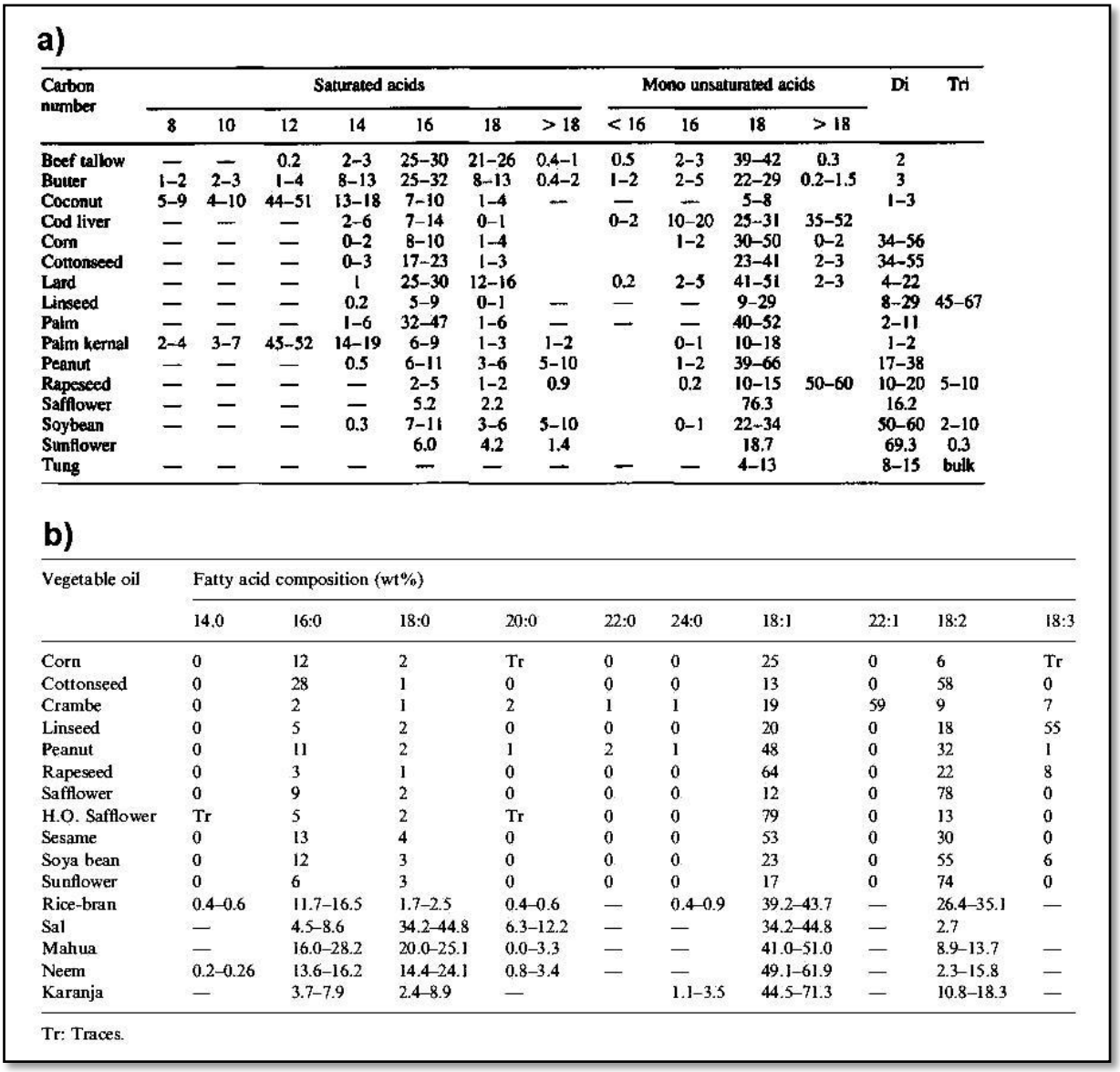

a)

Carbon number	Saturated acids							Mono unsaturated acids				Di	Tri
	8	10	12	14	16	18	> 18	< 16	16	18	> 18		
Beef tallow	—	—	0.2	2–3	25–30	21–26	0.4–1	0.5	2–3	39–42	0.3	2	
Butter	1–2	2–3	1–4	8–13	25–32	8–13	0.4–2	1–2	2–5	22–29	0.2–1.5	3	
Coconut	5–9	4–10	44–51	13–18	7–10	1–4	—	—	—	5–8		1–3	
Cod liver	—	—	—	2–6	7–14	0–1		0–2	10–20	25–31	35–52		
Corn	—	—	—	0–2	8–10	1–4			1–2	30–50	0–2	34–56	
Cottonseed	—	—	—	0–3	17–23	1–3				23–41	2–3	34–55	
Lard	—	—	—	1	25–30	12–16		0.2	2–5	41–51	2–3	4–22	
Linseed	—	—	—	0.2	5–9	0–1	—	—	—	9–29		8–29	45–67
Palm	—	—	—	1–6	32–47	1–6	—	—	—	40–52		2–11	
Palm kernal	2–4	3–7	45–52	14–19	6–9	1–3	1–2		0–1	10–18		1–2	
Peanut	—	—	—	0.5	6–11	3–6	5–10		1–2	39–66		17–38	
Rapeseed	—	—	—	—	2–5	1–2	0.9		0.2	10–15	50–60	10–20	5–10
Safflower	—	—	—	—	5.2	2.2				76.3		16.2	
Soybean	—	—	—	0.3	7–11	3–6	5–10		0–1	22–34		50–60	2–10
Sunflower					6.0	4.2	1.4			18.7		69.3	0.3
Tung	—	—	—	—	—	—	—	—	—	4–13		8–15	bulk

b)

Vegetable oil	Fatty acid composition (wt%)									
	14.0	16:0	18:0	20:0	22:0	24:0	18:1	22:1	18:2	18:3
Corn	0	12	2	Tr	0	0	25	0	6	Tr
Cottonseed	0	28	1	0	0	0	13	0	58	0
Crambe	0	2	1	2	1	1	19	59	9	7
Linseed	0	5	2	0	0	0	20	0	18	55
Peanut	0	11	2	1	2	1	48	0	32	1
Rapeseed	0	3	1	0	0	0	64	0	22	8
Safflower	0	9	2	0	0	0	12	0	78	0
H.O. Safflower	Tr	5	2	Tr	0	0	79	0	13	0
Sesame	0	13	4	0	0	0	53	0	30	0
Soya bean	0	12	3	0	0	0	23	0	55	6
Sunflower	0	6	3	0	0	0	17	0	74	0
Rice-bran	0.4–0.6	11.7–16.5	1.7–2.5	0.4–0.6	—	0.4–0.9	39.2–43.7	—	26.4–35.1	—
Sal	—	4.5–8.6	34.2–44.8	6.3–12.2	—	—	34.2–44.8	—	2.7	
Mahua	—	16.0–28.2	20.0–25.1	0.0–3.3	—	—	41.0–51.0	—	8.9–13.7	—
Neem	0.2–0.26	13.6–16.2	14.4–24.1	0.8–3.4	—	—	49.1–61.9	—	2.3–15.8	—
Karanja	—	3.7–7.9	2.4–8.9	—		1.1–3.5	44.5–71.3	—	10.8–18.3	—

Tr: Traces.

Fig. 2.2.1.2. The composition of vegetable oils and fats: a) adopted from [33], b) adopted from [41].

When compared to diesel fuel, PPOs have higher density and kinematic viscosity. The viscosity varies from source to source. However, the highest value can be noted for soya oil (around 65 cSt which is around 20 times higher than diesel). It can be seen that the calorific value for diesel is not required by EN590 norm (usually around 42 MJ/kg). Nevertheless, PPOs show lower value than diesel. In addition to this, the cetane number for SVOs is lower.

The main problem with fuelling diesel engine by SVOs/PPOs is their high kinematic viscosity. It can affect the fuel line, especially the pump, injectors and fuel spray characteristics. The viscosity of PPOs can be reduced by three techniques:

- heating the oil before it is introduced into the fuel injection system and the combustion chamber
- blending the oil with diesel fuel
- the transesterification process (discussed in the next section)

The influence of heating PPOs on their viscosity can be seen in ref. [42,51-53]. It has been shown that heating the oil to a temperature of about 70 - 80°C causes a reduction in the viscosity by a factor of 4. There are some benefits of heating over the blending method adopted to lower the viscosity of SVO/PPO. Blending limits the usage of SVO/PPO, as only small fractions provide lower viscosity. From a financial point of view, the heating method provides a viable option in making the best use of SVO/PPO in diesel engines. This can be facilitated by installing a heat exchanger in the fuel system of the engine. These types of heat exchangers are based on extracting the heat from the engine exhaust and the engine cooling system.

Moreover, the lower calorific value of PPOs leads to less energy output from an engine (when a constant fuel mass is considered) or more fuel consumption (when a constant engine load is considered). The cetane number provides information about ignitability, thus the lower value for PPOs affects their ignition leading to longer ignition delay and poorer engine performance. On the other hand, a high sulfur and phosphorous content in SVOs results in high soot emissions.

Generally, the usage of PPOs/SVOs in diesel engines causes short and long term problems [54,55]:

- Short-term
  - cold weather starting
  - plugging and gumming of filters, lines and injectors
  - engine knocking

- Long-term
  - coking of injectors and carbon deposits on the piston and the head of engine
  - excessive engine wear
  - failure of engine lubricating oil due to polymerization

Table 2.2.1.1. Properties of jatropha, rapeseed, soya oil based on literature and diesel, PPO fuel standards.

	Jatropha oil	Rapeseed oil	Soya oil	DIN V 51605 (PPO)	Diesel fuel EN590
Density, kg/m3	917±1, 917.7 (15°C), 918, 940 (15°C)	911.5, 778 (100°C), 912, 911.5, 900-930 (15°C)	913.8, 914, 913.8, 925 (15°C)	900 - 930 (15°C)	820 - 845 (15°C)
Kinematic viscosity, cSt	35.98±1.3 (40°C), 24.5 (15°C), 49.9, 36.9 (37.8°C), 49.9 (38°C)	37 (38°C), 46.68 (40°C), 37.3, 37 (40°C), 38 (40°C), 37 (38°C), 39.5 (40°C)	32.6 (38°C), 32.6, 32.6 (40°C), 33 (40°C), 32.6 (38°C), 65 (40°C)	max. 36 (40°C)	2.00 - 4.50
Cloud point, °C	9±1	-3.9, -3.9	-3.9,-3.9	-	-
Pour point, °C	4±1, 4, -3	-31.7, -12, -31.7	-12.2, -12.2	-	-
Flash point, °C	229±4, 225, 240, 99	246, 273, 258, 246, 280	254, 255, 254, 230	min. 220	above 55
Carbon residue, %	0.8±1, 1, 0.44	0.3, 0.4	0.27	max. 0.4	max. 0.30
Ash content, %	0.03±0, 0.8	0.054, 0.01	<0.01	max. 0.01	max. 0.01
Calorific value, MJ/kg	39.071, 38.65, 39.774, 42.084	39.7, 40.2, 39.52, 39.7, 35, 37.6	39.6, 39.44, 39.6, 37, 39.6	min. 36	-
Sulfur, %	0	0.01, 0.0022, 0.002	0.01	max. 10	0.001
Water content, %	1.4	0.075	-	max. 0.75	max. 0.2
Acid value mgKOH/g	28	2, 1.14	0.2	max. 2.0	-
Cetane number	45, 40-45	37.6, 37.6, 37.6	37.9, 37.9, 38, 37.9	min. 39	min. 51
Iodine number, g/100g		91-131, 100-120, 94-120	117-143	95 - 125	-
Specific gravity	0.918	0.914	0.92	-	-
Phosphorous content, mg/kg	-	-	-	max. 12	-

In the case of applying SVOs in passenger cars, usually the fuel line is modified and consists of an auxiliary fuel tank, solenoid valves and a central control unit. In addition to this, because of cold start problems, the car has to start with diesel fuel and then it can be switched to SVO and changed back to diesel just before the end of the journey.

2.2.2 The transesterification process

Transesterification is a well defined chemical process where mono-alkyl esters are produced by the reaction of triglyceride with an alcohol [33,34]. The glycerol is a common by-product that is formed during the transesterification process. Mono-alkyl esters are normally referred to as biodiesel. Figure 2.2.2.1 shows the scheme of the transesterification reaction.

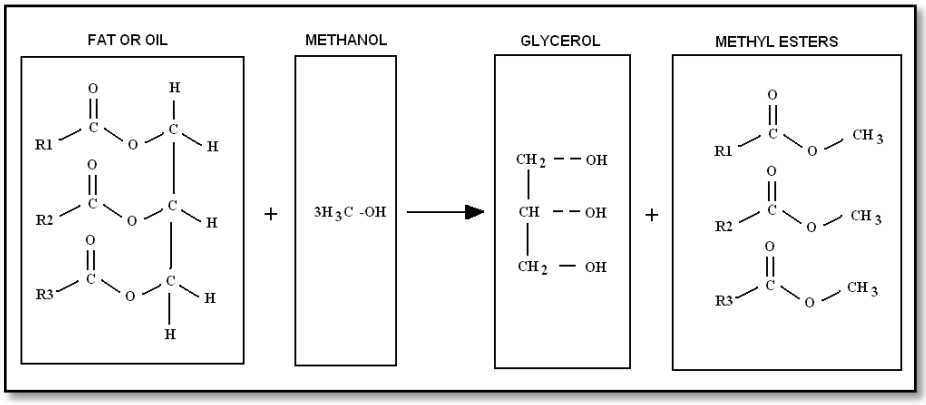

Fig. 2.2.2.1. The diagram of the transesterification process.

In the case of vegetable oil's transesterification process, the glycerol is removed from the triglyceride molecule and long-chain alkyl (methyl, propyl or ethyl) esters are formed (depending on the alcohol used in the process). However, methyl alcohol is common to all types of PPOs. Moreover, the fatty acid composition for biodiesel remains the same as for the vegetable oil used in the process. For quantifying this process, the mass based balance is presented in the following formula [33]:

$$\frac{1000kg}{(Fat)} + \frac{107.5\ kg}{(Methanol)} \rightarrow \frac{1004.5kg}{(Methyl\ ester)} + \frac{103kg}{(Glycerol)} \tag{2.24}$$

The by-product glycerol is usually used in the production of soap.

2.2.3 Biodiesel characterisation

Biodiesel can be made from different types of vegetable oils as well as from waste cooking oils. The name of the specific type of biodiesel usually consists of a name of XME, where the first letter X replaces the first letter of PPO, i.e. RME – rapeseed methyl ester. The blending rate of biodiesel is usually described as BY, where Y is a percentage of biodiesel in the blend, i.e. B50 – 50% of biodiesel in the blend. When the origin of biodiesel does not play any significant role, it generally becomes fatty acid methyl esters (FAME).

After the process of transesterification, biodiesel offers properties closer to diesel. For instance, most importantly, the kinematic viscosity is reduced to almost the same level as diesel. The cetane number and the calorific value are improved. The EN 14214 standard describing properties of FAME as a fuel in diesel engines, is shown in Table 2.2.3.1.

Table 2.2.3.1. The EN 14214 standard describing fuel properties of FAME.

Property	Units	lower limit	upper limit
FAME content	% (m/m)	96,5	-
Density at 15°C	kg/m³	860	900
Viscosity at 40°C	mm²/s	3,5	5,0
Flash point	°C	> 101	-
Sulfur content	mg/kg	-	10
Carbon residue remnant (at 10% distillation remnant)	% (m/m)	-	0,3
Cetane number	-	51,0	-
Sulfated ash content	% (m/m)	-	0,02
Water content	mg/kg	-	500
Total contamination	mg/kg	-	24
Copper band corrosion (3 hours at 50 °C)	rating	Class 1	Class 1
Oxidation stability, 110°C	hours	6	-
Acid value	mg KOH/g	-	0,5
Iodine value	-	-	120
Linolenic Acid Methylester	% (m/m)	-	12
Polyunsaturated (>= 4 Double bonds) Methylester	% (m/m)	-	1
Methanol content	% (m/m)	-	0,2
Monoglyceride content	% (m/m)	-	0,8
Diglyceride content	% (m/m)	-	0,2
Triglyceride content	% (m/m)	-	0,2
Free Glycerine	% (m/m)	-	0,02
Total Glycerine	% (m/m)	-	0,25
Group I metals (Na+K)	mg/kg	-	5
Group II metals (Ca+Mg)	mg/kg	-	5
Phosphorus content	mg/kg	-	4

Apart from having almost the same fuel properties as diesel fuel, biodiesel has disadvantages of its use in diesel engine. Generally, FAMEs have a more intensive negative effect on filters clogging and on fuel lines made from rubber derived material. However, because of its lower kinematic viscosity, the cold weather engine start effects are negligible. The usage of biodiesel is simplified as it does not need any engine modification such as fuel preheating (fuel delivery system). On the other hand, the transesterification is a more complex and expensive method for the use of PPOs/SVOs in a diesel engine.

2.2.4 Emission characteristics for PPO and FAME fuels

In this section emission characteristics from the usage of PPO or FAME are discussed from already published literature.

Recently, Rakopoulos et al. [43] have compared the emission performance of different PPOs and biodiesels in concentrations of 10 and 20% with diesel fuel under low and high load engine operating conditions. The engine was single cylinder, naturally aspirated with direct injection system. Engine operating conditions were: 2000 rpm, injection timing of 29 deg

bTDC at two loads, where high load corresponds to 75% and low load corresponds to 38% of maximum power. The fuels were tested in constant BMEP mode allowing 30 minutes of stabilization time between changing the fuels. It has been found that soot and CO emissions were higher for PPOs but lower for biodiesels, compared to those from diesel fuel. In addition to this, NO_x emissions were found to be lower for PPO and biodiesel blends. The HC emissions from PPOs were also found to be higher than those from diesel. However, variations in the HC emissions for methyl esters were very sensitive to the feedstock and blending rate.

Agarwal et al. [42] have studied emissions performance using jatropha oil in a direct injection diesel engine. The engine used in this experiment was naturally aspirated and with single cylinder. The engine was run at constant BMEP of 6.21 bar at 1500 rpm. In their investigation, the injection pressures were optimized for different fuels from 180 to 240 bar. They found, the smoke and the gaseous emissions, such as CO and HC, emitted from the combustion of Jatropha oils were higher at all loads when compared to diesel. In their investigation, the injection pressures were optimized for different fuels from 180 to 240 bar.

Using coconut oil blends with diesel, Machacon et al. [56] found that the NO_x emissions were lower when compared to diesel fuel for all blends under all loads. It was also noticeable that the reduction of smoke emission for all the blends of coconut oil under all load conditions was achieved, comparing to diesel fuel. The experiments were done in a single cylinder, direct injection fuel system. The engine speed was always constant of 2800 rpm and whole range of engine loads was tested. The injection timing was always kept at 17 deg bTDC.

Scholl et al. [57] have tested soya methyl esters (SME) in a DI, naturally apirated, 4 cylider diesel engine for two different injector nozzle diameters (0.279 mm and 0.229 mm). The engine was equipped with rotary distribution pump and it was operated always at constant speed of 1800 rpm. In the case of soot emissions, they have found lower values for SME for all engine loads and for both injectors. The NO_x have been found lower for SME only when a larger diameter of injector nozzle was applied. Generally, the THC emissions were lower for SME but further significant reduction was possible when the injector with larger nozzle was used. In addition to this, a reduction of CO emission was possible only for a smaller injector nozzle, while for a larger nozzle it remained at the same level as for diesel fuel.

Alin et al. [58] published results from the tests using different fuels: diesel oil, sunflower oil, sunflower methyl ester (SfME), cottonseed oil, cottonseed methyl ester (CME), soyabean oil, soyabean methyl ester (SME), corn oil, opium poppy oil and rapeseed oil. They used single cylinder, direct injection diesel engine with injection timing of 27 deg bTDC. The vegetable oils were preheated to temperature of 90 degC and after changing the fuel the engine was run for around 20 minutes for proper installation flushing. The gaseous emissions were

recorded always at the maximum engine torque at engine speed in range from 900 to 1800 rpm. In their work, the CO and soot emissions have been found higher than those of diesel fuel. However, there were fluctuations between biofuels i.e. the highest smoke number value belongs to corn oil while the highest CO emission to rapeseed oil. On the other hand, the NO_2 emission was found to be lower for all used fuels, comparing to diesel's NO_2 emission, where the highest reduction applies to corn oil. Generally, the CO_2 emission was lower than that of diesel but in the case of sunflower oil, SfME and soybean oil it has been found equal to the diesel's CO_2 emissions.

The usage of different methyl esters has been studied by Banapurmath et al. [59] where optimized injection timing and injection pressure were applied. The optimization process was based on possibly the highest brake thermal efficiency. They found that, for diesel, honge oil methyl ester (HOME), jatropha oil methyl ester (JOME) and sesame oil methyl ester (SOME), the optimized injection timing was at 23, 19, 27 and 27 CAD bTDC, respectively. In addition to this, the injection pressure was found to be 220 bar for JOME and SOME and 205 bar for HOME. Under these operating conditions, the smoke opacity was the highest for JOME, then for HOME, SOME and the lowest for diesel fuel at all tested engine's loads. The same trend could be noticed in the case of THC and CO emissions. Furthermore, the NO emission was found to be in the fluctuation limit of diesel at lower loads but significantly lower for methyl esters at high load. They have also found that the ignition delay and the duration of combustion were longer in the case of biodiesels.

The analysis of the influence of the EGR on the rapeseed oil methyl ester (RME) and its blends with ultra low sulfur diesel (ULSD) fuel was done by Tsolakis et al. [60]. In the case of the EGR influence, the soot, CO and THC increased, while NO_x decreased with a higher EGR percentage for all available fuels and blends. However, when the concentration of RME in the blend increased, the soot, CO and THC were reduced, already being lower than those of diesel. The opposite effect could be seen for NO_x emissions, where a higher concentration of RME increased their emissions. When compared to diesel fuel, the NO_x emissions for RME were always higher.

The time-resolved emissions measurement for two passenger cars was done by Vojtisek – Lom [61]. Transient emissions monitoring proceeds at a total of 20.9 km route for both cars. In his experiment, various origin mixtures of waste, filtered and de-watered vegetable oils were tested. The route has been divided into six sections: start, suburban segment, acceleration to freeway, freeway cruise, central business distinct and city-urban segment. Generally, the percentage change in respect to diesel fuel was: -8%, 28%, 21%, 4% and 29%, in the case of NO_x, THC, CO, CO_2 and PM, respectively. The same emission trends for the second car have been achieved but at different percentages (-20%, 34%, 60%, 5% and 14% for NO_x, THC, CO, CO_2 and PM, respectively).

A detailed study of using the jatropha oil has been reported by Reksowardojo et al. [62]. Their measurements were done for blends of 10 and 100% of jatropha oil as well as the same blends but for degummed jatropha oil. They have found that the effect of adding 10% of jatropha oil did not have any significant influence on the emission characteristics. However, for pure jatropha oil, the effects on THC and CO emissions are evident and they are higher than those of diesel fuel. On the other hand, NO_x and soot emissions were lower for 100% of jatropha oil. A degumming process of the oil provided better results in the case of CO and THC emissions, while the NO_x emission, after degumming, remained almost the same.

In the case of vegetable oils, it has been reported that for peanut, sunflower, cottonseed and soybean oil, during the injection process, there is a breakdown of the high molecular weight, unsaturated fatty acids, predominately linoleic (C18:2) and linolenic (C18:3) to lower molecular weight fatty acids [63]. In this case, the autoignition process of low molecular weight fatty acids (or hydrocarbons) could be faster.

Luft et al. [51] have tested injection parameters using rapeseed oil in two different injection systems: the inline pump system and the common rail system. They have found that the usage of rapeseed oil causes longer spray cones which leads to unfavourable cylinder wall wetting effect. However, when used the common rail system, this effect seemed to be less harmful.

2.3 Electrostatic classification of soot particles

Recent interest in particulate matter emissions from diesel engines has forced the design of a device which is capable of accurate measurement. For this purpose, the device based on electrostatic soot particles classification has been developed. This system is capable to detect mobility particle diameters within the range of 1000 nm to 10 nm or even 5 nm. The output of the system is a soot particle size distribution, where the given size (diameter) of particle is described by its concentration number. Generally, soot particles from diesel engines have been observed as bimodal in distribution [64,65]. The nucleation mode describes particles at a diameter below 50 nm with its peak at about 10 nm. In this mode, the nucleation process takes place, where new soot particles are formed on a hydrocarbon molecule base after the process of combustion. Usually, the nuclei mode contains 1-20% of the particles mass but around 90% of the particle number [66]. On the other hand, the accumulation mode ranges in size from around 50 nm to 500 nm. In this mode, particles from the combustion or from the nucleation process grow up through the condensation of hydrocarbons or agglomeration with other particles. The model of soot particle size distributions and their modes, proposed by Kittelson et al., is shown in Figure 2.3.1 [66].

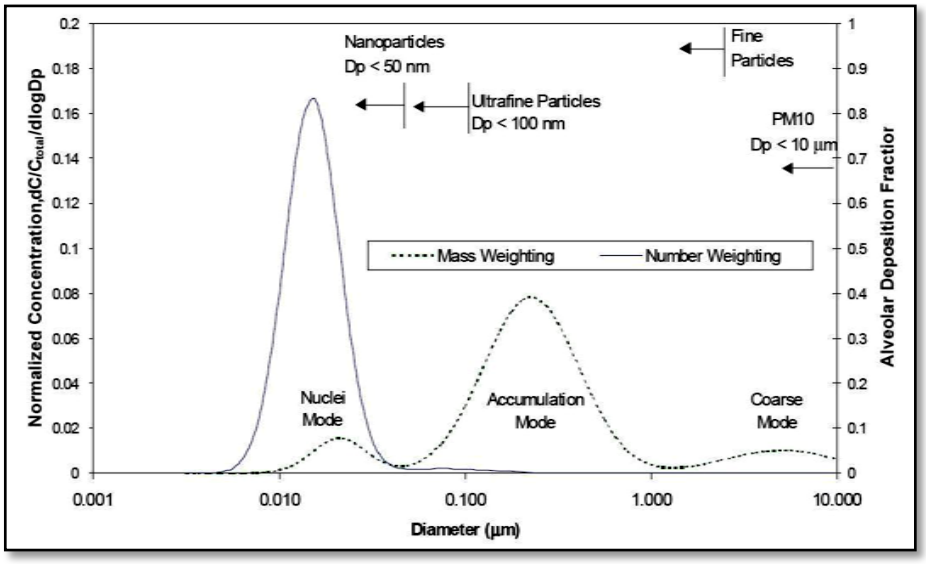

Fig. 2.3.1. The model of soot particles size distribution [66].

The soot particles from diesel engines are simultaneously sampled and diluted. The dilution process of the soot particles is used to prevent further strong coagulation and condensation and to simulate the mixing process with ambient air. The dilution ratio is one of the important factors which influences the particle size distribution. Moreover, factors such as dilution air temperature, primary dilution ratio, residence time and relative humidity cause significant artefacts to the measurement of soot particles. In the already published literature, the effect of low dilution ratios (20-30) resulted in a high concentration of particles in the nucleation mode [66-68]. The way in which the aerosol is diluted is also very important. The same dilution ratio in two different systems can result in varied particle size distribution as aerodynamics of the system has a strong influence.

2.3.1 Principle of Differential Mobility Analyser (DMA)

A general description of a differential mobility analyser can be found in ref. [69]. The DMA consists of two metal coaxial cylinders. The inner cylinder plays the role of the inner electrode and the outer cylinder the role of the outer electrode. The space between them is used for classifying the soot particles. A schematical diagram of the DMA principle is shown in Figure 2.3.1.1.

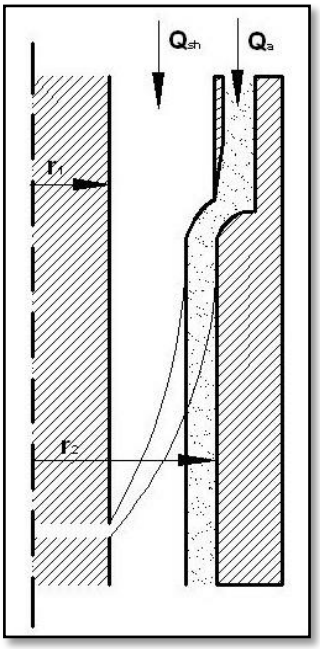

Fig. 2.3.1.1. The diagram of schematic DMA principle method [69].

Diluted particles (aerosol) are allowed to pass through the neutralizer to get a uniform and known charge distribution. The charged aerosol is introduced to the DMA, where sheath air flow is used to separate the aerosol flow from the inner electrode. For the central electrode of the DMA, different ranges of voltages are applied. The given electric field for a given voltage causes the movement of particles towards the inner electrode. At the end of the central electrode, only a certain size (certain electric mobility) particles can be collected through the small size exit. Moreover, for a given electric field, the particles with higher mobility will stick to the central electrode and particles with lower mobility will not move from the aerosol flow. Because of this effect, only particles corresponding to a given electric field and mobility will be classified. The radial electric field (E_r) inside the DMA can be described as follows, according to the applied voltage:

$$E_r = \frac{V}{r ln\left(\frac{r_1}{r_2}\right)} \tag{2.25}$$

Where:

- r_1 and r_2 – radius of central electrode and outer cylinder
- V – voltage

Moreover, radial motion of a particle with mobility Z_p due to this field is:

$$\frac{dr}{dt} = Z_p E_r(r) \tag{2.26}$$

In addition to this, particles have to be accurately specified by charge distribution, which is a major assumption in this method. The charge distribution is usually achieved by passing aerosol through a bipolar charger, where charging efficiency also has to be considered. Another assumption consists of uniform, laminar and well balanced sheath air and aerosol flows inside the DMA. Moreover DMA's electrodes have to be precisely fabricated with very good quality non-corrosive material in exactly the same radial dimensions along the whole length of the DMA.

2.3.2 Dilution systems for particles size distribution

Detailed reviews on different dilution techniques used for exhaust soot measurements are described by Burtscher [70] and Lyyranen et al. [71]. The most commonly used system for simulating atmospheric dilutions is the Constant Volume Sampler (CVS). This method can be used as a Full Exhaust Flow Dilution Tunnel (FEFD-tunnel), or Partial Exhaust Flow Dilution Tunnel (PEFD tunnel). The principle of this method is to route all exhaust gases into the large tunnel where the dilution air is added (Figure 2.3.2.1). Besides the good simulation of dilution with environmental air, it is also possible to determine the total mass concentration (for example for European Drive Cycles). For the test with heavy duty engines, this system usually becomes very large and expensive as the exhaust flow is very high. Commonly, CVS operates on a moderate dilution ratio of below 1:10 and usually without heating the dilution air.

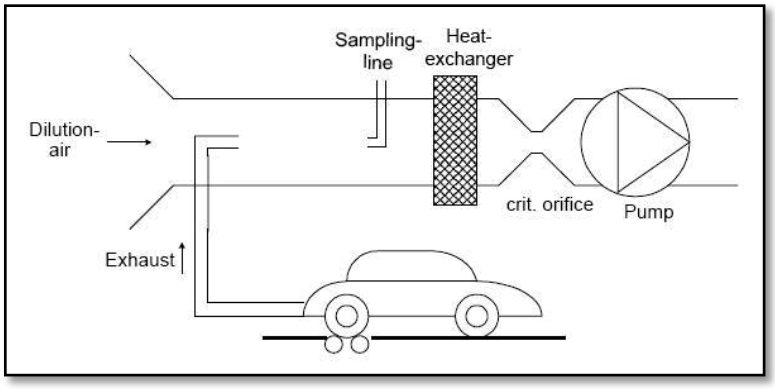

Fig. 2.3.2.1. The diagram with schematic full flow dilution tunnel (FFDT) [70].

The ejector diluter is based on the Venturi nozzle principle (Figure 2.3.2.2). The dilution air and diluter can be heated which gives more control of the dilution process. A single diluter is capable of obtaining 1:10 dilution ratios. However, the compact design allows the setting of a couple of units in the cascade mode, where the total dilution ratio is a multiplication of dilution ratios from each unit.

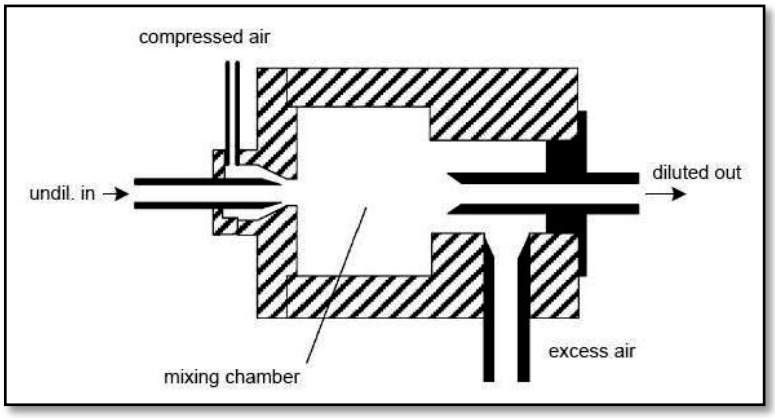

Fig. 2.3.2.2. The diagram with schematic ejector diluter [70].

The rotating disk dilutor allows the achievement of high dilution ratios from 1:30 to 1:1000 (Figure 2.3.2.3). Dilution air can be heated separately, which gives the opportunity to study the nucleation effects. This is the ideal dilutor for particles below 1000 nm while the measurement of larger particles causes errors.

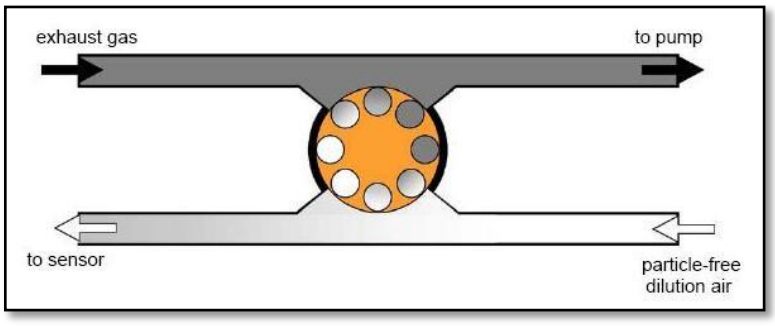

Fig. 2.3.2.3. The diagram with schematic rotating disk diluter [70].

Another type of dilution system that has been recently used is a porous tube dilution system (PTD) (Figure 2.3.2.4). The dilution gases flow through a porous tube and mix with the exhaust. PTD is designed for handling the aerosols at low dilution ratios. In the experiment done by Lyyranen et al. [71], they confirmed that PTD is the best method of dilution for obtaining unchanged, “real” number size distributions.

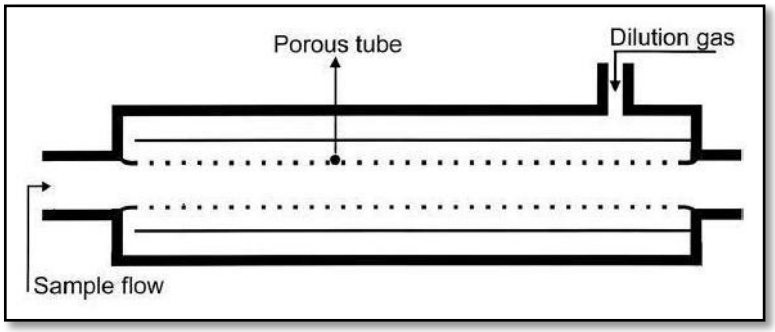

Fig. 2.3.2.4. The diagram with schematic porous tube diluter (PTD) [70].

The hot and cold dilution processes have been presented by Kasper [72] on a phase diagram graph (Figure. 2.3.2.5).

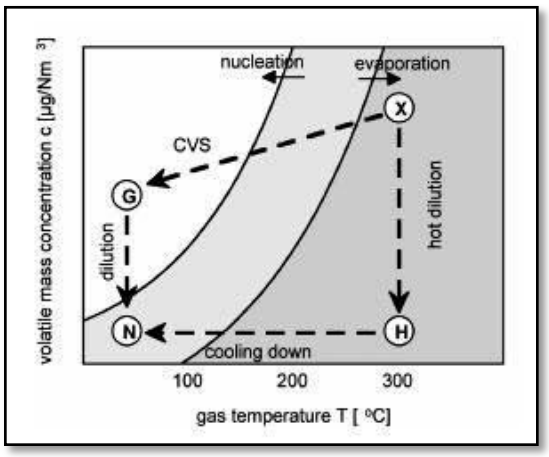

Fig. 2.3.2.5. The diagram with hot and cold dilution processes [72].

He illustrates the principle of hot and cold dilution processes with separating nuclei particles. The main goal is to decrease volatile mass fraction while simultaneously cooling down the aerosol. Therefore, a hot dilution process takes place in two dilution stages. Firstly, the hot dilution stage provides reduced temperature but still a high concentration of volatile fraction. The second dilution, at ambient temperature, is used only to remove the volatile fraction. On the other hand, the hot dilution process requires only one dilution stage. Thus, hot dilution air reduces the volatile concentration to the required level and only then the cooling process of diluted particles takes place.

3 CHAPTER 3 – Experimental setup

In this chapter the experimental setup of the Ford automotive diesel engine will be presented. Additionally, the Electrostatic Mobility Spectrometer (EMS), fuel properties and data analysis are described.

3.1 Ford automotive diesel engine

The schematic experimental engine setup is presented in Figure 3.1.1. All engine equipment is described in the next sections.

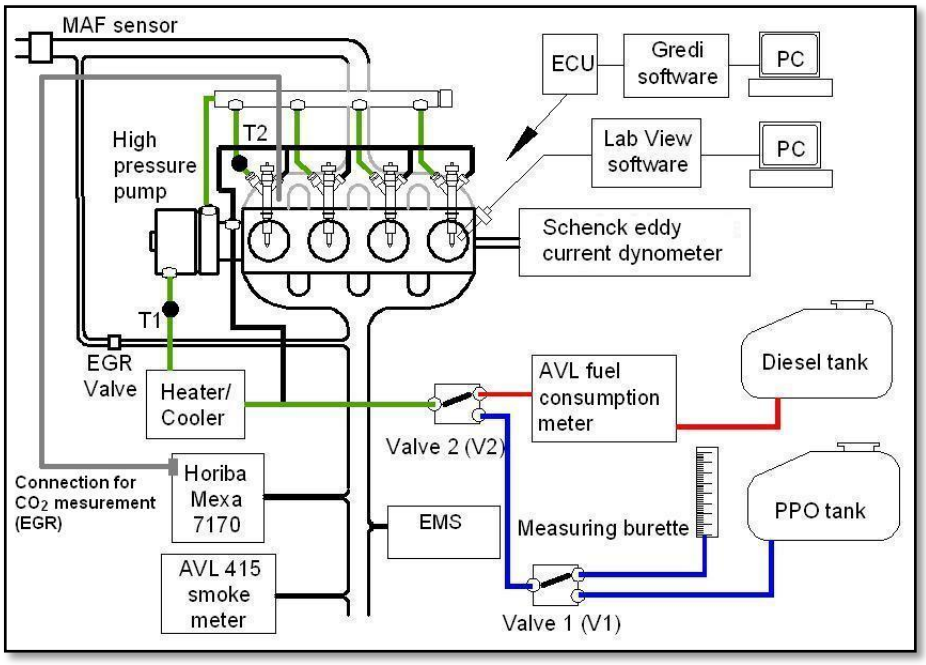

Fig. 3.1.1. The schematic engine experimental setup.

3.1.1 Engine and Dynamometer

All experiments in this study were done using Ford's Duratorq (Puma) diesel engine. The engine was supplied by Ford as a prototype production unit which recently powered Ford Transits and Mondeo cars. This is a four cylinder, High Speed Direct Injection (HSDI) diesel engine. The engine head was designed with a double camshaft and four valves per cylinder. The engine specification can be seen in Table 3.1.1.1. The engine is also equipped with a turbocharger. However, the engine was operated as naturally aspirated avoiding the effects of a different level of air in the combustion chamber under varied engine operating conditions. Only the results described in Section 4.4, were done under turbocharged engine operation. The fuel injection system is production Delphi's direct injection common rail

system. The injectors are designed having six holes with a nominal diameter of 0.154 mm and a spray hole angle of 154 deg. The maximum fuel injection pressure can reach 1600 bar at high engine speed. The details of combustion chamber can be seen in Figure 3.1.1.1.

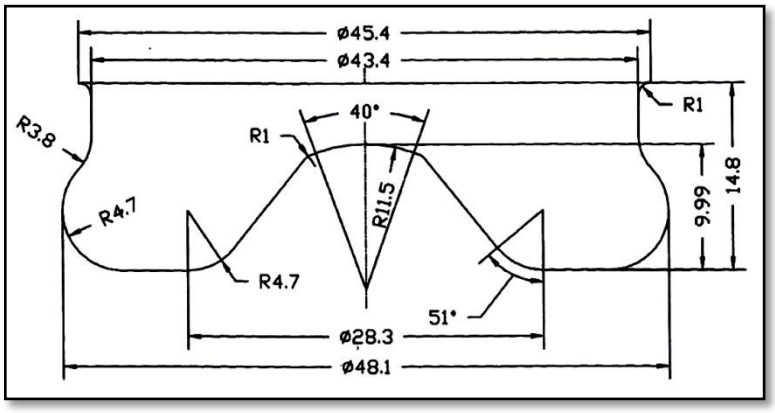

Fig. 3.1.1.1. The piston bowl (combustion chamber) details.

The engine cooling system consists of two circuits. The first is used for engine cooling water and the second for cooling the engine oil. The engine coolant and the water that cools the engine oils pass through a Bowman heat exchanger where the cold water is supplied from the reservoir tank. For all experiments, the engine was warmed up to a temperature of 50 degC under idle conditions. The engine coolant temperature was kept constant during all experiments at around 70 degC. The cooling system is equipped with safety cut-off which stops the engine if the coolant water temperature rises up to 100 degC. The engine oil level was kept constant and its temperature was always below 95 degC during the test.

Table 3.1.1.1. The engine specification.

HSDI diesel engine	
Displacement, cm^3	1998.23
Cylinder numbers	4
Compression ratio	18.2 : 1
Bore, mm	86
Stroke, mm	86
Cod-Rod length, mm	155

In order to control the engine load and speed, the engine is coupled to a W130 Schenck eddy - current dynamometer. A schematic diagram of this eddy - current dynamometer is shown

in Figure 3.1.1.2. The direct current in the exciter coil produces a magnetic field. The magnetic field pulsates with the frequency of the passing rotor teeth and generates eddy currents which produce magnetic field lines opposing the exciter field, causing a braking action on the rotor. The braking force is transported through the dynamometer housing and the arm to the electronic force meter. Knowing the current force and length of the arm, the signal is calculated, achieving the engine torque.

The engine can be controlled in two dynamometer modes: constant torque or constant speed. In the first mode, the engine torque is fixed by the dynamometer and further increases in the fuel quantity rises the engine speed. Similarly, the second mode allows fixing the engine speed and a regulation in the fuel quantity sets the required engine torque.

The dynamometer controller is connected to the safety circuit which detects potential engine failures, causing emergency shutdown of the engine.

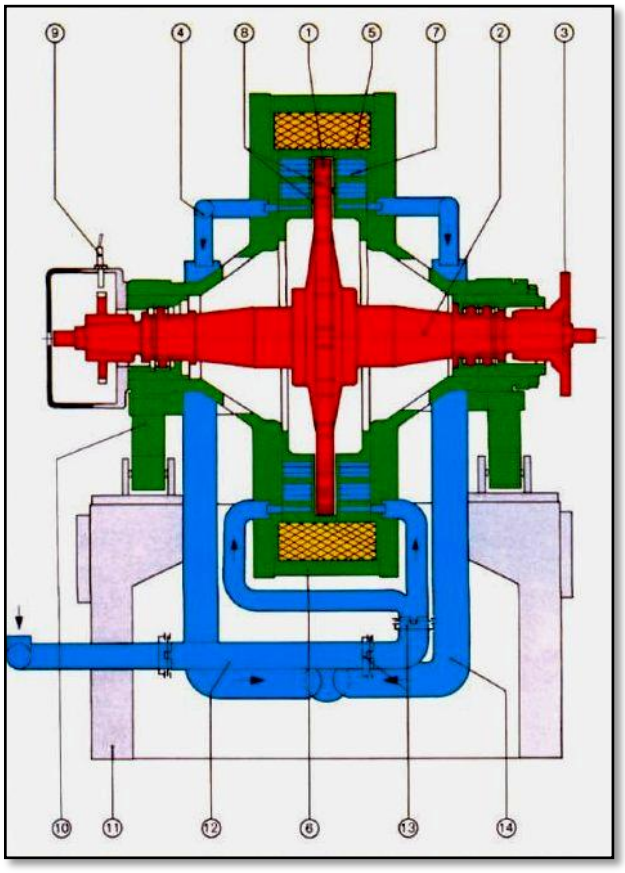

Fig. 3.1.1.2. The schematic diagram of eddy-current dynamometer, where: 1) rotor, 2) rotor shaft, 3) coupling flange, 4) water outlet with thermostat, 5) excitation coil, 6) dynamometer housing, 7) cooling chamber, 8) air gap, 9) speed pick-up, 10) flexure support, 11) base, 12) water inlet, 13) joint, 14) water outlet pipe.

3.1.2 Gas analyser and smoke meter

The exhaust gaseous emissions CO, THC, NO_x were measured by the Horiba MEXA-7170DEGR gas analyser while the AVL – 415S smoke meter was used to measure the smoke number. A Non-Dispersive Infrared Method (NDIR) has been used to measure the CO and CO_2 emissions. The NO_x emissions have been measured using the chemiluminescence method whereas the total unburned hydrocarbons (THC) were measured using the flame ionisation detection technique.

The separate module AIA-72X in the gas analyser was used for the NDIR method. The principle of this method is illustrated in Figure 3.1.2.1. The CO_2 and CO gases have different infrared abortion spectras, thus the measurement of the transmitted infrared light is a proportional measure of the concentration of these gases. The typical NDIR module consists of two cells where the first is used for sampling gases and the second for comparison, usually filled with gas which does not absorb infrared radiation. The infrared beam passes through the sampling cell and then through the band pass filter and is measured by the detector. Furthermore, the signal detected from the sampling cell is compared to the same light source passed through the comparison cell. The acquired pre-amplified signal is proportional to the CO_2 or CO concentrations.

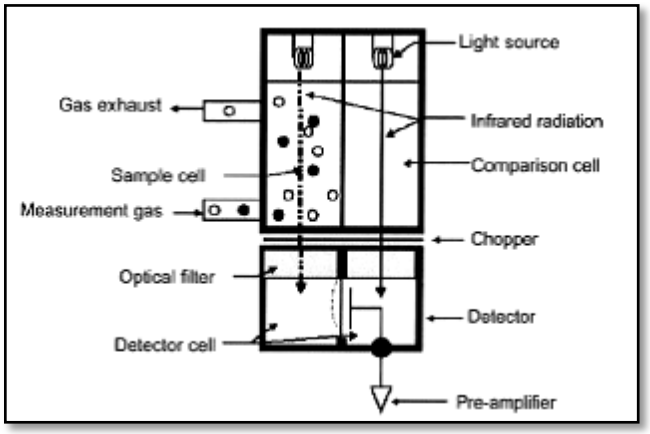

Fig. 3.1.2.1. The schematic diagram of the principle of the NDIR method (adopted from Horiba Users manual).

Another module, MPA – 720, is used for the measurement of the O_2 concentration. Its principle is shown in Figure 3.1.2.2. The O_2 molecules are detected by the magneto-pneumatic method. When appropriate current is applied to the electro magnet, the electric field attracts the oxygen molecules, changing the level of the local pressure. The difference in pressure is detected by the condensed microphone and is proportional to the O_2 concentration.

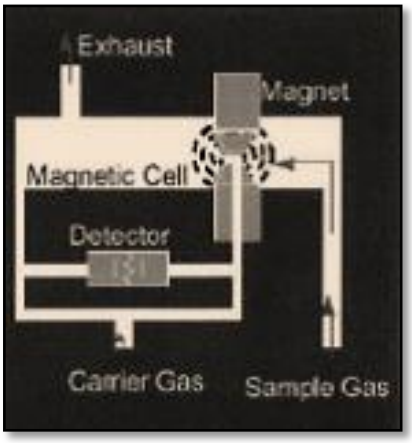

Fig. 3.1.2.2. The schematic diagram of the principle of the magneto-pneumatic method (adopted from Horiba Users manual).

The flame ionisation detection method (FID) is used to measure THC as a concentration of the total carbon molecules. The Horiba analyser consists of the FIA-720 module, which measures the THC concentration. Unburned hydrocarbons are introduced to the chamber and burned in the hydrogen/air flame. The ions, as a result of combustion, are proportional to the THC concentration. They are further collected on the one of the electrodes by applying electric voltage, giving the signal for analysis.

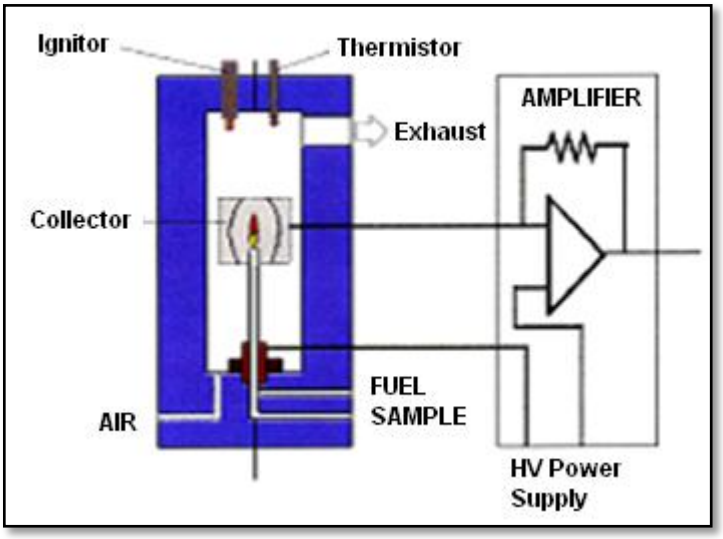

Fig. 3.1.2.3. The schematic diagram of the principle of the FID method (adopted from Horiba Users manual).

The CLA-720A module in the Horiba analyser is responsible for the measurement of NO_x. The chemiluminescence method has been adopted to detect the NO_x. This is based on the chemical reaction of NO_2 with ozone, which produces excited NO_2 in the reaction chamber. When newly produced NO_2 return to the ground state, they emit the light. The light passes through the band pass filter and is being detected proportionally to the NO_x concentration in the sample.

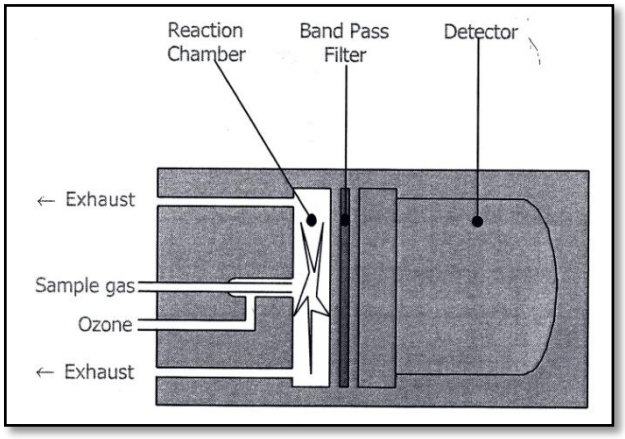

Fig. 3.1.2.4. The schematic diagram of the principle of the chemiluminescence method (adopted from Horiba Users manual).

The soot particle emissions from the exhaust gases are measured by the smoke meter. The principle of the smoke meter is shown in Figure 3.1.2.5. Generally, a well defined exhaust sampling volume passes though the paper filter. Carried by the exhaust gases, soot particles are collected on the filter (up to a certain size), causing its blackening. The light transmission through the soot on the paper is proportional to the soot quantity. The smoke number is measured from 0 to 10, where 0 corresponds to the white paper filter while 10 to totally black paper. On the other hand, value 0 corresponds to a soot concentration of 0 mg/m^3 while value 10 to the soot concentration of 32000 mg/m^3.

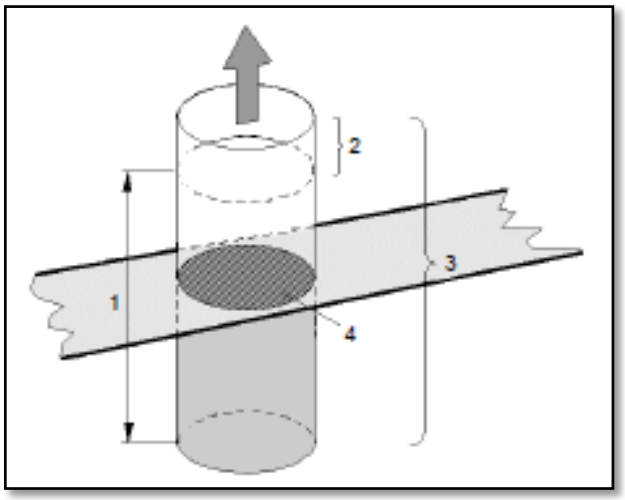

Fig. 3.1.2.5. The schematic diagram of the principle of the smoke meter (adopted from AVL Users manual), where: 1) effective volume, 2) dead volume, 3) sampled volume, 4) filter area.

During all experiments, gaseous emissions as well as the smoke number were measured three times under given steady state engine operating conditions. Basically, for each engine steady state condition the gaseous emissions and smoke number were sampled three times

in 5 minutes period. Afterwards the result was averaged over the three readings. Moreover, apart from the test in Chapter 6, all emissions and smoke number were measured from raw engine exhaust, without the installation of any of the after treatment systems.

3.1.3 Fuel consumption metering devices

Regarding the usage of RSO, SO or RME, the fuel consumption was measured by the burette. Measurements were always performed three times under each engine operating condition. Inside the burette are marks of the fuel volume where the time of specific fuel volume is measured. Afterwards, the volumetric fuel consumption is converted to mass, by multiplying the fuel density. On the other hand, the fuel consumption for diesel was measured by the AVL – 7030 fuel consumption meter. This is based on the gravimetric method. On the beginning of the measurement, the vessel (around 300 ml) is filled with the fuel and then the fuel supply to the engine is measured. The change in the mass of the vessel and fuel is measured in specified, set time. The error of the flow is determined as follows: from three readings, the difference of maximum and minimum value is divided by average value. Each engine steady state condition gives one fuel flow error measurement. For instance, averaged error of fuel flow for tests done in Chapter 4 is around 1.28% for measurements from the 75ml burette. Likewise, the diesel flow measurement showed similar error value of 1.18%. Errors of the fuel flow in Chapter 5 were around 1% for AVL device and 1.55% for the burette. Detailed error bars are shown in Section 4.1.3. The comparison of averaged fuel consumption from these two devices gives good result. However, the usage of measuring burette leads to possible higher errors as it is highly dependent on the operator. On the other hand, application of this method is certainly the cheapest and the fastest way to check the consumption of biodiesel or vegetable oils.

3.1.4 Fuel line modifications

In order to run the engine with RSO and SO the engine fuel system has been modified as shown in Figure 3.1.1. The main modification in the fuel line was to route the fuel through the controlled fuel heater/cooler, maintaining the fuel at a constant temperature. Two-way valves were used to change the fuel supply from the diesel tank or from the vegetable oil tank. The fuel consumption of vegetable oils was measured using a burette connected to the modified fuel line. Valve 2 was used to switch the fuel from diesel oil to vegetable oil and vice versa. Once switched to vegetable oil, valve 1 was used to route the vegetable oil either directly from its tank or through a burette in order to measure the fuel consumption. The burette was filled using a separate pump fixed between the vegetable oil tank and the burette. The return fuel line from the high pressure common rail pump was connected to

the inlet fuel line before the heater/cooler. After several preliminary investigations, the temperature in the fuel pipeline close to the injector tip was fixed at 70°C to reduce the viscosity of the vegetable oils. The fuel temperature in the system was measured at two locations in the fuel pipeline, the thermocouple T_1 was fixed after the heater/cooler but before the high pressure pump and the second thermocouple T_2, was placed close to the injector. Without disruption in the high pressure fuel pipeline, the thermocouple was fixed using a temperature resistant silicone gel. The measured data from thermocouple T_2 is assumed to be a close representative of the actual fuel temperature.

In order to overcome the problem of high fuel viscosity and cold start, the engine was always started using diesel fuel and then switched to vegetable oil. The engine was allowed to run for approximately 45 to 50 minutes to make sure that all diesel fuel was flushed out by the vegetable oil before the actual start of the measurements. Similarly, while shutting down, the engine was switched back from vegetable oil to diesel fuel and run for another 45 minutes to ensure that only diesel fuel was left inside the fuel system to avoid problems associated with cold start. The time of the fuel line flushing was determined by the measurements of the exhaust gaseous emissions such as CO, THC and NO_x at engine operating conditions of 2.7 bar BMEP at 1500 rpm, 800 bar of injection pressure, 0% EGR and 9 deg bTDC of injection timing. The results are shown in Figure 3.1.4.1 and it can be seen that the emissions are stable after 45 to 50 minutes.

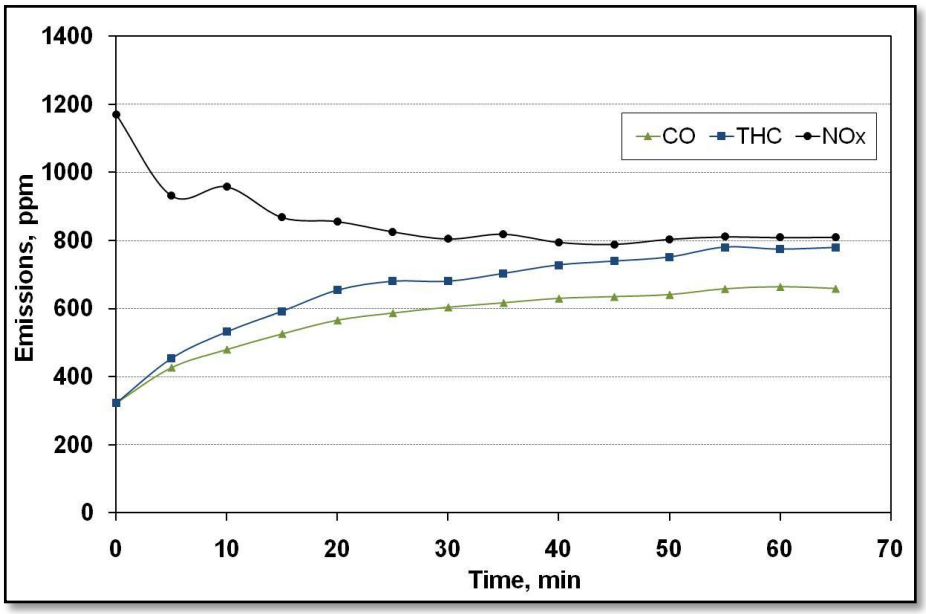

Fig. 3.1.4.1. The stabilization time for switching the fuel from diesel to PPO.

Relatively long time is needed for flushing as the return pipe from high pressure pump was connected before heater/cooler which is placed roughly one meter before injectors.

Generally, before each test the engine was running on diesel fuel. Just before switching to different fuel the quick emission check was performed in order to keep the engine in health state.

3.1.5 In-cylinder pressure data acquisition system

The in-cylinder pressure was measured by the Kistler PiezoQuartz 6125 A pressure transducer. The transducer was fitted into the first cylinder in a glow plug hole. Usually, pressure transducers require a separate cooling system but this version was resistant to thermal shock. The quartz crystal provides the proportional charge to the level of the cylinder pressure. Then, a charge signal (16 pC/bar) is amplified by the charge amplifier and captured by the PC with the installed labview software. The pressure transducer was periodically calibrated by Kistler.

For accurate measurement, the top dead centre of the engine has to be synchronized with pressure data. For this purpose, the GEL pickup and 360 toothed wheels with a separate TDC position was used. The TDC can be set by the manual threaded adjuster installed on the GEL's pickup arm. The TDC of the first cylinder was obtained by the detection of the piston peak and adjusted by the pickup arm. This method provided correct setting of static TDC.

3.1.6 ECU software (Gredi)

The engine control unit (ECU) software management Gredi allows controlling the engine parameters in real time. Moreover, it is possible to change and reprogram the engine maps. Generally, the software shows tables with variables (monitoring of engine parameters) and parameters (changing engine parameters). The main engine parameters are as follows: injection timing, injection pressure, EGR and single or dual injection mode. Each parameter has its own map created by the producer or by the user which engine can follow during the test. However, there is a possibility to be independent from the engine maps and change these parameters manually. The engine can also start without Gredi software but, in this case, all parameters will remain as the last saved in the ECU flash memory.

3.1.7 EGR control

The EGR level is also controlled via Gredi software. The EGR valve opens and closes according to the level of the vacuum pressure, regulated by the solenoid valve. Basically, the mass air flow (MAF) is measured by the MAF sensor fitted into the inlet line before the EGR mixer. In the Gredi software, there is a possibility of setting the required mass air flow.

Therefore, if the set value is lower than the current air flow, the EGR valve opens, reducing the air flow. For instance, if the engine air flow is 100 kg/h then the set value of 80 kg/h will reduce the air flow to the required value by EGR addition. The proportion of the reduced air flow can be used as an expression of the EGR percentage. However, the Horiba gas analyser has a second, separate CO_2 emissions measurement line which can be used to determine a real and more accurate EGR level. The EGR percentage is calculated by the following formula:

$$EGR = \frac{CO_{2in}}{CO_{2exh}} \cdot 100\% \quad (3.1.7.1)$$

Where:

- CO_{2in} – CO_2 concentration in the inlet manifold
- CO_{2exh} – CO_2 concentration in the exhaust tail pipe

The CO_2 in the exhaust is measured by the main analyser connection while the additional connection provides CO_2 concentration in the inlet manifold. The actual EGR percentage, calculated by the Formula 3.1.7.1, is displayed on the analyser's screen.

In this study, the production unit EGR was cooled by engine coolant. However, the cooling efficiency was too low to use it as a cooled EGR therefore a high inlet temperature at high EGR can have a negative effect on emissions such as soot.

3.2 Electrostatic mobility analyser setup

3.2.1 Primary dilution

The primary dilution system was designed to improve the quality of the results. Detailed characterisation of the system is described in Section 5.1. Figure 3.2.1.1 shows a schematic diagram of the primary dilution system.

The exhaust gases (aerosol flow) enter the dilution system through the perforated end fitted in the exhaust tail pipe. The particle flow into the system depends on the exhaust gas pressure. At high engine speed, the pressure increases resulting in higher flow. The aerosol flow passes through the high temperature resistant regulating valve, where it can be adjusted. Then, particles are transported to the next pipe which is blocked at the end. The only way to escape for the particles is perforation (around 18 cm long perforations). The perforations are covered by the large diameter pipe which is connected to the dilution gas (in front of the perforations). The dilution system is designed in such a way that the mixing process occurs in a concentric tube arrangement. The dilution gas used in this system is nitrogen as it is a neutral gas, which can not influence the soot oxidation process at higher

temperatures. Additionally, the particles enter the chamber, which allows checks on the aerosol condition, before it enters to the secondary dilution system. The three connections on the top are designed to measure the temperature and relative humidity of the mixture as well as CO_2 concentration. On the other hand, the one way (non return) valve is installed at the bottom connection allowing to flow out the excess of the sample. At the end of the chamber, another connection is used to attach secondary dilution with soot particles classification system.

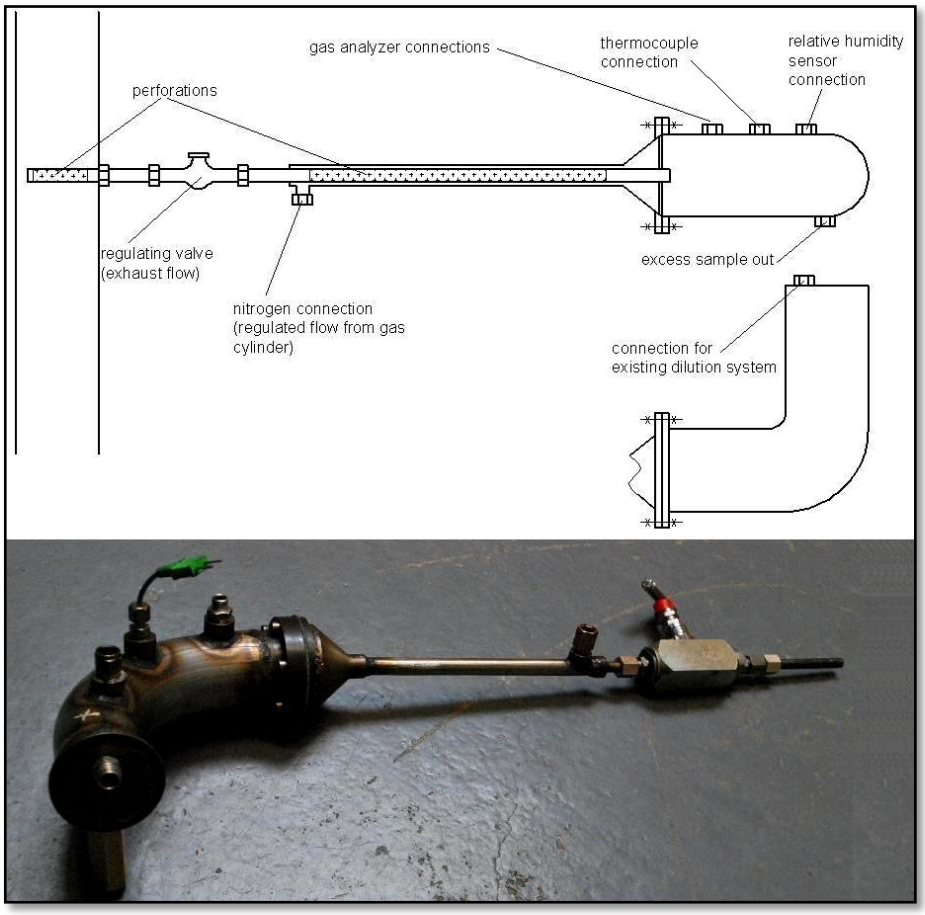

Fig. 3.2.1.1. The diagram with schematic primary dilution ratio system.

The primary dilution ratio (PDR) for this system is obtained as a measurement of CO_2 in the exhaust tail pipe and in the chamber after the mixing process and applies to the following formula [73]:

$$PDR = \frac{CO_{2m} - CO_{2a}}{CO_{2e} - CO_{2a}} \quad (3.2.1.1)$$

Where:

- CO_{2m} – CO_2 concentration in the mixture (after the mixing process)
- CO_{2e} – CO_2 concentration in the exhaust raw gases (before the mixing process)
- CO_{2a} – CO_2 concentration in the ambient air

The main gas analyser probe is connected to the exhaust tail pipe while the additional EGR line is used to measure the CO_2 concentration in mixture after the dilution process. Under constant engine operating conditions, the CO_{2e} is constant. However, the CO_{2m} can be adjusted by the quantity of nitrogen in the system thus the required PDR level is achieved. This system provides flexible dilution ratio regulation ranging from 0 to around 10 and is limited only by the range of the nitrogen flow meter. Application of wider range of nitrogen flow meter could be difficult as the crucial role in dilution process plays a mixing pressure. Wider range can produce higher pressure in the system where nitrogen can be blown back to the exhaust pipe or disturb the well balanced flow in the EMS system. Moreover, the dilution gas (nitrogen) is introduced to the system at ambient temperature which is attributed to the cold dilution process.

3.2.2 Secondary dilution and classification systems

The Electrostatic Mobility Spectrometer (EMS) consists of a Differential Mobility Analyzer (DMA) coupled with a Faraday Cup Electrometer (FCE), a neutralizer and a dilution probe where the exhaust soot particles are simultaneously diluted and heated up. A detailed scheme of the EMS and the dilution probe is presented in Figure 3.2.2.1.

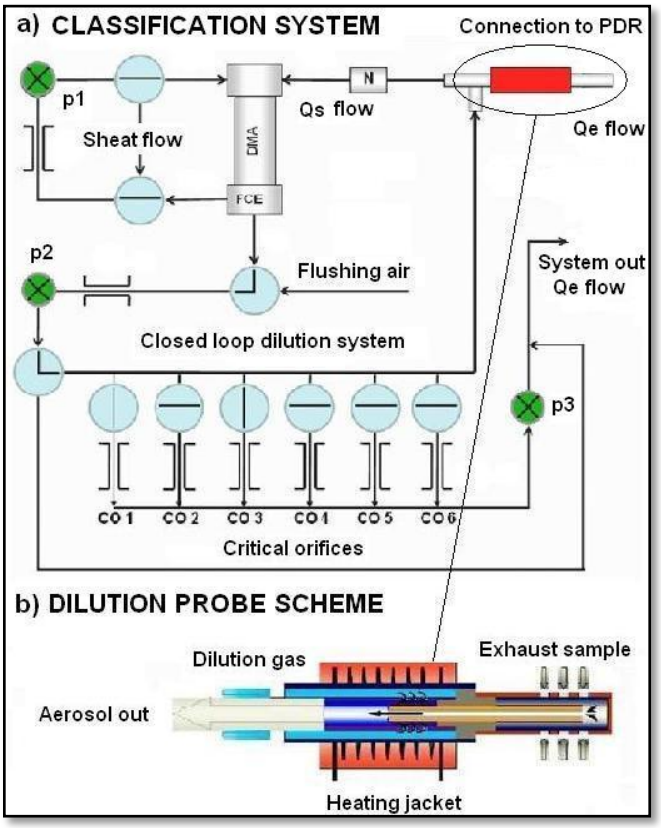

Fig. 3.2.2.1. The schematic diagram of, a) the EMS, b) the secondary dilution probe (adopted from EMS user manual).

The secondary dilution system is based on the closed loop dilution idea. Generally, the pump p2 and its critical orifice produce a constant and stable flow of around 2.6 l/min. Moreover, this flow circulates through the DMA, FCE, the critical orifices system and the dilution probe. Additionally, before the dilution probe, the absolute filter is installed for cleaning and further usage of the gas in the dilution process. If one of the valves opens, the pump p3 will take out a part of the main flow determined by the critical orifice or their combination. Automatically, the main flow is balanced by the same quantity as was subtracted by the new aerosols flow through the dilution probe. It is possible to apply ten different dilution ratios by the combinations of the six critical orifices. In this system, the required dilution ratio is achieved as different ratios of the aerosol to dilution flow in always constant flow of around 2.6 l/min. Table 3.2.2.1 shows the flows through the critical orifices and the accordingly obtained dilution ratios. Generally, the SDR is calculated by the following formula:

$$SDR = \frac{Q_S}{Q_e} \tag{3.2.2.1}$$

Where:

- Qs – sample flow (generated by the pump p2 , always 2.6 l/min)
- Qe – aerosol flow, adjusted by the critical orifices

Table 3.2.2.1. The flows through the critical orifices and corresponding SDR.

Q_s, l/min	SDR	%	Q_e, l/min	Orifice combination
2,60	32,50	3,08	0,08	**Co1**
2,60	23,64	4,23	0,11	**Co2**
2,60	17,33	5,77	0,15	**Co3**
2,60	11,30	8,85	0,23	**Co1+Co3**
2,60	8,13	12,31	0,32	**Co4**
2,60	5,53	18,08	0,47	**Co4+co3**
2,60	4,73	21,15	0,55	**Co5**
2,60	3,33	30,00	0,78	**Co1+Co5+Co3**
2,60	2,08	48,08	1,25	**Co6**
2,60	1,44	69,23	1,80	**Co6+Co4+Co3+Co1**

The total dilution ratio of the whole system is a multiplication of the PDR and SDR. Assuming the highest PDR of 10 and SDR of 32.5, the total dilution ratio reaches 325. The SDR can be heated to the temperature of around 300 degC. In the case of maintenance, the Q_e flow at the dilution probe should be periodically checked for blockages, ensuring the proper functioning of the EMS. It always has to be done according to the flow values summarized in Table 3.2.2.1.

3.2.3 Neutraliser

The neutraliser is used to get uniform charge distribution. In this case, the Am-241 neutraliser with alpha activity of 60 MBq was used. The radioactive source applies to a 110mm long, 20 mm wide and 0.2 mm thick silver foil covered by a 3 mm thick layer of gold and platinum. Figure 3.2.3.1 shows the real image as well as the sketch of the neutraliser.

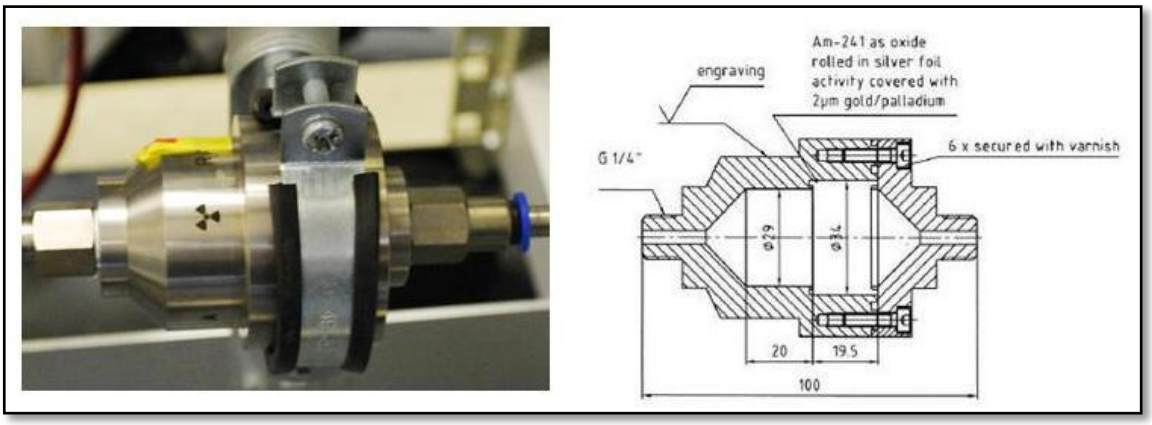

Fig. 3.2.3.1. The picture and scheme of neutraliser (adopted from EMS user manual).

3.2.4 Differential mobility analyser

The scheme of Differencial Mobility Analyser (DMA) is presented in Figure 3.2.4.1. A different design of mobility analyser provides a different range of detected soot particles.

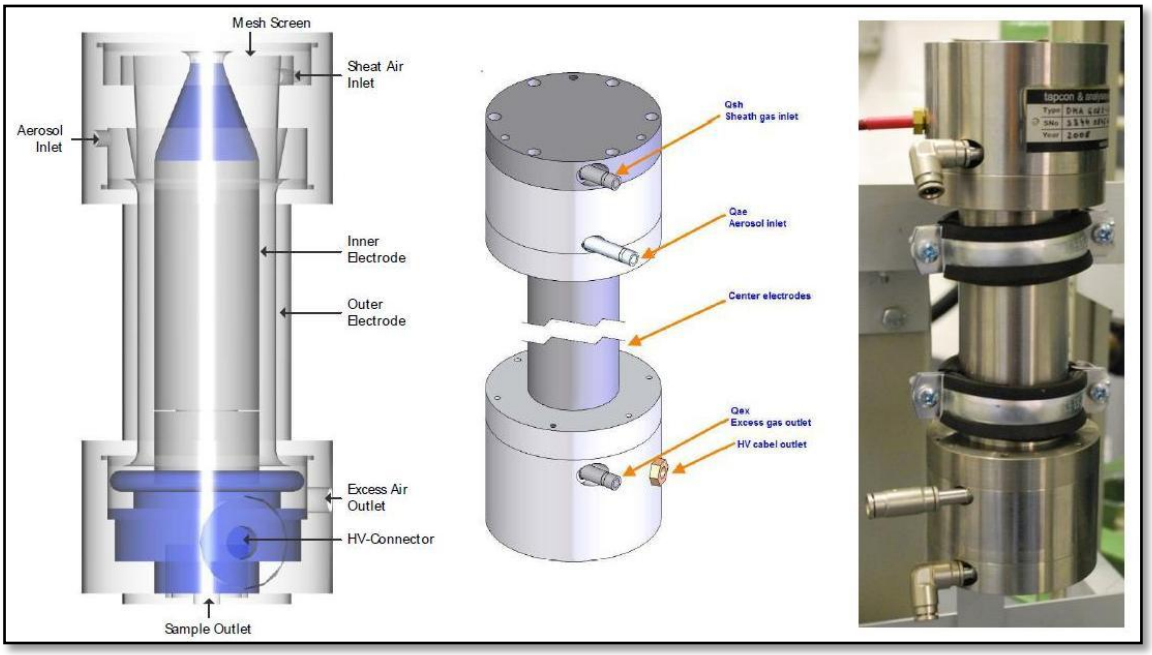

Fig. 3.2.4.1. The schematic cross section and real picture of DMA (adopted from EMS user manual).

The EMS system can be equipped with two different DMA. The main criteria are their length and radius of the electrodes. A short DMA150 has an effective length of 150 mm and is capable to measure particles from 1 nm to 150 nm. The long DMA600 is 600 mm long and provides the particles diameter range from around 5 nm to 650 nm. Both have the same radial dimensions of the inner electrode of 16 mm and the outer of 22.5 mm. Moreover, a stainless steel material was used to manufacture these DMAs. The recent version of DMA600 has been changed from stainless steel to aluminium. The effective length remained the same while the inner and outer radiuses of the electrodes were changed to 17.5 mm and 24 mm, respectively.

3.2.5 Faraday cup electrometer

Faraday cup is a high performance, computer controlled electrometer specially designed for soot particles detection. The type of FCE is the FCE – 11/A and the measurement range is from 1.0e-15 to 0.5e-10 A. A schematic cross section of FCE is presented in Figure 3.2.5.1.

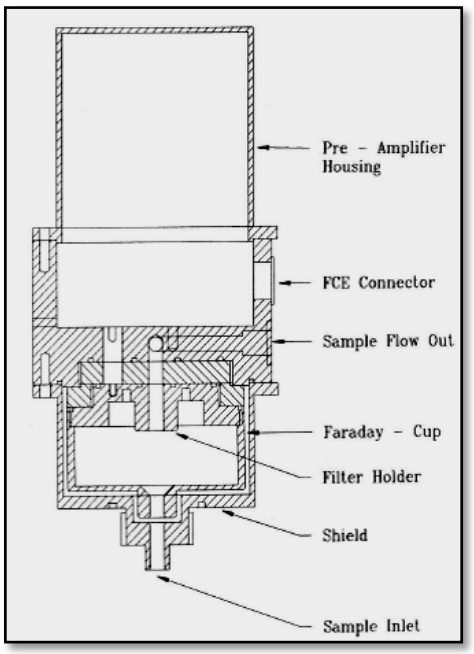

Fig. 3.2.5.1. The schematic cross section of FCE (adopted from EMS user manual).

The operation of FCE is based on the principle of a Faraday Cage. Aerosol from the sample outlet of a DMA is drawn through the Faraday Cup and then deposited on an absolute filter. The electrical charges carried by the particles into the cage are compensated by a current to the outside of the Faraday Cup which is measured using sophisticated electronics.

3.2.6 Software

The EMS system is entirely controlled by software. There is a separate control of the sheath/excess air to the DMA and sample flow. Additionally, the SDR can be set in the software. The type of DMA, FCE and critical orifices can be changed in the software's configuration tab. Figure 3.2.6.1 presents the screenshot from the software. The main area is a current measurement where x-axis is a diameter in nm and y-axis the concentration number in $1/cm^3$. On the right hand side, it is possible to preview the current parameters for selected particles detection (red bars).

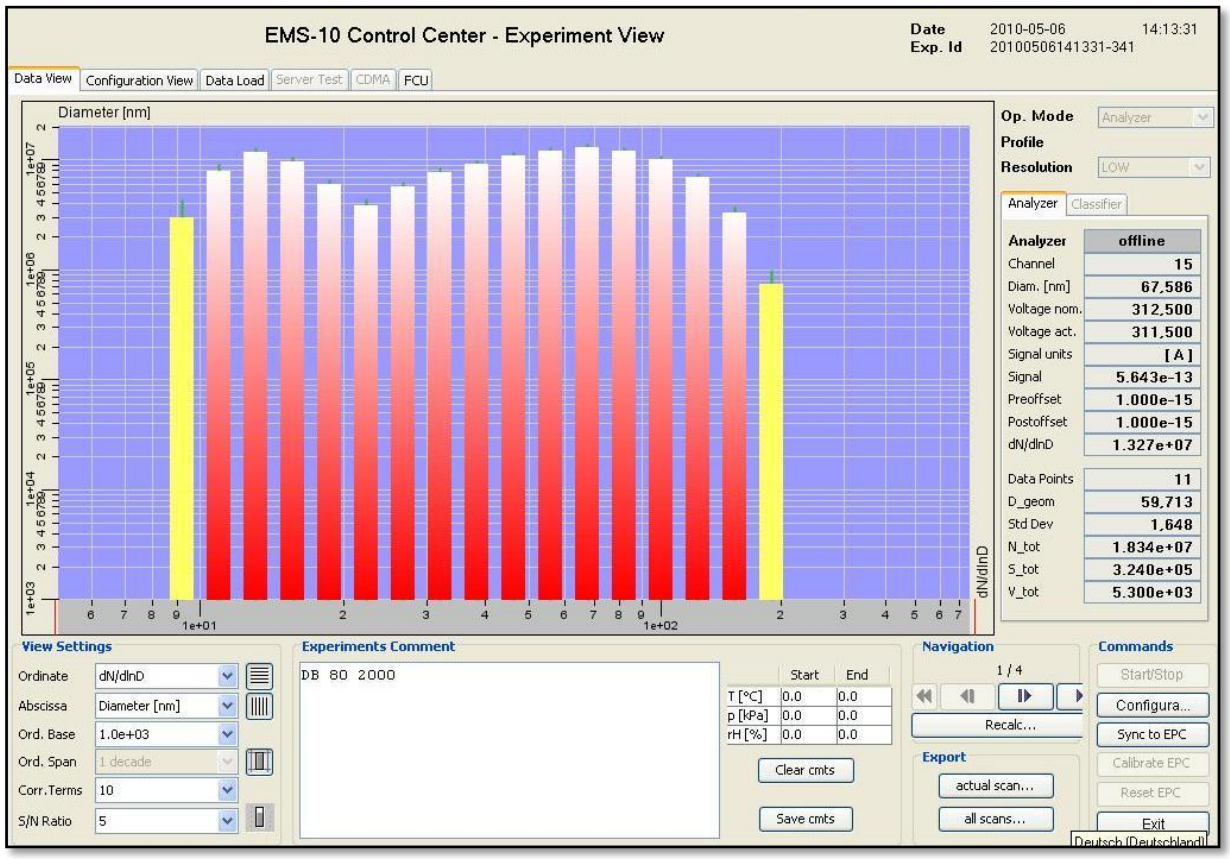

Fig. 3.2.6.1. Screenshot from the EMS software.

Moreover, the EMS can work in three resolutions – low, medium and high. The lowest resolution divides the measurement range into only 20 channels (20 detections) while the highest, most accurate, divides the measurement range into 100 channels. One soot particle size distribution corresponds to the results from Figure 3.2.6.1 and is usually termed as a single scan. The output file with the results is saved in *.csv where the data is delimited by semicolon. It can be easily exported to MS Excel or Matlab and further analysed.

3.3 Fuel properties

Three kinds of fuels were used in this study. The rapeseed oil (RSO) and soya oil (SO) were provided by a local UK company Regenatec. The rapeseed methyl ester (RME) was provided by Shell Global Solutions. Moreover, diesel fuel was ordinary lab diesel fuel. Although the properties of soya oil were not given, they were close to that of edible oil and can be further referred to the properties summarized in Table 2.1 from the already published literature. However, the properties of RSO, RME and diesel were known and are summarized in Table 3.3.1.

Table 3.3.1. The properties of the fuels used in the experiments.

Parameter	Units	RME	RSO	DIESEL
Cetane Number	-	49.8	49.5	52.1
Density @ 15 degC	kg/m^3	837.4	920.9	853.8
Flash point	degC	-	236	68
Carbon residue	%	-	0.28	0.2
Viscosity @ 40 degC	cSt	2.891	34.32	2.5
Sulphur content	mg/kg	7.5	52.5	10
Cloud point	degC	-17	-	-10
Ash content	%	-	0.003	<0.005
Water content	mg/kg	-	841	61
Total aromatics	%	24	-	10.5
Carbon	%	86.5	-	86.2
Hydrogen	%	13.5	-	13.4
Oxygen	%	<0.04	-	0
Calorific value	kJ/kg	45959.1	37354	44800
Oxidation stability	hrs	>48	5.6	14 g/m3

3.4 Data analysis

3.4.1 In-cylinder volume

The in-cylinder volume is calculated based on crank-piston geometry (Figure 2.2). Generally, the cylinder volume at any crank position is:

$$V = V_C + \frac{\pi B^2}{4}(l + a - s) \qquad (3.4.1.1)$$

Where:

- V_c – clearance volume
- B – cylinder bore

- l – connecting rod length
- a – crank radius
- s – distance between the crank axis and the piston pin axis

The distance s can be written as:

$$s = a\cos\theta + \sqrt{l^2 - a^2 sin^2\theta} \quad (3.4.1.2)$$

By replacing the distance s in Equation 3.4.1.1, by Equation 3.4.1.2 gives the in-cylinder volume at any given θ (crank angle degree):

$$\frac{V}{V_c} = 1 + \frac{1}{2}(r_c - 1)\left[R + 1 - cos\theta - \sqrt{R^2 - sin^2\theta}\right] \quad (3.4.1.3)$$

Where:

- r_c – compression ratio (eq. 2.1)
- R – ratio of connecting rod length to crank radius, l/a

3.4.2 Apparent and cumulative heat release rate

Generally, the heat release during combustion process can be defined as gross and apparent. The gross heat release rate reflects the losses by crevices and heat transfer to the cylinder walls. However, in this study, the net heat release calculation has been used. This heat release rate has been calculated by Formula 3.4.2.3.

Generally, the heat release rate calculations are based on the first law of thermodynamics. It is calculated as an energy balance of the combustion chamber.

$$\delta Q_{ch} = dU_s + \delta Q_{ht} + \delta W + \sum h_i dm_i \quad (3.4.2.1)$$

Where:

- U_s – internal energy
- Q_{ht} – convective heat transfer to the cylinder walls
- W – work output
- $h_i dm_i$ – the losses by the crevices

The final formula for the gross heat release rate can be written as:

$$\frac{dQ_{ch}}{d\theta} = \frac{\gamma}{\gamma - 1} p \frac{dV}{d\theta} + \frac{1}{\gamma - 1} V \frac{dp}{d\theta} + V_{cr} \frac{dp}{d\theta} + \frac{dQ_{ht}}{d\theta} \quad (3.4.2.2)$$

Furthermore, without correction for heat loss to the cylinder walls:

$$\frac{dQ_{cha}}{d\theta} = \frac{\gamma}{\gamma-1} p \frac{dV}{d\theta} + \frac{1}{\gamma-1} V \frac{dp}{d\theta} \quad (3.4.2.3)$$

Where:

- γ- adiabatic index (specific heats ratio)
- p - the in-cylinder pressure
- V- the cylinder volume
- Θ - crank angle degree

The net (apparent) heat release rate calculations apply to the first two terms and represent a sensible energy change and work transfer to the piston (eq. 3.4.2.3).

It is well known that a specific heat ratio has a strong influence on the peak of the heat release rate [74,75]. The value of adiabatic index normally varies between 1.3 and 1.35 [1]. Since this work is focused on comparing the effects of various fuels and different engine operating conditions, a constant adiabatic exponent of 1.35 was used.

The cumulative heat release rate is calculated as a sum of net heat release rates at each of the CAD, beginning from the start of injection and can be expressed by the following formula:

$$cHRR = \sum_{SOI}^{CAD=720} \frac{dQ_{ch}(i)}{d\theta(i)} \cdot k(i) \quad (3.4.2.3)$$

Where k is the resolution of the heat release rate expressed in 1/measured points in 1 CAD.

3.4.3 Start of combustion, end of combustion, duration of combustion and ignition delay

The start of injection is a command from the ECU software.

The start of combustion (SOC) was estimated from the heat release rate and it is defined as the CAD at which the heat release curve crosses x-axis (from negative to positive values).

The end of combustion (EOC) was obtained from the 90% value of the normalized cumulative heat release rate and is defined in terms of CAD.

The ignition delay was calculated as a difference between the SOC and SOI in terms of CAD, by the following formula:

$$ID = SOC - SOI \quad (3.4.3.1)$$

The duration of the combustion (DOC) was obtained as a difference between the EOC and the SOC:

$$DOC = EOC - SOC \tag{3.4.3.2}$$

The premixed and diffusion combustion phases are distinguished by using the second differential of the heat release rate [74]. An overall view on determining all mentioned values is presented in Figure 3.4.3.1.

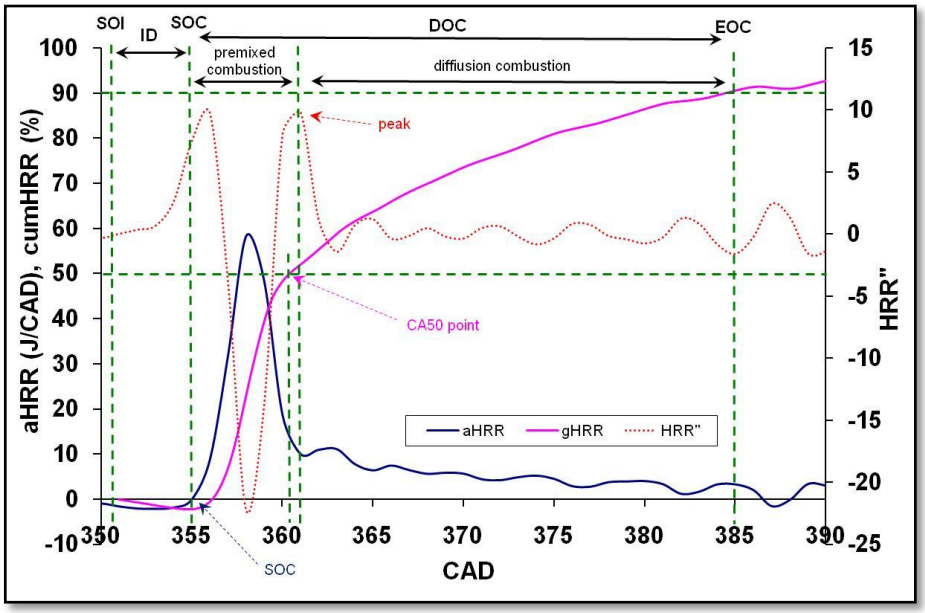

Fig. 3.4.3.1. The schematic diagram of determining of the SOC, EOC, DOC, ID, premixed and diffusion phases and CA50 point.

3.4.4 Combustion efficiency

The combustion efficiency is calculated as a loss of energy by the incomplete combustion. Usually products of incomplete combustion are CO and THC. It can be described via the following formula:

$$\eta_c = \frac{\sum_i x_i Q_{HVi}}{\left[\frac{m_f}{(m_a + m_f)}\right] Q_{HVf}} \tag{3.4.4.1}$$

Where:

- x_i – mass fraction of the unburned species
- Q_{HVi} – lower heating values of these species

- m_f/m_a – mass flow of the fuel and air, respectively
- Q_{HVf} – lower heating value of the fuel

3.4.5 The brake specific fuel consumption

The brake specific fuel consumption describes the fuel consumption acquired from the unit of engine power, by the following formula:

$$BSFC = \frac{\dot{m}_f}{P} \tag{3.4.5.1}$$

Where:

- m_f – mass flow of the fuel
- P – engine output power

3.4.6 Cumulative particles concentration number

The soot particles cumulative concentration number (CCN) can be calculated by the following Equation:

$$CCN = \sum_{i=1}^{n} \left[\frac{dN}{dlnD(i)} \cdot dlnD(i) \right] \tag{3.4.6.1}$$

Where:

- n – consecutive particles diameter (number of channel)
- $\frac{dN}{dlnD}$ – particles concentration number
- $dlnD$ – width of the size interval for a channel

The CCN in the nucleation and accumulation modes is calculated by the same formula but in different particles diameter ranges.

3.4.7 Coefficient of variation for soot particles size distribution

The coefficient of variation (COV) has been calculated in order to quantify the repeatability of soot particles size distributions. It has been calculated by the following formula. It also can be used to determine the repeatability from day to day or from scan to scan.

$$COV = \frac{\sigma}{\mu} = \frac{\sqrt{\frac{1}{n}\sum_{i=1}^{n}\left[x_i - \left(\frac{1}{n}\sum_{i=1}^{n}(x_i)\right)\right]^2}}{\frac{1}{n}\sum_{i=1}^{n}(x_i)} \tag{3.4.7.1}$$

Where:

- σ – standard deviation
- μ – mean
- n – number of data points
- x – data point

3.4.8 The DPF filtration efficiency

The filtration efficiency based on the total cumulative concentration number has been calculated by the following Equation and expressed in percentage:

$$\eta_{CNN} = \left(1 - \frac{CNN_a}{CNN_b}\right) \cdot 100\% \quad (3.4.8.1)$$

Where:

- CNN_a – cumulative concentration number after the DPF
- CNN_b – cumulative concentration number before the DPF

4 CHAPTER 4 – Emission characteristics and engine performance

4.1 Combustion and emission performance of rapeseed oil, soya oil and their blends.

4.1.1 Test matrix

The RSO, SO and their bends with diesel have different fuel properties compared to diesel. In order to compare the combustion and emission characteristics for these fuels the engine was always operated under a constant load of 2.7 bar BMEP at 1500 rpm (engine torque of 42.7 Nm ± 0.5 Nm at engine speed of 1500 rpm ± 10 rpm). The corresponding engine operating conditions are shown in Table 4.1.1.1. The load (about 20% of the maximum power) and speed conditions have been chosen to represent the widely used operating point of the stationary driving cycle for automotive diesel engines. The properties of RSO were confined within the range given in the DIN V 51605 (Section 3.3) apart from the sulphur, phosphorous and water content. The properties of SO were close to that of the edible oil.

Table 4.1.1.1. The engine operating conditions.

Engine conditions	
Engine speed	1500 rpm
Engine load	2.70 bar BMEP
Injection pressure	800 bar
EGR rate	0%
Injection timing	9 CAD bTDC

4.1.2 Combustion characteristics

Figures 4.1.2.1a and b show the in-cylinder pressure traces and the peak of in-cylinder pressures for all fuels (RSO, SO, diesel fuel and 30%, 20%, 10%, of RSO and SO in diesel fuel blend). The in-cylinder pressures were averaged over 25 cycles. It is noticeable that for RSO and SO the in-cylinder pressure peaks are lowest by comparison with those for the blends and for diesel fuel. The maximum difference in the peak cylinder pressure is about 4 bar. In Figure 4.1.2.1b it can be seen that, the peak pressure decreases with an increase in the

concentration of RSO/SO in blends. Additionally, it can be seen that SO and its blends show a lower peak pressure compared to RSO and its blends. The relative differences in peak pressure are attributed to high molecular weight fractions (fatty acids) and other fuel properties such as viscosity and cetane number, which affect the combustion process of RSO, SO and their blends. Thus, the peaks of in-cylinder pressure are lower than for diesel. General trend of decreasing peak pressure for increased percentage of RSO and SO in the blend can be seen. However, apparent dip for 10% RSO and SO blend is marginal about 2 bar which is in the range of measurement error.

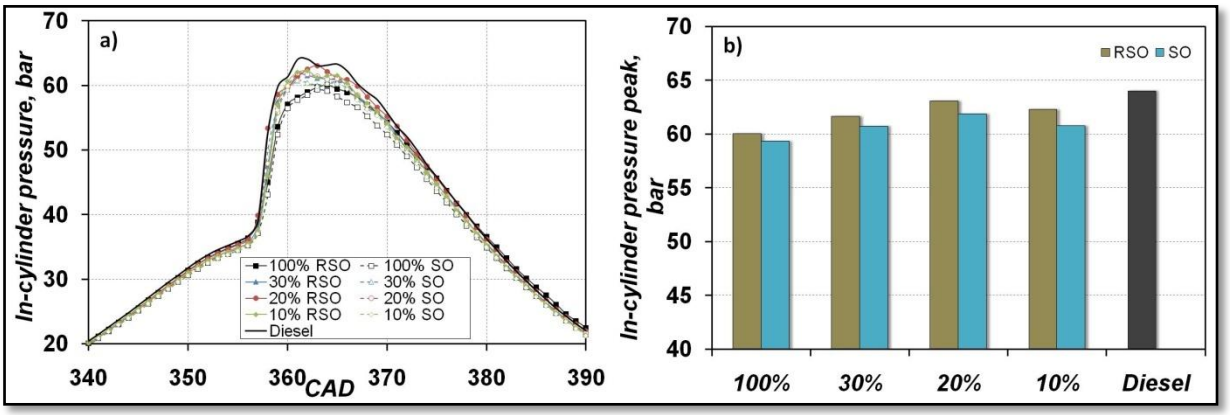

Fig. 4.1.2.1. The diagrams of a) in-cylinder pressure, b) in-cylinder pressure peak for RSO, SO and their blends.

Using the in-cylinder pressure data, the apparent in-cylinder heat release rate was obtained using the basic thermodynamic Equation 3.4.2.3.

Figure 4.1.2.2a shows the heat release rate for all the fuels. It could be seen that the heat release rates are different for different fuels. The start of combustion (SOC) for vegetable oils and their blends with diesel is almost the same as for diesel fuel. The peak value of the heat release rate for pure RSO, SO and their blends is lower compared to that of diesel fuel and it decreases with an increasing concentration of SVO in diesel. The peak values of the apparent heat release rates are presented in Figure 4.1.2.2b. Diesel has the highest peak value of about 83 J which decreases to about 58 J and 60 J for RSO and SO, respectively. The lower magnitudes of the peak of heat release rates are attributed to higher viscosity and poor air utilization of RSO/SO and their blends compared with diesel fuel. The variations in the ignition delay (the time between the start of injection (SOI) and the start of combustion (SOC)) for RSO, SO, their blends and diesel fuel are negligible (Figure 4.1.2.3a).

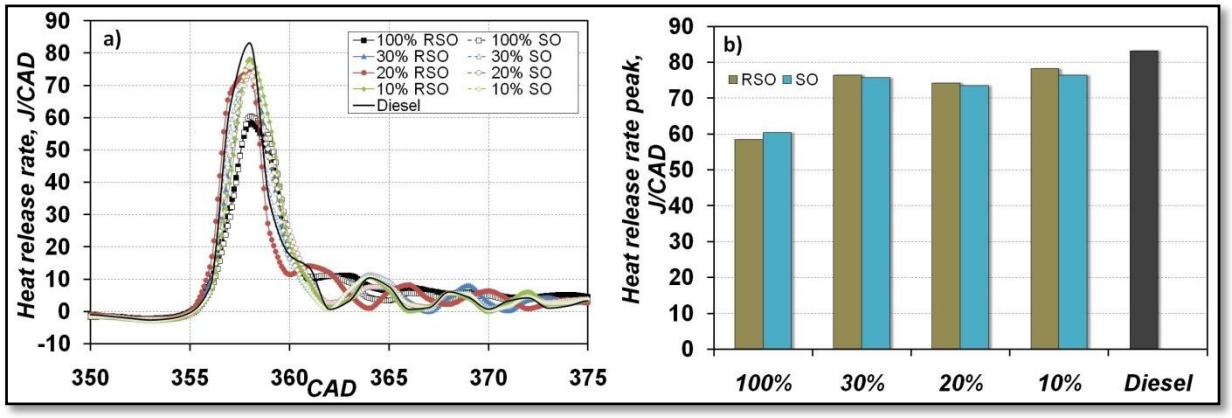

Fig. 4.1.2.2. The diagrams of a) heat release rate, b) heat release rate peak for RSO, SO and their blends.

Generally the cetane number (CN) is a good indicator of the ignition delay and for fuels with higher CN the ignition delays are shorter. Considering the ignition delay and cetane number it can be seen that RSO and SO with lower CN have almost the same ID as for diesel fuel. This effect could be mainly due to the cracking of heavier molecules and the chemical reactions that are leading to the formation of low boiling point fractions during the injection period. Ignition could be initiated mainly by the low molecular fractions which are formed at the periphery spray during the cracking process of high molecular fractions when injected into the engine combustion chamber, as described in [63]. The high molecular fractions that are present in the core of the spray also cause longer combustion duration. Moreover, the presence of the oxygen content in the vegetable oil enhances the formation of a stoichiometric mixture sooner than for non oxygenated diesel fuel. In addition to this, fuel preheating can also slightly advance the start of combustion due to the enhanced temperature of the mixture. Therefore, using vegetable oils with higher molecular weight compared to diesel fuel results in negligible variations in the ignition delay.

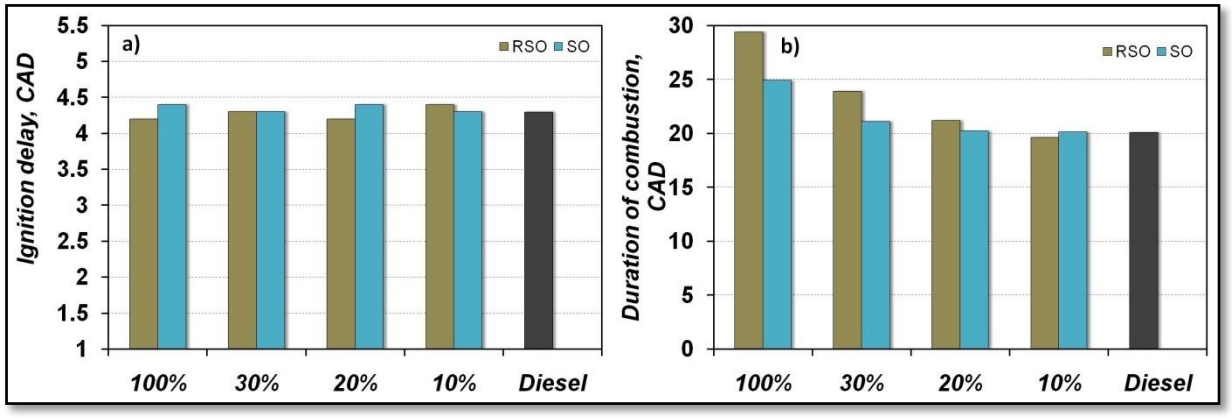

Fig. 4.1.2.3. The diagrams of a) ignitions delay, b) duration of combustion for RSO, SO and their blends.

Figure 4.1.2.3b shows the plot of combustion duration for diesel, neat RSO, SO and their blends. It is noticeable that duration of combustion is longer for vegetable oils compared to

diesel fuel. Moreover, as the percentage of vegetable oil in diesel increases, the duration of combustion also increases. This could be the effect of poor air utilisation by the higher boiling point fractions that are present mainly in the core of the spray. Comparing both the neat RSO and SO, the combustion duration for RSO is longer than that for SO.

Figure 4.1.2.4a provides information about the duration of combustion in the premixed phase as well as in the diffusion phase. The premixed and diffusion combustion duration are distinguished using the second differential of the heat release rate. The durations of the premixed combustion phase for the vegetable oil and its blends are slightly lower than for diesel and without any specific trends. The combustion of diesel, RSO, SO and their blends has a longer diffusion phase compared to the premixed burning. Despite shorter premixed burn duration, the magnitude of heat that is released during this phase is higher compared to the magnitude of heat that is released in the diffusion phase (Figure 4.1.2.4b).

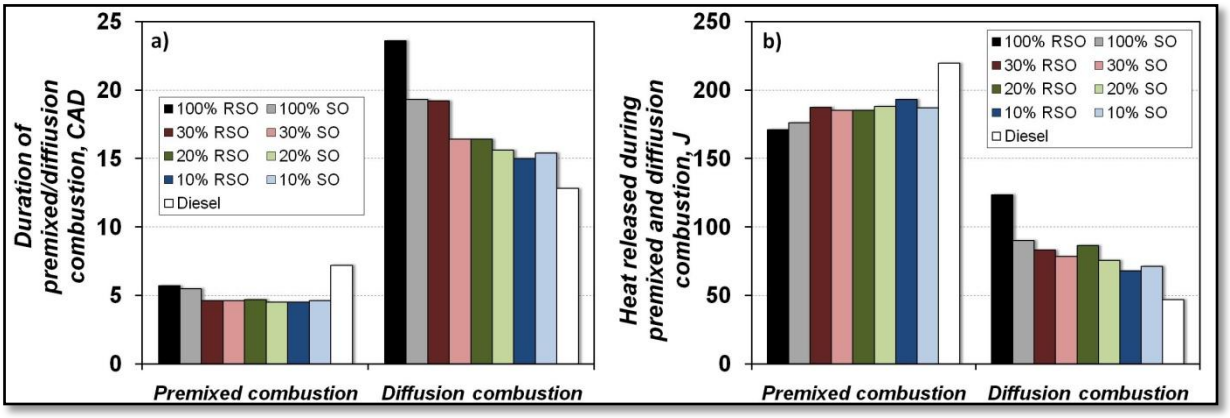

Fig. 4.1.2.4. The diagrams of a) duration of combustion in the premixed and diffusion phases, b) heat released in the premixed and diffusion phases for RSO, SO and their blends.

The magnitude of heat released during the premixed phase is lowest for pure RSO and SO and slightly increasing with lower concentration of these oils in blend. The lower magnitude of heat released by the RSO and the SO indicates that the global combustion temperatures are low, influencing the in-cylinder emissions formation process. The magnitude of heat released by the vegetable oil and its blends during the diffusion combustion is higher compared with diesel. As the concentration of SVO in diesel increases, the magnitude of the diffusion combustion increases, strongly influencing the soot production.

Figure 4.1.2.5 shows the combustion efficiency of RSO, SO and their blends with diesel fuel. This has been calculated by the Equation 3.4.4.1. As expected, pure RSO and SO have the lowest combustion efficiency. However, lower concentrations of RSO, SO in blends show improved combustion efficiency. Generally, products of incomplete combustion (CO, THC) indicate the magnitude of combustion efficiency. Due to high viscosity and poor atomization,

the emissions of CO and THC are higher for pure RSO and SO, which result in low combustion efficiency.

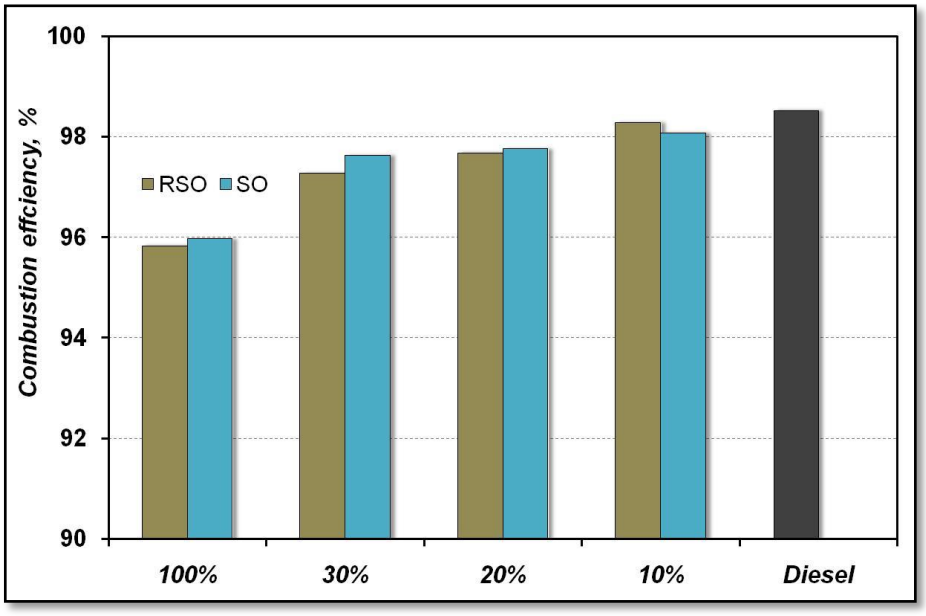

Fig. 4.1.2.5. The combustion efficiency for RSO, SO and their blends.

4.1.3 Emission characteristics

The emissions characteristics and the fuel consumption of RSO, SO and their blends with diesel fuel at 30%, 20% and 10% are presented in Figure 4.1.3.1. All results are compared against the emissions of diesel under the same operating conditions. As previously discussed the global heat release rates for RSO and SO are lower than that for their blends and diesel. This indicates that the global in-cylinder temperatures for neat vegetable oils are lower than their blends and diesel. Lower combustion temperature also lowers the formation of NO_x emission from the combustion of RSO and SO as shown in Figure 4.1.3.1a. Consequently, the NO_x emissions for RSO and SO are reduced by about 30% and 40% respectively, compared with diesel. By blending 10% of RSO with diesel, the NO_x emissions are lowered by 6% and similarly, blending 10% of SO with diesel results in a reduction of NO_x emissions by 9% compared to that of diesel fuel. However, SO and its blends show a greater reduction in the NO_x emissions compared to RSO and its blends. Differences in NO_x emissions between rapeseed oil and soya oil and their blends could be attributed to the differences in fuel properties and their effects on the stoichiometric mixture formation and combustion. The main causes of the formation of NO_x emissions during the combustion process are the in-cylinder temperature, availability of oxygen and ignition delay. The availability of oxygen in the fuel structure and its readiness to form local stoichiometric A/F ratios in the spray at high

cylinder temperature influences the formation of NO_x emissions. The heat released during the premixed phase has a strong effect on the formation of NO_x emissions. In the case of SVO, the high viscosity results in poor mixture formation which subsequently affects the premixed combustion phase as shown in Figure 4.1.2.4b. A low heat released by premixed combustion of SVO also leads to a reduction of global in-cylinder temperature. Moreover, it could be seen that the heat released during the premixed combustion for RSO and SO is lower compared to that of diesel fuel. This indicates that the in-cylinder temperatures are low, eventually resulting in lower NO_x emissions.

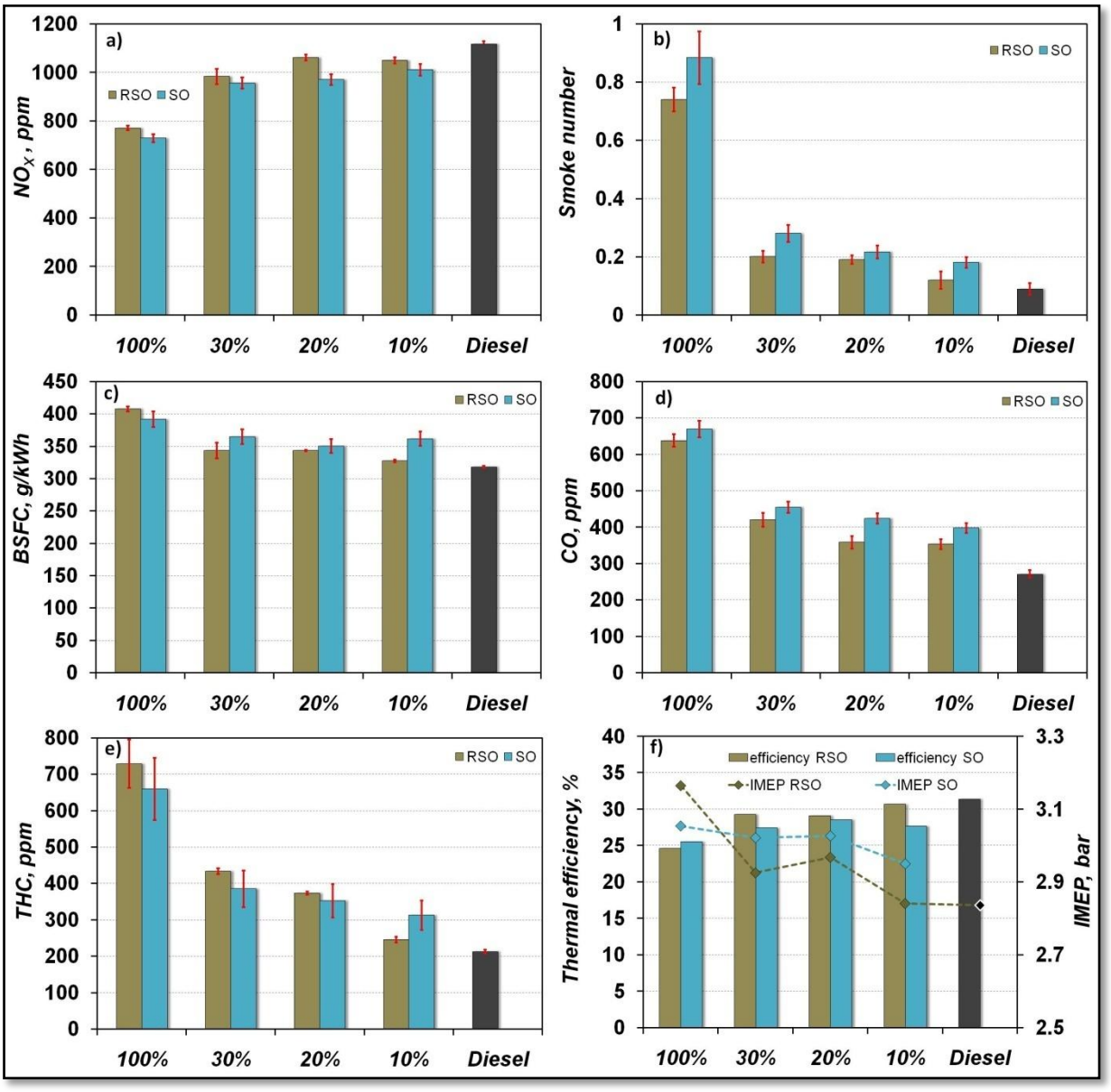

Fig. 4.1.3.1. The diagrams of a) nitrogen oxides emissions, b) smoke number, c) brake specific fuel consumption, d) carbon monoxide emission, e) total unburned hydrocarbons emissions, f) thermal efficiency and IMEP.

Figure 4.1.3.1b shows the smoke emissions from diesel, RSO, SO and their blends with diesel fuel. A significant increase in the smoke number (SN) was observed for pure RSO and SO. In comparison with diesel fuel, neat vegetable oils (RSO, SO) have higher SN of about 640% and 780%, respectively. Also, the smoke number increases when higher fractions of RSO and SO are added to the diesel blend. Variations in the soot emissions between RSO and SO are caused by differences in the fuel properties such as sulphur, phosphorous and oxygen content. As previously discussed, not all properties of RSO are in compliance with the DIN V 51605 specification. High content of sulphur and phosphorous in fuel causes higher soot emissions, however the oxygen content helps to reduce SN. These two processes are competing against each other. Although vegetable oils have higher oxygen content, the soot production is still high due to longer diffusion combustion of higher boiling point fractions shown in Figure 4.1.2.3b and 4.1.2.4a. Despite preheating the vegetable oils to temperatures up to 70°C, their viscosities are still higher than of diesel, which leads to poor atomization of vegetable oils and consequently formation of relatively larger fuel droplets compared to diesel. This causes poor air utilisation, incomplete vaporization and local rich mixtures which eventually cause higher soot production from the combustion of RSO and SO.

The Brake Specific Fuel Consumption (BSFC) for diesel, RSO, SO and the blends of RSO and SO with diesel are shown in Figure 4.1.3.1c. The BSFC increases with an increase of the RSO, SO concentration in the blend. Neat oils, RSO and SO have higher specific fuel consumption compared to diesel. The main reason for the increase in the BSFC is the lower calorific value of vegetable oils. In order to maintain the engine at the same load, more fuel is injected into the engine combustion chamber leading to higher fuel consumption. The BSFC for RSO and SO increases by 28% and 23%, respectively compared to that of diesel. Figure 4.1.3.1d shows the variation of carbon monoxide (CO) emission for diesel, RSO, SO and the blends with diesel. The CO emission for RSO, SO and blends is higher than for diesel. It could be seen that even a small addition of 10% of vegetable oil in diesel results in higher CO emissions. By adding 10% of RSO to diesel, the CO emissions increase by 30 % and similarly by adding 10% of SO to diesel the CO emission increases by 46%. When using neat RSO and SO, the CO emission is increased by 135% and 146% respectively, compared to diesel. It is evident that increasing concentration of vegetable oil in diesel causes an increase in the CO emissions. Generally, SO and its blends show a higher CO emission compared to RSO and its blends. Figure 4.1.3.1e shows the variation in the THC emissions from diesel, RSO, SO and also for the blends of RSO and SO in diesel. Both CO and THC are products of incomplete combustion. The combustion of vegetable oils (RSO, SO) is affected mainly by their high viscosity, which leads to poor mixing and increase in the CO, THC, soot and fuel consumption. The THC emissions for RSO are higher by 243% and similarly the THC emissions for SO are higher by 210% compared to diesel. By adding 10% of RSO to diesel, the THC emissions increase by 15%, likewise by adding 10% of SO to diesel increases the THC

emissions by 47%. As previously discussed a reduced heat release rate for vegetable oils causes low combustion temperatures, partial oxidation and flame quenching of the cylinder walls. These effects contribute to higher hydrocarbons emissions. Luft et al. [51] compared atomization, vaporization and spray cone shapes between diesel and rapeseed oil. They found that the combustion of rapeseed oil caused a longer spray cone penetration due to poor atomization and vaporization. Generally, the CO and THC emissions are mainly dependent on the local in-cylinder air fuel ratio. Higher viscosity leads to poor atomization, formation of larger droplets, partial vaporization, local rich mixtures and low combustion temperatures, which eventually result in incomplete combustion. In addition to this, fuelling rates for vegetable oils are higher due to their lower calorific value. As the percentage of vegetable oil in the blend increases the engine operates on a relatively richer mixture also leading to incomplete combustion and higher THC and CO emissions.

Figure 4.1.3.1f shows thermal efficiency and IMEP for RSO, SO and diesel fuel. It can be seen that maximum efficiency of 31.41% belongs to diesel. In the case of vegetable oils, the thermal efficiency decreases with an increase of the RSO/SO percentage in the blend. Moreover, the blends with RSO show always higher efficiency than for SO. For pure vegetable oils thermal efficiency decreases to approximately 25%. The calorific value is a major factor which influences the thermal efficiency but a slight increase of IMEP for higher percentage of vegetable oils in the blend also can be one of the reasons.

The tests done in this section provide basic information about application of different fuels in diesel engine, their behaviour and emission characteristics. Academic purposes of this study resulted in developed procedures of controlling and fuelling the engine. Moreover, these preliminary tests are used as a good background for further test procedures.

4.1.4 Conclusions

The experiments were performed to investigate the combustion and emission characteristics of RSO, SO and the blends of 30%, 20% and 10% of RSO and SO in diesel. The fuel injection system was modified to accommodate these fuels in the HSDI diesel engine. Some of the main findings from this investigation are summarised as follows:

- The combustion analysis revealed that the ignition delays for the RSO and SO and its blends are almost the same as for diesel but RSO and SO have a longer duration of combustion due to higher viscosity and the presence of heavier molecular fractions in the vegetable oil.
- The smoke number and the gaseous emissions such as CO and THC are higher for vegetable oils, compared with diesel. On the other hand, the NO_x emissions for RSO

and SO are much lower than for diesel. A decrease in NO_x emissions was observed even in the case of a small addition of 10% vegetable oil in diesel.

- The blending effect causes an increase in the THC, CO and soot emissions but decrease in the NO_x emissions, for a gradually higher concentration of RSO and SO in blends. The differences between RSO and SO and their blends in terms of their emissions and combustion characteristics are caused by differences in the fuel properties.
- The usage of vegetable oils such as RSO and SO provides benefits in terms of CO_2 emissions due to the closed loop of carbon cycle, which helps avoiding climate changes. On the other hand, the fuel consumption for RSO and SO was about 25% higher due to the lower calorific value.

4.2 Influence of injection parameters and EGR on the performance of rapeseed oil and its blends

4.2.1 Test matrix

The main focus of this work was to investigate the effects of varying fuel injection parameters such as fuel injection pressure, fuel injection timing and also the different levels of EGR in order to understand the combustion and emission characteristics of rapeseed oil (RSO) and its blends in a high speed direct injection diesel engine. As a fuel for the diesel engine, rapeseed oil and its blends at 10%, 20%, 30% and 50% were used to explore the engine performance under different fuel injection pressures (800 bar, 1000 bar and 1200 bar), EGR percentages (0%, 10% and 20%) and injection timings (9 bTDC, 4 bTDC and TDC). All these variations were carried out under a constant engine load and speed of 2.7 bar BMEP and 1500 rpm, respectively. All the results acquired for rapeseed oil and its blends have been compared against diesel fuel at a reference engine operating condition (injection pressure of 800bar, EGR percentage of 0% and injection timing of 9 deg bTDC). Table 4.2.1.1 provides an overview of all tested fuels and engine operating conditions. The fuel properties are summarized in Section 3.3.

Table 4.2.1.1. The engine operating conditions and tested fuels, where: 1, 2, 3 – effect of the injection pressure, 1, 4, 5, - effect of the EGR percentage, 1, 6, 7, - effect of the injection timing.

Engine conditions			**Tested fuels**
Injection pressure, bar	**EGR, %**	**Injection timing, cad bTDC**	
800 bar	0% EGR	9deg bTDC [1]	Diesel fuel, 10%, 20%, 30%, 50%, 100% RSO
1000 bar	0% EGR	9deg bTDC [2]	10%, 20%, 30%, 50%, 100% RSO
1200 bar	0% EGR	9deg bTDC [3]	
800 bar	10% EGR	9deg bTDC [4]	
800 bar	20% EGR	9deg bTDC [5]	
800 bar	0% EGR	4deg bTDC [6]	
800 bar	0% EGR	TDC [7]	

4.2.2 The influence of fuel injection pressure

COMBUSTION CHARACTERISTICS

Figures 4.2.2.1a-d show the variation of the in-cylinder pressures, heat release rates, peaks of the in-cylinder pressures and ignition delay for RSO and their blends with diesel for different fuel injection pressures. In Figure 4.2.2.1a it can be seen that as the fuel injection pressure increases from 800 bar to 1200 bar the combustion starts earlier. In addition to this, the in-cylinder pressure peak increases with a higher fuel injection pressure. It is noticeable that the in-cylinder pressure peak is about 4 bar lower for pure RSO as compared to that of diesel under the same fuel injection pressure and at the same engine operating conditions. Increasing the fuel injection pressure from 800 bar to 1200 bar for pure RSO has led to the same in-cylinder pressure peak as that of diesel under the reference engine operating condition. For a higher injection pressure of 1200 bar, all RSO blends apart from 30% RSO showed even higher in-cylinder pressure peak as compared to diesel at reference engine conditions. At an injection pressure of 1000 bar a higher in-cylinder pressure peak can be noticed only for blends of 10% and 20% RSO. Figure 4.2.2.1b shows the variation of the heat release rate for different fuel injection pressures. As the fuel injection pressure increases from 800 bar to 1200 bar the peak of the heat release rate as well as the combustion phasing of RSO advances due to the reduction of the ignition delay through better air entrainment and mixing. The position of the CA50 point for 100% RSO was determined to be at 361.5, 357.5 and 356.1 CAD for 800 bar, 1000 bar and 1200 bar respectively. It clearly shows that a higher injection pressure leads to faster ignition and combustion. Besides the advanced combustion at high injection pressure, the peaks of heat release rate for RSO are still lower compared to that of diesel under the reference engine operating condition. In Figure 4.2.2.1c it can be seen that as the concentration of RSO in the blend increases the in-cylinder pressure peak marginally decreases. For any of the blends, the higher injection pressure causes a rise of the in-cylinder pressure peak.

Based on the in-cylinder pressure and the heat release rate it can be noticed that combustion performance of pure RSO is much poorer than that of diesel at the same engine operating conditions. In the case of blends, when the concentration of RSO in diesel is less, the combustion performance is similar to that of diesel fuel. Increasing the fuel injection pressure for RSO and its blends enhances the in-cylinder pressures and the heat release rates, eventually resulting in the same combustion performance as that of diesel. Moreover, the rise in the momentum of the fuel spray leads to better entrainment of air into the core of the fuel spray. In addition to this, a high injection pressure provides more energy to break up higher viscous fuels into smaller droplets, leading to faster evaporation at the periphery

of the fuel sprays and faster ignition of the fuel vapour. Even though there are advantages gained from the increase of the fuel injection pressure, the overall outcome is minimised due to the effect of higher viscosity of RSO.

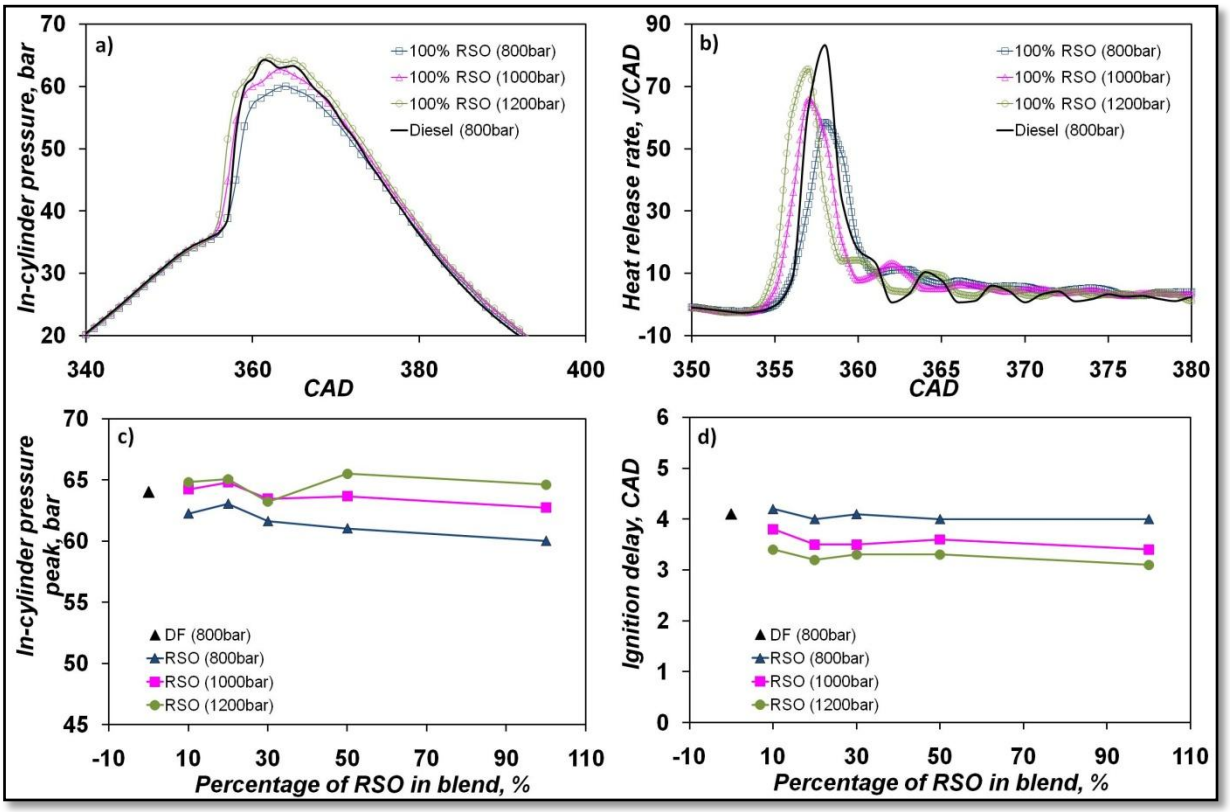

Fig. 4.2.2.1. The influence of injection pressure on a) in-cylinder pressure, b) hear release rate, c) in-cylinder pressure peak, d) ignition delay.

Figure 4.2.2.1d shows the ignition delay for RSO, its blends for different fuel injection pressures and for diesel fuel. The ignition delay and SOC were obtained accordingly to the description in Section 3.4.3. It can be seen that the ignition delay decreases with an increase in the injection pressure. On average, a reduction of about 1 CAD was observed between 800bar and 1200 bar for pure RSO and blends. The variations in the ignition delay for RSO and for different RSO blends at a given injection pressure are negligible. Higher injection pressure causes a better mixing process which reduces ignition delay. On the other hand, more heat release especially in the premixed phase, under high injection pressure operation leads to higher in-cylinder temperatures and eventually higher NO_x emissions.

Figure 4.2.2.2a shows the duration of combustion of the premixed and the diffusion combustion phases for different fuel injection pressures.

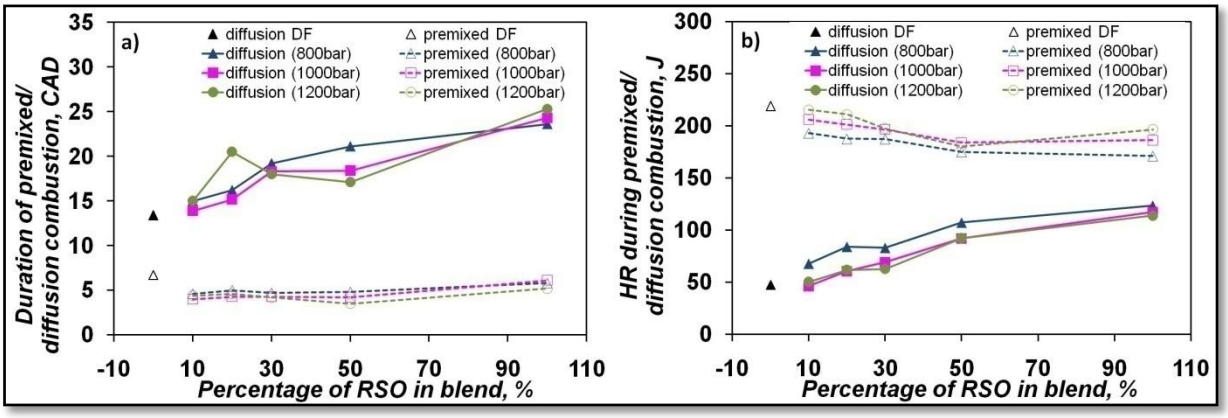

Fig. 4.2.2.2. The influence of injection pressure on a) duration of combustion in the premixed and diffusion phases, b) heat release during the premixed and diffusion phases.

The duration of premixed combustion for RSO and its blends is shorter when compared to diesel while the duration of the diffusion combustion for RSO and its blends is always longer than that of diesel. As the concentration of RSO in the diesel blend increases, the duration of diffusion combustion becomes higher but the duration of premixed combustion phase remains nearly the same for all blends except for a very small rise for the neat RSO. Thus the total duration of combustion (the sum of premixed and diffusion phases) shows an increasing trend with high concentration of RSO in the blend, the trend is similar to that of the diffusion combustion as the duration of premixed combustion is almost constant for different RSO blends. It is interesting to note that the injection pressure did not have any clear trends on the duration of combustion for these two phases even though it affects the amount of heat that is released during these two phases.

In Figure 4.2.2.2b it can be seen that the amount of heat released during the premixed phase is higher, compared to that of diffusion phase for all fuels. The heat released during the premixed combustion phase is lower for pure RSO and its blends when compared against diesel. In addition to this, it can be seen that as the concentration of RSO in the blend increases, the premixed heat marginally decreases for a given injection pressure. However, by increasing the injection pressure, the heat released during the premixed phase slightly increases. The heat released during the diffusion combustion for pure RSO and its blends is higher when compared to that of diesel. Furthermore, the magnitude of heat that is released during the diffusion combustion increases significantly with a higher concentration of RSO in the blend. An increase in the injection pressure from 800 to 1200 bar causes a reduction in the diffusion combustion phase for RSO and its blends.

Generally, the amount of heat released in the premixed combustion phase is strongly connected to the formation of NO_x through the correlation of increased in-cylinder combustion temperature. A shorter duration of combustion and lower heat released in the premixed phase leads to lower NO_x formation. On the other hand, better atomization due to

higher injection pressure produces better entrainment, more efficient fuel vaporization and mixture formation. This leads to faster combustion and higher heat release rate in the premixed phase resulting in a favourable environment of higher in-cylinder temperature and higher NO_x emissions. The diffusion phase of combustion is strongly correlated to the soot emission from the engine, thus longer duration of diffusion combustion eventually leads to higher soot formation.

EMISSION CHARACTERISTICS

Figures 4.2.2.3a - e show the variation of the nitrogen oxides emissions (NO_x), the smoke number (SN), the Brake Specific Fuel Consumption (BSFC), the carbon monoxide emissions (CO) and the total unburned hydrocarbons emissions (THC) for all fuels under different injection pressures.

In Figure 4.2.2.3a, it can be seen that the NO_x emissions for RSO and its blends are lower compared to those of diesel under the same engine operating conditions. A reduction of more than 30% of NO_x emissions was achieved for neat RSO when compared against diesel for the same operating condition. As the concentration of RSO in the blend increases, the NO_x emissions decrease. However, an increase in the fuel injection pressure leads to higher NO_x emission. When compared against diesel it could be seen that a reduction in NO_x emissions was achieved for all blends at 800 bar injection pressure as well as for a blend of 50% RSO and for 100% RSO at 1000 bar fuel injection pressure. In the case of 1200 bar injection pressure, the NO_x emissions were higher for all concentrations of RSO in diesel fuel. The reduction of about 30% NO_x for pure RSO was achieved mainly through the reduction of in-cylinder temperature as indicated by the lower in-cylinder pressure peak and lower magnitude of heat released during the premixed phase compared to that of diesel. As previously mentioned, the NO_x emissions from engines are strongly influenced by the amount of heat released in the premixed combustion, the in-cylinder pressure peak and the resultant in-cylinder temperatures. These factors increase with higher fuel injection pressures through better air entrainment and mixture formation leading to faster combustion. Consequently, it results in higher magnitudes of heat release rate in the premixed phase causing higher in-cylinder temperatures and higher NO_x emissions. However, when compared against similar injection pressures and similar operating conditions, RSO and its blends resulted in lower NO_x emissions.

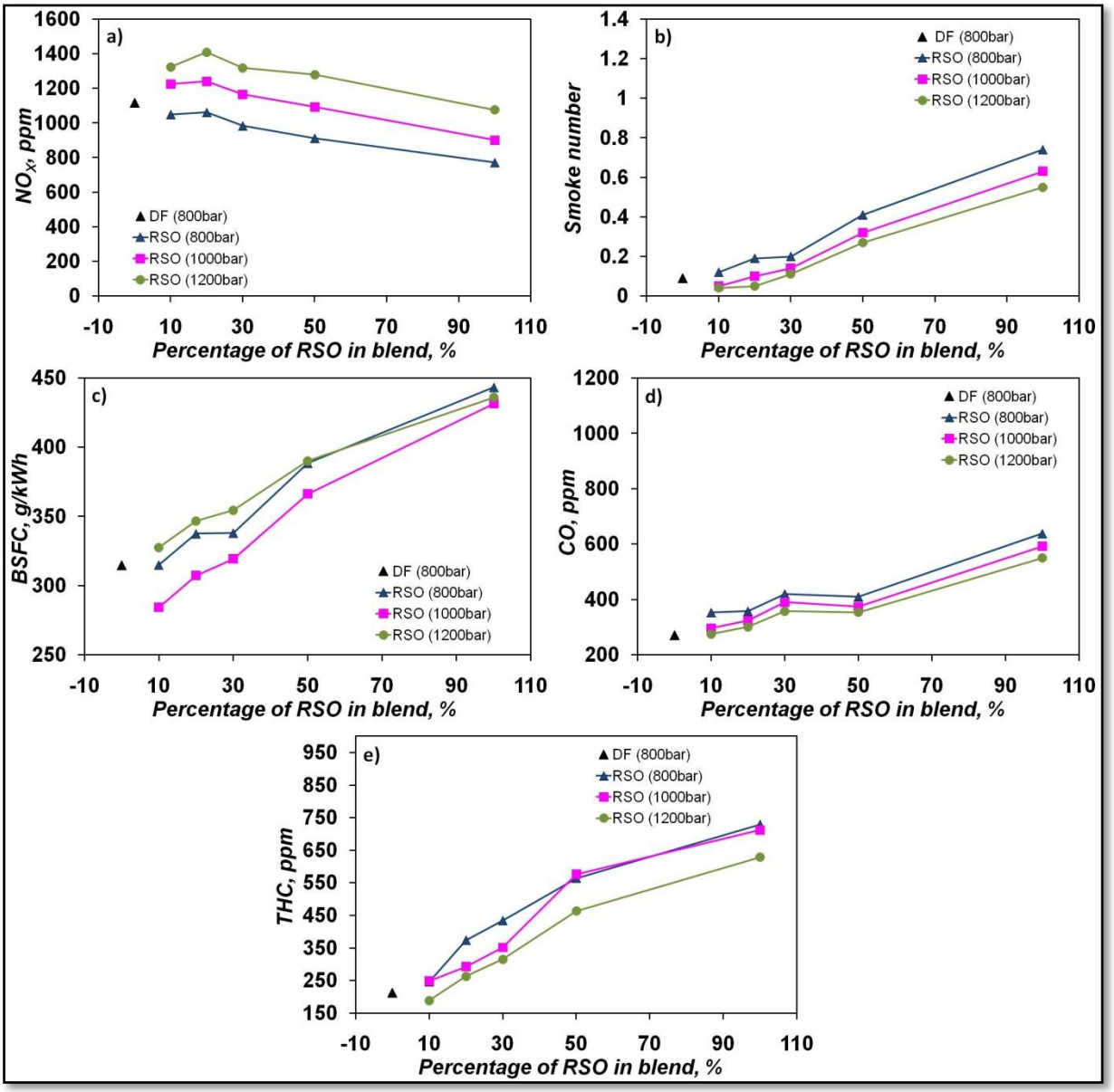

Fig. 4.2.2.3. The influence of fuel injection pressure on: a) nitrogen oxides emissions, b) smoke number, c) brake specific fuel consumption, d) carbon monoxide emission, e) total unburned hydrocarbons emissions.

Figure 4.2.2.3b shows the variations in the soot emissions for RSO and their blends under different injection pressures and for diesel. It is noticeable that the soot emissions for RSO and their blends are lowered by increasing the fuel injection pressure. Higher injection pressure leads to the formation of smaller fuel droplets and faster fuel vaporization due to better entrainment which eventually results in the reduction of smoke emissions. It is also evident that as the concentration of RSO in the blend increases, the soot emission rises. When compared against diesel under the same fuel injection pressure of 800 bar, it can be seen that the soot emissions from RSO are much higher. However, by increasing the injection pressure of the fuel blends from 800 bar to 1200 bar, it is possible to reduce the soot emissions below the diesel soot levels for the blends of up to 30% of RSO. For blends greater than 30% RSO, the soot emissions are higher than diesel even at higher injection

pressures. The high soot yield for RSO and their blends are mainly attributed to fuel properties, such as high viscosity, high sulphur and phosphorous content. In Table 3 it could be seen that several properties of RSO do not comply with the DIN V 51605 specifications. A high content of sulphur and phosphorous in RSO causes higher soot emissions. At the same time, the presence of relatively high oxygen content when compared to that of diesel should favour the soot oxidation process which tends to reduce SN. These two processes are in competition against each other. However, the content of sulphur and phosphorous seem to be dominant during combustion. Although, the RSO was preheated to the temperature of up to 70°C, its viscosity is still higher than that of diesel, leading to poorer atomization and formation of relatively larger size droplets. This causes poor air utilisation, incomplete vaporization and locally rich mixtures which eventually result in a higher production of soot from the combustion of RSO. A longer duration of combustion, particularly the diffusion combustion also contributed to higher smoke number.

The Brake Specific Fuel Consumption (BSFC) for diesel, RSO and their blends is shown in Figure 4.2.2.3c. It could be seen that the BSFC for RSO and their blends is higher than that of diesel under the same fuel injection pressure of 800 bar. The BSFC increases with higher concentration of RSO in the blend, attributed to lower calorific value of RSO and its blends compared to that of diesel fuel. In order to maintain the engine at the same load, more fuel was injected for RSO and its blends because of their lower energy content when compared to diesel. The BSFC for 100% RSO increases by 41 % compared to that of diesel under the same operating conditions. When the fuel injection pressure was increased from 800 bar to 1000 bar the BSFC for RSO and its blends decreased. However, for the blends of 10%, 20% and 30% of RSO, the BSFC was even lower compared to that of diesel. The benefit of lower fuel consumption was achieved through the higher momentum of the fuel jet by increasing the fuel injection pressure from 800 bar to 1000 bar. This leads to increased entrainment, better air utilisation and eventually more efficient combustion. However, when the fuel injection pressure was further increased from 1000 bar to 1200 bar, the BSFC deteriorated and increased even more compared to the case of 800 bar fuel injection pressure. The further increase in the fuel injection pressure should lead to better entrainment and better combustion, but in the case of RSO and its blends a penalty of higher BSFC could be observed. Similar effects of unclear trends in the fuel consumption have been reported for different fuel injection pressures [76]. As previously mentioned the addition of RSO to the blend should increase the BSFC. However, almost the same values as for diesel can be seen for 10% RSO at 800 bar of injection timing. This is attributed to higher error obtained during measurements done by the burette for all alternative fuels.

Figures 4.2.2.3d and e show the variation of CO and THC emissions for RSO, its blends at different fuel injection pressures and for diesel. In Figure 4.2.2.3d it can be seen that for RSO

and its blends, the CO emissions are higher when compared to those of diesel. Moreover, the CO emission increases with a high concentration of RSO in the blend. Under the same engine operating conditions, the CO emission from 100% RSO is around 135% higher when compared to that of diesel. It is also evident (Figure 4.2.2.3d) that as the fuel injection pressure increases, the CO emission decreases. However, by operating the engine with a blend of 10% RSO at the fuel injection pressure of 1200 bar, the CO emission is comparable to that of diesel. Figure 4.2.2.3e shows the variation of the THC emissions for diesel, RSO and its blends at different fuel injection pressures. As the concentration of RSO in the blend increases, the THC emissions are higher. The THC emissions decrease with a high fuel injection pressure. However, the general emission trends for both THC and CO are similar. The THC emissions for the 100% RSO are around 243 % higher compared to those of diesel. Both CO and THC emissions are the products of incomplete combustion and they tend to decrease with higher injection pressures. The unburned hydrocarbons emissions are generally formed as a result of flame quenching. The formation of higher CO and THC emissions with increasing concentration of RSO in diesel blends are strongly related to the higher viscosity of vegetable oils. Higher viscosity also leads to longer spray penetration. As a result, wetting of the cylinder walls eventually leads to the formation of higher CO and THC emissions by incomplete combustion.

4.2.3 The influence of EGR

The EGR is one of the strategies most effectively used to reduce the NO_x emissions in diesel engines. However, the addition of the EGR leads to an increase of the soot emissions [77-80]. In this section, the effect of using EGR on the combustion and emission performance of RSO will be discussed.

COMBUSTION CHARACTERISTICS

Figures 4.2.3.1 show the variation of the in-cylinder pressure, its peak and the oxygen concentration in the inlet air, as well as the heat release rate under different levels of EGR. In this study the temperature of the inlet gas was not measured as it was not able to do with current engine setup. In Figure 4.2.3.1a it can be seen that the in-cylinder pressures for 100% RSO at 0% EGR are lower when compared to diesel under the same engine operating conditions. The addition of 10% and 20% EGR under RSO operation did not show any significant difference in the in-cylinder pressure traces and in the in-cylinder pressure peaks. In Figure 4.2.3.1b it can be seen that as the concentration of RSO in the blend increases, the peak of the in-cylinder pressure decreases. As the EGR percentage increases, the in-cylinder pressure peak shows a marginal decrease in its magnitude. Generally, as the exhaust gases

are introduced into the combustion chamber, the concentration of oxygen that will be available to participate in the combustion lowers. This eventually affects the ignition, combustion and soot processes. Moreover, the presence of higher specific heat capacity gases in the combustion chamber causes the global temperature of the charge in the cylinder to decrease, which affects NO_x formation processes. As the percentage of EGR increases, the effect of lower oxygen concentration and the lower bulk gas temperature will delay the ignition process. This effect should be reflected in the in-cylinder pressure trace. However, in this study, under low load operating condition and under moderate percentages of EGR, the reduction in the inlet oxygen concentration due to EGR was not significant, as shown in Figure 4.2.3.1c. Similar effects of negligible difference in the in-cylinder pressure traces due to low oxygen concentration have been observed in the already published literature [81]. In addition to this, the presence of the oxygen content in the RSO and its burnt gases would also contribute to the existing oxygen content of the inlet charge under EGR operation. Thus the net effect of EGR under the RSO operation results in a marginal reduction of the oxygen concentration of the inlet charge.

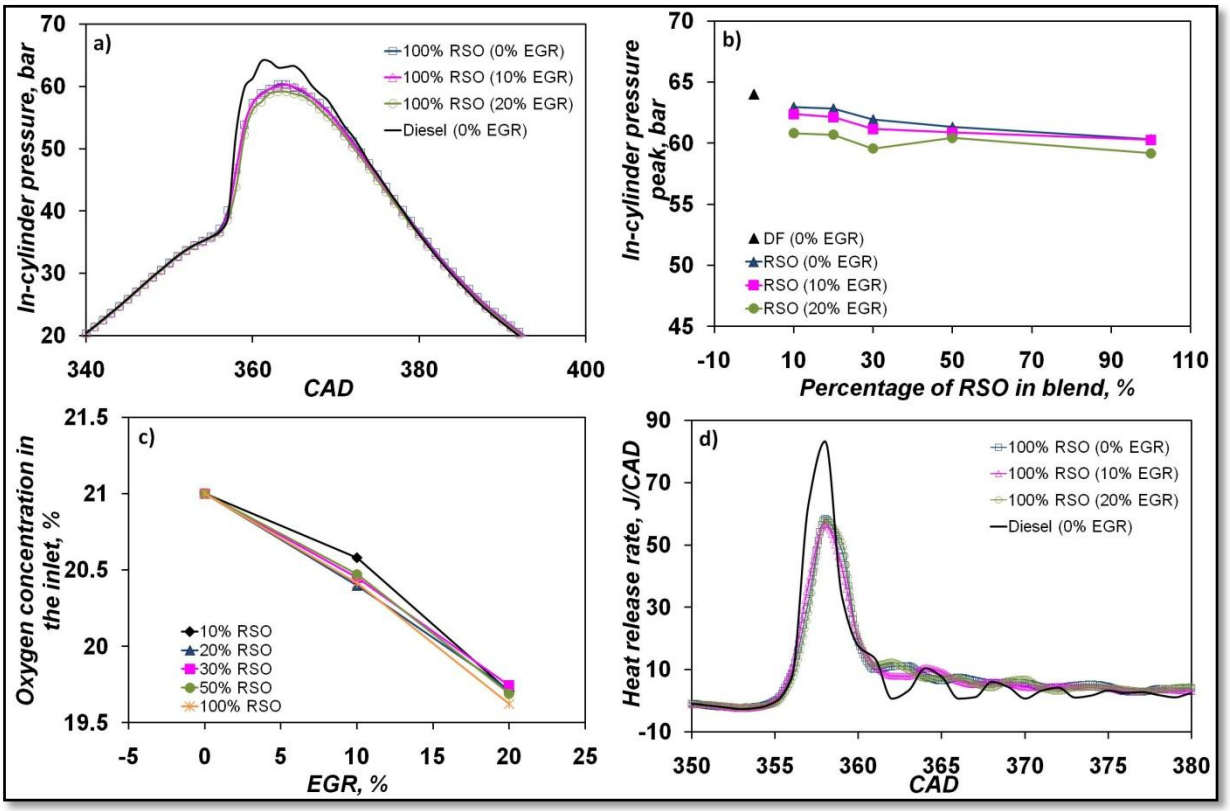

Fig. 4.2.3.1. The influence of EGR on: a) in-cylinder pressure, b) in-cylinder pressure peak, c) oxygen concentration in the inlet, d) heat release rate.

Figure 4.2.3.1d shows the variation of the heat release rates for 100% RSO under different percentages of EGR and for diesel without EGR. It is noticeable that the heat release rate for 100% RSO is lower than that of diesel. Moreover, the effect of adding different percentages

of EGR on the RSO heat release rates is negligible. Thus differences in the ignition delay and in the position of CA50 point for RSO and its blends for different percentages of EGR are negligible and their variations are only within their fluctuation limits.

Figures 4.2.3.2a and b show the duration of combustion in the premixed and diffusion phases as well as the amount of heat released during these phases. The duration of the premixed phase for RSO and its blends is almost constant with a high concentration of RSO in the blend and their magnitudes are always lower than those of diesel. In contrast, the duration of diffusion combustion is always longer for RSO and its blends. In the case of 10% RSO, an increase in the percentage of EGR leads to longer duration of combustion in the diffusion phase. It is also noticeable that the duration of combustion in the diffusion phase increases with higher concentration of RSO in the blend for any given percentage of EGR. Even though the duration of the premixed combustion is shorter than diffusion combustion, heat released during the short premixed combustion phase is much higher than the heat released from the long diffusion combustion phase. Thus, the magnitude of heat released in the premixed combustion phase for RSO and its blends (Figure 4.2.3.2b) is always lower than in the case of diesel and almost constant with increasing concentration of RSO in the blend.

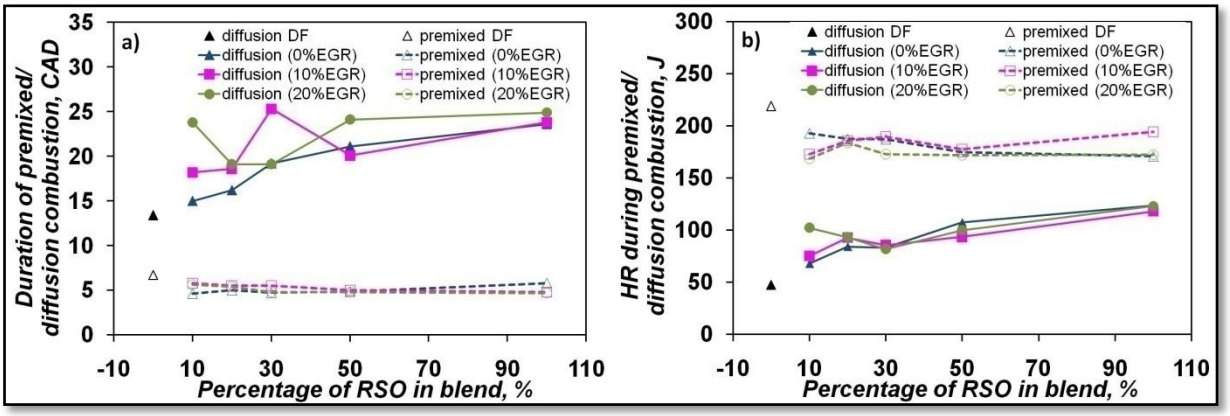

Fig. 4.2.3.2. The influence of EGR on a) duration of combustion in the premixed and diffusion phases, b) heat release during the premixed and diffusion phases.

On the contrary, the heat released during the diffusion phase is always higher than that of diesel and increases with higher concentration of RSO in the blend. For 10% RSO blend, the effect of EGR on the amount of heat released during the diffusion as well as the premixed phases is evident. For the rest of the blends, the trends associated with the effect of EGR on the duration and magnitude of heat released during the premixed and diffusion phases are not clear. The results presented from the combustion analysis (Figures 4.2.3.2a and b) show that the duration and the amount of heat released during the premixed combustion phases suggest that the NO_x emissions for RSO can be lower when compared to that of diesel. Moreover, the trends from the duration of combustion and heat released in the diffusion

phase suggest that the soot emissions for RSO could be higher than that of diesel. They can further increase with higher concentration of RSO in the blend.

EMISSION CHARACTERISTICS

Figures 4.2.3.3a – e show the variation of nitrogen oxides emissions (NO_x), smoke number (SN), brake specific fuel consumption (BSFC), total unburned hydrocarbons emissions (THC) and carbon monoxide emissions (CO) for different blends of RSO. In Figure 4.2.3.3a, the NO_x emissions tend to decrease as the percentage of RSO in the blends increases. The highest reduction of the NO_x emissions was achieved in the case of 100% RSO. Despite small differences in the in-cylinder pressure peaks for different percentages of EGR (Figure 4.2.3.1b), the addition of EGR caused an effective reduction in the amount of NO_x emitted from RSO and its blends. When the engine was operated using RSO and its blends, the average reduction in NO_x emissions of about 39% was achieved by using 20% EGR. However, a significant reduction of about 60% was achieved by using neat RSO with 20% EGR when compared against diesel under the reference operating condition. When compared to diesel fuel, RSO has a lower in-cylinder pressure and temperature due to higher viscosity which contributes to charge cooling. In addition to this, the presence of higher specific heat capacity of the exhaust gases from EGR lowers the global temperature in the combustion chamber and the flame temperature, which subsequently reduces the reaction rates that are leading to the formation of NO_x emissions. As discussed above, the lower heat release rates and the shorter duration of the premixed combustion (Figure 4.2.3.2a and b) for RSO also results in a favourable environment for lowering the NO_x emissions.

Figure 4.2.3.3b shows the effects of EGR on soot emissions from RSO and its blends and from diesel fuel under reference operating conditions. It is evident that the soot emissions are highest for 100% RSO and tend to increase with a higher percentage of RSO in their blend. Moreover, the soot formation rate is enhanced as the percentage of EGR in the cylinder increases. When the engine was operated using RSO and its blends, an average increase in soot emissions of about 58% was achieved using 20% EGR. However, a significant increase of approximately 1160% was achieved by using neat RSO with 20% EGR when compared with diesel under the reference operating condition. The addition of the exhaust gases into the inlet manifold results in a slight reduction of oxygen content in the cylinder. The formation as well as the oxidation process of the soot is primarily influenced by the engine operation on gradually richer mixtures and slightly by lower oxygen content of the fresh charge, due to EGR addition. The combined effect of fuel properties, lower combustion temperature and lower oxygen content reduces the soot oxidation process which eventually results in higher soot emissions.

Figure 4.2.3.3c shows the brake specific fuel consumption for RSO, its blends at different percentages of EGR and for diesel. Due to the low calorific value of RSO, the brake specific fuel consumption is higher than that of diesel fuel and it increases with higher concentration of RSO in the blend. At lower percentages of EGR, the variation in BSFC was not clear. However, the addition of 20% EGR resulted in lower BSFC for all RSO blends.

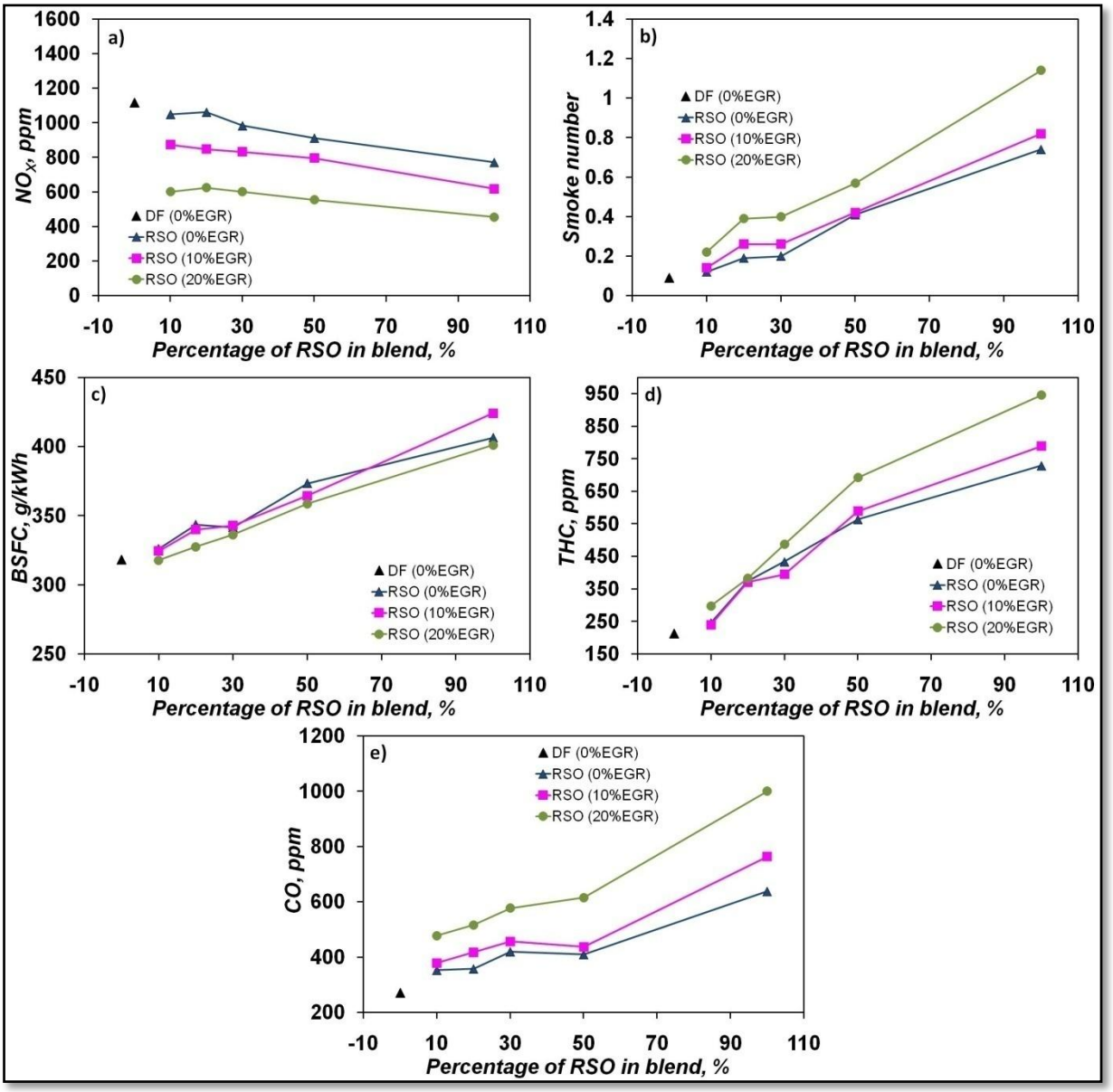

Fig. 4.2.3.3. The influence of EGR on: a) nitrogen oxides emissions, b) smoke number, c) brake specific fuel consumption, d) total unburned hydrocarbons emissions, e) carbon monoxide emission.

Figure 4.2.3.3d and e provide an overview of the total hydrocarbons (THC) and carbon monoxide (CO) emissions. Due to the EGR addition, the engine operates on rich mixture resulting in poorer air utilisation by the fuel spray leading to higher CO and THC emissions. Thus the THC and the CO emissions for RSO and its blends increase with higher percentages of EGR. The THC and CO emissions also increase with a higher concentration of RSO in the

blend. Generally, the unburned hydrocarbons are formed as the result of flame quenching effects and incomplete combustion. In this case, the higher concentration of THC emissions from RSO occurs mainly because of the longer fuel spray core compared to that of diesel [51]. The average increase in the THC emissions for RSO and its blends when comparing 0% EGR and 20% EGR was about 16% while the maximum increase in THC emission between pure RSO at 20% EGR and diesel under reference operating condition was about 345%. Incomplete combustion of RSO leads to a relatively high concentration of CO emissions when compared with diesel. The average increase in the CO emissions for RSO and its blends when comparing 0% EGR and 20% EGR was about 44% while the maximum increase in CO emission between pure RSO at 20% EGR and diesel under reference operating condition was about 270%. The recirculation of exhaust gases into the cylinder effectively reduces the NO_x emissions but the SN, THC and CO emissions are higher resulting in lower combustion efficiency.

4.2.4 The influence of injection timing

COMBUSTION CHARACTERISTICS

Figures 4.2.4.1a-d show the variations of the in-cylinder pressure, its peaks, the heat release rate and the ignition delay for RSO, its blends at different fuel injection timings and for diesel fuel. The in-cylinder pressure data in Figure 4.2.4.1a clearly shows the shift in the combustion phase and its corresponding pressure peaks. The late injection of fuel in the compression stroke or even at TDC leads to a lower pressure peak due to the occurrence of combustion in the expansion stroke. In Figure 4.2.4.1b it can be seen that the in-cylinder pressure peak decreases significantly for retarded injection timing and slightly decreases with a higher concentration of RSO in the blend at all injection timings. When compared against diesel, the average differences in the pressure peaks for RSO and its blends are about 4%, 12% and 20% for the injection timings of 9, 4 and 0 deg bTDC respectively.

In the case of the heat release rate (Figure 4.2.4.1c), it is noticeable that the retardation of the injection timing causes a reduction in the heat release rate and the combustion phase is shifted towards the expansion stroke. The position of the CA50 point is at about 361.5, 365 and 370.5 CAD for the injection timings of 9, 4 and 0 deg bTDC respectively. A lower peak of the heat release rates for RSO is due to poor atomization and vaporization of larger fuel droplets caused by higher viscosity. The ignition delay (Figure 4.2.4.1d) for diesel was found to be approximately 4 CAD and was measured as the difference between SOC and SOI (Section 3.4.3). For up to 20% of the blend, the ignition delay at all injection timings was

within the fluctuating limits of diesel. However, for the blends containing more than 30% of RSO, the ignition delay was lower than that of diesel fuel for the injection timings of 4 and 0 deg bTDC. Moreover, a slight reduction of ignition delay with higher concentrations of RSO in the blends can be seen, especially for these two injection timings. A small fraction of oxygen in RSO composition, increased fuel temperature, higher in-cylinder pressure and temperature before the start of injection can help to ignite the fuel faster, thus shorter ignition delay can be observed for retarded injection timing

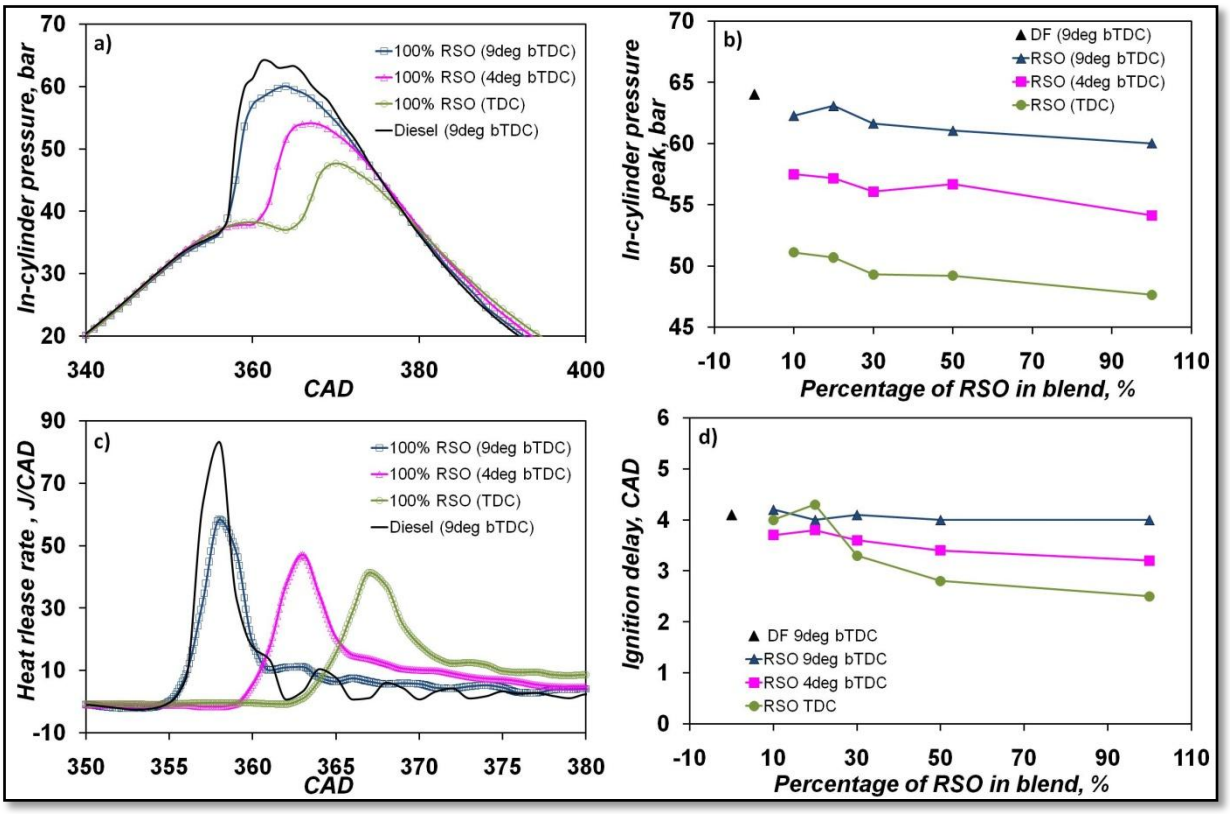

Fig. 4.2.4.1. The influence of fuel injection timing on: a) in-cylinder pressure, b) in-cylinder pressure peak, d) heat release rate, e) ignition delay..

Figure 4.2.4.2a shows the duration of premixed and diffusion combustion phases for different blends of RSO under different injection timings. It is noticeable that for the RSO blends, the duration of the premixed combustion phase is shorter compared to that of diesel fuel and the different fuel injection timings did not show any significant effects on the duration of the premixed phase. In addition to this, the duration of the premixed combustion was not significantly affected by increasing the concentration of RSO in the blend. On the contrary, the duration of combustion in the diffusion phase for RSO and its blends is always longer than that of diesel fuel. As the concentration of RSO in the blend increases, the duration of diffusion combustion phase becomes longer but the effect of the injection timing on the diffusion combustion phase is inconclusive.

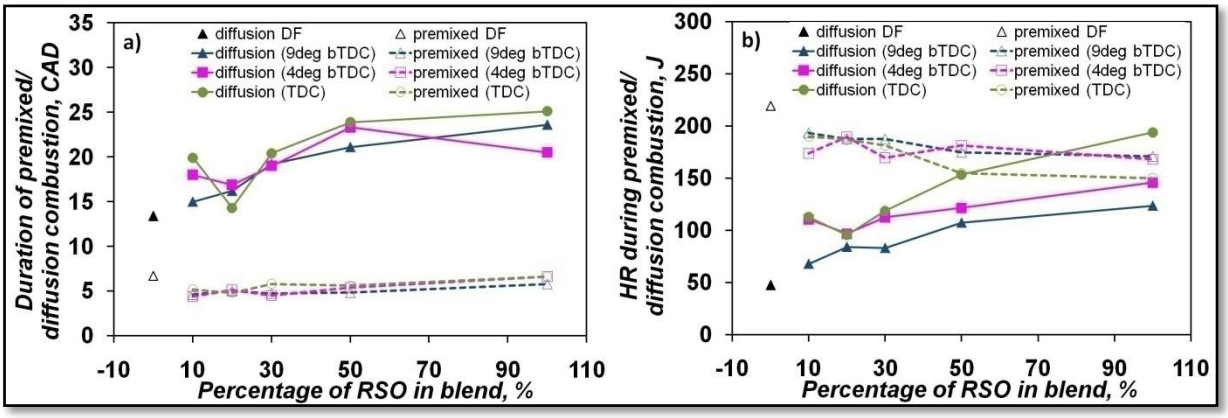

Fig. 4.2.4.2. The influence of fuel injection timing on a) duration of combustion in the premixed and diffusion phases, b) heat release during the premixed and diffusion phases.

Figure 4.2.4.2b shows the amount of heat released during the premixed and diffusion combustion phases for RSO and its blends at different injection timings. The amount of heat released in the premixed combustion phase is lower compared to that of diesel fuel. With increasing concentration of RSO in the blend, the amount of heat released during the premixed combustion phase gradually decreases while its duration is almost constant (Figure 4.2.4.2a). The injection timing did not have any significant effect on the duration and magnitude of heat that was released during the premixed combustion phase. In the case of the diffusion combustion phase, the magnitude of heat released is higher than that for diesel and it increases with higher concentration of RSO in the blend. Moreover, for the retarded injection timing, RSO produces more heat in diffusion combustion. It can also be noticed that in the case of injection at TDC for pure RSO, the heat released in the diffusion phase is higher than the heat released in the premixed combustion phase.

EMISSION CHARACTERISTICS

The analysis obtained from the heat release is helpful for understanding the NO_x and soot emissions from RSO and its blends. A lower magnitude of heat released in the premixed phase, may lead to lower NO_x emissions compared to that of diesel. On the other hand, higher heat release in the diffusion combustion phase leads to higher soot emissions. Furthermore, the retardation of the injection timing produces more heat in the diffusion phase, thus it can suggest that soot emissions for RSO and its blends could be higher at late fuel injection timing.

Figures 4.2.4.3a-e show the emission characteristics of NO_x, soot, Brake Specific Fuel Consumption, THC and CO for RSO and its blends for different injection timings. According to Figure 4.2.4.3a, RSO and its blends show lower NO_x emissions than diesel. Higher viscosity of RSO causes a global decrease in the in-cylinder and flame temperatures. Therefore, as the concentration of RSO in the blend increases, the NO_x emissions relatively decrease. In addition to this, the retarded injection timing significantly reduces the NO_x emissions

because of the low in-cylinder temperature resulting from the shift of the combustion into the expansion stroke. Compared to diesel operation, a maximum reduction of NO_x emissions of 67% was achieved for 100% RSO when the fuel was injected at TDC. The minimum reduction was approximately 6% in the case of 10% RSO when the fuel was injected at 9 deg bTDC. The NO_x formation during combustion mainly depends on the Zeldovich mechanism where formation reactions are more intensive in a high temperature environment leading to higher NO_x emissions [1]. In the case of diesel engines, the highest in-cylinder temperature occurs during the premixed combustion phase where the formation of NO_x is dominant. The previous analysis of HRR (Figure 4.2.4.2a and b) clearly shows that a lower heat release rate and a shorter premixed combustion occur for RSO and its blends, which eventually results in lower NO_x emissions.

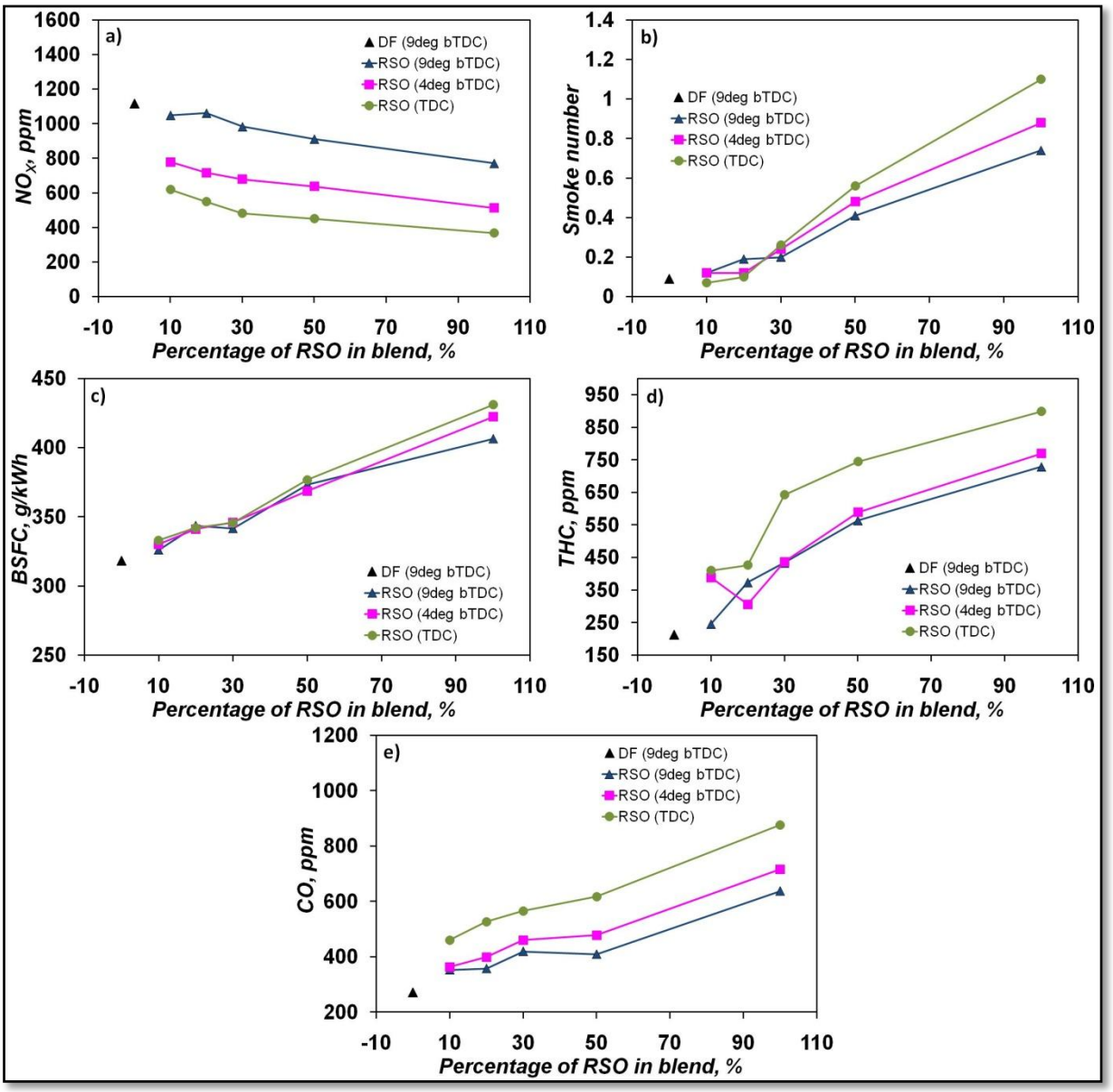

Fig. 4.2.4.3. The influence of fuel injection timing on: a) nitrogen oxides emissions, b) smoke number, c) brake specific fuel consumption, d) total unburned hydrocarbons emissions, e) carbon monoxide emission.

Figure 4.2.4.3b shows the measured smoke number for RSO, its blends at different injection timings and diesel fuel under reference engine operating condition. Generally, the soot emissions for RSO and its blends increase with a higher concentration of RSO in the blend. It can be seen that the smoke number is the highest for retarded injection timing. It is interesting to note that for 10-20% RSO blends, the smoke numbers are comparable to that of diesel when the blends are operated under retarded injection timing. On the other hand, the maximum difference between diesel and 100% RSO at TDC is as high as 1122%. Poor atomization due to the high viscosity of the RSO leads to an increase in the soot formation during the diffusion combustion phase. Less efficient air utilization of the larger fuel droplets also plays a significant role. Moreover, the retarded injection timing increases the soot emissions due to poor oxidation process. This process implies lower combustion temperatures obtained mainly in the expansion stroke. In addition to this, unfavourable fuel properties, such as high sulphur and phosphorous content of RSO emphasize the high soot emissions. Previous calculations have shown that the combustion of RSO is longer. It is increasing with a high concentration of RSO in the blend and retarded injection timing which favours soot formation. The combustion of high molecular weight compounds [63], different composition, chain length and the number of carbon double bonds in the structure of the RSO's fatty acids [82,83] also lead to high soot formation.

The Brake Specific Fuel Consumption for RSO and its blends (Figure 4.2.4.3c) is higher when compared against diesel, the main reason being the lower calorific value. The BSFC increases with a higher concentration of RSO in the blend. The effect of injection timing on the BSFC is not clear for the blends but it increases for pure RSO operation as the fuel injection timing is retarded. However, due to the less efficient combustion in the expansion stroke, compared to the combustion under normal fuel injection timing, more fuel will be consumed in order to achieve the same engine load. The maximum increase in the BSFC was about 35% between diesel and 100% RSO at TDC injection timing.

Figures 4.2.4.3d and e show the variation of THC and CO emissions for different blends of RSO in diesel and also for different fuel injection timings. Both emissions show a similar trend: CO and THC are higher compared to diesel and increase with a higher concentration of RSO in the blend. The effect of the retarded injection timing is the same for both emissions but the trends are clearer in the case of CO emissions. Late injection causes much higher THC and CO compared to the reference injection timing. The maximum increase in THC and CO between diesel and 100% RSO at TDC injection timing is about 324% and 223% respectively. As mentioned above, both emissions are formed as a result of incomplete combustion, mainly due to the combustion taking place at low temperature in the expansion stroke. Moreover, the spray-wall impingement could be much greater for the injection of fuel at TDC.

4.2.5 Summary

In the case of compression ignition engines, the soot and NO_x emissions are the most important as they are higher than those emitted from spark ignition engines and are under strict emission regulations. For this purpose, summarised analysis was made to show the effect of different injection strategies and EGR on NO_x and soot emissions. Well known for diesel engines, the soot - NO_x trade off has been proposed in Figure 4.2.5.1. The data shown in Figure 4.2.5.1 was limited to 100%, 50% and 30% RSO blends as the rest of the blends have shown the same trends but at respectively lower level of soot and higher level of NO_x emissions. By increasing the injection pressure, it can be clearly seen that for a given RSO blend, the smoke number can be effectively reduced with a simultaneous increase in the NO_x emission, moving the operating point towards the right-down side from the reference operating point. The use of EGR and retarded injection timing provides significant reduction in NO_x emissions but an increase in the smoke number shifting operating points towards the left-up side from the reference operating point. The use of the retarded injection timing seems to achieve better results than the use of the EGR strategy. However, from the fuel economy point of view high EGR would be better and high smoke number can be reduced by after treatment systems. For given RSO blend, the retarded injection timing provides less smoke number and less NO_x when compared to the EGR strategy. For instance, in the case of EGR addition, combustion characteristics such as ignition delay, in-cylinder pressure peak, and combustion phase maintain almost constant and have been noticed to be in the fluctuation limits. However, the retarded injection timing provides a shifted combustion phase towards the expansion stroke, lower in-cylinder pressure peaks and also shorter ignition delays.

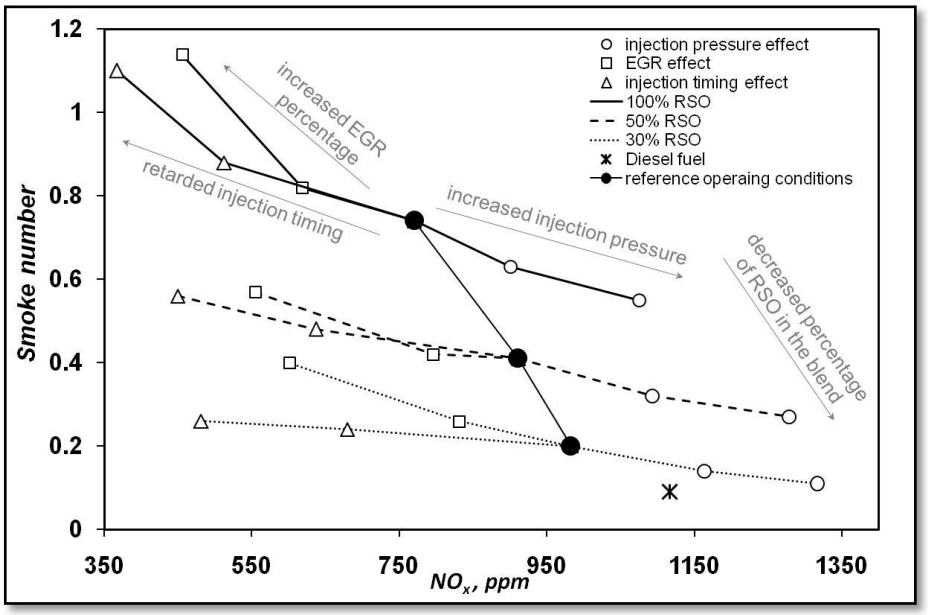

Fig. 4.2.5.1. The soot – NO_x trade of as summarized effects of injection pressure, EGR and injection timing.

When comparing Figures 4.2.2.2b, 4.2.3.2b and 4.2.4.2b, it is interesting to note that for different injection pressures and for different EGR percentages the variations in the premixed heat release for a given blend are minimum. However, the heat released in the premixed phase varies significantly with different injection timings. It can be seen that as the concentration of RSO in the blend increases, more heat is released in the premixed phase while the injection timing is retarded. Their magnitude approached the magnitude of the heat that is released in the diffusion combustion phase. Retarded injection timing provides different combustion characteristics, as the entire combustion takes place in the expansion stroke, which are reflected in the heat released during the premixed and diffusion phases.

As the concentration of RSO decreases at the given operating condition the position of the reference operating point in the trade off moves to right-down side increasing NO_x and significantly reducing soot emissions. Generally, a lower concentration of RSO leads to lower viscosity of the blend which significantly improves combustion characteristics that result in lower soot but higher NO_x emissions.

This work provides the influence of a single parameter on the emission and combustion characteristics from RSO fuel. Therefore, by combining injection timing and injection pressure, even better results than those for diesel fuel can be obtained. It can be seen that the high injection pressure improves combustion, without incomplete combustion compounds in the exhaust gases. An operation at such a high injection pressure should allow the reach of a stable combustion and engine operation even at an injection timing of 2 or 3 deg aTDC. This strategy can give sufficient reduction of NO_x emissions for their further increase by high injection pressure. The magnitude of reduction of NO_x caused by retarded injection timing is much higher that the magnitude of increase in NO_x caused by high injection pressure, eventually resulting in lower NO_x level compared to that of diesel fuel. The opposite effect could be achieved for soot emissions as retarded injection timing leads to a high smoke level. However, this could be reduced by high injection pressure. In this case, more research can be done for further analysis and quantifying the effect of combining injection pressure and injection timing parameters.

4.2.6 Conclusions

In this experimental study, the effects of different engine operating conditions such as injection pressure, injection timing and EGR on the combustion and emission performance of rapeseed oil and its blends with diesel fuel have been investigated and the conclusions are summarised as follows:

Generally, when the RSO was used under the reference operating conditions a lower in-cylinder pressure and heat release rate was observed when compared to diesel. The

combustion duration of RSO was longer than that of diesel due to its higher viscosity and the presence of heavier molecular weight fractions. The smoke number and the gaseous emissions, such as CO and THC, are higher for RSO compared to diesel. On the other hand, the NO_x emissions for RSO are around 6% lower than that of diesel. A decrease in NO_x emissions was observed even for a small addition of 10% vegetable oil in diesel. The THC, CO, soot emissions and BSFC show an increase, while the NO_x emissions tend to decrease with a high concentration of RSO in the blend.

The increase of the injection pressure from the reference engine operating condition resulted in improved combustion and shorter ignition delay for RSO and its blends. A shorter ignition delay of RSO at high injection pressure also advanced the combustion, increasing the in-cylinder pressure, heat release rate and their peaks respectively. By increasing the injection pressure, the exhaust SN, THC and CO emissions were reduced. However, the NO_x emissions increased becoming higher than those of diesel.

The increase of the EGR from the reference engine operating condition did not have any significant effect on the in-cylinder pressure and HRR but their magnitudes were lower than those of diesel. Increasing the EGR to 20% resulted in a further reduction of NO_x emissions. By increasing the concentration of RSO in the blend, the NO_x emissions decreased by more than 65% for the case of 20% EGR. The benefit of NO_x reduction was achieved at the expense of higher SN, THC and CO emissions.

Retarding the fuel injection timing from 9 deg bTDC to TDC caused a shift of the combustion towards the expansion stroke and resulted in lower in-cylinder pressure peaks for RSO and its blends. Moreover, the NO_x emissions were reduced while the other emissions, such as THC and CO, were increased. It also prolonged the combustion duration which led to the penalty of higher SN.

By varying these engine operating parameters and varying the concentration of RSO in the blend, the combustion and emission characteristics can be adjusted to achieve similar or even better results than diesel fuel. Consequently, RSO and its blends can fully or partially replace diesel fuel. For instance, by simultaneously retarding the injection timing and increasing the injection pressure, the soot emissions can be effectively reduced by maintaining low NO_x emissions, particularly for blends up to 30% RSO with diesel. In this case, the injection parameters play a significant role in decreasing the soot emissions.

4.3 Simultaneous reduction of both soot and NO_x from 30% RSO blend

4.3.1 Test matrix

In this study, an attempt has been made to reduce the soot emission from the combustion of RSO to obtain the diesel equivalent level of soot emissions. A reduction of the soot emissions from combustion of RSO was done by changing injection parameters such as injection pressure and injection timing. Tests were carried out at a constant load of 2.7 bar BMEP at 2000 rpm of engine speed. In the case of this test, higher engine speed was chosen because of higher EGR stability. As previously mentioned, the engine EGR regulation is based on the air mass flow sensor. At such a higher engine speed the air mass flow was measured more precisely, resulted in higher accuracy of EGR rate. The reference injection parameters at this particular load correspond to an injection pressure of 800 bar and an injection timing of 9 deg bTDC. These parameters were swept from 800 bar to 1200 bar and from 13 deg bTDC to TDC to obtain the diesel equivalent level of soot emissions for RSO. Under the same soot levels, in-cylinder pressure, exhaust gaseous emissions and exhaust soot particles size distributions were compared between RSO and diesel fuel.

4.3.2 Results

Experimental results for pure RSO as well as for 10%, 20%, 30% and 50% blends of RSO with diesel fuel show a strong reduction in the NO_x emissions. On the contrary, the smoke number increases with higher concentration of RSO in the blend (Figure 4.3.2.1).

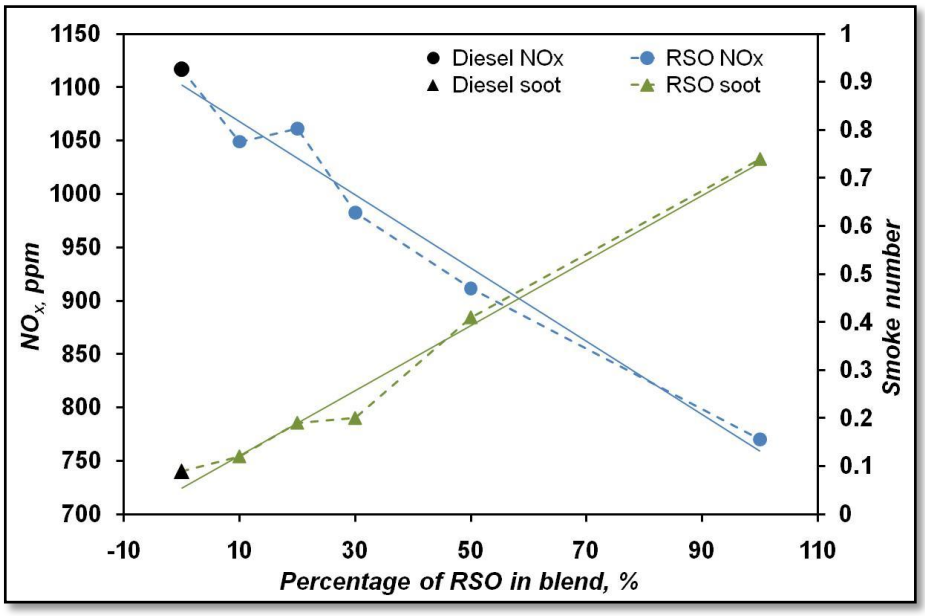

Fig. 4.3.2.1. The NO_x emissions and smoke number trends for RSO, diesel and their blends of 10, 20, 30, 50 % of RSO addition.

It is well known that RSO has a very high kinematic viscosity compared to diesel. Even after heating RSO to temperatures of up to 70 °C, its viscosity is around 10 cSt, approximately 7 cSt higher than that of diesel fuel. High viscosity causes poorer atomization and mixing which subsequently affects the combustion process. Poor evaporation characteristics of RSO lead to higher charge cooling, lower in-cylinder temperatures and incomplete combustion. Consequently, the in-cylinder pressures and in-cylinder temperatures are lower than in the case of diesel, resulting in lower NO_x emissions. On the other hand, the duration of combustion is longer due to slower air/fuel mixing which causes higher soot emissions. In Figure 4.3.2.1 it can be seen that 100% RSO has the lowest NO_x and the highest soot emissions compared to other RSO blends and diesel fuel. As the concentration of RSO in the blend decreases, the NO_x emissions increase whereas the soot emission decreases. This effect can be partly related to lower viscosity of the blend. By using a blend of 50% RSO in diesel, the NO_x emissions are lowered by 18% and the soot emission increases by 355% compared to diesel. Similarly, by using a blend of 30% RSO in diesel, the NO_x emissions are lowered by 12% and the soot emission increases by 122% compared to diesel. In order to utilize the advantage of lower NO_x emissions from RSO, different fuel injection strategies were applied to reduce their soot levels to those of diesel under reference engine operating conditions (injection pressure of 800bar, injection timing of 9deg bTDC, 0% of EGR, engine speed of 2000 rpm and engine load of 2.7 bar BMEP).

Since the smoke number for 100% RSO is very high compared to diesel, a first attempt was made to reduce the soot emissions for 50% RSO blend. Figure 4.3.2.2 shows the strategies adopted to reduce soot emissions for the 50% RSO blend to the diesel equivalent level of soot emissions.

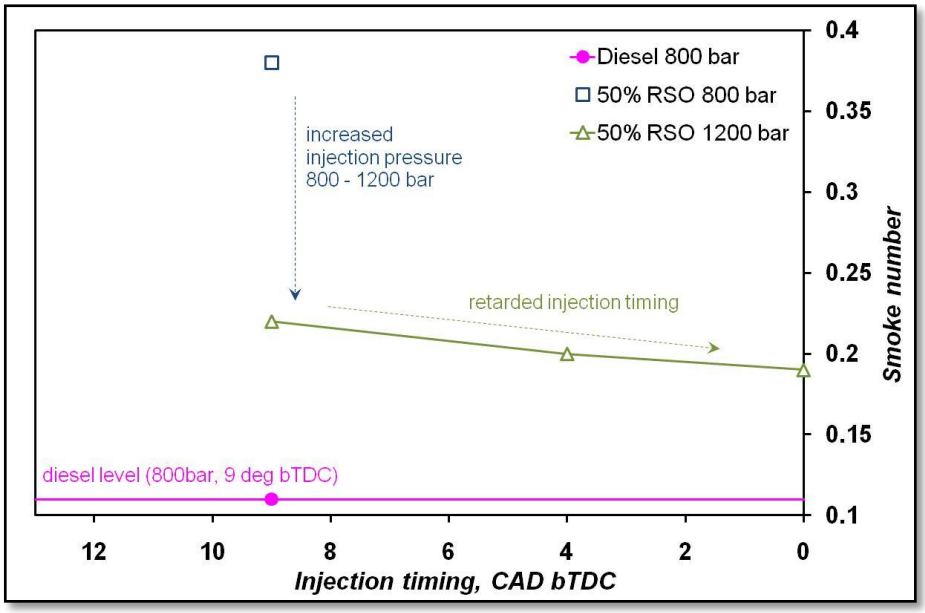

Fig. 4.3.2.2. The strategy adopted to reduce the soot emissions for the blend of 50% RSO.

It can be seen that by increasing the fuel injection pressure from 800 bar to 1200 bar, the smoke number was reduced from 0.7 to 0.2 but it was still higher than diesel. Higher injection pressure resulted in a better atomization and vaporization of 50% RSO blend. It also resulted in a better air entrainment, air/fuel mixing and shorter time for the soot precursors formation. At the injection pressure of 1200 bar, a further reduction of the soot emissions has been achieved by retarding the fuel injection timing. By sweeping the injection timing to TDC a simultaneous reduction of both soot and NO_x emissions has been obtained. Even though the injection parameters were set at the fuel injection timing of 0 deg bTDC and at a high injection pressure of 1200 bar, it was still not possible to reduce the soot emissions from 50% RSO to the same level of soot emitted from the combustion of diesel fuel. Under these conditions, the soot emission from 50% RSO is still higher by about 64% compared to diesel. Since the first attempt to reduce the soot from 50% RSO has not been successful, a second attempt was made for 30% RSO blend.

It can be seen from Figure 4.3.2.3 that the soot emission from 30% RSO blend was reduced to diesel soot levels for the fuel injection pressure of 1200 bar and the fuel injection timing of 3 deg bTDC. This strategy was applied only for academic purposes as from economical point of view retarded injection timing generates higher fuel consumption.

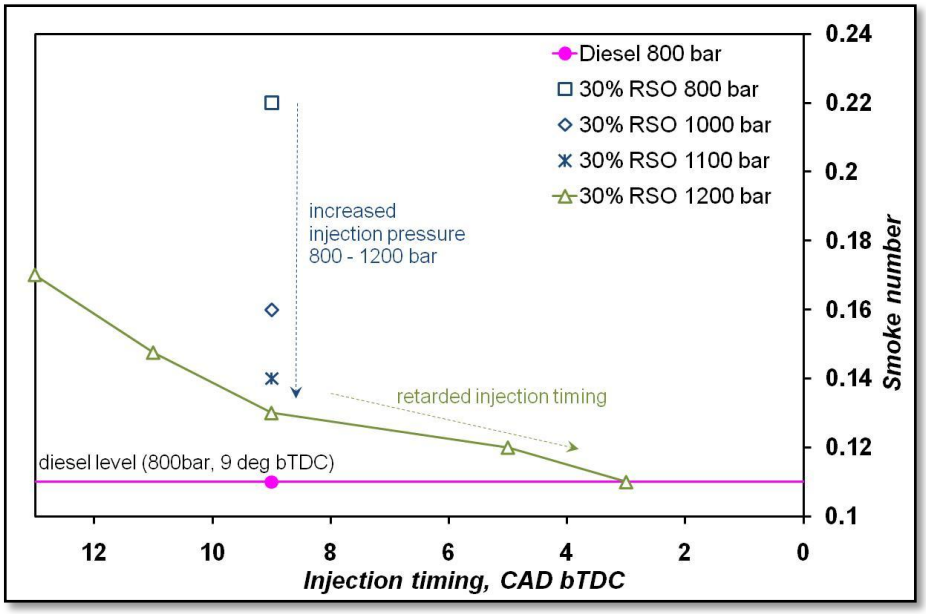

Fig. 4.3.2.3. The strategy adopted to reduce the soot emissions for the blend of 30% RSO.

Figure 4.3.2.3 also shows that the soot emission can be reduced even more by further retarding the fuel injection timing. This reduction can also be achieved by using RSO blends less than 30% in volume. On the other hand, even at an injection pressure of 1000 bar, the

diesel equivalent level of soot can be achieved in the case of 30% RSO. However, in this case, a further retardation of the fuel injection timing will be required.

Further analysis has been conducted to study the combustion and emission characteristics for diesel and 30% RSO under reference engine operating conditions as well as for 30% RSO under the diesel equivalent level of soot conditions. Figure 4.3.2.4a shows in cylinder pressures for diesel and 30% RSO at 800 bar, 9 deg bTDC and also for 30% RSO at 1200 bar, 3 deg bTDC (diesel soot equivalent conditions). Under reference engine operating conditions, the in-cylinder pressure for 30% RSO was lower than diesel and the combustion phase was slightly shifted. However, 30% RSO at diesel equivalent soot emissions showed a significantly shifted combustion phase and a lower in-cylinder pressure peak compared to diesel, because of retarded injection timing. The position of the CA50 point was about 360.4 CAD for diesel fuel and about 365.7 CAD for 30% RSO under the equivalent level of soot condition.

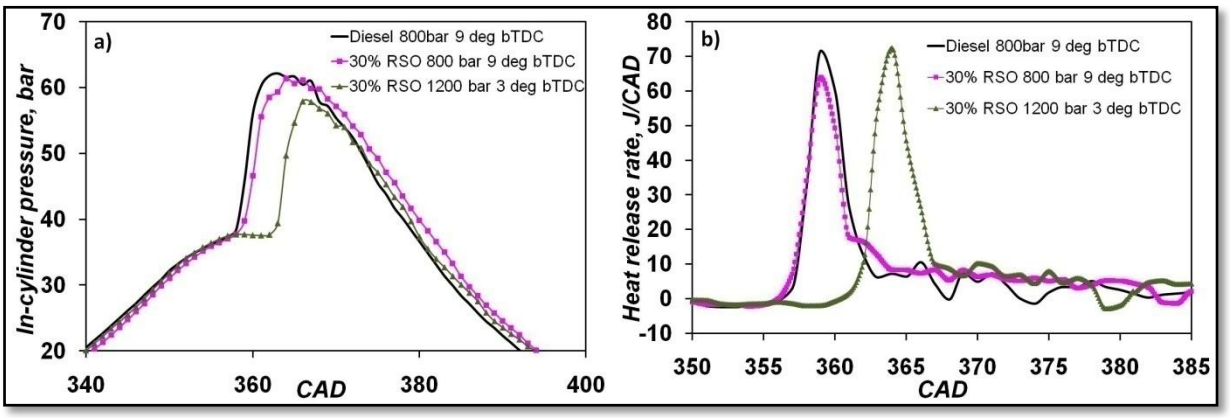

Fig 4.3.2.4. The diagrams of: a) the in-cylinder pressures, b) the heat release rates, for diesel, 30% RSO under standard engine operating conditions and for 30% RSO under diesel equivalent soot engine conditions.

On the other hand, it is noticeable that the heat release shapes are almost the same in all cases. However, the 30% RSO combustion has been shifted towards the expansion stroke (Figure 4.3.2.4b). It can also be seen that the 30% RSO under reference engine operating conditions has a lower peak of the heat release rate and a larger diffusion combustion phase compared to diesel. Lower in cylinder pressure causes lower in-cylinder temperatures, which eventually lead to lower NO_x emissions. However, the lower peak of the in-cylinder pressure for 30% RSO under the diesel equivalent soot conditions gives almost the same peak of the heat release rate as diesel. In this case, it can be noticed that higher injection pressure improves the combustion of the 30% RSO simultaneously maintaining a relatively lower combustion temperature.

Figure 4.3.2.5a shows the duration of combustion in the premixed and diffusion phases. In all cases, the duration of the premixed combustion phase was almost the same. When

comparing 30% RSO under the reference conditions against the diesel equivalent soot conditions (1200 bar, 3 deg bTDC), it can be seen that the duration of the premixed phase was slightly less under diesel equivalent soot operating conditions. The duration of the diffusion combustion for 30% RSO was higher compared to diesel when both operated under reference engine operating conditions. However, there has been a noticeable reduction in the diffusion combustion duration for 30% RSO under the diesel equivalent soot conditions.

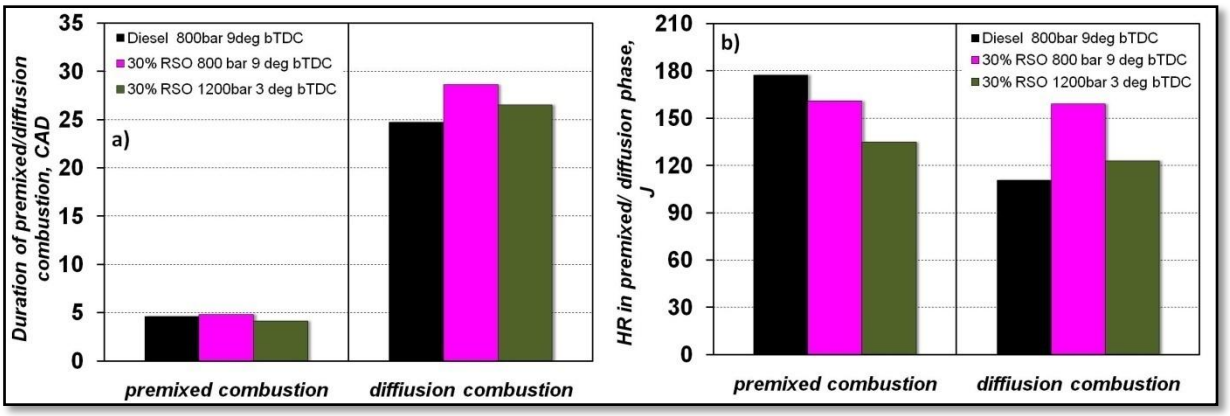

Fig. 4.3.2.5. The diagrams of: a) the duration of premixed and diffusion combustion phases, b) the heat released in the premixed and diffusion combustion phases, for diesel, 30% RSO under standard engine operating conditions and for 30% RSO under diesel equivalent soot engine conditions.

Figure 4.3.2.5b shows the magnitude of heat released during the premixed and diffusion phases. It can be seen that small variation in the duration of combustion can result in relatively huge differences in the heat release during these phases. In the case of diesel under reference conditions and 30% RSO under the diesel equivalent soot conditions, a negligible reduction in the premixed combustion duration was observed but there is a significant difference in the magnitude of the heat released between these cases (about 43 J). Likewise, a reduction in the diffusion combustion duration of about 2 CAD results in a reduction of heat release by 40 J for 30% RSO under the soot equivalent compared to 30% RSO under reference engine operating conditions. The diffusion combustion leads to a large field of flame zones in the combustion chamber where soot is mainly formed. A reduction in the amount of heat released during this phase suggests that the soot emissions can be less. On the other hand, the duration and the amount of heat released during the premixed combustion phase are connected to the formation of NO_x. In this case, the well known Zeldovich mechanism plays an important role, where high in-cylinder temperatures lead to increased formation of NO_x. The availability of oxygen and the formation of local stoichiometric mixtures are also contributory factors that influence the NO_x emissions.

The overall duration of the combustion (DOC) and ignition delay (ID) for diesel and 30% RSO under reference and diesel equivalent soot conditions are presented in Figure 4.3.2.6. The ignition delay was obtained as a difference between the start of combustion (SOC) and the

start of injection (SOI). The start of injection was a command from the ECU (engine control unit) software and the start of combustion was achieved from the heat release curve and defined in terms of CAD where the HRR curve becomes a positive value after the fuel injection. The overall DOC was calculated as the difference in the CAD between the EOC and the SOC. The end of combustion is defined in CAD as 90% of normalized cumulative heat release. The overall DOC is the sum of the premixed and the diffusion DOC. Within this sum, the premixed DOC shows almost constant values whereas the diffusion DOC has a dominant trend. Therefore, the overall DOC shares the same dominant trend as the diffusion DOC in all cases. It is noticeable that the DOC has been reduced for 30% RSO under the diesel equivalent soot conditions compared to 30% RSO under reference engine operating conditions.

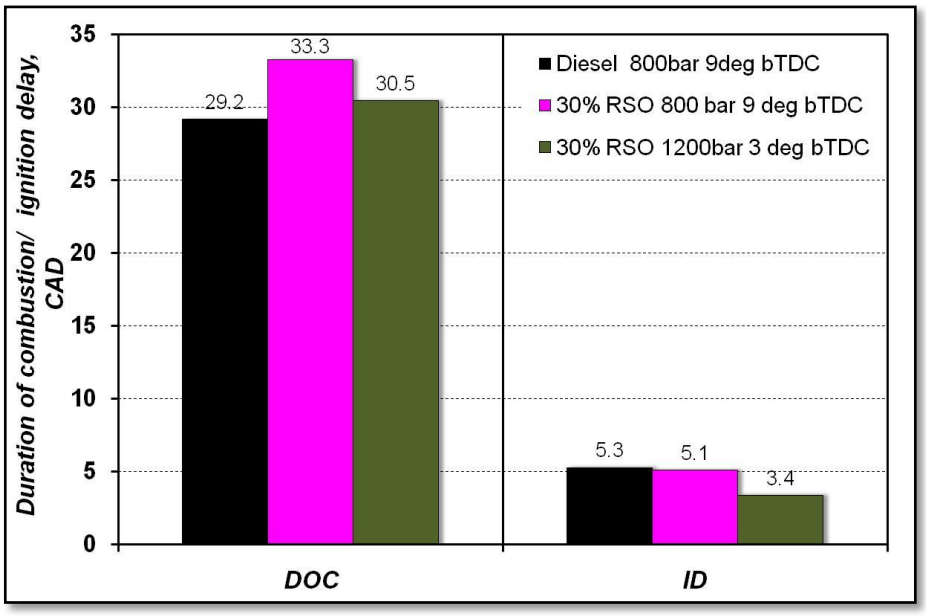

Fig. 4.3.2.6. The total duration of combustion and ignition delay for diesel, 30% RSO under standard engine operating conditions and for 30% RSO under diesel equivalent soot engine conditions.

Figure 4.3.2.6 also shows that the 30% RSO and diesel fuel had the same ID under the reference engine operating conditions. It would be likely that a higher viscosity of RSO would result in a longer ID for 30% RSO but the presence of oxygen content and fuel preheating result in a faster ignition. It has also been reported that during the injection of vegetable oil, there is a breakdown of the complex fuel compounds leading to the formation of low molecular weight compounds. Therefore, the fuel can be ignited faster [63]. On the other hand, it is noticeable that 30% RSO under the diesel soot equivalent conditions showed a reduction in the ID by 2 CAD. In this case, the late injection also caused a higher in-cylinder temperature of fresh air which improved the ignition process.

Figure 4.3.2.7a presents the emissions of total hydrocarbons (THC), carbon monoxide (CO) and Brake Specific Fuel Consumption (BSFC). Both THC and CO are products of incomplete

combustion and can be used to infer the quality of the combustion process. It can be seen that the CO and THC emissions are higher for 30% RSO when compared to diesel under the reference engine operating conditions. For 30% RSO under the diesel equivalent soot operating conditions, the CO emission is further increased but a reduction in the THC can be observed. Even though the THC emissions decrease, they are still higher than diesel. The high level of CO and THC emissions for 30% RSO under diesel equivalent soot conditions can be easily reduced by using oxidising catalysts. The BSFC was observed to be higher for 30% RSO when compared to diesel under reference engine operating conditions. In this case, the lower calorific value of RSO caused higher fuel consumption.

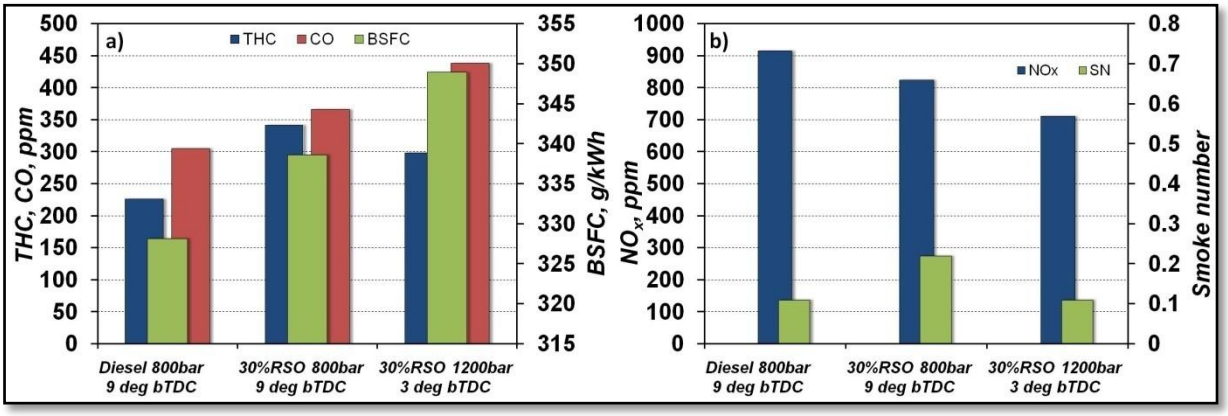

Fig. 4.3.2.7. The diagrams of a) the THC emission, CO emission and BSFC, b) the NO_x emissions and smoke number for diesel, 30% RSO under standard engine operating conditions and for 30% RSO under diesel equivalent soot engine conditions.

Figure 4.3.2.7b shows the nitrogen oxides emissions (NO_x) and smoke number (SN) for diesel and 30% RSO. It can be seen that, SN for 30% RSO under the same diesel engine operating condition is approximately 100% higher than that of diesel. However, by increasing the injection pressure and by retarding the injection timing, the SN was reduced to the same level as that of diesel fuel for 30% RSO. As previously discussed, increasing fuel injection pressure improves atomization and leads to faster evaporation. A better air utilisation and entrainment results in a faster diffusion combustion and a lower soot formation. In addition to this, late injection can eventually result in low temperature combustion (LTC) where both soot and NO_x emissions are reduced simultaneously. Generally, the NO_x emissions for 30% RSO blend were less compared to diesel. By using the proposed injection strategy, it was possible to achieve a further reduction of 22% in NO_x emissions for 30% RSO under the diesel equivalent soot conditions when compared to diesel under reference engine operating conditions. In this case, retarded injection timing and increased injection pressure influenced the NO_x emissions. It is well known that increasing injection pressure causes higher NO_x emissions while retarding the injection timing results in a reduction in NO_x emissions. Experiments show, the effect of the retarded injection timing overrides the

contributions from the increased injection pressure, leading to an efficient reduction of NO_x emissions.

The soot particles size distributions and cumulative concentration numbers for diesel and RSO under different engine operating conditions are presented in Figure 4.3.2.8. Soot particles emitted from the combustion of diesel fuel have a typical bi-modal size distribution, where the nucleation mode peak was observed at 13 nm and the peak of the accumulation mode was observed at a mobility diameter of approximately 32 nm.

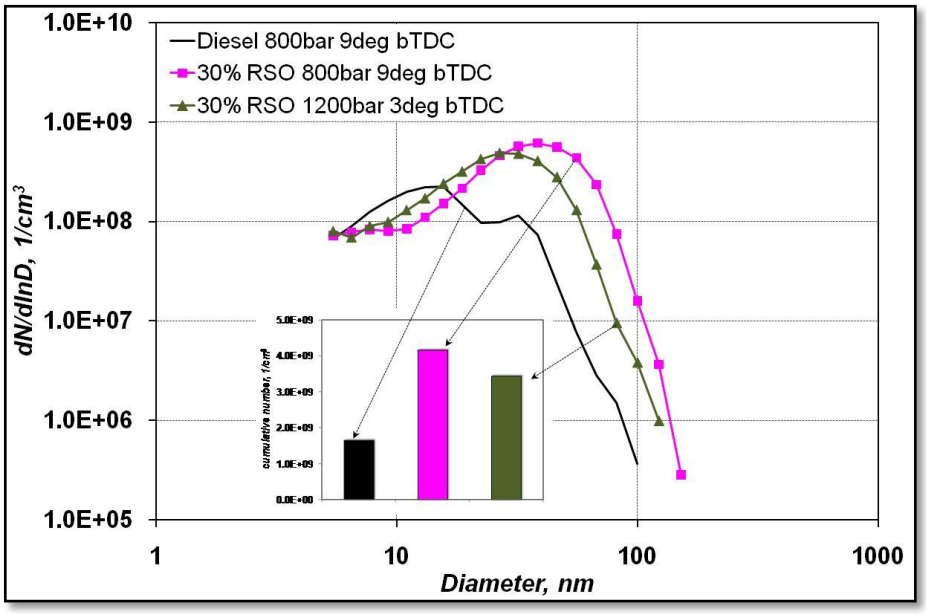

Fig. 4.3.2.8. The soot particles size distributions for diesel, 30% RSO under standard engine operating conditions and for 30% RSO under diesel equivalent soot engine conditions.

On the other hand, it is clear that for 30% RSO blend only one particles peak was observed under both engine operating conditions. Under the same engine operating conditions, particles showed a wider diameter range for 30% RSO. On the other hand, under the diesel equivalent level of soot, the same blend shows a reduction in the particles diameter range as well as in the concentration number, especially in the accumulation mode. However, the concentration number for 30% RSO under the diesel equivalent level of soot is still higher than that of diesel under the reference operating conditions. Generally, the number concentration in the nucleation mode for diesel is slightly higher than that of 30% RSO. The cumulative number concentration of soot particles is strongly dependant on the particles concentration in the accumulation mode. It can be seen that the cumulative particles concentration number is higher for 30% RSO when compared to that from diesel fuel under the same engine operating conditions. Nevertheless, under the diesel equivalent soot conditions, the cumulative number for 30% RSO is reduced but still higher than diesel. Each particle size distribution is averaged over the three scans. Additionally, the COV was around 14%, 21% and 6% for diesel, 30% RSO at 800 bar and 30% RSO at 1200 bar, respectively.

4.3.3 Conclusions

In this study, the advantage of lower NO_x emissions from the combustion of 30% blend of RSO in diesel fuel was further explored to reduce their soot emissions to the diesel equivalent level, through different fuel injection strategies. The main findings are summarized below.

- By using pure RSO and its blends, the NO_x emissions are lower when compared to diesel fuel.
- The diesel equivalent level of soot emissions was achieved for 30% blend of RSO by simultaneously retarding the injection timing up to 3 deg bTDC and increasing the injection pressure up to 1200 bar.
- A lower level of NO_x and soot emissions can be achieved by reducing the percentage of RSO in the blend (less than 30%), by increasing the injection pressure (>1200 bar) or further retarded injection timing (>3 deg bTDC).
- Further reduction of NO_x emissions by about 22% was achieved for 30% blend of RSO under the diesel equivalent soot engine operating conditions.
- 30% RSO blend can be successfully used in a DI diesel engine with a lower level of NO_x emissions and at the same or lower level of soot emissions when compared to diesel.
- The cumulative number concentration of the exhaust soot particles emitted from 30% RSO is higher when compared to that of diesel under same engine operating conditions. Even though the diesel equivalent level of soot emissions was achieved through varying injection strategies for 30% RSO, the concentration number is much higher than that of diesel.

4.4 Performance of RME and Diesel under turbocharged engine operation

The usage of boosted pressure of the inlet air provides more air in the combustion chamber and eventually reduces soot emissions. The regulation of boost pressure is important due to overboosting which can have devastating effects on the engine. Too high initial pressure inside the combustion chamber results in a significantly higher in-cylinder pressure peak. Consequently, it can affect the head gasket, the cylinder rings, producing huge blow-by power loss. In this test, a variable geometry turbocharger was applied. Generally, the level of boost pressure is regulated by the amount of under pressure which allows the movement of blades and achieves the required boost pressure. The maximum vacuum provides maximum boost pressure while the ambient pressure causes minimal boost pressure. The engine itself produces a vacuum, depending on the engine speed, which is used as a regulation signal for the EGR valve or boosting.

Basically, the boost pressure can be adjusted by Gredi software (Section 3.1.6) but because of this complicated procedure, the regulation of the turbocharger has been designed for manual use. This consists of a manual regulating valve which adjusts the amount of under pressure for the turbine's blades movement. The schematic diagram of the turbocharger coupled with EGR and the engine can be seen in Figure 4.4.1.

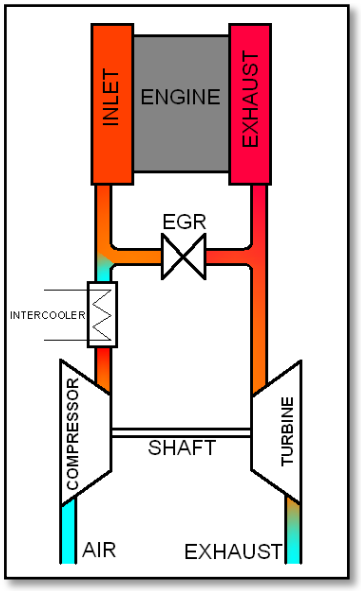

Fig. 4.4.1. A diagram of the turbocharger layout used.

Generally, in the manual regulation mode, the level of under pressure is regulated by an additional manual valve. The current value of boost pressure can be measured using a pressure transducer fitted in the inlet manifold.

The application of EGR causes a variation in the required boost pressure, depending on the EGR level. There are two effects: pressure balance of the returned exhaust gases and compressed air and amount of exhaust mass flow through the turbine. Therefore, the exhaust gases at high pressure mixes with high pressure of compressed air where their quantities can be different results in various percentage of EGR for the same EGR valve opening. On the other hand, for higher EGR rates more exhaust is returned into the inlet, thus lower flow drives the turbine. This results in less power produced by the turbine and an automatic decrease of the boost pressure. The characteristic of the boost pressure according to EGR is shown in Figure 4.4.2.

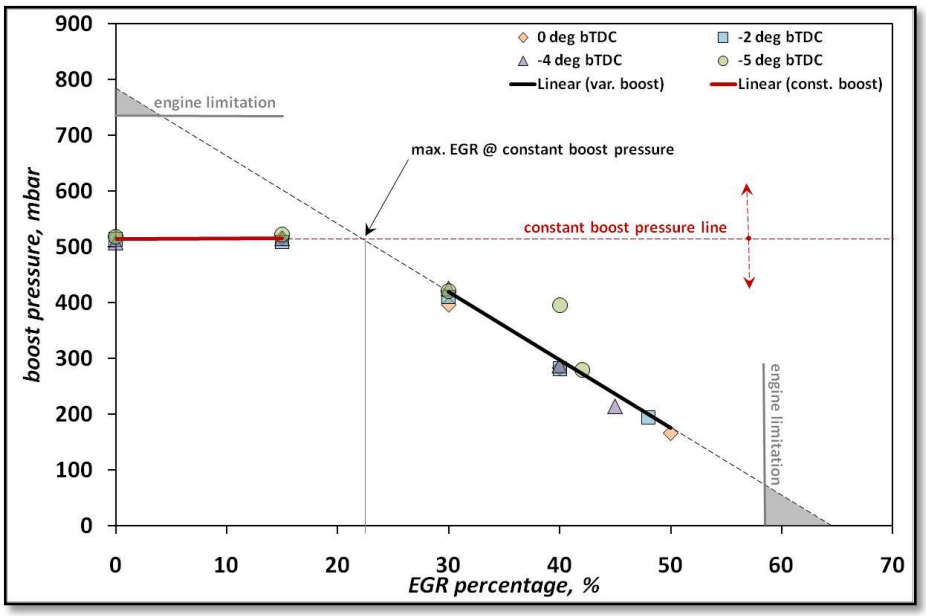

Fig. 4.4.2. The EGR and boost pressure trade off from the tested engine (2.7 bar BMEP at 2000 rpm).

It can be seen that without EGR, the boost pressure reaches the maximum value, which is limited by the design of the turbocharger and the engine. On the other hand, without boosting, the EGR percentage can reach the maximum but still limited by the engine design. The dashed black line on the graph shows the boost pressure - EGR level trade off for the engine used in this experiment. Thus, as the maximum boost pressure decreases, it is possible to apply higher EGR percentages. However, for a constant boost pressure of 1.5 bar (dashed red line), it is possible to operate the engine up to 23% of EGR. Any further increase in the EGR resulted in reduced boost pressure. All mentioned boost pressures apply to the absolute values.

4.4.1 NO_x – soot trade off for diesel fuel with and without boosting

Figure 4.4.1.1 shows the NO_x – soot trade off for diesel fuel at different engine parameters with and without boosting. The reference engine operating conditions apply to an injection pressure of 800 bar, injection timing of 9 deg bTDC, 0 % EGR at 2.7 bar BMEP and 2000 rpm. Without boosting, the position of the reference operating point is around NO_x of 855 ppm and SN of 0.11. An increase in EGR from 0% to 40% resulted in a reduction in NO_x but an increase in the smoke number. At maximum EGR (40%), the NO_x was reduced to 154 ppm and SN increased to 1.05. On the other hand, by retarding the injection timing from 9 deg bTDC to 3 deg bTDC under reference operating condition resulted in simultaneous reduction of NO_x and soot. The NO_x and soot emissions were reduced to around 516 ppm and 0.08, respectively, at a retarded injection timing of 3 deg bTDC. Additionally, it can be seen that as the inlet air was uncooled, the soot emissions became higher. The application of the turbocharger causes increased inlet air temperature after compression, which influences the soot emissions. In this test, the inlet air was always cooled under turbocharged engine operation. Moreover, the application of a boosting pressure of 1.2 bar resulted in a shift of reference operating conditions towards lower soot and NO_x emissions. Under these conditions, the NO_x were reduced to around 665 ppm and the soot emissions to around 0.04. The addition of EGR in boosted mode resulted in the same trend when compared to the naturally aspirated mode. However, the level of soot emissions was lower. The maximum EGR at a constant 1.2 bar boost pressure was about 43%. A further increase in EGR from 50% to 56% resulted in reduced boost pressure. Such a high EGR level in turbocharged mode was a result of more air in the mixture, which allows stable engine operation. Apart from this, higher EGR rates in turbocharged mode lead to a significant increase in SN and a decrease in NO_x. The maximum EGR (56%) provides the NO_x around 17 ppm and SN around 4.6. However, the retarded injection timing from 9 deg bTDC to 2 deg aTDC resulted in the same trend as without boosting. Thus, the NO_x and soot emissions are reduced to around 333 ppm and 0.023, respectively.

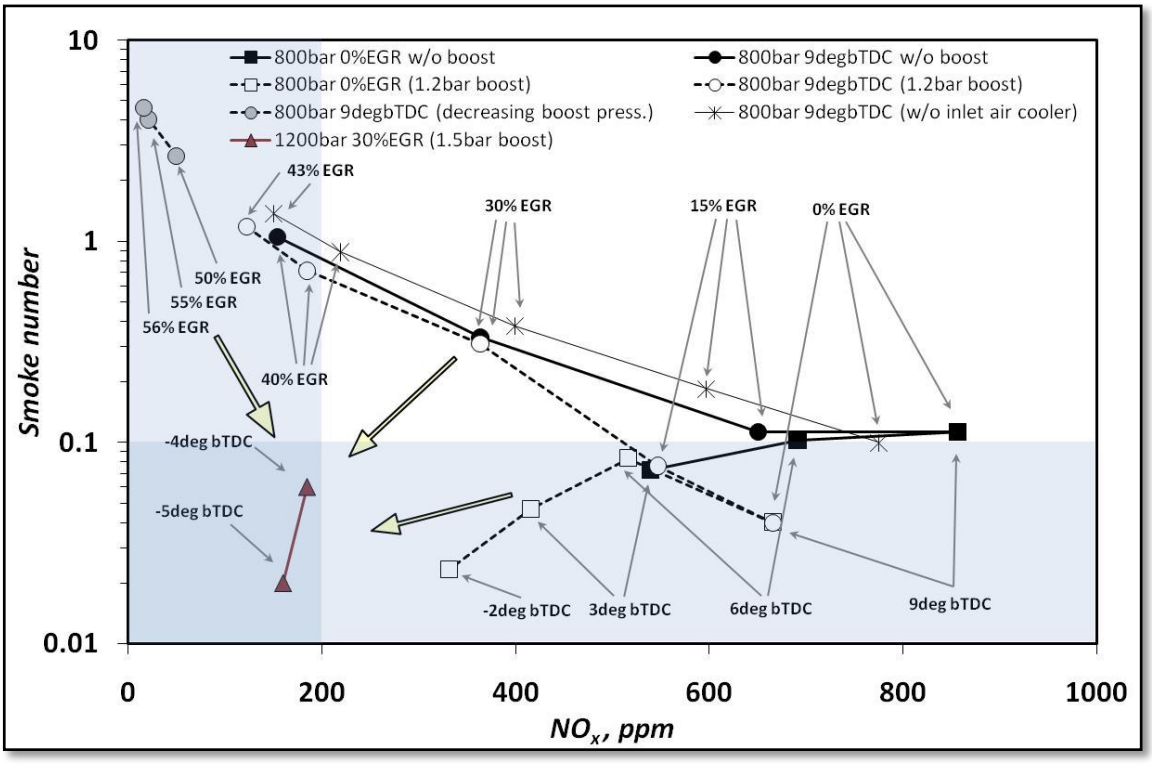

Fig. 4.4.1.1. The NO_x – soot trade off for diesel fuel with and without boosting.

The increase in SN with a higher EGR is attributed to lower oxygen concentration in the inlet as well as an increased inlet temperature due to uncooled EGR. The retarded injection timing resulted in longer ignition delay and more premixed combustion thus, the reduction of soot occurred. Moreover, the application of inlet air boosting gives the possibility of engine operation at late injection timings (2 deg aTDC when boosted). On the other hand, an increase of injection pressure results in the reduction of soot, due to enhanced air entrainment and mixing process.

The aim of this study was to reduce the NO_x and soot emissions to relatively low levels (smoke number below 0.1 and NO_x emissions below 200 ppm). Figure 4.4.1.1 presents an example of the results at high boost and injection pressure with an application of 30% EGR. Moreover, with a combination of late fuel injection, it was possible to obtain low levels of soot and NO_x emissions.

4.4.2 Test matrix and procedure

In order to obtain low NO_x and soot emissions, the late fuel injection, high boost and injection pressure were applied. The measurements were done according to the test matrix in Table 4.4.2.1. The engine was operated at 2.7 bar BMEP, 2000 rpm and injection pressure of 1200 bar. The boosting pressure was initially maintained at 1.5 bar. However, the previously discussed boost pressure – EGR characteristic allowed the application of only up

to 15 % EGR at constant boost pressure. At each injection timing, the EGR was changed from 0% to 50 % or maximum available. The test was done for two fuels: diesel and RME.

Table 4.4.2.1. Test matrix and engine operating conditions.

2.7 bar BMEP at 2000 rpm, boost press max 1.5 bar, injection pressure 1200 bar						
DIESEL RME		EGR,%				
		constant boost pressure		varied boost pressure		
		0	15	30	40	50 (or max)
injection timing, CAD bTDC	0	✓	✓	✓	✓	✓
	-2	✓	✓	✓	✓	✓
	-4	✓	✓	✓	✓	✓
	-5	✓	✓	✓	✓	✓

4.4.3 Combustion characteristics

Figure 4.4.3.1 shows the in-cylinder pressure for diesel and RME at an injection timing of TDC where different percentages of EGR were applied. There is a very strong effect of EGR on the in-cylinder pressure. Therefore, at high EGR, the in-cylinder pressure decreases and the combustion phase shifts towards the expansion stroke. At EGR levels of 0% and 15%, the pressures in the compression stroke for both fuels follow the same curve due to the same boosting pressure of 1.5 bar. A further increase in EGR resulted in a lower level of boosting pressure (according to Figure 4.4.2), which was around 1.4 bar, 1.3 bar and 1.2 bar at 30%, 40% and 50% of EGR, respectively. Moreover, the engine operation on RME fuel resulted in a slightly lower in-cylinder peak than for diesel. Generally, a high amount of exhaust gases in the inlet manifold causes the engine operation on gradually richer mixtures (lack of oxygen). Furthermore, the presence of triple atom molecules in the exhaust composition (mainly CO_2, H_2O) decreases the in-cylinder temperature due to their high specific heat capacities. During the combustion process, the in-cylinder temperature can be represented by the in-cylinder pressure. Therefore, a high EGR also leads to lower in-cylinder temperature. The EGR effect on the in-cylinder pressure, seen in the case of injection timing at TDC, is the same for other injection timings (2, 4 and 5 deg aTDC). The combustion process at such a high EGR rates was still stable. The calculated COV was always below 5%. For diesel fuel was 1.43% and 2.39% while for RME 1.38% and 1.83% at 0 % and 50% of EGR. The slight instability for diesel fuel at 50% EGR can be seen.

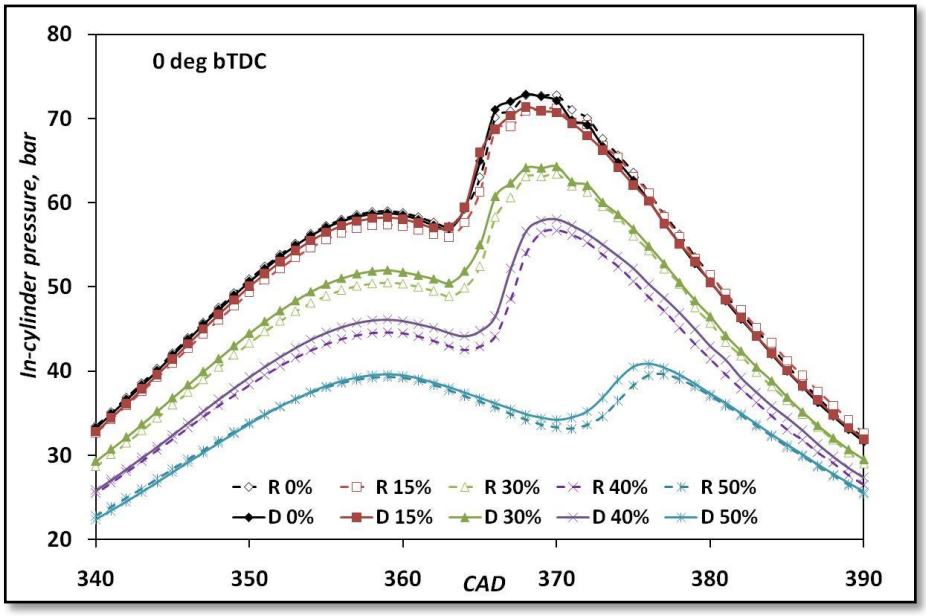

Fig. 4.4.3.1. The effect of EGR on the in-cylinder pressure at injection timing at TDC for both fuels.

The effects of injection timings on the in-cylinder pressure at a given EGR percentage are shown in Figure 4.4.3.2. It can be seen that, as the injection timing is retarded, the combustion phase is shifted and the in-cylinder pressure peak reduced. A shift in the combustion phase is the result of retarded injection timing while a reduction of the in-cylinder pressure peak is the consequence of gradually lower initial in-cylinder conditions (pressure and temperature). The differences in the compression pressure, especially at maximum EGR, are attributed to inaccurate regulation of boost pressure with a combination of high EGR. On the other hand, the influence of injection timing seems to be dominant in the case of diesel as it provides more shifted combustion phase. Moreover, the addition of EGR leads to narrowing the differences in the combustion phase for RME. It can be seen that at the highest EGR percentage, the injection timing did not influence the combustion phase as much as for diesel.

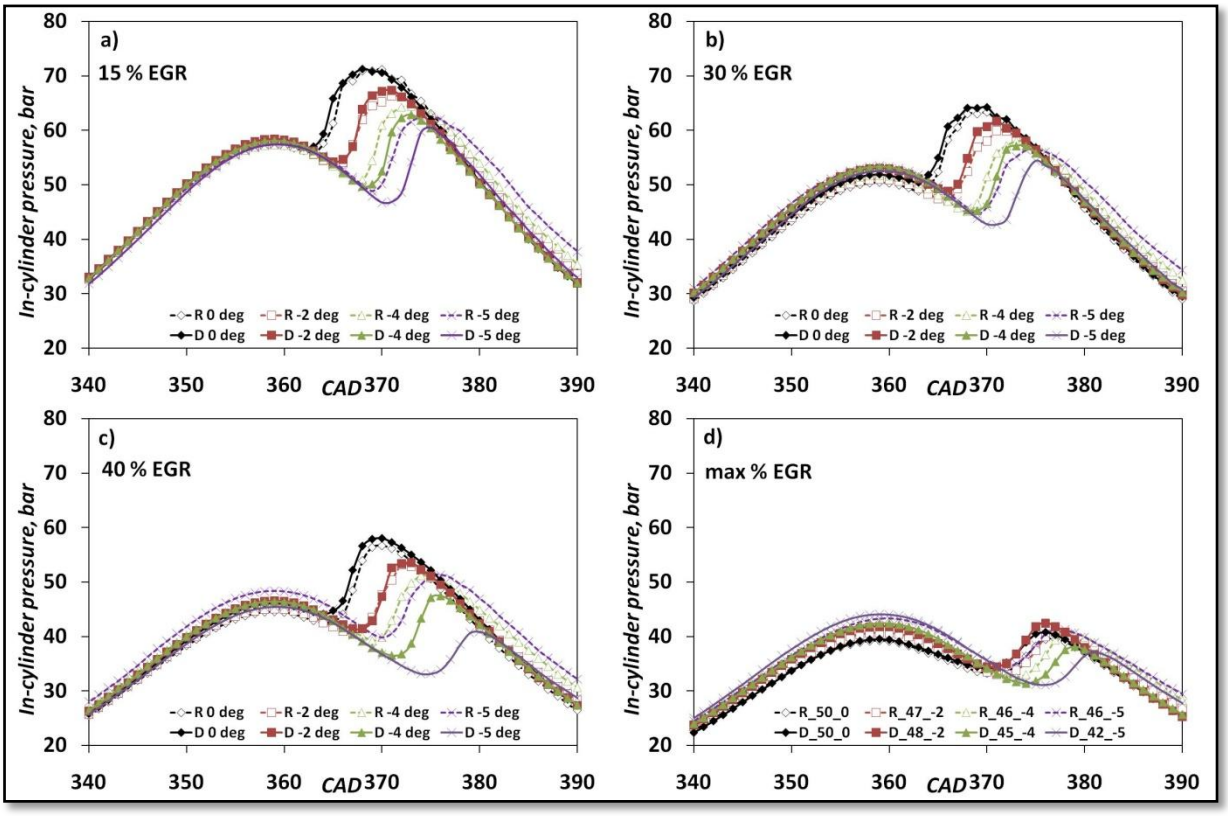

Fig. 4.4.3.2. The effect of injection timing on the in-cylinder pressure at different EGR percentages for both fuels at: a) 15% EGR, b) 30% EGR, c) 40% EGR and d) max. EGR (around 50%).

Figure 4.4.3.3 presents the in-cylinder pressure peak summarized from all engine operating conditions for both fuels. The position of the in-cylinder pressure peak provides the information on shift in the combustion phase while the peak shows the overall pressure level. Generally, the in-cylinder pressure peak is reduced and shifted towards the expansion stroke for retarded injection timings and higher EGR rates. However, the EGR has a stronger effect in the case of reducing the in-cylinder pressure peak. The reduction of the in-cylinder pressure peak because of the retarded injection timing was about 18 bar, while due to the influence of EGR around 32 bar. Moreover, both fuels show almost the same trends.

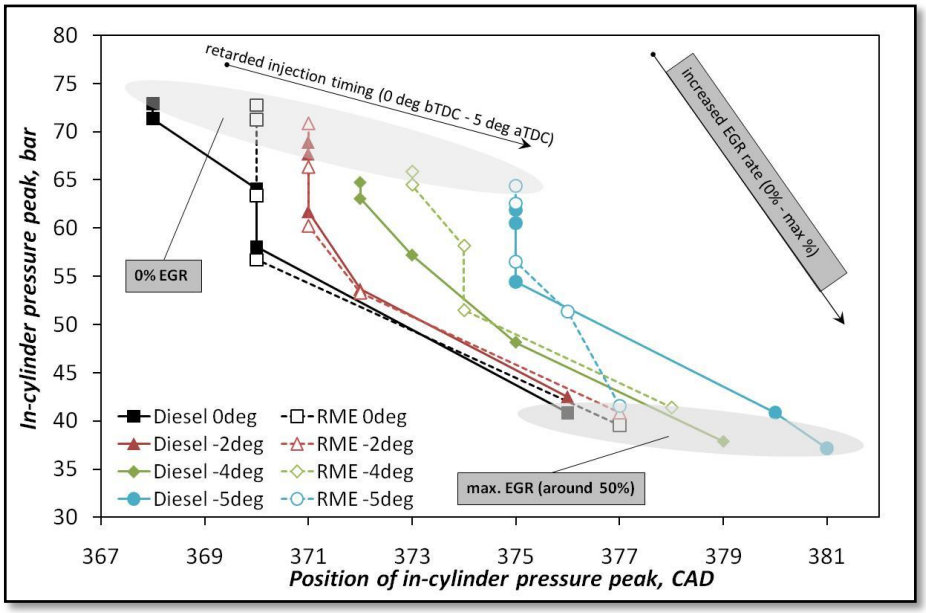

Fig. 4.4.3.3. The effect of injection pressure and EGR on the in-cylinder pressure peak for both fuels (values of the boost pressure can be seen in Figure 4.4.2).

Figure 4.4.3.4 shows the effects of EGR on the heat release rate (HRR) at an injection timing of 0 deg bTDC, for diesel and RME. Generally, high EGR causes the combustion to be shifted towards the expansion stroke and thereby reducing the peak of the heat release rate. Moreover, the combustion is prolonged, which can be seen especially in the premixed combustion phase at high levels of EGR.

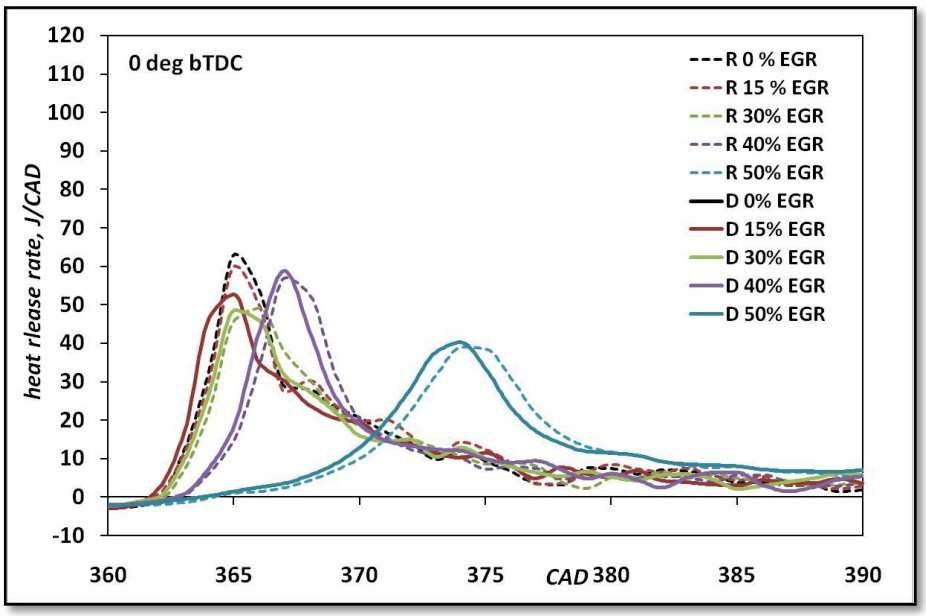

Fig. 4.4.3.4. The effect of the EGR on the heat release rate for both fuels at injection timing of TDC (values of the boost pressure can be seen in Figure 4.4.2).

On the other hand, Figure 4.4.3.4 presents the effects of injection timings on the HRR at a given EGR percentage for both fuels. At low EGR rates (0% – 30%), the retarded injection timing from TDC to 5 deg aTDC causes an increase in the HRR peak for both fuels. In the case of 40% EGR and maximum EGR, the HRR peaks are almost the same. The combustion phase is already shifted because of retarded injection timing. Moreover, it can be seen that there are noticeable differences between fuels, especially at injection timing from 4 to 5 deg aTDC. Therefore, RME seems to start the combustion process earlier than diesel. This effect applies for each given EGR rate. For this purpose, the ignition delay has been calculated.

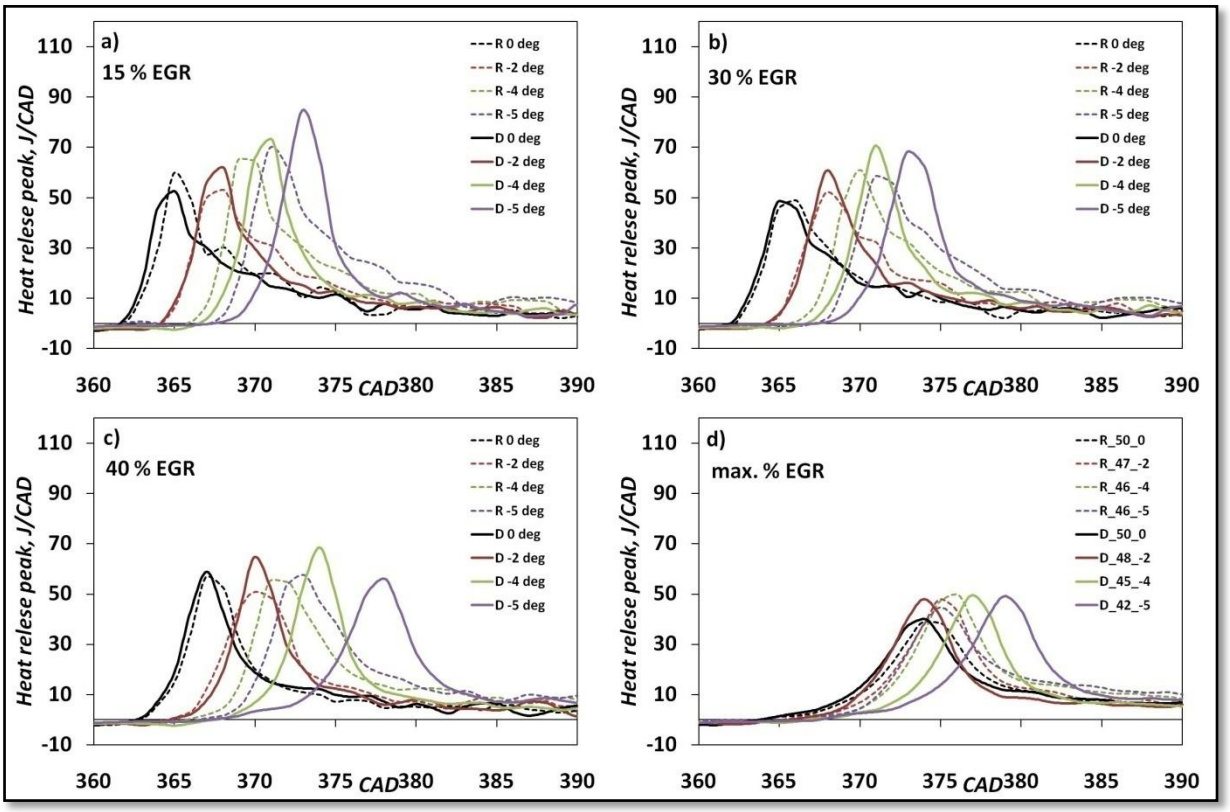

Fig. 4.4.3.4. The effect of injection timing on the heat release rate at different EGR percentages for both fuels at: a) 15% EGR, b) 30% EGR, c) 40% EGR and d) max. EGR (around 50%).

Generally, the ID is calculated as a difference between SOC and SOI where SOC is determined when the HRR curve crosses the x axis and becomes positive after the fuel injection (Section 3.4.3). However, in this measurement, the maximum EGR showed prolonged combustion so the detection of this point was complex and resulted in large errors. Thus, a small difference in HRR (around zero value) resulted in a couple of CAD differences. For this purpose, the calculation of SOC was done as a 10% threshold for each of the operating conditions. Firstly, all the HRRs were normalized and then SOC calculated as a 10% point in terms of CAD. This resulted in realistic trends of ID for both fuels. The calculated ID is summarized in Figure 4.4.3.4a. In the case of diesel, the ID is longer with a higher EGR and retarded injection timing. However, the effect of increased ID due to EGR is

dominant at higher EGR rates (from 30% EGR). The fuel injection after TDC resulted in longer ID because of gradually lower in-cylinder pressure and temperature (expansion stroke), thus more time is needed for fuel vaporization. In the case of EGR, the engine operates at gradually richer mixtures with lack of oxygen. Therefore, it takes more time to form proper air/fuel mixture when compared to the operation without EGR. The difference in ID for diesel fuel was around 2.4 CAD between 0 deg aTDC and 5 deg aTDC of injection timing at 0% EGR and around 4.8 between 0% and max. % of EGR at TDC of injection timing.

In the case of RME, the ID seems to be constant with retarded injection timing as opposite to ID from diesel. Moreover, the injection timing effect was inconclusive fluctuating within around 1 CAD. When compared to diesel's ID, RME showed definitely shorter ID at retarded injection timing. This is mainly attributed to the oxygen content in the elementary composition of RME. Thus, the mixing process and the formation of proper air/fuel mixtures is faster, resulting in shorter ID. On the other hand, the work done by Ryan III et al. [63] confirmed that a heavy molecular structure of fatty acids breaks down and forms low molecular weight compounds during injection. Also, a lack of oxygen due to EGR is compensated by elemental composition of oxygen in the RME structure. This may also help a faster ignition of the fuel in the combustion chamber. The effect of EGR on the RME's ID is almost the same as in the case of diesel. It increases with a higher EGR rate where also the lack of oxygen plays a dominant role.

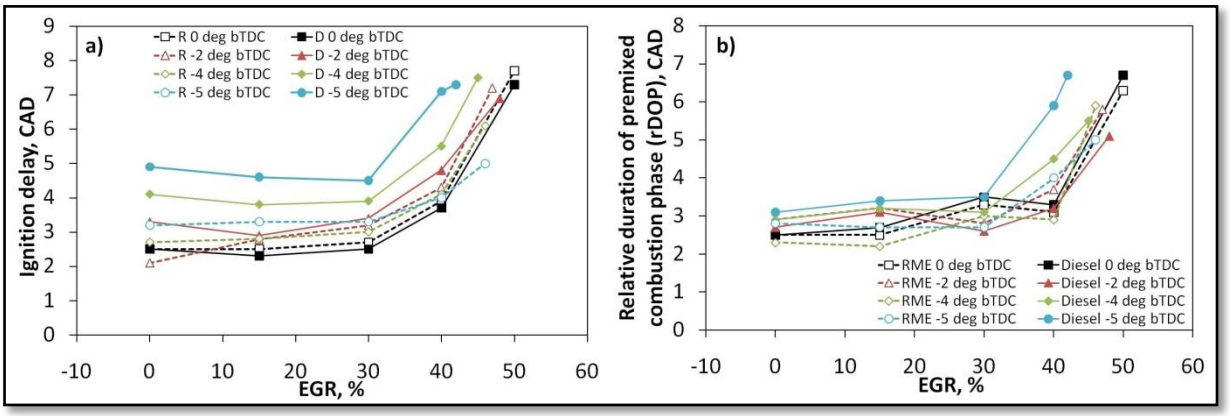

Fig. 4.4.3.5. The effect of injection pressure and EGR on the in-cylinder pressure peak for both fuels (values of the boost pressure can be seen in Figure 4.4.2).

Figure 4.4.3.5b shows the effects of EGR and injection timings on a relative duration of premixed combustion phase (rDOP) for both fuels. The rDOP has been calculated as a difference between the HRR peak and the SOC in terms of CAD. It can be seen that the premixed combustion phase is affected only by the high EGR rates for both fuels. Moreover, it is hard to distinguish any trend regarding the different fuels and retarded injection timings on the premixed combustion. As it could be previously seen in Figure 4.4.3.4, high EGR reduces the peak of HRR and prolongs the premixed phase. Generally, more premixed

combustion should increase the NO_x emissions. In this case, the premixed combustion is prolonged but the amount of heat release during this phase is dominant. Lower in-cylinder pressure and peak of the heat release rate are the main factors which influence the in-cylinder temperature. Therefore, even though the premixed phase is relatively longer, it proceeds at low temperatures reducing NO_x in the case of high EGR.

4.4.4 Emission characteristics.

Figure 4.4.4.1a presents the influence of the injection timing and EGR on NO_x emissions for both fuels. As the EGR increases, the NO_x emissions decrease for both fuels. A significant reduction of around 96% and 93% in NO_x occurred because of the addition of EGR, at injection timing of TDC for RME and diesel, respectively. Additionally, the retarded injection timing caused a reduction of around 16% and 20% in NO_x for RME and diesel, respectively. For all injection timings, apart from 5 deg aTDC, the differences between fuels were not distinguishable. Only at this injection timing, the RME showed higher NO_x emissions than diesel for all EGR cases. Generally, as the EGR percentage increases, the combustion temperature decreases resulting in lower NO_x emissions. It can be confirmed by decreasing the in-cylinder pressure as well as the heat release rate.

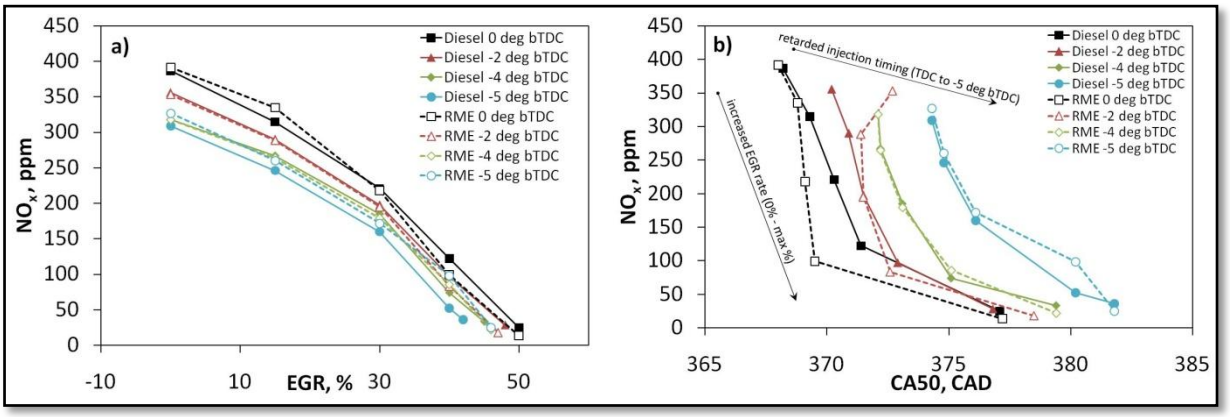

Fig. 4.4.4.1. The effects of EGR and injection timing on: a) the NO_x emissions, b) the NO_x and CA50 point (values of the boost pressure can be seen in Figure 4.4.2).

The combustion phase (CA50 point) has been calculated as 50% of normalized cumulative heat release rate in terms of CAD (Figure 4.4.4.1b). When the combustion phase shifts, due to high EGR or retarded injection timing, the NO_x emissions decrease. However, as previously mentioned, the strongest influence had the EGR. Even though the duration of premixed combustion is the longest at the highest EGR, the NO_x emissions are still reduced, because of lower combustion temperature.

Figure 4.4.4.2a shows the influence of injection timing and EGR on the smoke number for both fuels. In the case of diesel, the soot emissions increase with a higher EGR percentage at all injection timings. Moreover, the retarded injection timing caused a reduction in the smoke number for both fuels. It can also be seen that, generally, the soot emissions from RME were lower when compared to diesel. An increase in SN, because of an application of EGR, is attributed to the engine operation on gradually richer mixtures where the mixing process is slower. Additionally, the lack of oxygen and lower in-cylinder temperature led to slower oxidation rates and eventually higher soot emissions. On the other hand, the retarded injection timing does not cause any significant changes in the air/fuel mixture, thus the combustion temperature can only be attributed to the initial in-cylinder conditions before the fuel injection. As the injection timing is retarded, the initial in-cylinder temperature is lower. Nevertheless, various strategies of air/fuel mixing at different injection timings can have a significant influence on the reduction of soot emissions.

In the case of RME, the injection timing effect is the same as for diesel. However, at injection timing of TDC, an increase of EGR caused the reduction of soot emissions. The combustion enters the narrow window operation where it is possible to reduce the soot and NO_x emissions simultaneously (Figure 4.4.4.2b). This is a well known effect and it is termed as low temperature combustion (LTC). Generally, the whole combustion mainly consists of the premixed phase which proceeds at low in-cylinder temperatures. This narrow engine operating range usually appears at low engine load, very late or advanced injection timing and high EGR rates. Therefore, ID is much longer allowing better air/fuel mixing and eventually lower soot emissions.

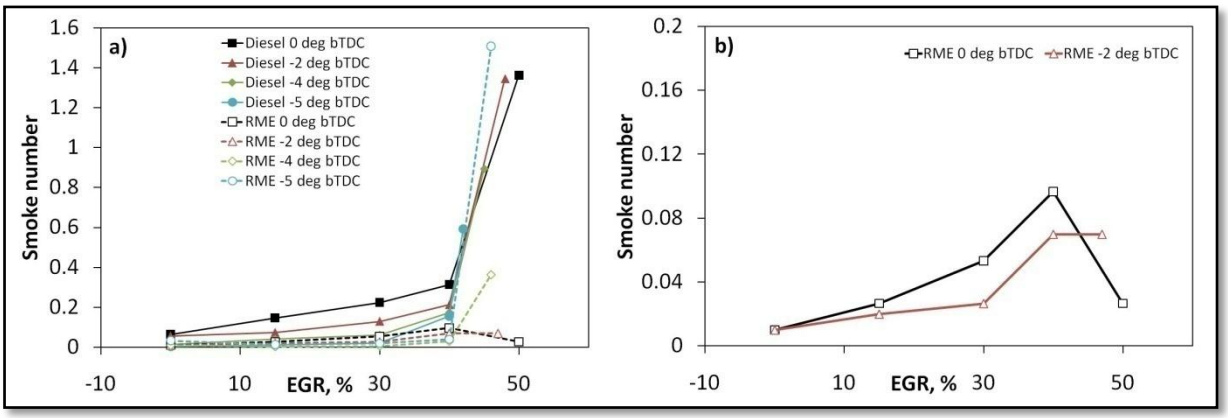

Fig. 4.4.4.2. The effects of EGR and injection timing on the smoke number, a) both fuels and all operating conditions, b) zoom for RME (reduction of smoke number).

In the case of retarded injection timing of 2 deg aTDC, this effect is still seen since the smoke number remains constant for high EGR (40% to 47%). For the next injection timing of 4 deg aTDC, the smoke number increases again with a higher EGR.

All the NO_x and SN results can be seen in Figure 4.4.4.3 as a NO_x – soot trade off for both fuels. The data for diesel without boosting is also shown. Generally, the retarded injection timing at given EGR causes a reduction of soot and NO_x emissions. A higher EGR rate leads to the reduction of NO_x but the increase of soot emissions (apart from RME at injection timing of TDC). The shaded areas in the Figure define the low NO_x and soot emissions. The range of 0 – 200 ppm has been adopted to represent low NO_x emissions while the range of 0 – 0.1 to represent low soot emissions. Some of the results obtained from test matrix are within these ranges.

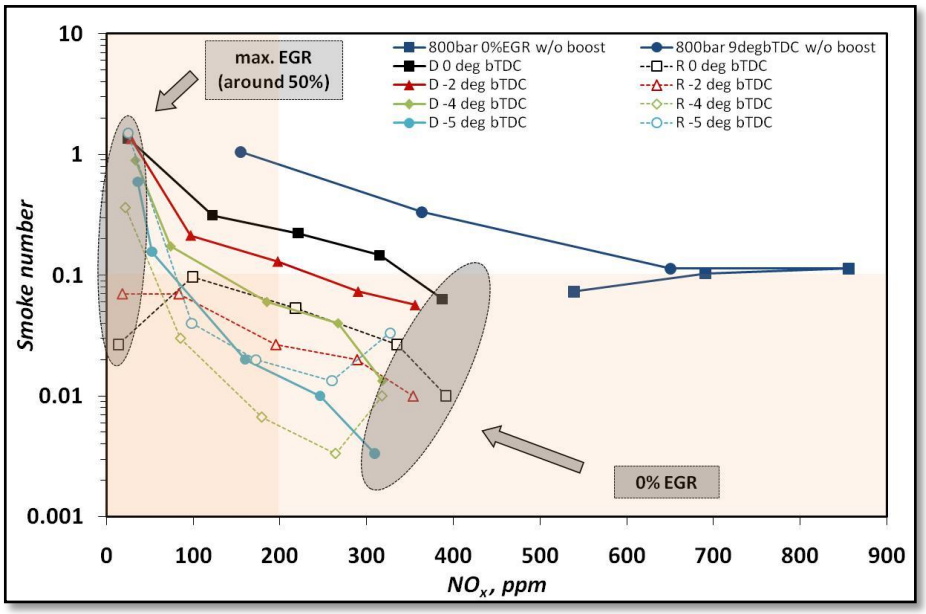

Fig. 4.4.4.3. The effects of EGR and injection timing on the smoke number and NO_x for both fuels.

The summarized engine operating conditions for low NO_x and soot emissions can be seen in the Table below:

Table 4.4.4.1. The engine operating condition at which low NOx and soot emissions have been obtained.

		RME	NO_x, ppm	SN	DIESEL	NO_x, ppm	SN
injection timing, CAD aTDC	0	50% (max)	13.6	0.026	-	-	-
		40% EGR	99.3	0.096	-	-	-
	2	47% (max)	18.0	0.07	-	-	-
		40% EGR	83.3	0.07	-	-	-
		30% EGR	196.0	0.026	-	-	-
	4	40% EGR	85.6	0.03	30% EGR	185.0	0.06
		30% EGR	179.3	0.006			
	5	40% EGR	98.3	0.04	30% EGR	160.0	0.02
		30% EGR	172.0	0.02			

The results obtained from RME seem to fit into the low NO_x and soot range under several engine operating conditions. It is because of naturally lower soot emissions for RME when

compared with diesel. Moreover, RME's advantage is the fact that it was possible to reduce the smoke number at a higher EGR, which automatically placed these conditions into a lower emissions zone.

Figure 4.4.4.4 shows the effects of EGR and injection timing on the THC (4.5.4.4a) and CO emissions (4.4.4.4a) for diesel and RME. The THC and CO emissions are products of incomplete combustion. It can be seen that as the injection timing retards, the THC and CO emissions become higher for both fuels. Therefore, the late fuel injection gradually causes unstable combustion with unburned products.

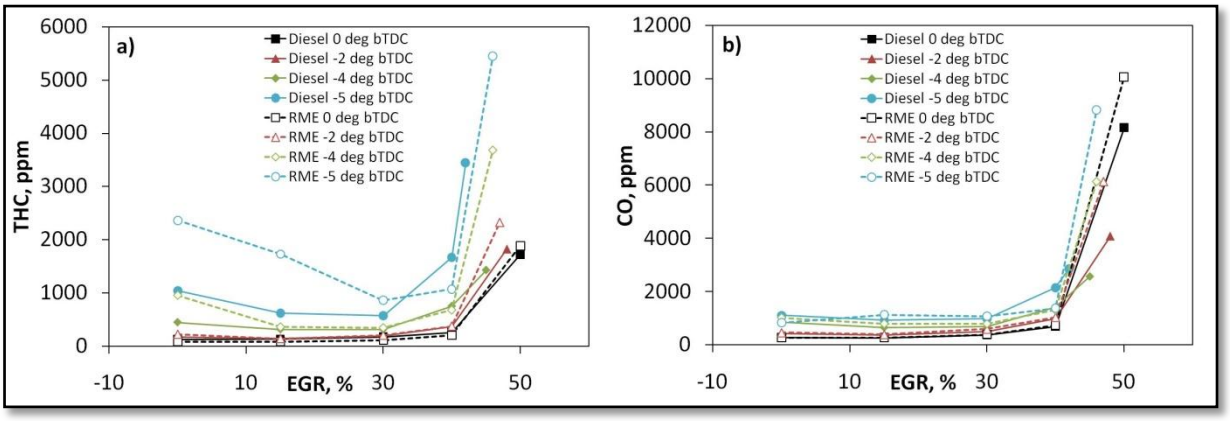

Fig. 4.4.4.4. The effects of EGR and injection timing on: a) THC emissions, b) CO emission (values of the boost pressure can be seen in Figure 4.4.2).

In the case of THC emissions, a higher EGR resulted in a decrease and then a significant increase at the highest EGR. Moreover, the highest possible CO emissions occur at maximum EGR. The application of EGR causes the engine operation on rich mixture, where the air utilisation is insufficient resulting in an incomplete combustion and the rise of CO and THC emissions. Generally, RME showed slightly higher THC and CO emissions than diesel, apart from the injection timing of 5 deg aTDC for THC emissions where the differences between RME and diesel were big, especially at low EGR percentages. Furthermore, as the simultaneous reduction of NO_x and soot was possible for RME at the highest EGR, the THC and CO emissions are the highest. However, this amount should still be efficiently burned in the oxidising catalysts.

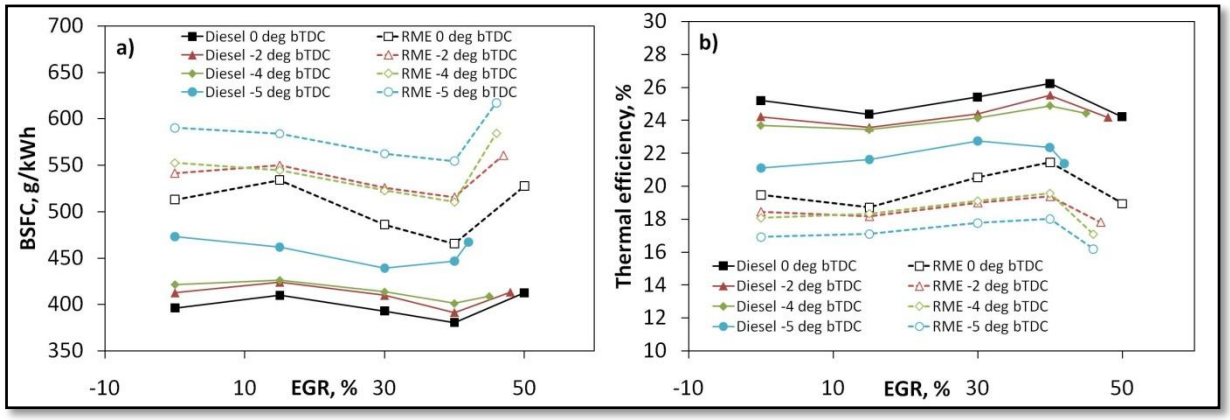

Fig. 4.4.4.5. The effects of EGR and injection timing on a) brake specific fuel consumption, b) thermal efficiency, (values of the boost pressure can be seen in Figure 4.4.2).

The brake specific fuel consumption (BSFC) for RME and diesel is presented in Figure 4.4.4.5a. Generally, the engine operation on RME results in higher fuel consumption than diesel. It is attributed to its lower calorific value. The retarded injection timing resulted in higher fuel consumption for both fuels. However, slightly lower values can be noted for diesel at injection timings from TDC to 4 deg aTDC and then significant increases at an injection timing of 5 deg aTDC.

Generally, more fuel is consumed for the retarded injection timing as a result of low combustion temperature and incomplete combustion. On the other hand, it can be seen that at the highest EGR, the fuel consumption significantly increases for both fuels at a given injection timing. It is a result of rich combustion with lack of oxygen in the combustion chamber thus more fuel is needed for obtaining the required engine load. The fuel injection of such a high amount of fuel, at maximum EGR, leads to the same engine energy output but significant THC, CO and soot emissions.

Figure 4.4.4.5b shows the thermal efficiency for diesel and RME at all engine operating conditions. The highest value of thermal efficiency is reached by diesel around 26%. The application of RME fuel at these engine conditions resulted in relatively poor performance of even 16% of thermal efficiency. This can be attributed to very late combustion conditions and high EGR. Generally, engine fuelled by RME had lower thermal efficiency than that of diesel.

The engine operation at such a high EGR and late injection strategy was motivated by academic studies. Relatively low thermal efficiency, especially for RME, does not comply with current trends in downsizing engines.

4.4.5 Conclusions

The conclusions from this work are summarized below.

- Generally, the turbocharged engine operation reduced soot and NO_x emissions.
- The usage of boost pressure of 1.5 bar and injection pressure of 1200 bar led to late and stable combustion even at an injection timing of 5 deg aTDC.
- Generally, the retarded injection timing caused a reduction in soot while a high EGR led to high soot emissions for both fuels (apart from one engine operating condition for RME).
- Soot emissions were lower in the case of RME.
- In the case of RME, a simultaneous reduction of smoke number and NO_x can be observed at injection timings of 0 and 2 deg aTDC and maximum EGR.
- The ID for RME was not as sensitive to the injection timing as diesel fuel.
- The EGR rate has been found to be a dominant parameter in increase of the relative premixed combustion duration.
- The NO_x emissions were decreasing with a high EGR and retarded injection timing for both fuels. Differences in NO_x emissions were negligible between fuels.
- Incomplete combustion at maximum EGR resulted in significantly high THC and CO emissions as well as increased fuel consumption.

5 CHAPTER 5 – Soot particles size distributions

This chapter describes the measurements of the soot particles size distribution using the EMS device. Because of high sensitivity of the measurement method on the final result in the first part of this chapter the analysis of different dilution systems and the usage of different DMA material has been described. The second part consists of the soot particles size measurement at constant dilution conditions for different engine operating parameters (injection timing, injection pressure and EGR) for fuels such as RME and diesel.

5.1 A comparison between primary and secondary dilution systems

A comparison between primary and secondary dilution systems has been made in order to characterise and choose a dilution condition suitable for the measurements of soot particles from the diesel engine. The engine operating conditions were always the same throughout the whole analysis as they provide almost the same soot emissions. The engine operating conditions were as follows: engine load and speed of 2.7 bar BMEP (42.7 Nm) at 1500 rpm, injection pressure of 800 bar, injection timing of 9 CAD bTDC and EGR at 0%.

5.1.1 Results from the existing dilution system (secondary dilution system)

For the characterisation of the existing system (secondary dilution system), the following investigations on soot particle size distribution have been made:

- The influence of dilution ratio and dilution temperature (measurements for steel DMA),
- The influence of dilution ratio and dilution temperature (measurements for aluminium DMA).

The test matrix for measurements on steel DMA can be seen in Table 5.1.1. All results (two sets) have been obtained twice to acquire information about the day to day repeatability of soot particle size distributions. Moreover, for each dilution condition, three or more full scans have been taken in order to get an overview on scan to scan repeatability.

Table 5.1.1. The dilution conditions of data set for characterisation of steel and aluminium DMA.

SET 1		dilution ratio									
		1.4	2	3.2	4.5	5.4	8	10.8	16.4	24.7	31.5
temperature	50 °C	✓	✓	✓	✓	✓	✓	✓	✓	✓	✓
	75 °C	✓	✓	✓	✓	✓	✓	✓	✓	✓	✓
	100 °C	✓	✓	✓	✓	✓	✓	✓	✓	✓	✓
	150 °C	✓	✓	✓	✓	✓	✓	✓	✓	✓	✓
	200 °C	✓	✓	✓	✓	✓	✓	✓	✓	✓	✓
SET 2		dilution ratio									
		1.4	2	3.2	4.5	5.4	8	10.8	16.4	24.7	31.5
temperature	50 °C	✓	✓	✓	✓	✓	✓	✓	✓	✓	✓
	75 °C	✓	✓	✓	✓	✓	✓	✓	✓	✓	✓
	100 °C	-	-	-	-	-	-	-	-	-	-
	150 °C	-	-	-	-	-	-	-	-	-	-
	200 °C	-	-	-	-	-	-	-	-	-	-

THE RESULTS FOR STEEL DMA

The soot particles size distributions at different temperatures and dilution ratios are presented in Figure 5.1.1. Figure 5.1.1a shows that at a dilution gas temperature of 50 degC, the concentration number decreases with a high dilution ratio especially in the diameter range of 10-100nm. This is an expected trend as more diluted exhaust should carry less soot particle. For higher dilution gas temperatures, the differences in size distribution for different dilution ratios seem to be gradually negligible for dilution gas temperature of 100 degC on Figure 5.1.1b. Moreover, a further increase in the dilution air temperature to 150 degC (Figure 5.1.1c) shows the inversed trend for different dilution ratios.

Generally, the lowest dilution ratio (1.4) causes the lowest soot particle concentration number. Further increase in the dilution ratio, for this particular temperature, caused higher concentration numbers for dilution ratios of up to 5.4. Furthermore, a higher dilution ratio (8.0) brought down the concentration number while increasing the dilution ratio again (8.0 to 31.5) resulted in a higher concentration number. Moreover, a higher dilution gas temperature of 200 degC caused an unclear trend for different dilution ratios.

Figure 5.1.2 shows the effect of a dilution gas temperature for selected constant dilution ratios. Generally, the low range of dilution ratios (1.4 to 3.2) (Figure 5.1.2.a) provided a clear trend, where the soot particles concentration number decreases with a high dilution gas temperature. However, for higher dilution ratios (Figure 5.1.2b), the trends are not clear.

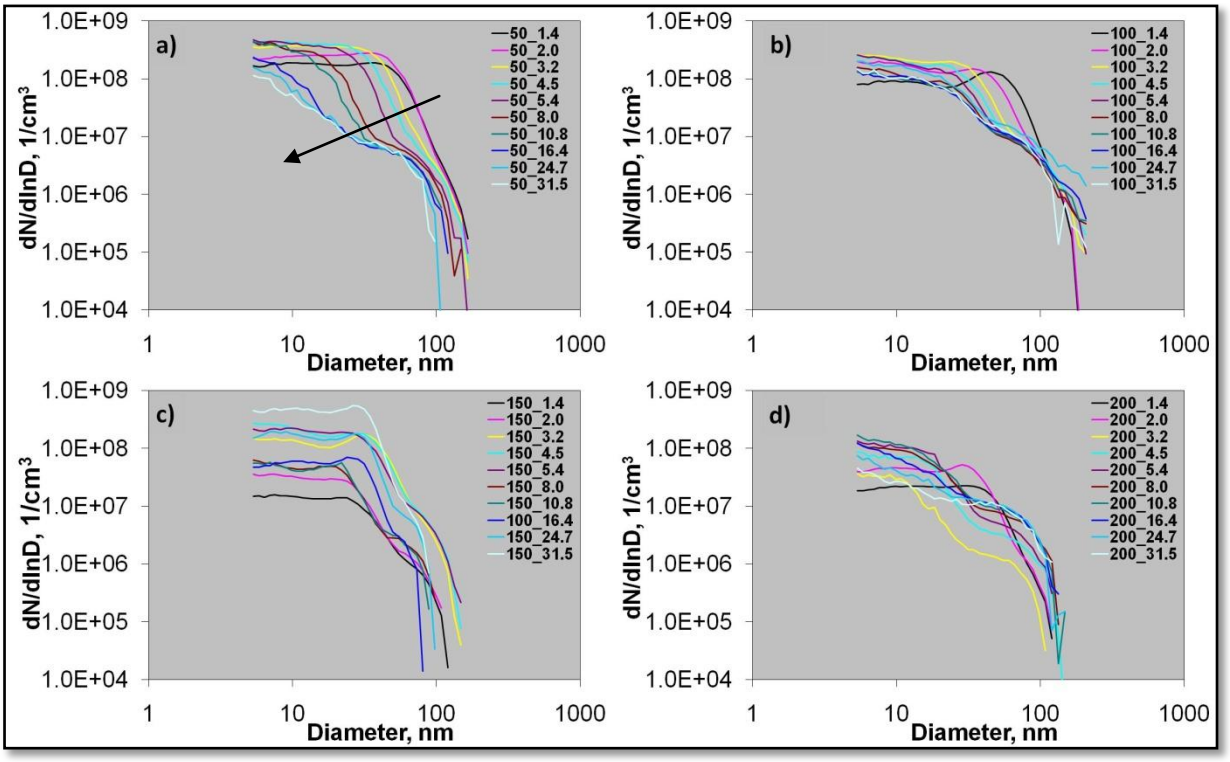

Fig. 5.1.1. The dilution ratio effects on soot particles size distribution for selected dilution gas temperatures of: a) 50deg C, b) 100 degC, c) 150 degC, d) 200 degC, from set 1 for steel DMA.

According to the literature [65,71], for higher dilution ratios and dilution gas temperatures, the soot particles concentration number decreases. Without heating the dilution system, the low temperature causes the condensation of the volatile fraction on soot particles. Moreover, particles grow and eventually concentration number increases. In the case of steel DMA, this dilution effect applies only to low dilution temperatures of 50-100 degC (Figure 5.1.1a, b). Additionally, the dilution gas temperature effect applies only to low dilution ratios of 1.4-3.2 (Figure 5.1.2a).

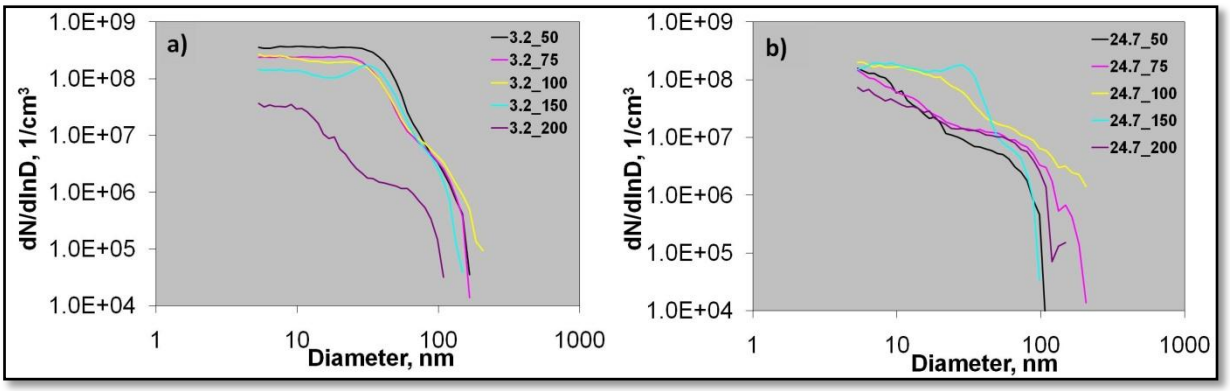

Fig. 5.1.2. The dilution gas temperature effects on soot particles size distribution for selected dilution ratios of: a) 3.2 , b) 24.7, from set 1 for steel DMA.

The next set of data (Table 5.1.1b), for the same DMA, provides information on day to day repeatability. As could be seen, the data for set 2 was not collected under all dilution conditions because the comparison of the repeatability of size distribution for different dilution ratios at dilution gas temperature of 50 and 75 degC from two different sets was sufficient for this analysis. Figure 5.1.3 shows selected dilution conditions as well as a comparison of the data from set 1 and set 2. Moreover, for each dilution condition all three scans are plotted, showing the variations from scan to scan.

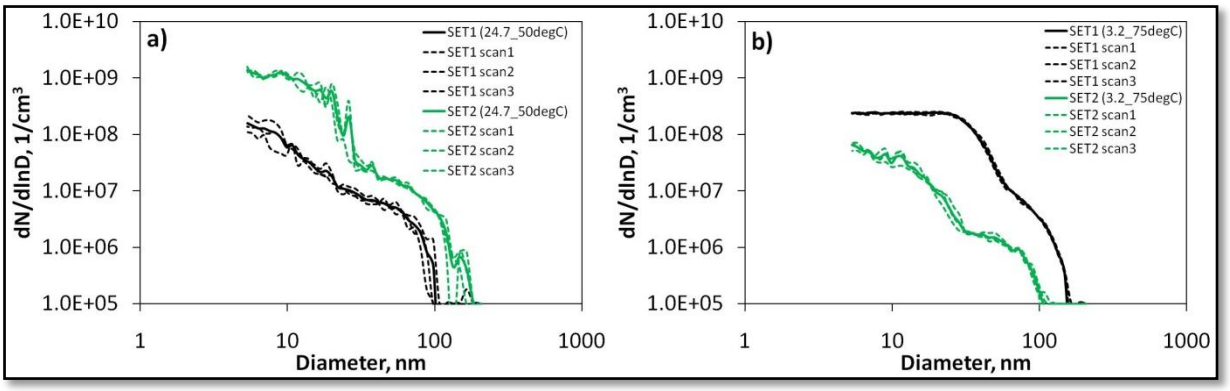

Fig. 5.1.3. The comparison of the soot particles size distributions for steel DMA from set 1 and set 2 from selected dilution condition of: a) dilution ratio of 24.7 at temperature of 50 degC, b) dilution ratio of 3.2 at temperature of 75 degC.

Under the dilution condition of 24.7 at 50 degC (Figure 5.1.3a) it can be seen that soot particles size distributions from day to day are completely different. In this case, the data from set 1 shows a much lower particles concentration number than from set 2. Moreover, the soot particles detection range for set 1 is narrower. The inverse trend could be seen under the dilution condition of 3.2 at 75 degC (Figure 5.1.3b). In this case, the particles concentration number is lower for data from set 2. For this reason, the data from set 2 was not fully obtained as the differences in size distributions for these two temperatures, at different dilution ratios, are significantly high. However, the tests for each dilution ratio condition showed good repeatability from scan to scan in all cases. For quantifying this effect, the coefficient of variation has been analysed by applying the Formula 3.4.7.1.

Figure 5.1.4 summarises the repeatability test under all conditions. It can be seen that, COV for day to day repeatability oscillates around 60 - 80 % (Figure 5.1.4a). Moreover, the COV increases for 50 degC case and decrease for 75 degC case with a high dilution ratio. The highest COV of 92% occurred under dilution conditions of 31.5 at 50 degC and the lowest of 36% under dilution conditions of 31.5 at 75 degC.

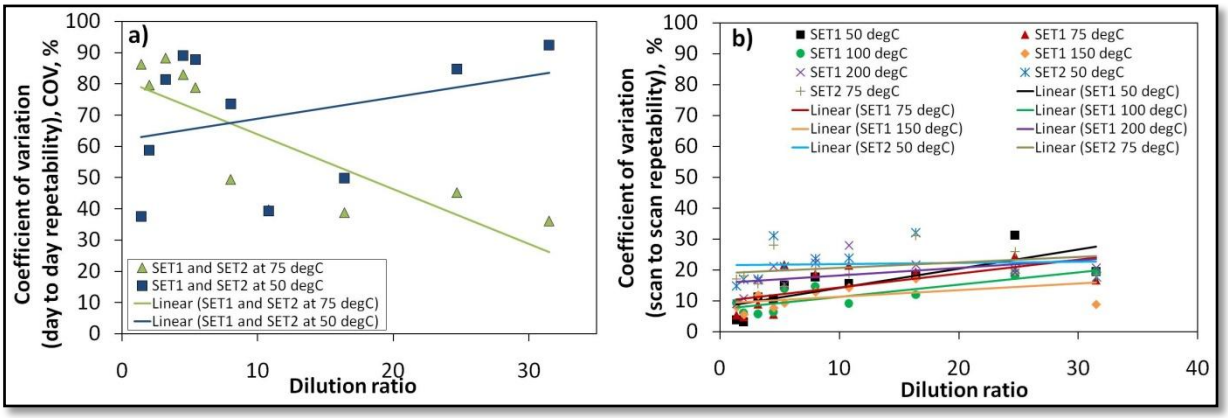

Fig. 5.1.4. The COV from measurements of soot particles size distribution based on: a) day to day analysis, b) scan to scan analysis for steel DMA.

However, the COV for scan to scan repeatability is improved, which equals to around 15% on average with the highest value of around 30% and the lowest of around 3% (Figure 5.1.4).

The results from the usage of steel DMA show unclear trends concerning the effects of different dilution ratios and dilution gas temperatures. Moreover, a poor day to day repeatability shown by the comparison of set 1 with set 2 forced changes being made in the system. One of the available methods was to check a different material of DMA.

THE RESULTS FOR ALUMINIUM DMA

All data was collected twice (two full sets) under all dilution conditions shown in Table 5.1.1a. The selected results of particle size distribution for aluminium DMA are shown in Figure 5.1.5. Regarding the data from set 1, the particle distribution at a temperature of 50 degC (Figure 5.1.5a) and a temperature of 200 degC (Figure 5.1.5b) shows that high dilution ratios cause a decrease in the particle concentration number especially for a particle diameter range of 5 – 40 nm. However, the particles concentration number for a diameter range higher than 40 nm did not show any significant effects. Moreover, this trend appears in the whole set 1 for each diluion gas temperature (50, 75, 100, 150 and 200 degC).

Additionally, exactly the same particle size distributions can be seen in the case of set 2. Selected data for different dilution ratios at temperatures of 50 degC and 200 degC from set 2 is shown in Figure 5.1.5c and d. Generally, the particles detection range is almost constant under all dilution conditions in set 1 as well as in set 2. However, slightly broader distributions can be seen in the case of lower dilution gas temperatures. Beside the negative influence of dilution ratio (increased concentration number with a high dilution ratio), the results seem to be consistent and with good repeatability.

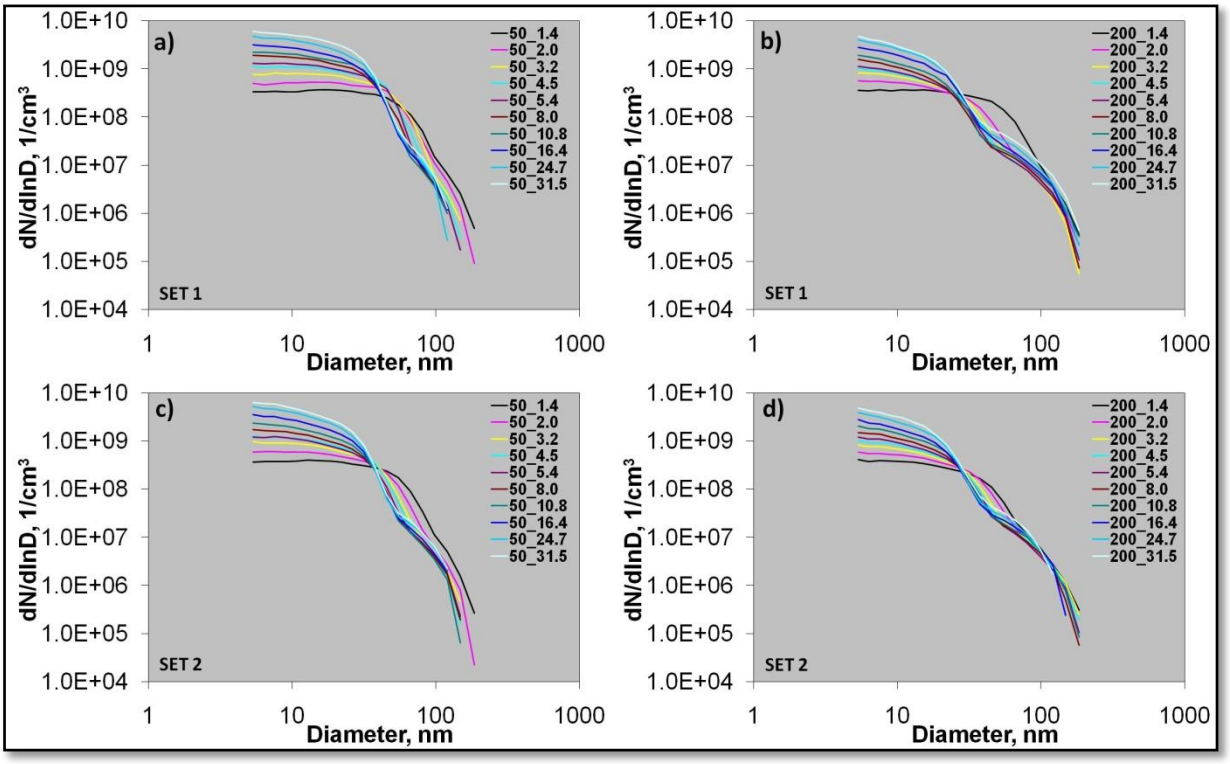

Fig. 5.1.5. The dilution ratio effects on soot particles size distribution for selected dilution gas temperatures of: a) 50deg C from set 1, b) 200 degC from set 1, c) 50 degC from set 2, d) 200 degC from set 2 for aluminium DMA.

The effect of dilution gas temperature on soot particles size distribution under selected dlution conditions from two sets is shown in Figure 5.1.6. Under all dilution conditions, from both sets, a high dilution temperature resulted in slightly lower particles concentration number. However, the slight differences could be in the fluctuation limits in some cases.

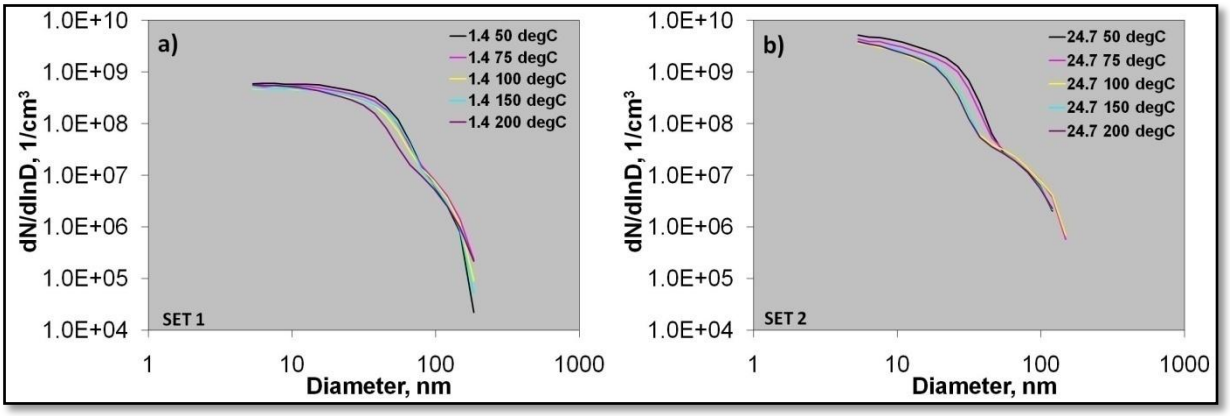

Fig. 5.1.6. The dilution gas temperature effects on soot particles size distribution for selected dilution ratios of: a) 1.4 from set 1, b) 24.7 from set 2 for steel DMA.

Due to the use of aluminium DMA, the coefficient of variation from day to day comparison has improved. The average value under all conditions is around 10% with the highest value of around 18% and lowest around 3% (Figure 5.1.7a). Moreover, the COV's trendlines

suggest that the day to day repeatability has improved at lower dilution ratios and higher temperatures. In the case of scan to scan repeatability, the data is shown only from set 1, as set 2 showed very similar results. On average, the COV from the scan to scan analysis was around 8%, with the highest value of around 14% and the lowest of around 3%. Furthermore, the COV from scan to scan analysis slightly decreases for a lower dilution ratio.

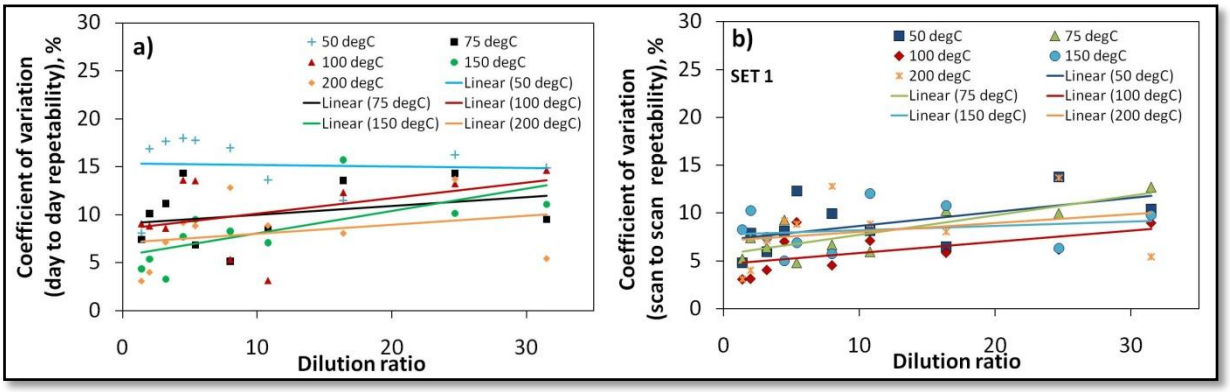

Fig. 5.1.7. The COV from measurements of soot particles size distribution based on: a) day to day analysis, b) scan to scan analysis for aluminium DMA.

The analysis from the usage of these two DMAs shows that steel DMA provides relatively high day to day COV. On the other hand, the aluminium DMA showed very good day to day repeatability. However, low COV from scan to scan analysis occurred for both DMAs. In the case of different dilution ratios and dilution gas temperature, the steel DMA caused deteriorated trends while trends from the aluminium DMA were consistent. The aluminium DMA with its good day to day repeatability has been chosen for further measurement as it provides an advantage over the steel DMA. Moreover the incorrect trend, where a high soot particle concentration occurs for high dilution ratios can be an artefact of dilution method and can be minified by the interference in the dilution system. Nevertheless, better results and repeatability from aluminium DMA can be attributed to differences in the material and design. Therefore, different electrical conductivity for aluminium, higher diameter of electrodes and different surface coarseness led to improved results.

Because of the high sensitivity of the results of the particles size distributions on different DMAs or dilution systems, the next measurements included the newly designed primary dilution system with nitrogen as a dilution gas. The unclear soot particles size distribution trends were partially eliminated by the application of the aluminium DMA and can be further minimized by the dilution method (mixing and cooling processes) as it is the most important for obtaining reliable results.

5.1.2 Results from the new dilution system (primary dilution system)

The inversed trends for dilution ratio effects compared to those seen in the literature [65,71] forced changes in the dilution system. The new dilution system was designed in order to eliminate deteriorated results. The full description and scheme of the primary dilution system is described in Section 3.2.1. In this case, as previously mentioned, the aluminium DMA was used as it provided good day to day and scan to scan repeatability. Moreover, the measurements were done under selected dilution conditions rather to check the size distribution trends and the effect of other parameters applied in the new dilution system. Thus, the repeatability is assumed to be good in the case of aluminium DMA for tests done with the primary dilution system. In these measurements, both dilution systems were coupled whereas PDR and SDR can be adjusted separately. For the first tests, the secondary dilution gas was not heated as the temperature effect will be discussed separately. Additionally, the influence of the exhaust valve opening and also the vacuum level on soot particles size distribution from the new primary dilution system will be discussed.

Figure 5.1.8 shows the effect of PDR on soot particles size distribution at zero of SDR, where the range of PDR was from 0 to 10.3. It can be seen that the concentration number is much lower for the new dilution system. It is almost 1.0E8 1/cm^3 when compared to steel DMA of around 1.0E9 1/cm^3 and aluminium DMA of around 1.0E10 1/cm^3. The main reason could be the particle losses in the primary dilution ratio because of its long design. Additionally, for each PDR, the particles size distributions have not shown the peak in the nucleation mode and can be treated as unimodal distributions. In this case, the length of the connecting pipes to the aluminium DMA and strong cooling effects presumably cause nuclei particles to be already condensed on other solid particles or coagulated, forming aggregates. The PDR effect is clear in this case and conforms to the effect seen in the literature. Therefore, a high dilution ratio decreases the soot particles concentration number. This is a good achievement especially when the previous test showed opposite trends for aluminium DMA. A slight decrease in concentration number can be seen for low range of dilution ratios from 1.17 to 2.32 and then a significant reduction for higher dilution ratios of 3.41 to 10.3. Furthermore, with a higher dilution ratio, the number concentration peak and its corresponding particle diameter decrease.

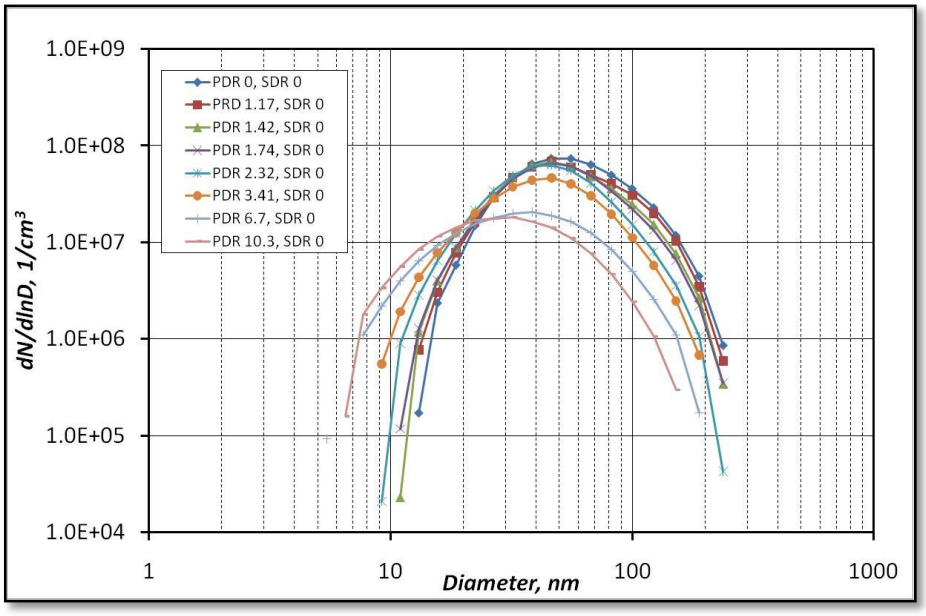

Fig. 5.1.8. The primary dilution effect of soot particles size distributions.

The following tests to characterize of this dilution system were done for selected, constant PDRs whereas SDR was varied. The soot particles size distributions at PDRs of 0, 2.32, 6.7 and 10.54 are shown in Figure 5.1.9a, b, c, and d, respectively. It is interesting to note that, when nitrogen, as gas in the primary dilution system, was not added, the soot particles concentration increases slightly with a higher SDR (Figure 5.1.9a). Nevertheless, the usage of PDR still prevents the formation of the peak of nuclei particles. However, even a small addition of nitrogen (PDR of 2.32) caused the concentration number to decrease with higher SDRs (Figure 5.1.9b). Also, the application of higher SDRs resulted in a slight decrease of the range of detected particles diameters. The same effects could be seen in the case of PDR of 6.7 (Figure 5.1.9c), but at a lower concentration number level. Moreover, at higher PDR, the effect of SDR seems to be dominant in the case of concentration number differences and in decreasing the diameter range of soot particles. In the case of PDR of 10.54, the influence of SDR is very strong (Figure 5.1.9d). A higher SDR causes a significant reduction in the concentration number and particles diameter range. In this case, the highest total dilution ratio was around 332:1. The particles loss was relatively high and is reflected in the particle concentration number and diameter.

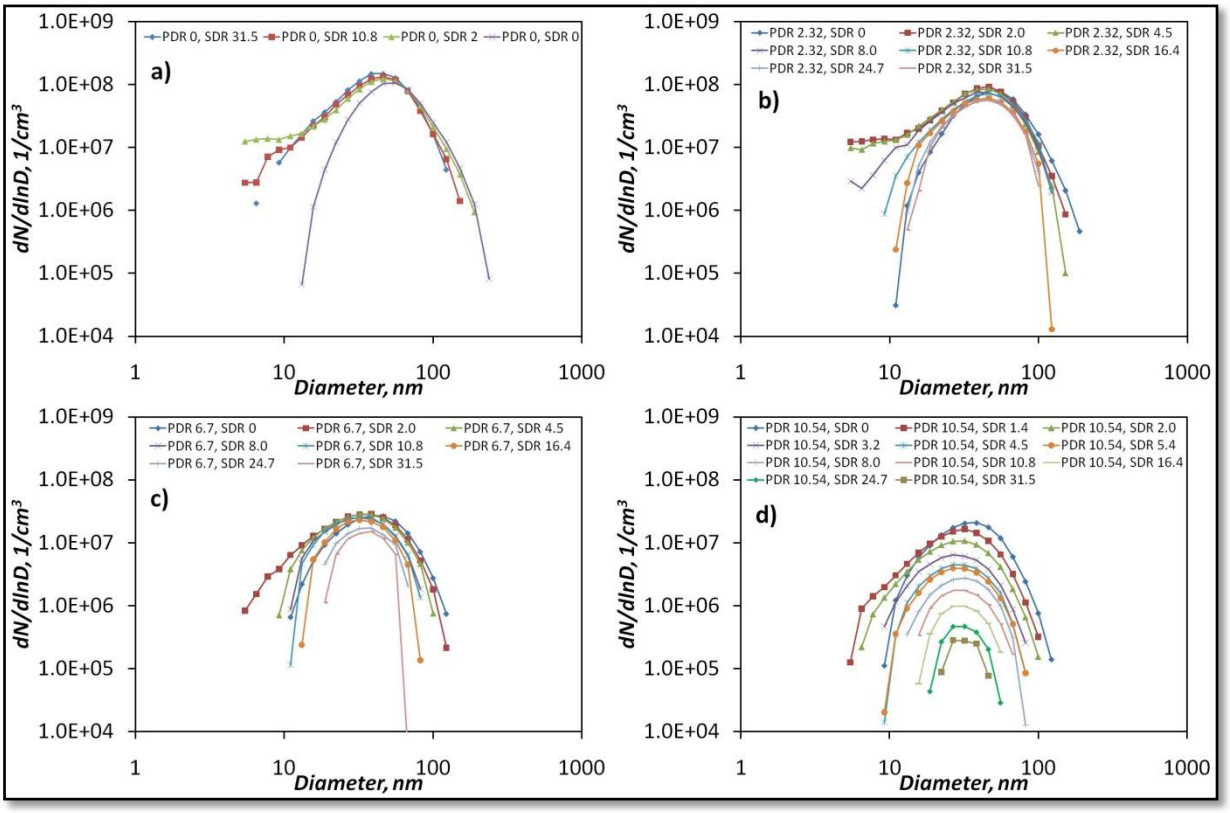

Fig. 5.1.9. The influence of SDR of the soot particles size distributions for selected PDR of: a) 0 PDR, b) 2.32 PDR, c) 6.7 PDR and d) 10.54 PDR.

This analysis shows that the application of the new primary dilution system provided the correct trend in particles concentration. Because of an unavoidable dilution instability, the error of measurements can be significant in the case of high PDR. For instance, Figure 5.1.9d shows big differences in the particles concentration as well as in the particles diameter for different SDR at a constant, high PDR of 10.54. For the purpose of further measurements, the PDR of 2.32 has been chosen as it provided a broader particles diameter range at a relatively high particles concentration.

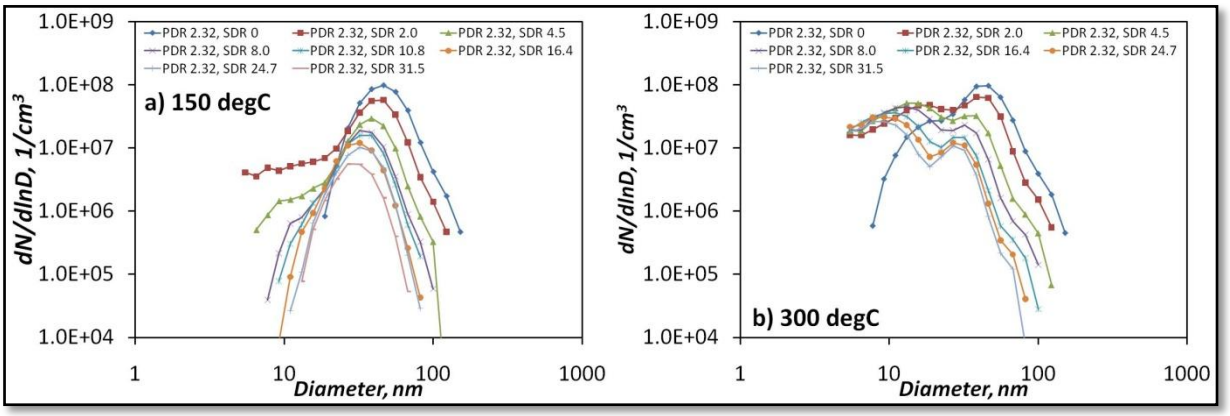

Fig. 5.1.10. The influence of SDR's temperature on soot particles size distributions: a) 150 degC, b) 300 degC.

Figure 5.1.10 presents the influence of the dilution gas temperature on the soot particles size distribution at 150 degC (Figure 5.1.10a) and 300 degC (Figure 5.1.10b) under different secondary dilution ratios at constant primary dilution ratio of 2.32.

It can be seen that, as the dilution temperature increases, the soot nuclei particles are detected by the system. In the case of a dilution gas temperature of 150 degC, the nuclei particles occur for SDR of 2.0, 4.5 and 8.0 with a slight peak in this range. However, a further increase in the dilution gas temperature to 300 degC causes the detection of nuclei particles for all SDRs beside the zero of SDR. At this particular SDR, the size distribution was not matched to the overall trend throughout the whole analysis (Figures 5.1.9 and 5.1.10). For this reason, the size distributions at zero of SDR are treated as an interruption of the dilution system and are not considered for further measurements. Nevertheless, the high dilution gas temperature of 300 degC provides the nuclei particles peak and even a small instability in SDR should not affect this mode.

Moreover, two more important parameters can be adjusted in the new dilution system. The exhaust valve opening (Figure. 5.1.11a) and the vacuum in the system (Figure 5.1.11b). The exhaust valve is a crucial parameter in getting a stable dilution ratio. However, it can be seen that the position of the valve's needle did not affect the particles distribution where the regulation range from half to four revolutions of the valve has been tested. A marginal increase of the soot particles diameters range can be noted when the exhaust valve was fully opened. Nevertheless, the influence of the exhaust valve opening on the soot particles size distribution is negligible.

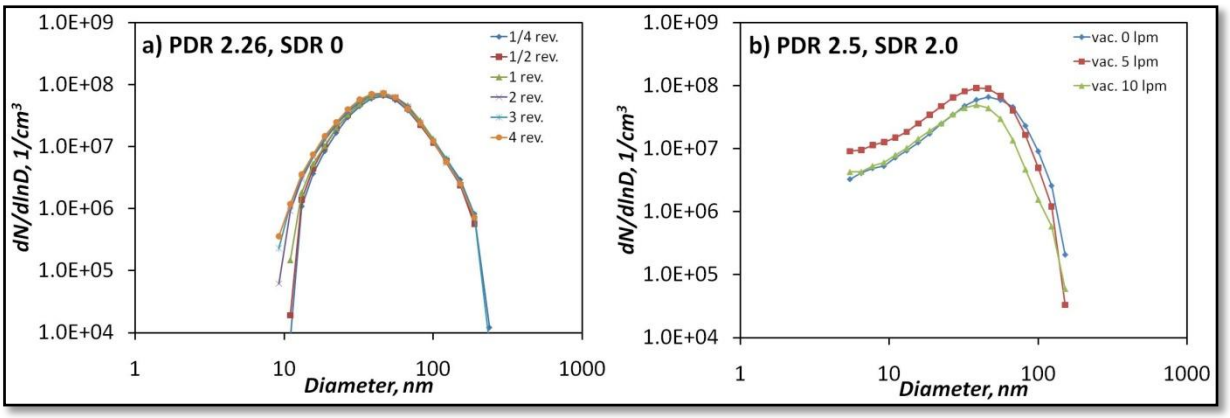

Fig. 5.1.11. The influence of: a) exhaust valve opening and b) vacuum level, on soot particles size distributions.

Another parameter was a vacuum level in the new dilution system (primary) caused by an additional sucking section connected to the excess sample out (Figure 3.2.1). The flow from the system was measured by connected flow meter with a regulating valve. The dilution conditions were constant for this test and were around PDR of 2.5, SDR of 2.0 at ambient temperature. The first test was done without any additional vacuum flow. Then, a flow of 5

lpm caused a higher soot particles concentration number especially for smaller particles while larger particles were almost the same. However, a higher flow of 10 lpm caused a lower concentration number for larger particles while smaller particles remained at the same level as those without applied vacuum. Therefore, the application of the vacuum in the system has a strong influence on the soot particles size distribution. Moreover, it seems to be a critical vacuum level for this system where the particles loss is significant, which was shown by 10 lpm of additional flow. The usage of the flow up to 5lpm shows that the particles concentration can be increased. The additional vacuum in the system has a strong influence on the mixing and cooling of the aerosol. Thus, for further experiments, the vacuum from the gas analyzer (around 1.4 lpm) was applied for the continuous control of the dilution ratio (measurement of CO_2) and to obtain a possibly higher particles concentration number.

5.1.3 Conclusions

The first test on the secondary dilution system, only with steel DMA, showed unclear trends for different dilution ratios and different dilution gas temperatures. The replacement of steel DMA with an aluminium DMA still resulted in improper rise in the particle concentration number for different dilution ratios. However, the temperature effects were clearer and a slight decrease of particle concentration number for higher temperatures could be noticed. Furthermore, the results from aluminium DMA were repeatable with the COV of around 10% and 8% for day to day and scan to scan analysis, respectively. The good consistency and repeatability from the usage of aluminium DMA are the main advantages compared to steel DMA. Therefore, further analysis was done on aluminium DMA. The main differences can be attributed to the varied material properties such as electrical or thermal conductivity. Additionally, the aluminium DMA has a slightly different design, especially the diameters of the electrodes. All the changes are updated in the software for a correct calculation of the particles concentration number and diameter but the process of particles classification can be influenced. The negative influence of dilution ratio (increased concentration number with a high dilution ratio) for aluminium DMA forced the design a new dilution system. The application of a two stage dilution system resulted in correct trends for different PDR as well as SDR. For further measurements, the following dilution conditions have been chosen:

- PDR of 2.32 (relatively higher concentration number with broader particles range, negligible influence of dilution ratio instability on size distribution)
- SDR of 2.0 (relatively higher concentration number with broader particles range)
- Temperature of SDR of 300 degC (visible nuclei particles in the case of all dilution ratios)

- Connection of the gas analyser (constant vacuum inside the secondary dilution system, continuous monitoring of the dilution ratio, relatively higher concentration number).

The measurement under these conditions gives a relatively real picture of the soot particles size distribution and can be used as a method of comparison between different engine operating conditions and different fuels.

5.2 Soot particles size distributions under different engine operating conditions

In this study, the soot particles size distributions were measured in order to obtain information about the influence of the engine operating condition. Two engine loads of 42.7 Nm (2.7 bar BMEP) and 80 Nm (5.0 bar BMEP) at 2000 rpm were maintained constant during the test. This work provides information about the influence of injection pressure, EGR and injection timing on soot particles size distribution. Additionally, the effects of different fuels have been provided as the fuels used in this work were diesel and RME (properties Section 3.3).

5.2.1 Test matrix and test conditions

For the two engine loads (2.7 bar and 5 bar BMEP) and for the two fuels (RME and diesel), the injection pressure was varied from 800 bar to 1200 bar, EGR from 0 % to maximum value and the injection timing from 9 to 3 deg bTDC. Generally, at each injection timing, the effects of injection pressure and EGR have been tested, separately. Detailed engine operating conditions for both fuels and maximum achieved levels of EGR can be seen in Table 5.2.1. As previously mentioned, the dilution conditions for the whole test were constant (PDR of 2.32, SDR of 2.0 at 300 degC of dilution gas temperature). Moreover, under all operating conditions, each particles size distribution measurement was taken three times (three scans) and then averaged. The results are presented in two main sections according to low and high engine load operations. Each section describes soot particles size distributions for different injection pressures, EGR levels and injection timing.

Table 5.2.1. The engine operating conditions. 1 – the influence of the injection pressure, 2 – the influence of EGR, 3 - the influence of the injection timing

42.7 Nm (2.7 bar BMEP) at 2000 rpm			80 Nm (5.0 bar BMEP) at 2000 rpm		
DIESEL			**DIESEL**		
9 deg bTDC	6 deg bTDC	3 deg bTDC	9 deg bTDC	6 deg bTDC	3 deg bTDC
800bar, 0% EGR [1,3]	800bar, 0% EGR [1,3]	800bar, 0% EGR [1,3]	800bar, 0% EGR [1,3]	800bar, 0% EGR [1,3]	800bar, 0% EGR [1,3]
1000bar, 0% EGR [1]	1000bar, 0% EGR [1]	1000bar, 0% EGR [1]	1000bar, 0% EGR [1]	1000bar, 0% EGR [1]	1000bar, 0% EGR [1]
1200bar, 0% EGR [1]	1200bar, 0% EGR [1]	1200bar, 0% EGR [1]	1200bar, 0% EGR [1]	1200bar, 0% EGR [1]	1200bar, 0% EGR [1]
800bar, 15% EGR [2]	800bar, 15% EGR [2]	800bar, 15% EGR [2]	800bar, 15% EGR [2]	800bar, 15% EGR [2]	800bar, 15% EGR [2]
800bar, 30% EGR [2]	800bar, 30% EGR [2]	800bar, 30% EGR [2]	800bar, 30% EGR [2]	800bar, 25% EGR [2]	800bar, 25% EGR [2]
800bar, 40% EGR [2]	800bar, 40% EGR [2]	800bar, 40% EGR [2]	800bar, 36% EGR [2]	800bar, 32% EGR [2]	800bar, 29% EGR [2]
RME			**RME**		
9 deg bTDC	6 deg bTDC	3 deg bTDC	9 deg bTDC	6 deg bTDC	3 deg bTDC
800bar, 0% EGR [1,3]	800bar, 0% EGR [1,3]	800bar, 0% EGR [1,3]	800bar, 0% EGR [1,3]	800bar, 0% EGR [1,3]	800bar, 0% EGR [1,3]
1000bar, 0% EGR [1]	1000bar, 0% EGR [1]	1000bar, 0% EGR [1]	1000bar, 0% EGR [1]	1000bar, 0% EGR [1]	1000bar, 0% EGR [1]
1200bar, 0% EGR [1]	1200bar, 0% EGR [1]	1200bar, 0% EGR [1]	1200bar, 0% EGR [1]	1200bar, 0% EGR [1]	1200bar, 0% EGR [1]
800bar, 15% EGR [2]	800bar, 15% EGR [2]	800bar, 15% EGR [2]	800bar, 15% EGR [2]	800bar, 15% EGR [2]	800bar, 15% EGR [2]
800bar, 30% EGR [2]	800bar, 30% EGR [2]	800bar, 30% EGR [2]	800bar, 30% EGR [2]	800bar, 30% EGR [2]	800bar, 30% EGR [2]
800bar, 40% EGR [2]	800bar, 40% EGR [2]	800bar, 40% EGR [2]	800bar, 33% EGR [2]	800bar, 33% EGR [2]	800bar, 32% EGR [2]
800bar, 50% EGR [2]	800bar, 50% EGR [2]	800bar, 50% EGR [2]			
800bar, 70% EGR [2]	800bar, 70% EGR [2]	800bar, 63% EGR [2]			

In the case of soot particles size distribution, an enormous amount of data forced to show only representative trends concerning the influence of the injection pressure, EGR level and injection timing.

5.2.2 Results from low load engine operation

SOOT PARTICLES SIZE DISTRIBUTIONS – LOW LOAD

The representative influence of the injection pressure on the soot particles size distributions for diesel and RME is presented in Figure 5.2.2.1. In this case, the representative injection timing of 6 deg bTDC was chosen as similar trends were seen for 9 and 3 deg bTDC.

A significant difference in the soot particles size distributions in a diameter range from 5 nm to 40 nm (nucleation mode) occurs between diesel and RME. Thus, particles emitted in the nucleation mode from RME showed almost an order of magnitude lower concentration number. Moreover, the particles size distributions for both fuels were not affected by different injection pressures and their results are within the fluctuation limits. In the case of the influence of the injection pressure on other injection timings (9 and 3 deg bTDC), the difference in concentration number in the nucleation mode between diesel and RME seems to be bigger for retarded injection timings (3 deg bTDC) (Figure 5.2.2.2.). Additionally, at retarded injection timing (3 deg bTDC), the injection pressure effect in the nucleation mode is visible whereas the soot particle concentration number decreases with a higher injection pressure for both fuels.

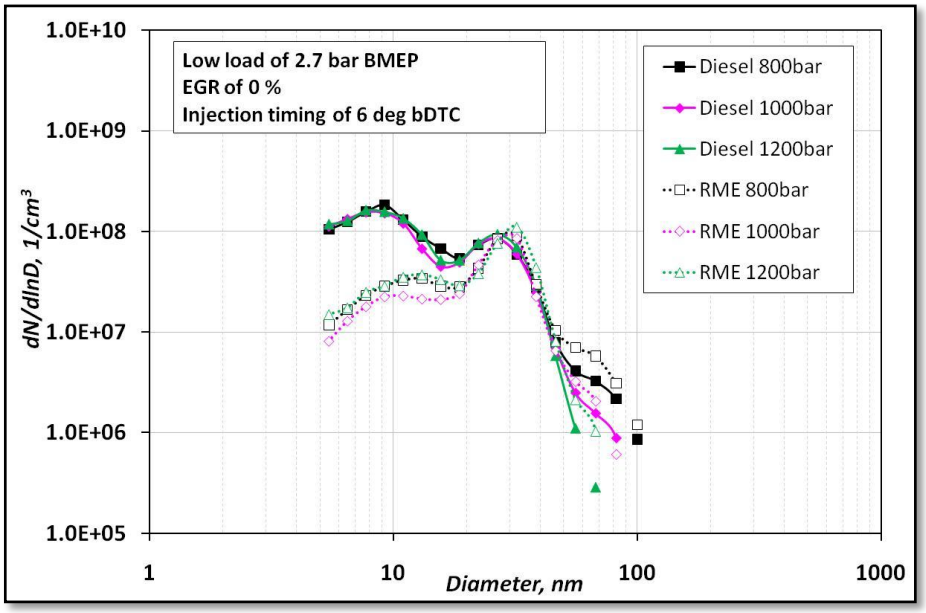

Fig. 5.2.2.1. The influence of injection pressure on soot particles size distributions for diesel and RME at low load engine operation.

On the other hand, the injection pressure had an effect on the particles diameter larger than 40 nm (accumulation mode). Moreover, within the accumulation mode, both fuels showed almost the same particles size distribution in a diameter range of 40 nm to 50 nm. For all the injection timings, the particles concentration number as well as the detection diameter range decreases with a higher injection pressure. Furthermore, the concentration number for diesel fuel was always lower when compared to RME.

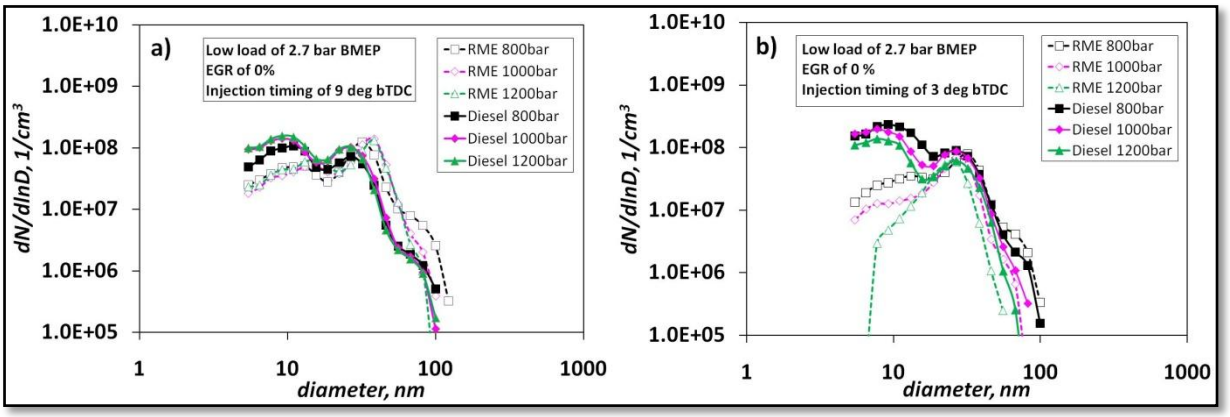

Fig. 5.2.2.2. The influence of injection pressure on soot particles size distributions for diesel and RME at low load engine operation a) for 9 deg bTDC, b) for 3 deg bTDC

A lower particle concentration number in the nucleation mode, for RME, could be attributed to a higher content of volatile fraction which is efficiently vaporized during the secondary dilution stage at 300 degC. On the other hand, it is well known that the increased injection pressure causes a better fuel atomization, resulting in improved air entrainment, vaporization process and air/fuel mixing. These advantages contribute to lower soot

emission. This effect is well known in the case of measuring the soot mass collected on filter paper. Therefore, the filtered particles mass corresponds mainly to their larger diameters reflecting this in the accumulation mode.

Figure 5.2.2.3 shows the representative soot particles size distributions for different levels of EGR for diesel and RME. The EGR percentage was varied from 0% - 40% in the case of diesel, from 0% - 70% in the case of RME under injection timing of 9 and 6 deg bTDC and from 0% - 65% for RME under injection timing of 3 deg bTDC. The presented EGR effect on soot particles size distributions for injection timing of 6 deg bTDC is the same at injection timings of 9 and 3 deg bTDC. It can be seen that the soot particles concentration number in the nucleation mode (< 40 nm) decreases with a high EGR level for both fuels. However, the concentration number for RME is always lower than for diesel. The exception is an EGR level of 40% for diesel, where its concentration number is the lowest. Moreover, the peak of nuclei particles disappears with a higher level of EGR, resulting in a unimodal size distribution with one peak in the accumulation mode. In this mode, an increase in the EGR causes a higher concentration number and a range of detected particles diameter. The addition of 70% of EGR resulted in the highest soot particles concentration number in the case of RME.

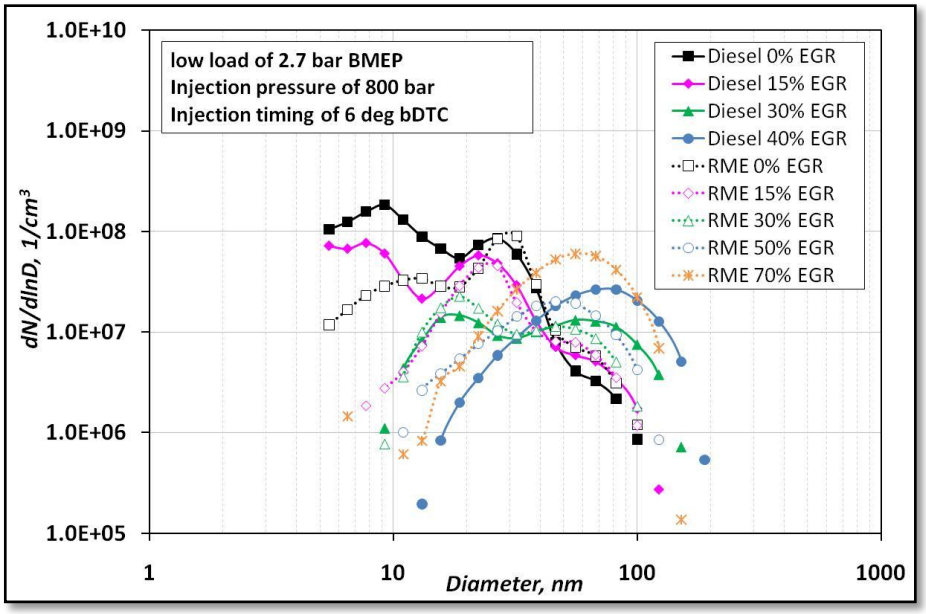

Fig. 5.2.2.3. The influence of EGR on soot particles size distributions for diesel and RME at low load engine operation.

The EGR technique is well known for the reduction of NO_x emissions. However, it has an adverse effect on the soot formation. In the case of high EGR, the engine operates on richer mixtures where the availability of oxygen in the combustion process is limited. These are favourable conditions for an incomplete soot oxidation process resulting in a high soot emission. Additionally, more soot is emitted in a given exhaust volume due to a high EGR

creates a more likely environment for coagulation, accumulation and condensation of volatile fractions on the particles resulting in the detection of a higher concentration of larger diameter particles in the accumulation mode.

Figure 5.2.2.4 shows the soot particles size distributions at different injection timings for diesel and RME. The injection timing effect can be presented under each operating condition from Table 5.2.1 but the conditions of the injection pressure of 1000 bar at 0% of EGR have been chosen for representative of the influence of the injection timing.

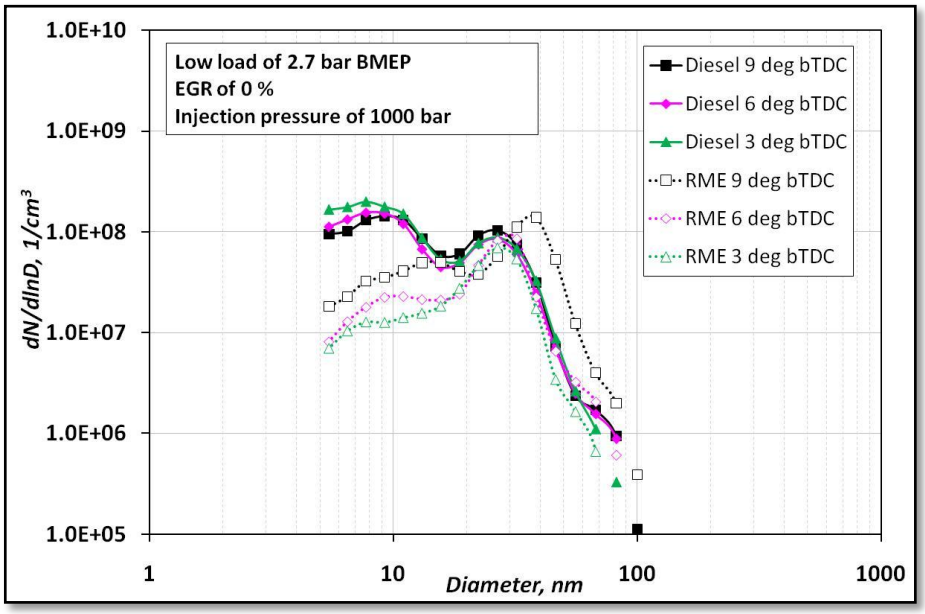

Fig. 5.2.2.4. The influence of EGR on soot particles size distributions for diesel and RME at low load engine operation.

Under all engine operating conditions, RME always has a lower concentration number in the nucleation mode. The injection timing effect in this mode was different for RME and diesel. Therefore, the retarded injection timing generally caused a higher concentration number in the case of diesel and a lower for RME. Moreover, in most cases, the differences in concentration number were within the fluctuation limits. In the accumulation mode, RME showed a decreased particles concentration number and the diameter range for retarded injection timing under all engine operating conditions. However, the retarded injection timing did not show any effects on the concentration number and particles diameter range in the accumulation mode for diesel. Moreover, the differences were within the fluctuation limits. The detection soot particles diameter was usually from 5 to around 85 nm for all fuels and engine operating conditions.

Generally, the retarded injection timing causes a shift of the combustion phase towards the expansion stroke. This consequently decreases the in-cylinder pressure and eventually the in-cylinder temperature. In some cases, the retarded injection timing results in a

simultaneous reduction of soot and NO_x emissions, for instance in the low temperature combustion (LTC) mode.

The analysis of the influence of these three engine parameters showed that the EGR has a stronger effect on soot particle size distributions, entirely changing the soot particles diameter and concentration number for both fuels.

THE CUMULATIVE CONCENTRATION NUMBER – LOW LOAD

The cumulative concentration number (CCN) can be calculated by Equation 3.4.6.1. The cumulative number in the nucleation and accumulation mode has been calculated by the above formula but in different particles ranges. Thus, the particles smaller than 40 nm have been counted into the nucleation mode whereas the particles larger than 40 nm applied to the accumulation mode. Figure 5.2.2.5 presents the effect of injection pressure, injection timing and EGR effects on the cumulative concentration number in the two modes for both fuels. The injection timing did not influence the cumulative concentration of nucleation mode for both fuels (Figure 5.2.2.5a).

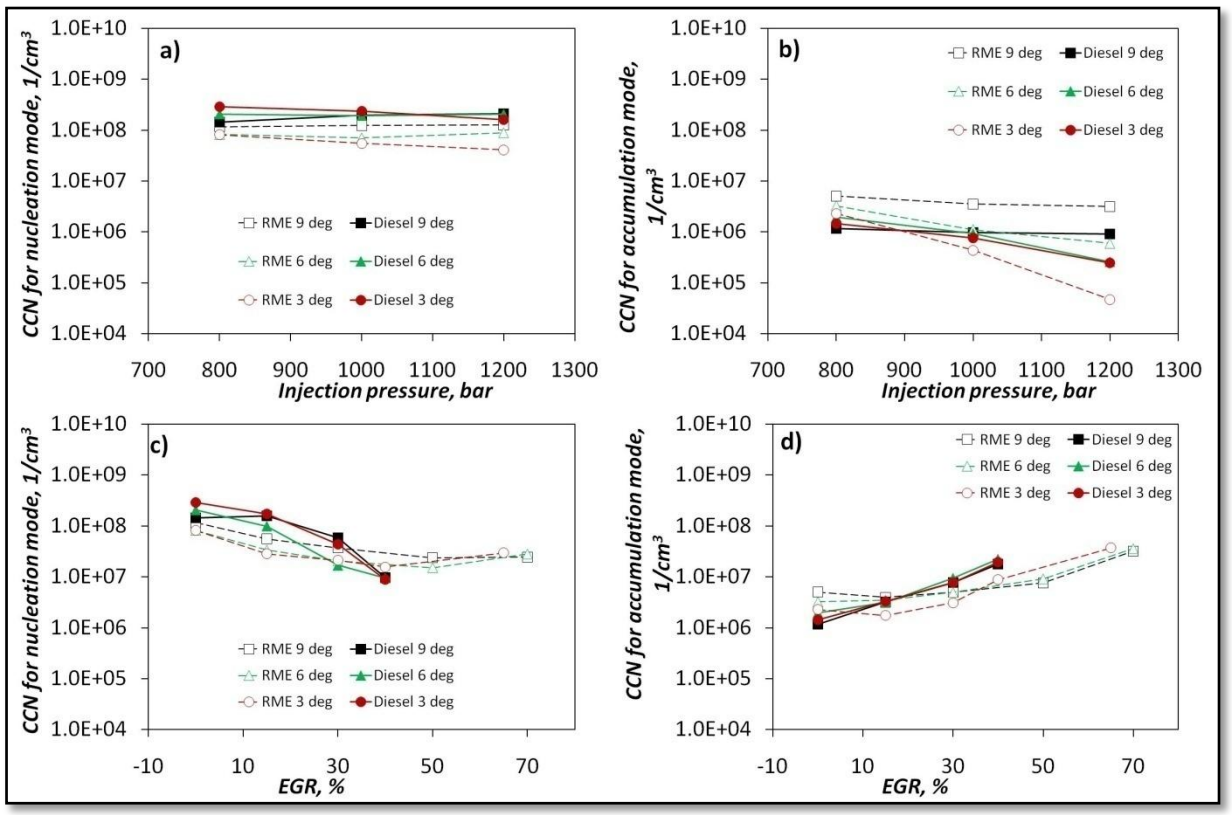

Fig. 5.2.2.5. The cumulative concentration numbers at low load engine operation for: a) nucleation mode - influence of injection pressure, b) accumulation mode - influence of injection pressure, c) nucleation mode - influence of EGR, d) accumulation mode – influence of EGR.

Especially for diesel, the particle cumulative concentration number is not changed by the injection pressure or injection timing and fluctuates around 2.3e08 1/cm^3. However, in the case of RME, the injection pressure and injection timing effects were more visible. Therefore, the particles CCN in the accumulation mode seem to decrease slightly with a higher injection pressure, especially in the case of 3 deg bTDC of injection timing. Moreover, the particles CCN decrease with a retardation of injection timing, especially at 1200 bar of injection pressure. When compared to diesel, RME always shows lower CCN in the nucleation mode. On the other hand, the particles CCN in the accumulation mode are significantly lower when compared to the particles CCN in the nucleation mode (Figure 5.2.2.5b). Especially for diesel, about two orders of magnitude difference can be noticed (1.0e06 1/cm^3). Likewise, in the nucleation mode, diesel showed an unclear trend in particles CCN in the accumulation mode. However, an increase in the injection pressure and retarded injection timing lowered the particles CCN in the accumulation mode for RME. This can especially be seen under the engine operating conditions of injection timing of 3 deg bTDC and injection pressure of 1200 bar.

Figure 5.2.2.5c shows the CCN in the nucleation mode according to different EGR for both fuels. It can be seen that the addition of EGR significantly decreases the CCN. The maximum reduction is approximately 1.9e08 and 5.3e07 1/cm^3 for diesel and RME, respectively, between 0 and maximum EGR. The injection timing did not have any significant influence on CCN in this particles mode. On the other hand, the CCN in the accumulation mode showed a significant increase with higher percentage of EGR (Figure 5.2.2.5d). At the maximum EGR percentage, the CCN is higher (around 1.7e07 and 3.7e07 1/cm^3) than in the case of 0% EGR for diesel and RME, respectively. Moreover, particles in the accumulation mode showed lower CCN than in the nucleation mode.

Generally, higher injection pressure results in lower soot emissions. This trend could be seen in slight decreases of CCN in the accumulation mode, especially for RME. From another point of view the addition of EGR corresponds to a higher soot formation. The EGR effect on particles CCN is the same for both fuels. For higher EGR percentage, particles in the nucleation mode seem to coagulate and form larger particles aggregates in the accumulation mode. Additionally, a lower concentration in the accumulation mode refers to differences in the particles sizes in these two modes. Generally, a high concentration of small diameter particles accumulates, results in low concentration but larger diameters. This effect can be seen in Figure 5.2.2.5c and d.

PARTICLES DIAMETER AT CORRESPONDING PEAK OF CONCENTRATION NUMBER – LOW LOAD

The particle diameter at the corresponding peak of the concentration number (Df(pCN)) has been analysed. Figure 5.2.2.6a presents the Df(pCN) according to different injection pressures for both fuels. In the case of diesel, the Df(pCN) is constant, around 27 nm. The injection pressure and timing did not have any influence. The RME case showed that at an injection pressure of 800 bar, the Df(pCN) is the same for all injection timings and is around 32 nm. However, at an increased injection pressure from 800 bar to 1000 bar and 1200 bar, the retarded injection timing resulted in the reduction of Df(pCN). The maximum difference in Df(pCN) between 9 deg bTDC and 3 deg bTDC of injection timing at 1000 and 1200 of injection pressure equals to around 11 nm. Generally, the Df(pCN) for RME is higher than in the case of diesel.

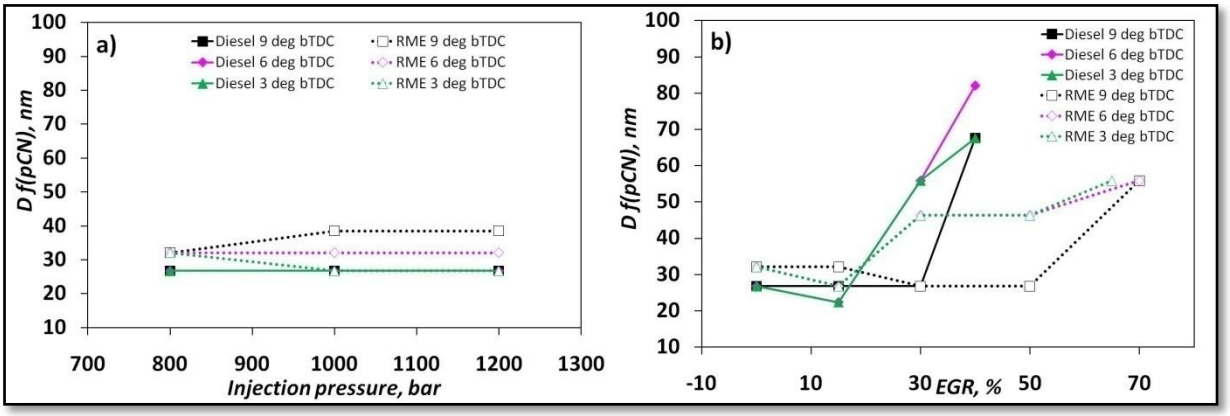

Fig. 5.2.2.6. The peak of the soot particles diameter in the function of a) injection pressure, b) EGR percentage for low engine load.

On the other hand, the addition of EGR causes a shift in the Df(pCN) towards a larger particles range (Figure 5.2.2.6b). In this case, the maximum difference was around 23.8 nm and 55.3 nm for RME and diesel respectively. Moreover, the maximum Df(pCN) about 82 nm occurred for diesel at 50% EGR and 6 deg bTDC of injection timing. The change in the injection timing did not cause any visible variations. Beside a higher concentration of particles from RME, its Df(pCN) is lower than that of diesel.

Generally, an increase in the EGR caused a large shift of the Df(pCN) while a higher injection pressure resulted in only slight differences of around 11 nm.

5.2.3 Results from high load engine operation

SOOT PARTICLES SIZE DISTRIBUTIONS – HIGH LOAD

Figure 5.2.3.1 shows the representative influence of injection pressure on soot particles size distributions under high load engine operation. A bi-modal size distribution can be seen only at 1000 bar and 1200 bar of injection pressure for both fuels. Generally, the nucleation mode shows a lower particles concentration number when compared to low load engine operation. Moreover, the accumulation mode seems to be at a slightly higher level of concentration number and the particles range is shifted towards larger diameters. However, in the case of high engine load, a higher injection pressure leads to increase in the concentration number of soot particles in the nucleation mode and decrease in the accumulation mode for both fuels. Generally, the soot particles size distribution was always at a lower concentration for RME when compared to diesel in the accumulation mode at particular injection timing. Moreover, the case of the nucleation mode shows a lower concentration number for RME at a given injection timing.

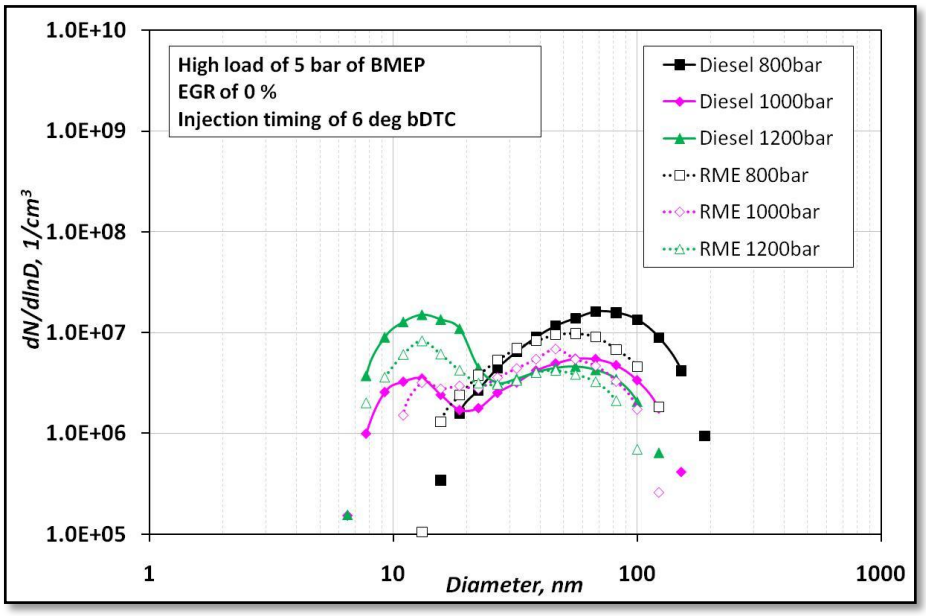

Fig. 5.2.3.1. The influence of injection pressure on soot particles size distributions for diesel and RME at high load engine operation.

The differences in size distribution at low and high engine loads are attributed to various combustion processes, in-cylinder pressure and mixture formation (higher soot emissions). Generally, more fuel is consumed in order to achieve a higher engine load and the combustion process takes place on richer mixtures. A high concentration of particles in the nucleation mode at low engine load is reduced by the particle accumulation process. Therefore, fewer particles can be seen in the nucleation mode but more in the accumulation

mode when compared to low load engine operation. Moreover, high injection pressure improves air entrainment in the fuel spray and mixing process leading to lower soot emissions. In this case, a high soot emission at an injection pressure of 800 bar is reflected as unimodal size distribution with the highest concentration number in the accumulation mode for both fuels. As the injection pressure increases to 1000 bar and then to 1200 bar, the soot emissions are reduced, thus the accumulation mode concentration decreases while the concentration number in the nucleation mode increases.

Figure 5.2.3.2 presents the representative condition for the influence of EGR on the soot particles size distributions at high engine load. The engine load of 5 bar BMEP resulted in higher soot emissions in comparison to the lower engine load. Additionally, a higher EGR percentage further increases soot emissions. Therefore, the particles range at the highest EGR percentages (36% for diesel and 33% for RME) is significantly higher than in the case of low engine load. This is around 6.5 nm – 682 nm and 38.5 nm – 682 for diesel and RME respectively, while at low load, the particles range was usually around 6.5 nm – 151 nm for both fuels. It can be seen that in all cases, the nucleation mode particles seem to follow the same distribution up to around 40 nm, without any influences from the EGR rate. However, in the accumulation mode, the EGR effect is dominant. Therefore, a high EGR percentage results in an increase of the concentration number and range of the particles. Moreover, the soot particles concentration number for RME is always lower when compared to diesel. The usage of high EGR rates causes a strong condensation and accumulation of the soot particles, which is reflected as a significantly low concentration number in the nucleation mode and high in the accumulation mode.

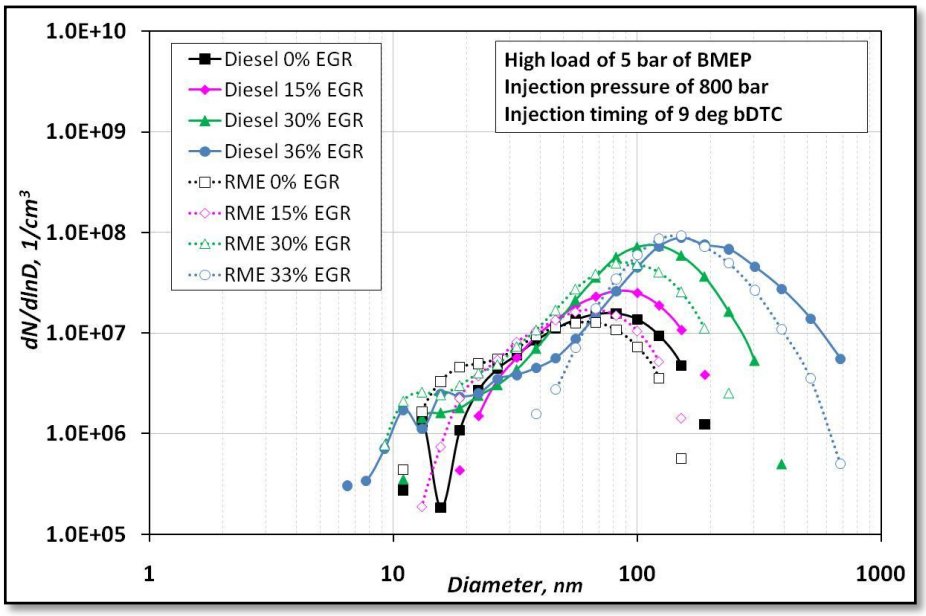

Fig. 5.2.3.2. The influence of EGR on soot particles size distributions for diesel and RME at high load engine operation.

Lower soot emissions from RME can be attributed to its higher oxygen content in the elementary composition, when compared to diesel. Generally, the formation of soot particles strongly depends on the soot precursors formation in rich reaction flame zones during combustion. Thus, soot precursors react favourably with elementary oxygen to form CO rather than aromatic compounds and soot. Additionally, very low sulphur content for RME compared to diesel contributes to lower soot particles number concentration, especially in the accumulation mode.

Figure 5.2.3.3 shows the representative influence of the injection timing on soot particles size distribution. It can be seen that the nucleation mode occurred under all conditions because of a high injection pressure of 1200 bar. Low level of soot emission provides a reduced possibility of accumulation of nuclei particles. In the case of diesel, the retarded injection timing caused a lower concentration of particles in the nucleation mode. Likewise, particles in the accumulation mode provide a slightly lower concentration number. In the case of RME, the particles number concentration in both modes follows the same trend as for diesel. Generally, the size distributions of particles from RME showed a lower concentration number than those from diesel. The influence of injection timing can be seen under all tested engine conditions, thus a similar trend, as described above, occurs in all cases.

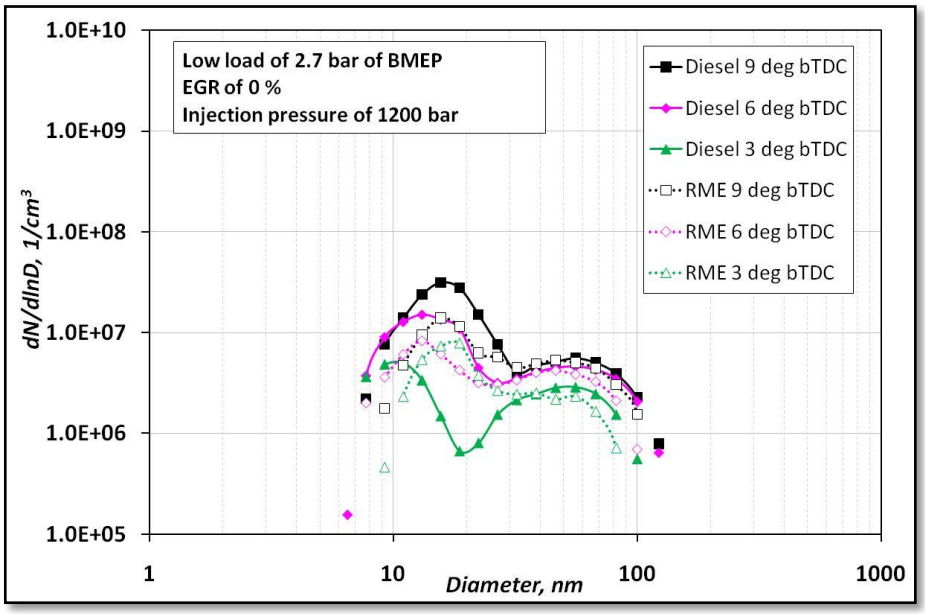

Fig. 5.2.3.3. The influence of injection timing on soot particles size distributions for diesel and RME at high load engine operation.

As well as in the case of the influence of injection pressure and EGR, the injection timing showed a reduction in the nucleation mode and an increase in the accumulation mode under a higher engine load operation.

THE CUMULATIVE CONCENTRATION NUMBER – HIGH LOAD

Figure 5.2.3.4 shows the cumulative concentration number in the nucleation and accumulation mode for all fuels and engine operating conditions. On average, the level of CCN in the nucleation mode regarding the influence of the injection pressure is about 1e07 1/cm^3 for both fuels (Figure 5.2.3.4a). In the case of diesel, the CCN slightly increases for a higher injection pressure, especially at an injection timing of 9 deg bTDC. Moreover, the retarded injection timing results in lower CCN. For RME, the retarded injection timing also resulted in lower CCN in the nucleation mode. However, the differences were smaller than in the case of diesel fuel. Additionally, variations of CCN in the nucleation mode are negligible thus it is almost constant with increased injection pressure.

When compared to a low load engine operation, it could be seen that CCN in the nucleation mode is on a much lower level. Generally, it is almost order of magnitude difference between these two loads. Additionally, the CCN in the nucleation mode for low load slightly decreases but for high load is higher with increased injection pressure. Furthermore, an inconclusive effect of the injection timing in the case of diesel under low load operation seems to be clearer in the case of high load operation. Likewise, CCN in the nucleation mode under high load is always lower for RME.

When the accumulation mode is considered, it can be seen that CCN decreases with a higher injection pressure (Figure 5.2.3.4b). On average, it is reduced from around 1.0e07 1/cm^3 to 1.2e06 1/cm^3. More soot emitted under a high engine load resulted in less CCN in accumulation when compared to a low load engine operation. Additionally, CCN in the accumulation mode is always lower for RME when compared to diesel at a given injection timing. As the CCN in the nucleation mode is almost constant (beside a slight increase for diesel at 9 deg bTDC) while the accumulation mode showed a reduction in CCN with a higher injection pressure.

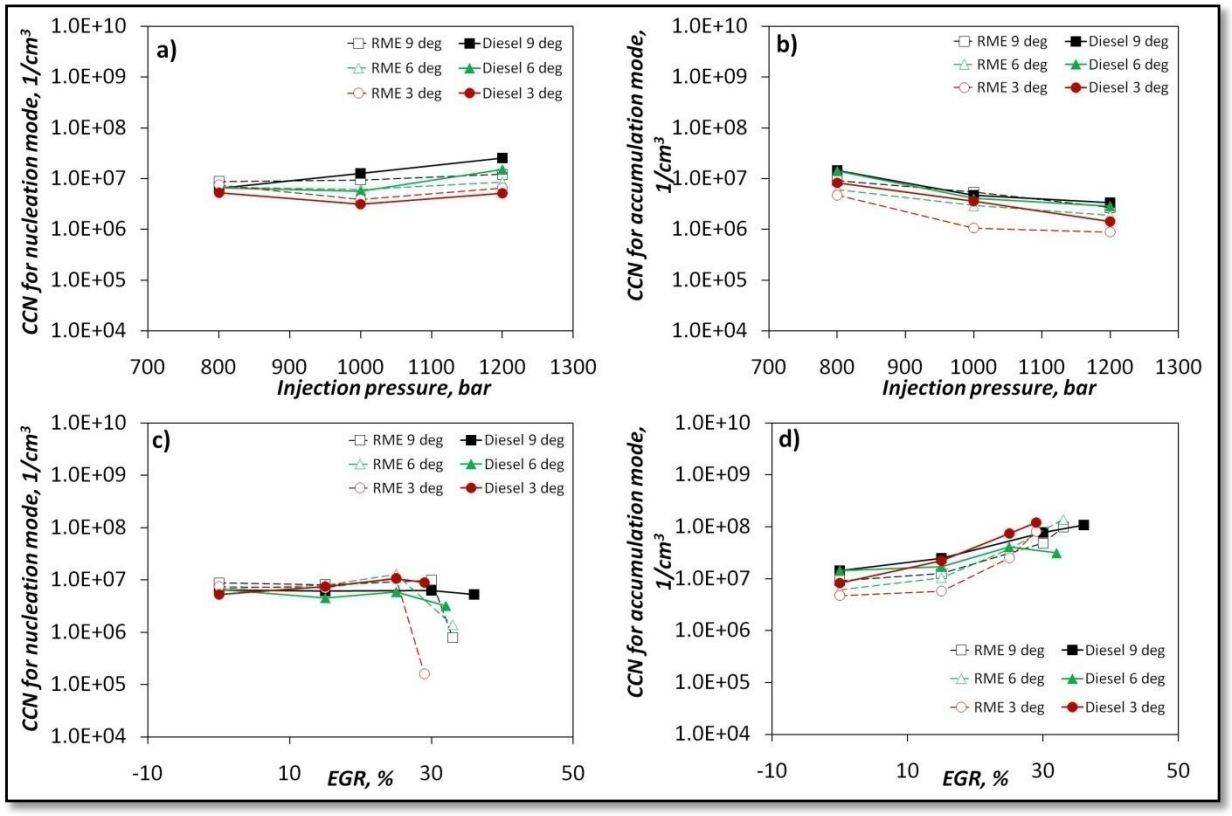

Fig. 5.2.3.4. The cumulative concentration numbers at high load engine operation for: a) nucleation mode - influence of injection pressure, b) accumulation mode - influence of injection pressure, c) nucleation mode - influence of EGR, d) accumulation mode – influence of EGR.

Larger particles diameter can be collected for a mass measurement using a smoke meter, thus the trend of CCN in the accumulation mode may correspond to the smoke number. Moreover, a higher injection pressure reduces soot emissions as a consequence of a better mixing and vaporization of a fuel.

The effect of EGR on the particles nucleation mode is shown in Figure 5.2.3.4c. It can be seen that as the EGR increases, the CCN in the nucleation mode decreases, especially for RME. Moreover, at the highest EGR level, the CCN significantly decreases. However, in the case of diesel, the CCN is almost constant with increased EGR and it is around 6.5e06 1/cm^3. Generally, the injection timing effect was unobserved for both fuels. Once again, the CCN in the nucleation mode under the influence of EGR was at a lower level when compared to low load engine operation. Additionally, a significant difference in CCN in the nucleation mode can be noted between diesel and RME at the highest EGR level. On the other hand, it can be seen that CCN in the accumulation mode significantly increases with higher EGR percentages (Figure 5.2.3.4d). At the maximum EGR, the CCN showed the lowest values in the nucleation mode but the highest in the accumulation mode, especially for RME at injection timing at 9 deg bTDC. Generally, low load and high load cases showed the same trends but, for a high load, CCN in the accumulation mode was at a higher level. Additionally, at a given injection

timing, the RME showed lower CCN than diesel. Particles from the nucleation mode agglomerated to form larger diameters as well as aggregates which are detected in the accumulation mode for higher EGR percentages. The effect of the injection timing can not be seen for both fuels. The soot emissions at high load and EGR rate are relatively high as the engine operates at rich mixtures. This provides the highest concentration of particles in the accumulation mode, which can be easily detected even by the conventional smoke meter.

THE Df(pCN)– HIGH LOAD

The injection pressure and EGR effects on Df(pCN) are presented in Figure 5.2.3.5 for both fuels. In Figure 5.2.3.5a, it can be seen that, as the injection pressure increases, the Df(pCN) shifts towards smaller sizes. Generally, the Df(pCN) is lower for RME when compared to diesel. However, an operation on a high engine load produces the highest concentration numbers at larger diameters, when compared to low engine load. On average, the Df(pCN) was found to be around 60 nm. The maximum difference occurred between diesel (9 deg bTDC, 800 bar) and RME (9 and 3 deg bTDC, 1200 bar) and was around 36 nm. The Df(pCN) was affected by the injection timing but without any viewable trends for both fuels. A slight shift in the Df(pCN) towards a smaller particles size is a consequence of the soot emissions reduction for a higher injection pressure.

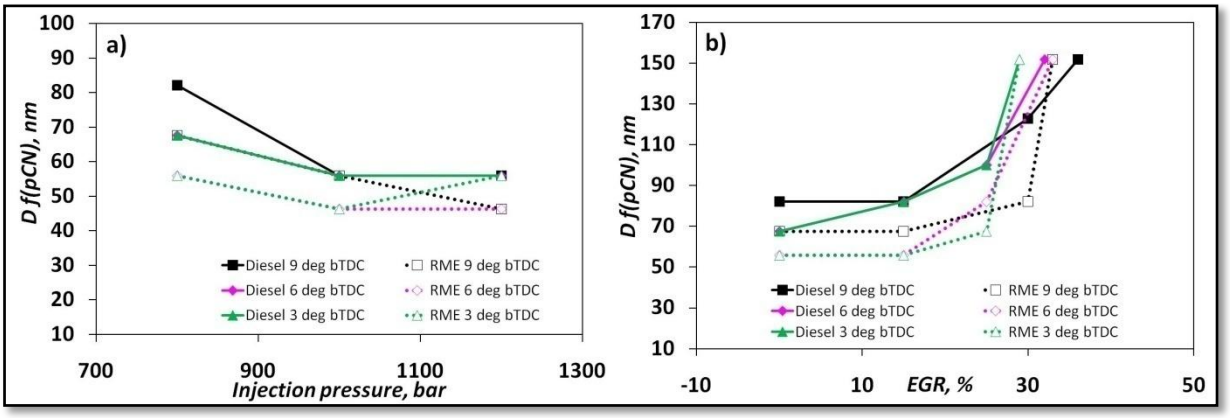

Fig. 5.2.3.5. The peak of the soot particles diameter in the function of a) injection pressure, b) EGR percentage, for high engine load.

On the other hand, high EGR percentages in the inlet caused an increase in the Df(pCN) for both fuels (Figure 5.2.3.5b). The operation at a higher engine load resulted in about two times larger Df(pCN) when compared to a low engine load. The difference between Df(pCN) at 0 % EGR and at maximum percentage of EGR is around 77 nm and 90 nm for diesel and RME, respectively. Generally, when compared to diesel, RME showed smaller Df(pCN) in most cases (beside maximum EGR). It can be noticed that, at low EGR percentages (0 to 30%), a higher Df(pCN) appears at an injection pressure of 9 deg bTDC for both fuels.

The influence of EGR showed the strongest effects on the Df(pCN) at low and high load. The soot emissions at high EGR led to strong condensation and agglomeration of small particles resulting in a shifted Df(pCN) towards larger particles range.

5.2.4 Conclusions

In this study, the particles size distributions under different engine operating conditions (injection timing, injection pressure, EGR, engine load) for two fuels have been analysed.

In the analysis of these two different fuels, RME always showed lower soot particles concentration than diesel under given engine operating conditions. It has been confirmed by a lower CCN in both particles modes and engine loads mainly due to higher oxygen content in the elementary composition of RME. Consequently, it could be justified by higher available EGR percentages. Moreover, when compared to the particle concentration numbers emitted from the same fuel quantity (RME and diesel), the soot emissions from RME could be even lower as this test was done at a constant engine load where the low fuel calorific value for RME was dominant.

The influence of the engine load is clear and understandable. At low engine load, more particles were visible in the nucleation mode. This condition provides low soot emissions as a result of lean mixture combustion. The nuclei particles were visible as a result of limited condensation and agglomeration. An increase in the engine load to 5 bar BMEP caused the combustion mixture to be richer and favourable for higher soot emissions. All small particle diameters are not seen as they have already been coagulated and agglomerated to form a larger size of particles. Therefore, the accumulation mode, in the case of higher engine load, has always been wider and at a higher particles concentration number.

The addition of EGR caused particles from the nucleation mode to agglomerate in the accumulation mode. This effect is visible at a low engine load while a higher load only generated a higher accumulation mode. A combination of high load and EGR resulted in the detection of significantly higher particle diameters. It was also shown that Df(pCN) was shifted towards a larger size of particles due to the gradually higher soot emissions.

The effect of injection timing was clear at a low load only in the accumulation mode. The soot particles concentration number decreased with a higher injection pressure. This can be also seen in the CCN in this mode. Moreover, an increase in the injection pressure caused a higher concentration number in the nucleation mode, especially at a higher engine load.

The interaction between the nucleation and accumulation particles mode can be attributed to the agglomeration and accumulation rate in the cubic unit of exhaust volume.

Presumably, higher soot emissions, thus a higher number of particles, in the same volume, could result in favourable conditions for accumulation and condensation of volatile fractions. This effect was always reflected as a high concentration number of large particles in the case of high soot emissions. High soot emissions, strong agglomeration and condensation processes can happen earlier in the combustion chamber or later during the dilution systems.

The effects of injection timing, EGR and engine load on soot particles in the accumulation mode are similar to those achieved by the usage of the smoke meter. Therefore, a certain size of particle determines the detection limit for this device.

6 CHAPTER 6 – The application of diesel particulate filter (DPF)

Diesel particulate filters (DPF) are widely used in passenger diesel cars and heavy duty diesel engines to reduce the soot particles matter emissions. It is well known that the efficiency of these filters can go even up to 90%. The main objective of this work was to check the soot particles size distribution before and after DPF and gather information about particles sizes which might pass through.

6.1 Test matrix and procedure

The DPF substrate was supplied by Johnson & Matthey. This is standard silicon carbide (SiC) substrate with 400 canals per square inch at 4 mili inch of wall thickness (400/4). The diameter of used in experiment was about 152.4 mm (6 inch). In order to equip the engine with this substrate, the whole existing exhaust system was modified. Figure 6.1.1 presents the manufactured DPF casing used in this experiment. The casing was made in such a way that can accommodate different substrates. It gives an opportunity for testing different DPF materials and porosities. The special connections before and after the filter were made to measure the particles size distribution, temperature, pressure, gaseous emissions and smoke number.

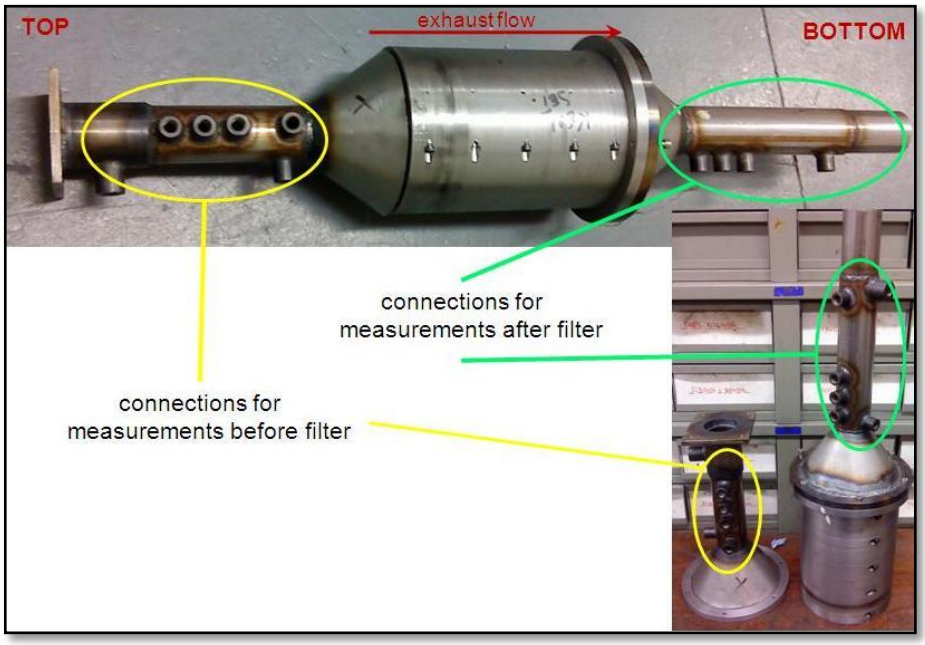

Fig. 6.1.1. The manufactured DPF casing.

In this test, the efficiency of the DPF was tested at three different engine speeds and at four different engine torques for each of the speed. The fuel used in this experiment was diesel. A full test matrix is presented in Table 6.1.1. Other engine operating conditions were kept

constant at 800 bar of injection pressure, 0 % of EGR and 9 deg bTDC of injection timing. The exhaust gas dilution conditions for the EMS were the same as in the case of measurements discussed in the previous chapter (Section 5.2.1). The primary and secondary dilution ratios were 2.32 and 2.0 at 300 degC, respectively.

Table 6.1.1. The engine operating conditions for DPF test.

DIESEL												
engine speed, rpm	1500				2000				2500			
engine torque, Nm	20	40	60	80	20	40	60	80	20	40	60	80
BMEP, bar	1.26	2.51	3.77	5.0	1.26	2.51	3.77	5.0	1.26	2.51	3.77	5.0
measurements after	✓	✓	✓	✓	✓	✓	✓	✓	✓	✓	✓	✓
measurements before	✓	✓	✓	✓	✓	✓	✓	✓	✓	✓	✓	✓

Measurements before and after the DPF were not simultaneous which is the main disadvantage of this test. Limitations in the equipment such as EMS, gas analyser, smoke meter, pressure and temperature sensors forced measurements to be done separately before and after the filter. The test sequence and procedure are illustrated in Figure 6.1.2.

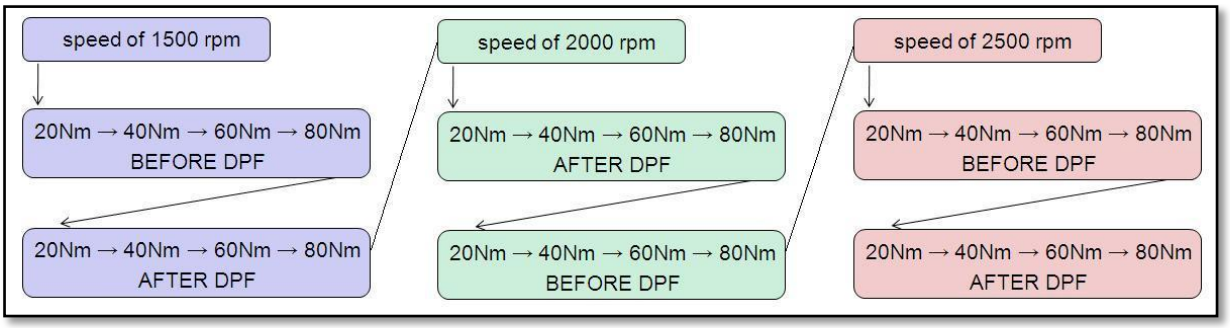

Fig. 6.1.2. The test sequence and procedure.

The test was started at an engine speed of 1500 rpm. The first measurements were done for 20 Nm, 40 Nm, 60 Nm and 80 Nm of engine torque when all devices were connected before the filter. Under these engine conditions, soot particles size distributions (three scans), smoke number, gaseous emissions, fuel consumption and the in-cylinder pressure (averaged over 100 cycles) were measured. In the case of in-cylinder pressure data acquisition system, recording of more than 100 cycles was not possible due to data storage limitations. Moreover, there was not need to record higher amount of cycles as in-cylinder pressure variations were described by COV lower than 5%. The operation at the highest engine tourqe (80 Nm) caused a rise in the engine exhaust system and overall engine temperatures. In this case, the engine was cooled down to a reasonable temperature which allows changing the

connection of all devices for measurement after the filter. Afterwards, the engine torque was changed again from 20 Nm to 80 Nm and all measurements were taken after DPF. For the next set of measurements, the engine speed was changed to 2000 rpm while the devices remained connected after the filter. Once again the measurements were done for the set of engine loads (20 Nm to 80 Nm) and then the devices were reconnected for measurement after DPF when engine was cold. The same procedure was applied for the next set of engine operating conditions. Generally, measurements before and after the DPF should be done simultaneously. The possible differences in measurements before and after the DPF could be attributed to the difference in time between a swap of the devices connection and fact that the engine combustion could be affected by different levels of exhaust back pressure.

The engine loads and speeds were chosen for the representative conditions of different soot emissions levels.

6.2 Combustion and emission characteristics

Once the filter was fitted in the case and attached to the exhaust manifold, the system was ready to run. The first set of measurement was performed to check the exhaust pressures and temperatures before and after the filter. In this case, the engine was running for two hours and the measurements were taken at 10 minutes intervals (Figure 6.2.1a) for the engine torque and speed of 75 Nm and 2000 rpm. It can be seen that the exhaust pressure after DPF as well as the temperature before and after were stabilised fast, after 20 minutes of engine run. However, the back pressure (exhaust pressure before filter) was rising slightly. After two hours of running, all the parameters were stable and the filter was ready to test according to Table 6.1.1.

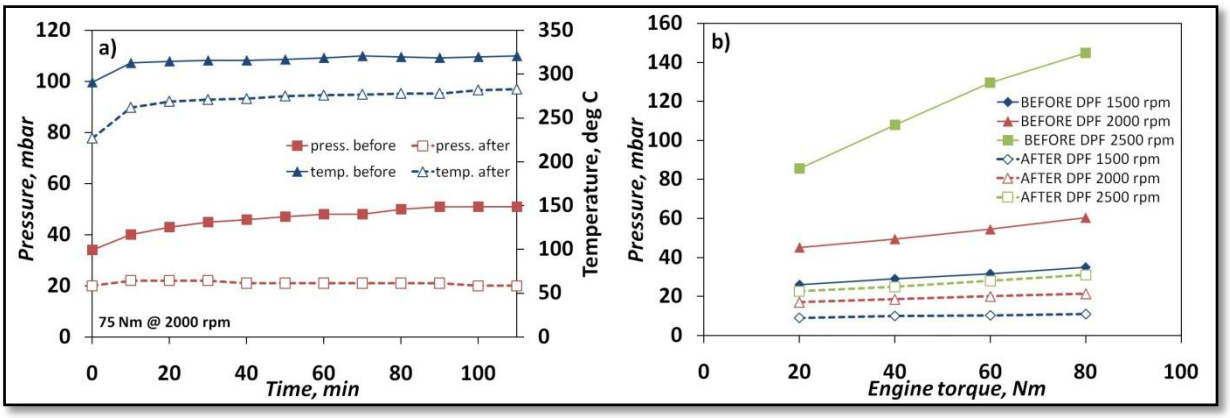

Fig. 6.2.1. The graphs of a) DPF stabilization, b) the effects of engine torque and speed on the pressure before and after DPF.

The exhaust back pressure is the main parameter which represents the condition of DPF. High pressure provides information about a possible blockage of the filter by soot deposition on its walls. Figure 6.2.1b shows the measured pressure before and after DPF for the test conditions described in Table 6.1.1. It can be seen that, the exhaust pressure slightly increases with a higher engine speed and torque. Generally, it is caused by a higher exhaust flow which results in higher pressure. On the other hand, the operation of the engine at higher load consumes more fuel which eventually leads to higher exhaust flow. The effect of DPF on exhaust back pressure can be seen especially in the measurements before filter. Such high pressure differences are not caused only by engine speed and load. Therefore, the soot deposition on filter's walls is more intensive according to the test time. More deposits were built up during later stage of the test procedure (Figure 6.1.1). Moreover, the highest gradients of the back pressure (more soot deposits and higher engine speed and load) occurred at an engine speed of 2500 rpm. The maximum value was about 150 mbar at an engine torque of 80 Nm and engine speed of 2500 rpm. It is interesting to note that, during this experiment, the last measurement was done when the devices were connected after the filter. In reality, at the same time, the back pressure could be even higher than the one observed in the graph.

However, recorded in-cylinder pressure curves for the measurement before and after DPF show that the combustion performance was not affected much by the different levels of back pressure (Figure 6.2.2a). The in-cylinder pressure curves before and after applies only to different times of measurement. From the combustion characteristics point of view, the in-cylinder pressure peak increases with a higher engine torque but decreases with a higher engine speed.

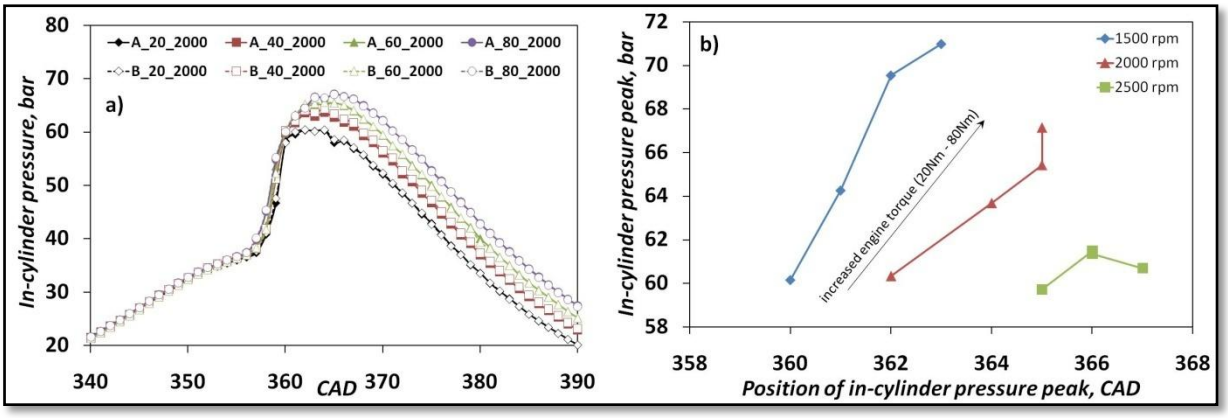

Fig. 6.2.2. The graphs of a) in-cylinder pressure peaks before and after DPF, b) the effects of engine torque and speed on the in-cylinder pressure peak.

Moreover, Figure 6.2.3 presents the ignition delay and the duration of combustion. All these values were calculated according to Section 3.4.3. It can be seen that as the engine speed increases the ID is longer. Additionally, the ID decreases slightly with a higher engine torque

for a given engine speed. As more fuel is injected, the overall engine temperature is higher, thus the fuel vaporizes and ignites faster.

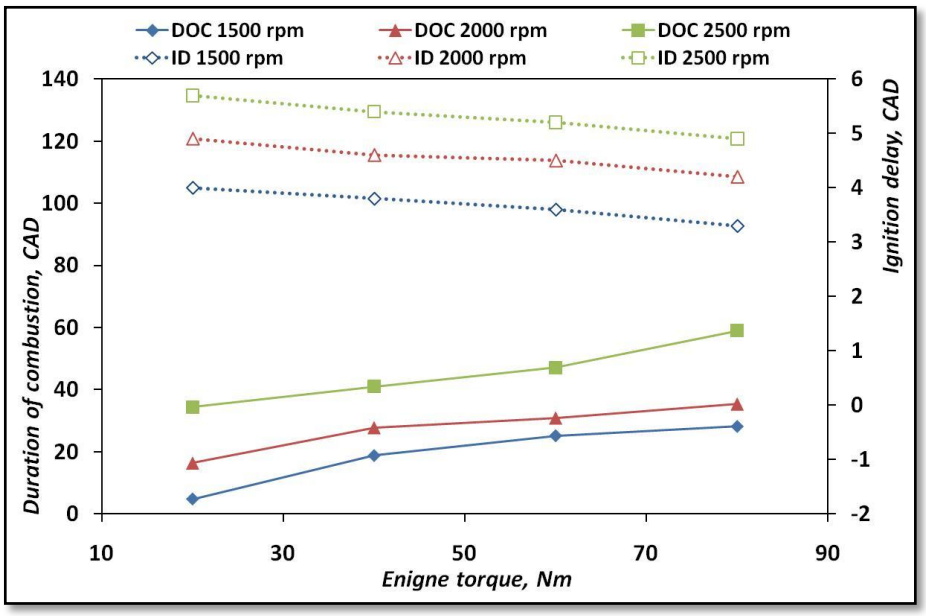

Fig. 6.2.3. The graphs of a) in-cylinder pressure peaks before and after DPF, b) the effects of engine torque and speed on the in-cylinder pressure peak.

In the same Figure the data of DOC is presented. It can be noticed that, as the engine torque and speed increases, the duration of combustion is longer. This is mainly attributed to the higher fuel consumption, thus more time is needed to complete the combustion process.

All emissions and fuel consumption were measured twice. The first measurement was done when all devices were connected before the filter and the second measurement after the filter, according to the test procedure. Figure 6.2.4a shows the variations of NO_x emissions and the smoke number in Figure 6.2.4b for different engine speed and torque.

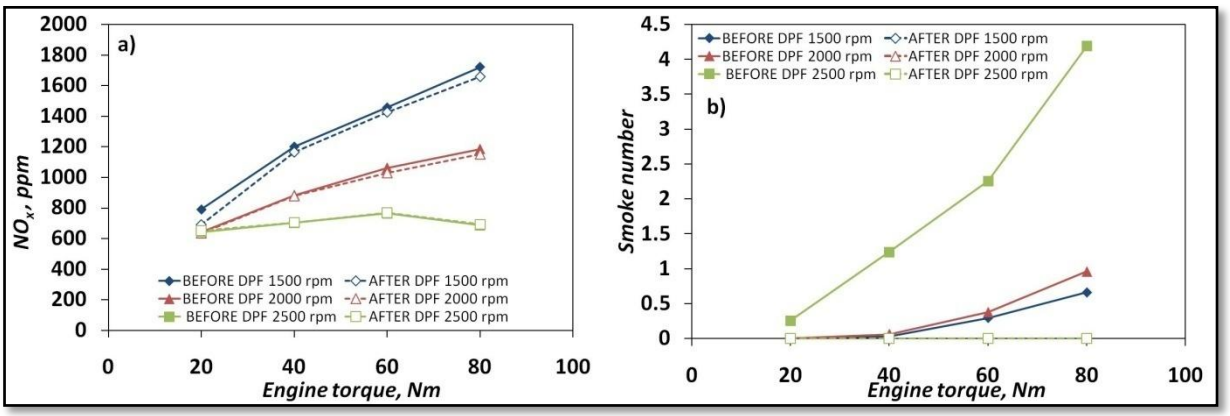

Fig. 6.2.4. The engine out emissions of: a) nitrogen oxides, b) filter smoke number.

It can be seen that, the NO_x decrease with a higher engine speed but increase with a higher engine torque. The measurements before and after the filter showed that DPF does not influence NO_x emissions.

Moreover, after the filter, they are the same as before with only small fluctuations. Generally, it is noticeable that NO_x are strongly linked to the in-cylinder pressure peak. The NO_x emissions follow the same trend as the cylinder pressure peaks. Therefore, NO_x are attributed to the in-cylinder temperature and the premixed combustion phase. Lower in-cylinder pressure and heat release peaks lead to the reduction of in-cylinder temperature eventually resulting in less NO_x.

On the other hand, the DPF effectively reduced soot emissions. In Figure 6.2.4b it can be seen that, as the engine torque and speed increase, the smoke number is higher before the DPF. Moreover, the measurement after the filter showed that the soot is below the detection limit of the AVL smoke meter under all engine operating conditions as small nuclei particles can easily pass through the paper filter. For this reason, a detailed analysis of soot particles size distribution after DPF was made and it is described in the next section. Generally, before the filter, the highest soot emission at an engine speed of 2500 rpm is a result of engine operation on gradually richer mixtures and at gradually raised exhaust back pressure. As the engine torque increases at a given engine speed, the smoke number also increases, mainly because of higher fuel consumption (richer mixtures).

Figure 6.2.5 shows the THC and CO emissions under all tested engine operating conditions for measurements done before and after the DPF. It has been found that these emissions were sensitive to the usage of the filter. Generally, filtered soot inside the DPF influences CO as well as THC emissions. In the case of THC emissions, measurements after DPF show that they are higher than before the filter for engine speeds of 1500 rpm and 2000 rpm but lower at 2500 rpm. This inconclusive trend can be attributed to the absorption of hydrocarbons by the carbon particles, strong condensation or oxidation at higher temperatures. Additionally, it can be affected by the test procedure where THC emissions were not measured simultaneously before and after the filter.

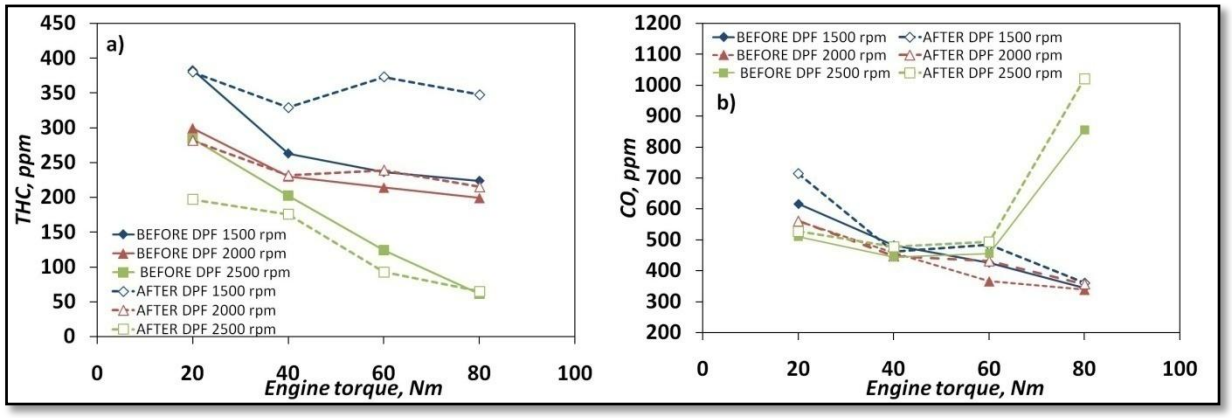

Fig. 6.2.5. The engine out emissions of: a) total hydrocarbons, b) carbon monoxides.

The CO emissions generally decrease with a higher engine torque and speed, before and after the DPF apart from the engine condition of 80 Nm at 2500 rpm where the significant peak of this emission can be seen. This can be the result of the highest exhaust back pressure and very rich combustion. Possibly, the differences in the measurements before and after DPF can be explained by partial soot oxidation which leads to higher CO after DPF. However, the influence of DPF on the THC and CO emissions can be further studied and explored.

The fuel consumption is expressed as a brake specific fuel consumption (Figure 6.2.6a) and as a fuel consumption in grams per second (Figure 6.2.6b). Obviously, the fuel consumption increases with a higher engine speed and load. The fuel consumption indicates that the engine operating conditions are possibly maintained the same for measurements before and after the DPF.

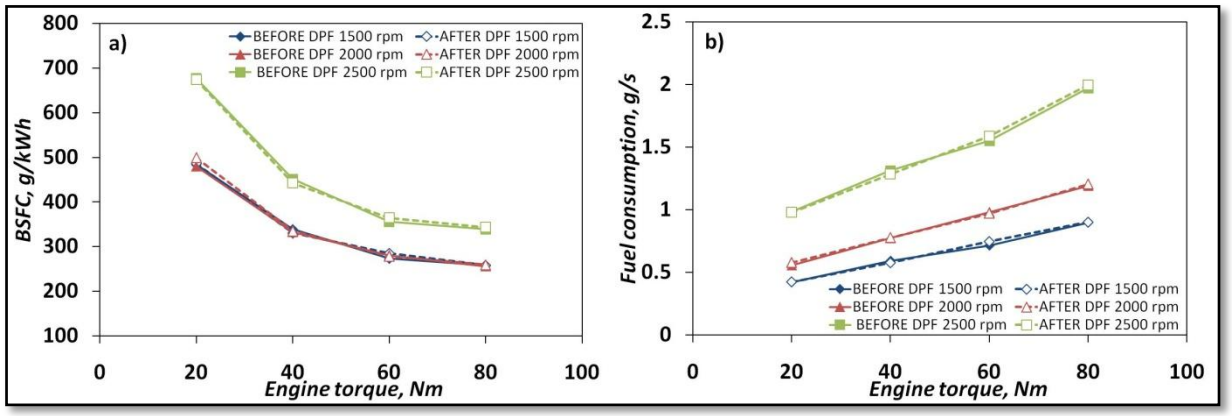

Fig. 6.2.6. The fuel consumption a) brake specific fuel consumption, b) fuel consumption in grams per second.

On the other hand, the BSFC resulted in the same values at engine speeds of 1500 rpm and 2000 rpm. Moreover, it decreases with the engine torque for a given engine speed. Relatively, at a higher engine load, less fuel is consumed for one kWh of engine output energy.

The previously discussed effects of gradually soot built up, increased back pressure and time differences in the measurements, the engine operating conditions remained constant. It can be seen especially from the measurements before and after the DPF (time difference) of NO_x (Figure 6.2.4a) and fuel consumption (Figure 6.2.6a, b), where good agreement of data has been achieved.

6.3 Soot particles size distributions

The soot particles size distribution was measured three times (three scans) and then averaged. For all engine operating conditions, as well as before and after DPF, the dilution conditions were the same.

Figure 6.3.1 shows the soot particles size distributions at an engine speed of 1500 rpm, before and after the filter. Generally, the soot particles size distributions can be divided into two particles modes. The first describes small diameter, nuclei particles in a diameter range from 5 nm to 40 nm while the second larger particles in a diameter range from 40 nm to 700 nm. In the case of measurements before the filter, it can be seen that as the engine torque increases the particles concentration number is reduced. However, the particles concentration number in the accumulation mode increases with a higher engine torque. Moreover, the detection diameter range is broader (up to 238 nm). This trend can be attributed to higher soot emissions at richer mixtures engine operation (Figure 6.2.4b). Therefore, more soot particles in the same exhaust volume tend to grow the size of the particle. The possibility of increasing the size can be attributed to agglomeration, accumulation, coagulation or condensation of VOF. The smoke number is strongly linked to the accumulation mode particles. Therefore, an increase in the concentration in this mode is represented by a gradually higher smoke number. The measurements after the DPF filter show that at a low engine torque (20 Nm and 40 Nm) the particles were not detected. Nevertheless, as the engine torque increased to 60 Nm and 80 Nm, small particles were detected by the EMS system in a narrow diameter range. At the engine torque of 60 Nm and 80 Nm, the detection particles diameter range was approximately 8 – 26 nm and 5 – 26 nm, respectively. The concentration peak corresponds to the diameter of around 18 nm. The concentration levels are similar to those from measurements before filter especially at their peak region. At this engine speed, the filter was effectively reducing the soot particles within a diameter larger than 26 nm. It is interesting to note that at engine torque of 80 Nm, the number concentration of particles in diameter of 10.9 and 13.1 nm after the filter was higher than before. This could be attributed to the nucleation process which occurs through the filter.

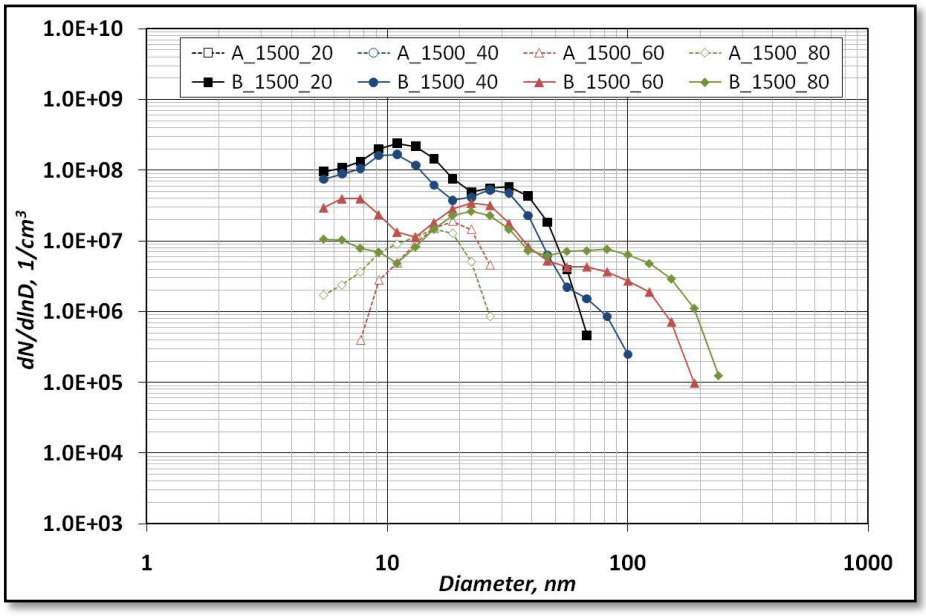

Fig. 6.3.1. The soot particles size distributions at engine speed of 1500 rpm, before and after DPF.

The soot particles size distribution before and after the filter for the engine speed of 2000 rpm are shown in Figure 6.3.2. The same trend in particles size distribution before the DPF can be seen in the case of the engine speed of 2000 rpm.

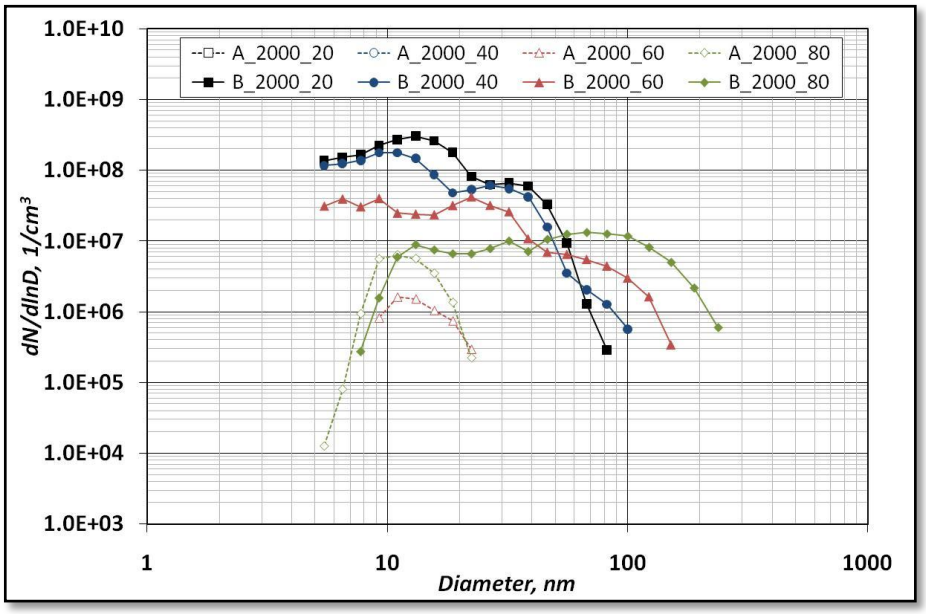

Fig. 6.3.2. The soot particles size distributions at engine speed of 2000 rpm, before and after DPF.

The nuclei particles decrease in concentration while in the accumulation mode the concentration increases with a higher engine torque. Generally, the particles size distributions at these two engine speeds are similar. As well as in the case of the engine speed of 1500 rpm, the detection diameter range increases with a higher engine torque. The maximum detected diameter is around 238 nm at an engine torque of 80 Nm. The particles

concentration number seems to be higher than in the case of the engine speed of 1500 rpm for all engine torques. However, the particles size distribution in the nucleation mode is lower than in the case of the engine speed of 1500 rpm. Generally, the soot particles size distributions are comparable to each other, which can be attributed to low differences in the smoke number or fuel consumption between these two engine speeds. On the other hand, the measurements after the filter showed that the particles diameter detection range is about 9 – 22 nm and 5 – 22 nm at an engine torque of 60 Nm and 80 Nm, respectively. The soot particles were effectively filtrated in the case of the engine torque of 20 Nm and 40 Nm. However, the concentration number is significantly lower than in the case of the engine speed of 1500 rpm. As well as at the engine speed of 1500 rpm, the concentration number of particles after the DPF is higher than at the measurement before for particles diameter range from 10.9 to 5.4 nm at an engine torque of 80 Nm. Relatively lower particles concentration after the filter can be attributed to a gradually better filter efficiency due to more soot deposition on the filter's walls.

Figure 6.3.3 shows the soot particles size distributions at an engine speed of 2500 rpm, measured before and after the filter.

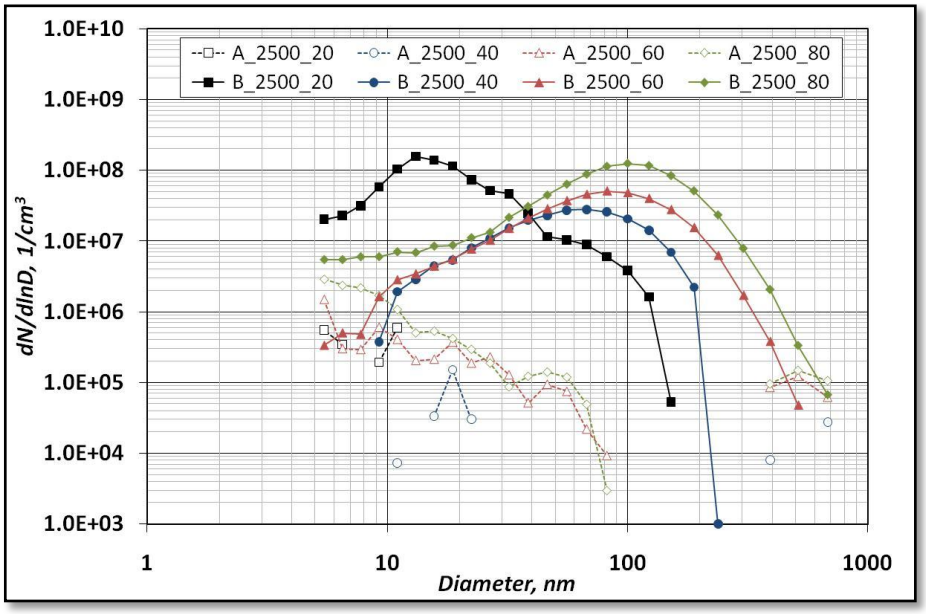

Fig. 6.3.3. The soot particles size distributions at engine speed of 2500 rpm, before and after DPF.

The particles sizes before the filter are entirely different than at the engine speeds of 1500 rpm and 2000 rpm. Generally, the trend remains the same as the nuclei particles decrease and the accumulation mode increases with a higher engine torque. However, apart from the engine torque of 20 Nm, the peak of the nucleation mode is reduced and the concentration levels are significantly lower than at any other engine speed. On the other hand, the particles in the accumulation mode are at significantly higher concentration levels and particles diameter detection range increases from 151 nm at 20 Nm to 682 nm at 80 Nm. A

different size distribution pattern at 2500 rpm can be attributed to higher differences in the smoke number as well as fuel consumption (Figures 6.2.4b and 6.2.5b, respectively) when compared to other engine speeds. The highest concentration number can be seen at the highest engine torque (80 Nm), where the smoke number and the fuel consumption also had their peaks. Moreover, the highest engine load and soot conditions lead to soot particles being passed through the filter in broader diameter ranges when compared to other engine speeds. The diameter range was about 5 nm to 82 nm at both engine torques of 60 Nm and 80 Nm. However, detected particles after the DPF were at significantly lower concentration levels when compared to other engine speeds. At lower engine torques, the soot particles were detected as single points in diameter ranges from 5 nm to 10 nm, 10 nm to 22 nm at 20 Nm and 40 Nm, respectively. It is interesting to note that all soot particles passed though the filter under all engine conditions are detected in low diameter range (low speed) or low concentration number (high speed). Moreover, all these particles were beyond the detection limit of the smoke meter. As well as at the previous engine speeds, the measurement after the filter showed higher number concentration than before but only at engine torque of 60 Nm and particles diameter of 5.4 nm.

Figure 6.3.4 shows the cumulative concentration numbers under all engine operating conditions before and after the DPF. The CCN has been calculated by the Equation 3.4.6.1.

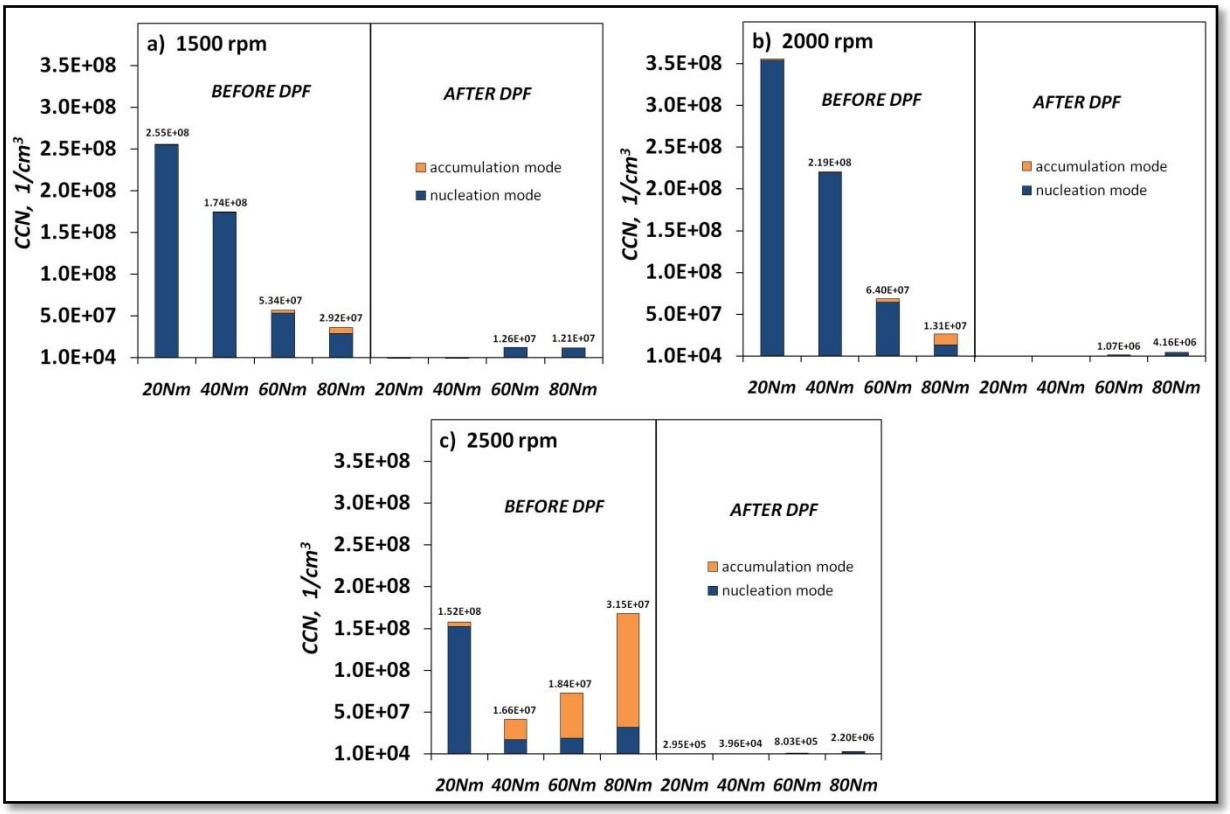

Fig. 6.3.4. The CCN in the nucleation and accumulation modes before and after the DPF at engine speeds of: a) 1500 rpm , b) 2000 rpm, c) 2500 rpm.

In the case of the engine speed of 1500 rpm (Figure 6.3.4a), it can be seen that the total CCN before the filter decreases with a higher engine torque (mainly the nucleation particles mode). However, the engine operation at gradually higher load leads to the formation of larger particles diameters. Their CCN in the accumulation mode increases with a higher engine torque. After the filter, the particles appear only in the nucleation mode at 60 Nm and 80 Nm of engine torque. Their concentrations are significantly lower than those before the filter. In the case of a higher engine speed of 2000 rpm (Figure 6.3.4b), the CCN before the filter, especially at a lower engine torque, is higher than at 1500 rpm. Moreover, a higher engine load leads to a gradually lower total CCN (mainly the nucleation mode) and higher CCN in the accumulation mode. It can be seen that the CCN in the accumulation is higher than in the case of an engine speed of 1500 rpm. On the other hand, the particles which passed through the filter are detected only in the nucleation particles mode at an engine torque of 60 Nm and 80 Nm. Their CCN is significantly lower than for the particles before filter as well as at the engine speed of 1500 rpm. The soot deposition inside the DPF at a later stage of experiment was more intensive thus lower CCN than at the engine speed of 1500 rpm can be observed. The CCN before and after the DPF at the highest engine speed of 2500 rpm are presented in Figure 6.3.4c. Because of relatively high soot emission at this engine speed, the CCN in the nucleation mode is significantly reduced. At the previous engine speeds, the dominant fraction in the total CCN was a nucleation mode while at 2500 rpm this role takes over the accumulation mode. It can be seen that in the case of the highest engine torque of 80 Nm, the CCN in the accumulation mode is equal to around 80% of total CCN. Generally, the particles in the nucleation mode are reduced by favourable conditions of accumulation or agglomeration, leading to larger particles in the accumulation mode. The total CCN increases with a higher engine tourqe from 40 Nm to 80 Nm beside 20 Nm which contribute to a high CCN in the nucleation mode under this condition due to less soot production in the exhaust. On the other hand, it can be seen that particles are detected for each of torques after the filter. However, the CCN levels are significantly lower when compared to other engine speed at the same engine torques. Moreover, the CCN consists of particles only from the nucleation mode. The CCN in accumulation mode corresponds to the measured smoke number. For instance, the highest CCN in the accumulation mode is reflected by the maximum value of the smoke number at the highest engine speed.

The filtration efficiencies are illustrated in Figure 6.3.5 and have been calculated by the Formula 3.4.8.1. The particles diameter filtration efficiency has been calculated using the same equation but the CCN after and before the filter is replaced by the concentration number before and after for a given particles diameter.

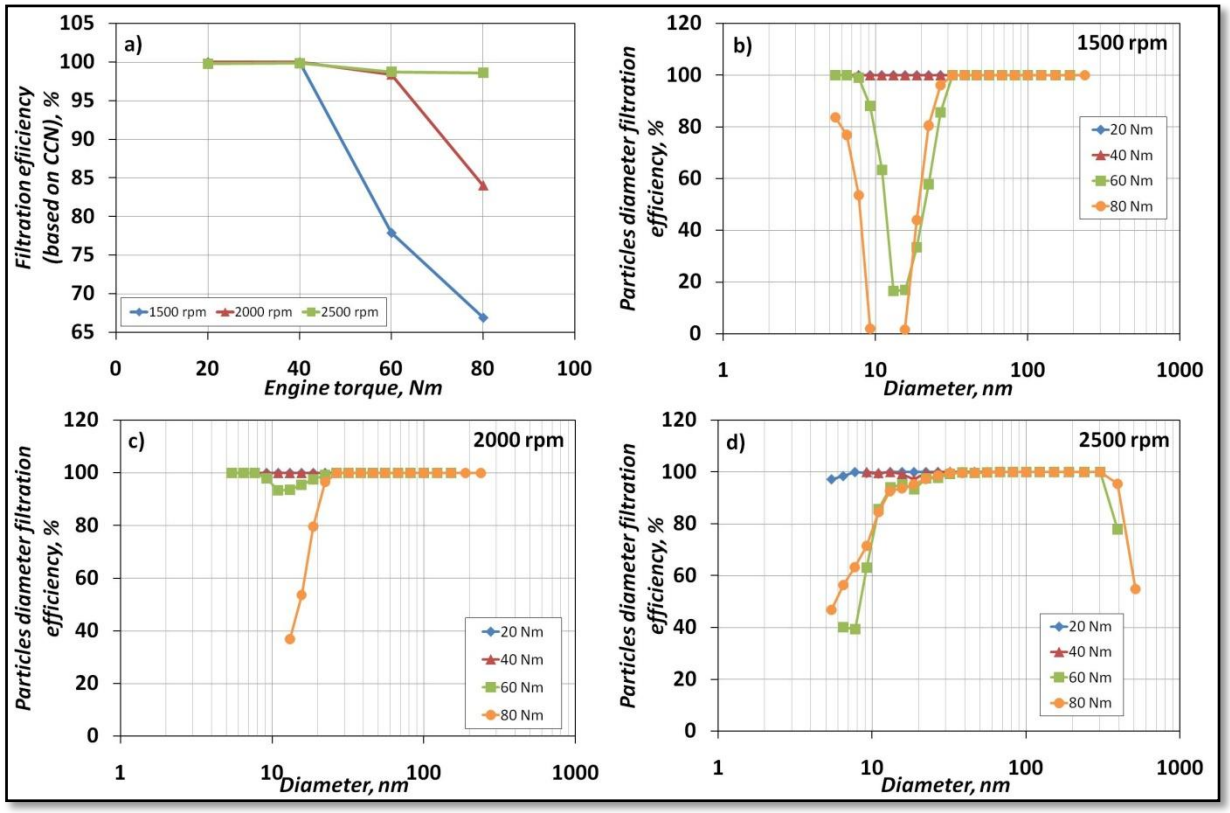

Fig. 6.3.5. The filtration efficiencies calculated based on: a) cumulative concentration number, b), c) and d) based on each of particles diameter for engine speed of 1500 rpm, 2000 rpm and 2500 rpm, respectively.

Based on the CCN, it can be seen that an increase in the engine speed improves the filtration efficiency (Figure 6.3.5a). The efficiency equals to 100% in the case of the engine speed of 1500 and 2000 rpm for engine torque at 20 Nm and 40 Nm. Under these engine operating conditions, the EMS system did not detect any soot particles after the DPF. On the other hand, an increase in the engine torque diminishes the efficiency. At the highest engine torque of 80 Nm, the filtration efficiency was about 67%, 84% and 98% at engine speeds of 1500 rpm, 2000 rpm and 2500 rpm, respectively.

The best filter performance can be observed at the highest engine speed of 2500 rpm. The efficiency varies from 99 % to 98 %. There are two factors which can result in such a high efficiency. These are higher soot emissions at higher engine speed and the duration of the experiment. At a later stage of the experiment the filter could be partially blocked resulting in the highest exhaust back pressure (Figure 6.2.1b) where the filtration is automatically improved. On the other hand, higher soot emissions lead to the formation of larger diameter particles which are favourably filtered than a smaller diameter size.

Figures 6.3.5b, c and d present the filtration efficiency calculated for each particle diameter at an engine speed of 1500 rpm, 2000 rpm and 2500 rpm, respectively. For the engine speed of 1500 rpm, the efficiency was 100% for the whole range of particles at an engine torque of 20 Nm and 40 Nm. The engine operation on a higher load resulted in a high concentration of

particles after the filter for the engine torques of 60 Nm and 80 Nm. In the case of 60 Nm, the efficiency goes down to around 16% at particles diameter of 13 - 15 nm while at 80 Nm it is around 2% for particle diameters of around 9 – 15 nm. In the case of the engine speed of 2000 rpm (Figure 6.3.5c), as the particles were detected, the efficiency started to decrease. However, lower concentration numbers than at 1500 rpm lead to generally higher filtration efficiencies. At the engine torque of 20 Nm and 60 Nm, the filtration efficiency was 100% for all particles diameter range. The lowest efficiency for 60 Nm was around 36 % at particles diameter of 13 nm while for 80 Nm around 93% at particles diameter of 11 nm. Generally, the efficiency for each particles diameter was better at this engine speed. Figure 6.3.5d shows the efficiency at the highest engine speed of 2500 rpm. It is interesting that at an engine torque of 60 Nm and 80 Nm, the particles were detected from 5 to 82 nm while the filtration efficiency starts decreasing from 26 nm. Therefore, the filtration efficiency between 26 nm and 82 seems to be at around 99%. The minimum efficiency was around 40% and 46% for the engine torque of 60 Nm and 80 nm, respectively. Moreover, as previously mentioned, the single detections of particles took place in the case of low engine torques of 20 Nm and 40 Nm. This is reflected by slightly decreased efficiency under these engine conditions. Furthermore, it also occurred at a larger particles diameter, which decreases the efficiency at these particular particle diameters. However, these single detections are rather interruptions in the measurement method than a real result as the signal to noise ratio was high.

6.4 The condition of the DPF after the test

The whole modified exhaust system, together with DPF, has been again replaced and opened for inspection. Figure 6.4.1 shows images of the filter after the whole test. It can be seen that the entrance of the filter is highly deposited with soot (Figure 6.4.1a and b). The cross section area has been reduced which resulted in a higher exhaust back pressure. Moreover, the whole substrate has been pushed down in the casing as a consequence of a high exhaust back pressure. The fitting of the filter was very tight because after the opening of the case, the soot deposition could not been noted between the substrate and the casing's walls (Figure 6.4.1b and c). On the other hand, the outlet of the filter was very clean, without any soot depositions (Figure 6.4.1c and d). A small fragment on the edge of the filter, which can be seen on the picture in Figure 6.4.1d, is a result of substrate movement due to high exhaust pressure. The edge of the filter touched the cone's wall resulted in small fragmentation.

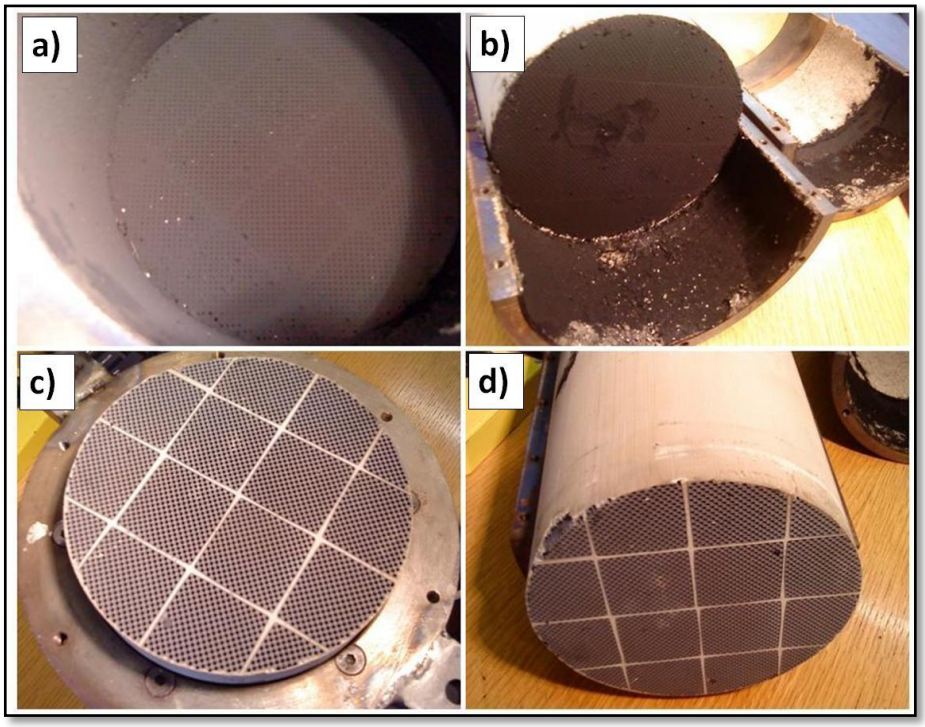

Fig. 6.4.1. The DPF after the test a) front of the filter closed case, b) front of the filter open case, c) back of the filter closed case, d) back of the filter open case.

6.5 Conclusions

The conclusions from this experiment are summarized below.

The soot particles after the DPF were not detected by the smoke meter as they were too small in diameter and easily passed through the paper filter. However, before the DPF, the smoke number increased with a higher engine speed and torque.

After the DPF, the particles were detected mainly at engine torque of 60 Nm and 80 Nm. The detection diameter range was around: 5 - 26nm, 5 - 22nm and 5 – 82 nm at an engine speed of 1500 rpm, 2000 rpm and 2500 rpm, respectively. On the other hand, the particles size distribution were similar at engine speeds of 1500 rpm and 2000 rpm while at 2500 rpm a reduction in nuclei particles and an increase in accumulation particles were noticed.

Moreover, it has been found that the particles accumulation mode is strongly connected to the smoke number as their values are represented by the same trend. Presumably, particles in a diameter larger than 100 nm can be collected and measured by the smoke meter. Otherwise, smaller particles are behind the detection limits of this device.

The filtration efficiency based on the CCN and particles diameter was 100% at low engine torque of 20 Nm and 40 Nm at all engine speeds. Generally, the filtration efficiency

increased with higher engine speed, which can be attributed to the high exhaust flow which partially blocked the substrate at a later stage of the experiment.

The NO_x emissions, in-cylinder pressure and fuel consumption, before and after DPF, indicated that the engine operating conditions were not affected by the time between measurements or by the increased back pressure.

The regeneration system of DPF and simultaneous monitoring of the engine parameters before and after the filter have to be developed for further investigations. Possibly by maintaining the same exhaust back pressure during measurements the results would better reflect the reality.

7 CHAPTER 7 - Conclusions and further work recommendations

Generally, the combustion characteristics of RSO, SO and their blends with diesel were poorer than for diesel. The in-cylinder pressure and the heat release rate for RSO and SO were lower when compared to diesel resulting in lower NO_x and high soot emissions. However, the ID was noted to be the same as that for diesel. The usage of RSO and SO also resulted in incomplete combustion (higher THC and CO emissions) as well as higher fuel consumption. Moreover, as the percentage of RSO or SO in the blend increased, the NO_x emissions were lowered but the fuel consumption, combustion efficiency, CO, THC and soot emissions were higher. Slight differences between RSO and SO are attributed to the differences in fuel properties. As a continuation of previous measurements the influence of three engine parameters on the combustion and emission characteristics for RSO and its blends is shown in Section 4.2. When RSO and diesel were compared under the same engine operating conditions, the combustion and emissions characteristics were the same as in the previous section. However, when the injection pressure was varied from 800 bar to 1200 bar, the soot emissions were lowered but the NO_x emissions increased for RSO and its blends. On the other hand, the usage of EGR reduced NO_x but increased the smoke number. The retarded injection timing reduced NO_x but increased the soot emissions for RSO and its blends. When compared to diesel, the summarised analysis shows that the combination of injection parameters (injection timing and injection pressure) can give the possibility of simultaneous reduction of soot and NO_x emissions. Additionally, a detailed analysis of EGR species from different fuel blends and their influence on the combustion and emission characteristics would be interesting as a recommendation for further work. The measurements in Section 4.3 show that it was possible to reduce the soot emissions from RSO to the diesel equivalent level of soot. The strategy for this reduction was to increase injection pressure and then to retard injection timing. First attempt was made for the blend of 50% RSO. However, high soot emissions from this blend were not reduced to the diesel equivalent level of soot. Moreover this strategy was successfully adopted for reduction of the soot from the blend of 30% RSO. The injection parameters for this blend were found to be 1200 bar of injection pressure and 3 deg bTDC of injection timing. Afterwards, a detailed comparative combustion and emissions analysis was done for 30% RSO at reduced soot conditions and diesel under reference engine operating conditions. The combustion analysis shows almost the same but shifted in-cylinder pressure and heat release rate curves when compared to diesel. Moreover, the NO_x emissions were further reduced for 30% RSO under the diesel equivalent soot engine operating conditions. Generally, the optimal engine operating conditions for the same soot emissions as diesel can be different. For instance, an injection pressure higher than 1200 bar would allow using a RSO percentage higher than 30% in the blend. From these measurements, the injection parameters for a given PPO blend are crucial in the reduction of soot emissions. Therefore, as a further study, different

diameters of the injector hole can be tested. It will provide a different PPO spray in the combustion chamber with longer lift-off lengths which could provide favourable conditions for further reduction of the soot emissions.

The full test matrix with different EGR and injection timing under turbocharged engine conditions for RME and diesel are presented in Section 4.4. The turbocharged operation further reduced the soot emissions and allowed the engine operation at a very late fuel injection, up to 5 CAD aTDC. When compared to diesel, under the same engine operating conditions, RME showed lower soot but higher NO_x emissions. In the case of RME, it was possible to reach the narrow engine operation window where the addition of EGR at TDC of injection timing resulted in low temperature combustion, where the simultaneous reduction of NO_x and soot emissions occurred. Moreover, the usage of RME resulted in stronger reduction than diesel in soot and NO_x emissions, thus more engine operating conditions for RME were fitted into low NO_x and soot emissions levels. As a recommendation for further measurements, the boost pressure could be maintained possibly at a constant level under high EGR percentages. Moreover, cooled EGR with a constant inlet manifold air/exhaust gas temperature could be applied. The above treatments would result in lower soot emissions at high EGR due to lower inlet temperature. Additionally, a constant (higher) boost pressure under a high EGR rate should further reduce the soot emissions. Consequently, the LTC effect could be dominant, leading to a reduced range of low NO_x and soot emissions on the NO_x-soot trade off graph.

Detailed characterisations of soot emissions and EMS system are presented in Chapter 5. The measurements for the existing dilution system using steel or aluminium DMAs showed a good scan to scan and day to day repeatability for aluminium DMA. The design and test of the primary dilution system showed that the particles concentration number was decreasing with a high dilution ratio, which was a correct trend. After several investigations, the favourable dilution conditions were found to be PDR of 2.32, SDR of 2.0 at 300 degC. They provided a relatively higher particles concentration, broader particles diameter range and visible nuclei particles. However, the detailed and systematic analyses of the whole system have to be done in order to obtain more real results. The design of the primary dilution system is very sensitive to changes in the particles size distribution. Therefore, a full dilution conditions matrix (PDR, SDR and SDR's temperature) could be done in order to investigate the influence of these parameters on soot particles size distributions. Moreover, it could be helpful to obtain information about flows and dynamics of the primary dilution system. Additionally, the characterisation of EMS system should be done for constant aerosol with known particles size distribution. In this way, the EMS system can be characterised and developed for further measurements.

The measurements of the soot particles size distribution for different engine parameters and fuels showed that, generally, the concentration number for RME was lower than for diesel. The nuclei soot particles were dominantly visible at a low engine torque, thus a higher torque resulted in a higher concentration number in the accumulation mode with a simultaneous broader range of the particles diameter. The biggest influence on soot particles size distribution can be seen in the case of EGR. Generally, soot particles from the nucleation mode agglomerate to form larger size aggregates in the accumulation mode. Moreover, the highest engine torque and EGR rate produced particles even up to 682 nm in diameter. On the other hand, a higher injection pressure caused a slight reduction only in the accumulation mode. Variations in the injection timing caused inconclusive trends. The influence of EGR or injection timing on the soot emissions can be attributed to the concentration number in the accumulation mode. An increase or decrease of the concentration number in this mode is linked to the soot emissions measured by the smoke meter, thus is higher or lower, respectively. A certain size of particles passes through the filter paper but only large diameter particles are measured.

The measurements in Chapter 6 showed that the application of DPF resulted in an efficient reduction of soot in the exhaust gases. The traditional measurements of the smoke number after the DPF were beyond the detection limit of the smoke meter. The analysis of the soot particles size distribution after the DPF showed low particles concentration numbers only in the nucleation mode at higher engine torques (60 and 80 Nm) and all tested engine speeds. However, the filtration efficiency based on CN was 100% at low engine torques (20 and 40 Nm) and all engine speeds. At the highest engine speed (2000 rpm), the detected range of particles diameter increased slightly from around 22 nm to 82 nm. Moreover, the measurements of soot particles size distribution before filter showed strong connection of the accumulation mode to the level of measured smoke number. This test was done without the simultaneous control of the parameters before and after the DPF. Especially, the exhaust back pressure is proportional to the time of measurement and increases during the test. Maintaining a constant back pressure requires the DPF's regeneration system which has to be developed for further measurements. Additionally, the casing for the DPF has been designed in such a way that allows using different types of substrates. A further study should involve different porosities of the DPF to check the filtration efficiency of different materials.

Bibliography

[1] J.B.Heywood. *Internal Combustion Engines Fundamentals*. McGraw-Hill Co, New York, 1988.

[2] *Internal Combustion Engine Handbook*. SAE, 2004.

[3] European Automobile manufacturers Association. *www.acea.be*.

[4] US Environmental Protection Agency. *www.epa.gov*.

[5] European Commission. *www.ec.europa.eu*.

[6] C.J. Hillard, R.W. Wheeler. Nitrogen Dioxide in Engine Exhaust. *SAE*, 790691 (1979).

[7] A.W. Majewsky, K.M. Khair. *Diesel Emissions and Their Control*. 2006.

[8] R.Stone. *Introduction To Internal Combustion Engines*. MacMillan Press LTD, 1999.

[9] J.E.Dec. A Conceptual Model of DI Diesel Combustion Based on Laser-Sheet Imaging. *SAE*, 970873 (1997).

[10] D.B.Kittelson. Engines and nanoparticles: a review. *Aerosol Science*, 29 (1998), 575-588.

[11] U. Mathis, R. Kaegi, M.Mohr, R. Zenobi. TEM analysis of volatile nonoparticles from partocle trap equipped diesel and direct-injection spark-ignition vehicles. *Atmospheric Environment*, 38 (2004), 4347-4355.

[12] A. Neer, U.O. Koylu. Effect of operating conditionson the size, morphology, and concentration of submicrometer particulates emitted from a diesel enigne. *Combustion and Flame*, 146 (2006), 142-154.

[13] K. Park, D. Kittelson, P. McMurry. Structural Properties of Diesel Exhaust particles Measured by Transmission Electron microscopy (TEM): Relationships to Particle Mass and Mobility. *Aerosol Science and Technology*, 38:9 (2004), 881-889.

[14] U. Kirchner, V. Scheer, R. Vogt, R. Kagi. TEM study on volatility and potential presence of solid cores in nucleation mode particles from diesel powered passenger cars. *Aerosol Science*, 40 (2009), 55-64.

[15] H. Zhao, N. Ladommatos. Optical Diagnostics for Soot and Temperature Measurement in Diesel Engines. *Progress in Energy and Combustion Science*, 24 (1998), 221-255.

[16] Y. Xu, C.F. Lee. Investigation of Soot Formation in Diesel Combustion Using Forward Illumination Light Extinction (FILE) Technique. *SAE*, 2004-01-1411 (2004).

[17] C.A.Pope. Epidemiology of fine particulate air pollution and human health: biologic mechanisms and who's at risk? *Environmental Heath Perpective*, 108 (2000), 713-723.

[18] K. Donaldson, X. Y. Li, W. MacNee. Ultrafine (nanometre) particle mediated. *Journal of Aerosol Science*, 29 (1998), 553-560.

[19] L.Wallace. Correlations of Personal Exposure to Particles with Outdoor Air. *Aerosol Science and Technology*, 32 (2000), 15 - 25.

[20] H.Yun, M.Sellnau, N.Milanovic, S.Zuelch. Development of Premixed Low-Temperature Diesel Combustion in a HSDI Diesel Engine. *SAE*, 2008-01-0639 (2008).

[21] M.Zheng, X.Han, Y.Tan, M.S.Kobler, S.K, M.Wang, M.C.Mulenga, J.Tjong. Low Temperature Combustion of Neat Biodiesel Fuel on a Common-rail Diesel Enigne. *SAE*, 2008-01-1396 (2008).

[22] N.Horibe, T.Ishiyama. Relations among NOx, Pressure Rise Rate, HC and CO in LTC Operation of a Diesel Enigne. *SAE*, 2009-01-1443 (2009).

[23] Earth System Research Laboratory, Global Monitoring Division. *http://www.esrl.noaa.gov/gmd/ccgg/trends/*.

[24] C.D. Keeling, R.B. Bacastow, A.E. Bainbridge, C.A. Ekdahl, P.R. Guenther, L.S. Waterman. Atmospheric carbon dioxide variations at Mauna Loa Observatory, Hawaii, Tellus (1976), 538-551.

[25] K.W. Thoning, P.P. Tans, W.D. Komhyr. Atmospheric carbon dioxide at Mauna Loa Observatory 2. Analysis of the NOAA GMCC data. *Journal of Geophysics and Research*, 94 (1989), 8549-8565.

[26] *CDIAC, Carbon Dioxide Information Analysis Centrer, cdiac.ornl.gov*.

[27] M. Guyon, P.Blanche, C.Bert, L.Philippe, I.Messaoudi. NOx-Trap System Development and Characterization for Diesel Enignes Emission Control. *SAE*, 2000-01-2910 (2000).

[28] T.Duesterdiek, W.Engeler, D.Neyer, J.Jocheim, D.Hesse, J.P.Warren, A.J.J.Wilkins, M.V.Twigg. A Study of the Catalytic Reduction of NOx in Diesel Exhaust. *SAE*, 962042 (1996).

[29] M.S.Brogan, N.S.Will, M.V.Twigg, A.J.J.Wilkins, K.Jordan, R.J.Brisley. Advances in DENOx catalyst technology for European Stage IV emissions levels. *Future Engine and System Technologies, Profesional Engineering Publications* (1998).

[30] Johnson&Matthey Catalysts. *www.matthey.com*.

[31] European Patent CRT EP 0835684.

[32] J.E.Dec. Advanced compression-ignition engines - understanding the in-cylinder processes (2009), 2727-2742.

[33] M.S.Graboski, R.L.McCormic. Combustion of fat and vegetable oil derived fuels in diesel enignes. *Progress in Energy and Combustion Science*, 24 (1998), 125-164.

[34] A.K.Agarwal. Biofuels (alcohols and biodiesel) applications as fuels for internal combustion engines. *Progress in Energy and Combustion Science*, 33 (2007), 233-271.

[35] K.Purushothaman, G.Nagarajan. Performance, emission and combustion characteristics of a compression ignition engine operating on neat orange oil. *Renewable Energy*, 34 (2009), 242-245.

[36] D.Kawano, H.Ishii, Y.Goto, A.Noda, Y.Aoyagi. Application of biodiesel fuel to modern diesel engine. *SAE*, 2006-01-0233 (2006).

[37] D.Kawano, H.Ishii, Y.Goto, A.Noda, Y.Aoyagi. Optimization of Enigne System for Application of Biodiesel Fuel. *SAE*, 2007-01-2028 (2007).

[38] USEPA. A comprehensive analysis of biodiesel impacts on exhaust emissions (2002).

[39] J.Cvengros, F.Povazanec. Production and treatment of rapeseed oil methyl esters as alternative fuels for diesel enignes. *Bioresource of Technology*, 38 (1996), 145-152.

[40] C.L.Peterson, H.Tood. Carbon cycle for rapeseed oil biodiesel fuesl. *Biomass and Bioerergy*, 14 (1998), 91-101.

[41] A.Srivastava, R.Prasad. Trigycerides-based diesel fuels. *Renewable and Sustainable Energy Reviews*, 4 (2000), 111-113.

[42] D.Agarwal, A.K.Agarwal. Performance and emissions characteristics of Jatropha oil (preheated and blends) in direct injection compression ignition engine. *Applied Thermal Engineering*, 27 (2007), 2314-2323.

[43] C.D.Rakopoulos, K.A.Antonopoulos, D.C.Rakopoulos, D.T.Hountalas, E.G.Giakoumis. Comperative performance and emissions study of a direct injection diesel engine using blends of diesel fuel with vegetable oils or bio-diesel of various origins. *Energy Conversion and Management*, 47 (2006), 3272-3287.

[44] A.Murugesan, C.Umarani, R.Subramanian, N.Nedunchezhian. Bio-diesel as an alternative fuel for diesel enignes-A review. *Renewable and Sustainable Energy Reviews*, 13 (2009), 653-662.

[45] A.Demirabas. Relationships derived from physical properties of vegetable oil and biodiesel fuels. *Fuel*, 87 (2008), 1743-1748.

[46] J.Narayana Reddy, A.Ramesh. Parametric studies for improving the performance of a jatropha oil-fuelled compression ignition engine. *Renewable Energy*, 31 (2006), 1994-2016.

[47] A.K.Tiwari, A.Kumar, H.Raheman. Biodiesel production from jatropha oil (Jatropha curcas) with high free fatty acids: An optimized process. *Biomass and Bioenergy*, 31, 569-575.

[48] F.K.Forson, E.K.Oduro, E.Hammond-Donkoh. Performance of jatropha oil blends in a diesel enigne. *Renewable Energy*, 29 (2004), 1135-1145.

[49] A.M.Williamson, O.Badr. Assessing the Viability of using Rape Methyl Ester (RME) as an Alternative to MIneral Diesel Fuel for Powering Road Vehicles in the UK. *Applied Energy*, 59 (1998), 187-214.

[50] A.S.Ramadhas, C.Muraleedharan, S.Jayaraj. Performance and emission evaluation of a diesel enigne fueled with methyl esters of rubber seed oil. *Renewable Energy*, 30 (2005), 1789-1800.

[51] M.Luft, S.Bernhardt, A.Velji, U.Spicher. Optimization of injection of pure rape seed oil in modern diesel enignes with direct-injection. *SAE*, 2007-01-2031 (2007).

[52] O.D.Hebbal, K.V.Reddy, K.Rajagopal. Performance characteristics of a diesel enigne with deccan hemp oil. *Fuel*, 85 (2006), 2187-2194.

[53] S.K.Haldar, B.B.Gosh, A.Nag. Studies on the comparison of performance and emission characteristics of a diesel engine using three degummed non-edible vegetable oils. *Biomass and Energy*, 33 (2009), 1013-1018.

[54] H.J.Harwood. Oleochemicals as a fuel: Mechanical and economic feasibility. *Journal of the American Oil Chemists' Society*, 61 (1984), 315-324.

[55] F.Ma, M.A.Hanna. Biodiesel production: a review. *Bioresource Technology*, 70 (1999), 1-15.

[56] H.T.C.Machacon, S.Shiga, T.Karasawa, H.Nakamura. Performance and emission characteristics of a diesel enigne fueled with coconut oil-diesel fuel blend. *Biomass and bioenergy*, 20 (2001), 63-69.

[57] K.W.Scholl, S.C.Sorenson. Combustion of soyabean oil methyl ester in a direct injection diesel enigne. *SAE*, 930934 (1993).

[58] R.Altin, S.Cetinkaya, H.S.Yucesu. The potential of using vegetable oil fuels as fuel for diesel engines. *Energy Conversion and Management*, 42 (2001), 529-538.

[59] N.R.Banapurmath, P.G.Tewari, R.S.Hosmath. Performance and emission characteristic of a DI compression ignition engine operated on honge, jtropha and sesame oil methyl esters. *Renewable Energy*, 33 (2008), 1982-1988.

[60] A.Tsolakis, A.Megaritis, M.L.Wyszynski, K.Theinnoi. Engine performance and emissions of a diesel engine operating on diesel-RME (reapseed methyl ester) blends with EGR (exhaust gas recirculation). *Energy*, 32 (2007), 2072-2080.

[61] M.Vojtisek-Lom. Time-resolved Emissions characteristics of MOdern Passenger Vehicle Diesel Enignes powered by Heated Vegetable Oil. *SAE*, 2007-24-0129 (2007).

[62] I.K.Reksowardojo, T.P.Brodjonegoro, W.Arismunandar, R.Sopheak, H.Ogawa. The combustion and exhaust gas emission of a direct injection compression ignition engine using physic nut oil (jatropha curcas L.oil). *SAE*, 2007-01-3622 (2007).

[63] T.W.Ryan III, M.O.Bagby. Identification of chemical changes occuring during the transient innjection of selected vegetable oils. *SAE*, 930933 (1993).

[64] D.B.Kittelson, W.F.Watts, J.P.Johnson. On-road and laboratory evaluation of combustion aerosols - Part1: Summary of diesel enigne results. *Aerosol Science*, 37 (2006), 913-930.

[65] U.Mathis, J.Ristimaki, M.Mohr, J.Keskinen, L.Ntziachristos, Z.Samaras, P.Mikkanen. Sampling Conditions for the measurement of Nucleation Mode particles in the Exhaust of a Diesel Vehicle. *Aerosol Science and Technology*, 38 (2004), 1149-1160.

[66] D.B.Kittelson, J.Johnson, W.Watts, Q.Wei, M.Drayton, D.Paulsen, N.Bukowiecki. Diesel Aerosol Sampling in the Atmosphere. *SAE*, 200-01-2212 (2000).

[67] B.Giechaskiel, L.Ntziachristos, Z.Samaras, V.Scheer, R.Casati, R.Vogt. Formation potential of vehicle exhaust nucleation mode particles on-road and in the laboratory. *Atmospheric Environment*, 39 (2005), 3191-3198.

[68] E.Vouitsis, l.Ntziachristos, Z.Samaras. Theoretical Investigation of the Nucleation Mode Formation Downstream of Diesel After-treatment Devices. *Aerosol and Air Quality Research*, 8 (2008), 37-53.

[69] S.C.Wang, R.C.Flagan. Scanning Electrical Mobility Spectrometer. *Aerosol Science and Technology*, 13 (1990), 230-240.

[70] H.Burtscher. Physical charcterization of particulate emissions from diesel enignes: a review. *Aerosol Science*, 36 (2005), 896-932.

[71] J.Lyyranen, J.Jokiniemi, E.I.Kauppinen, U.Backman, H.Vesala. Comparison of Different Dilution Methods for Mesuring Diesel Particle Emissions. *Aerosol Science and Technology*, 38 (2004), 12-23.

[72] M.Kasper. The Number Concentration of Non-Volatile Particles - Design Study for an Instrument According to the PMP Recommendations. *SAE*, 2004-01-0960 (2004).

[73] P.Eastwood. *Particulate Emissions from Vehicles*. John Willey & Sons Ltd, Chichester, 2008.

[74] U. Horn, R. Egnell, B. Johansson, O. Andersson. Detailed Heat Release Analyses With Regard To Combustion of RME and Oxygenated Fuels in an HSDI Diesel Engine. *SAE*, 2007-01-0627 (2007).

[75] R.Lanzafame, M.Messina. ICE gross heat release strongly influenced by specific heat ratio values. *International Journal of Automotive Technology*, 4 (2003), 125-133.

[76] K.Acharya, M.Dahodwala, W.Bryzik, N.Henein, N.Sova. Effect of different biodiesel blends on autoignition, combustion, performance and engine-out emissions in a single cylinder HSDI diesel engine. *SAE*, 2009-01-0489 (2009).

[77] A. Maiboom, X. Tauzia, JF, Hetet. Experimental study of various effects of exhaust gas recirculation (EGR) on combustion and emissions of an automotive direct injection diesel engine. *Energy*, 33 (2008), 22-34.

[78] A. Mailboom, X. Tauzia, JF. Hetet, M. Cormerais, M. Tounsi, T. Jaine, S. Blanchin. Various effect of EGR on combustion and emissions on a automotive DI Diesel engine: numerical and experimental study. *SAE*, 2007-01-1834 (2007).

[79] T. Suzuki, T. Kakegawa, K. Hikino, A. Obata. Development of Diesel Combustion for Commercial Vehicle. *SAE*, 972685 (1997).

[80] R. Schubiger, A. Bertola, K. Boulouchos. Influence of EGR on Combustion and Exhaust Emissions of Heavy Duty DI-DIesel Engines Equipped with Common-Rail Injection System. *SAE*, 2001-01-3497 (2001).

[81] M.Zheng, M.Wang, G.T.Reader, M.C.Mulenga, J.Tjong. An improvement on low temperature combustion in neat biodiesel engine cycles. *SAE*, 2008-01-1670 (2008).

[82] A.Schonborn, N.Ladommatos. Effect of the molecular structure of individual fatty acid alcohol esters (biodiesel) on the fromation of NOx and particulate matter in the diesel combustion process. *SAE*, 2008-01-1578 (2008).

[83] A.Schonborn, N.Ladommatos, J.Willims, R.Allan, J.Rogerson. Effects on diesel combustion of the molecular structure of potential synthetic bio-fuel molecules. *SAE*, 2007-24-0125 (2007).